BIORESPONSIVE NANOMATERIALS FOR MULTIMODALITY IMAGING AND THERAPY

EDITED BY: Dalong Ni, Hyung-Jun Im and Dawei Jiang
PUBLISHED IN: Frontiers in Chemistry

frontiers Research Topics

frontiers

ISSN 1664-8714
ISBN 978-2-88971-650-0
DOI 10.3389/978-2-88971-650-0

About Frontiers

Frontiers is more than just an open-access publisher of scholarly articles: it is a pioneering approach to the world of academia, radically improving the way scholarly research is managed. The grand vision of Frontiers is a world where all people have an equal opportunity to seek, share and generate knowledge. Frontiers provides immediate and permanent online open access to all its publications, but this alone is not enough to realize our grand goals.

Frontiers Journal Series

The Frontiers Journal Series is a multi-tier and interdisciplinary set of open-access, online journals, promising a paradigm shift from the current review, selection and dissemination processes in academic publishing. All Frontiers journals are driven by researchers for researchers; therefore, they constitute a service to the scholarly community. At the same time, the Frontiers Journal Series operates on a revolutionary invention, the tiered publishing system, initially addressing specific communities of scholars, and gradually climbing up to broader public understanding, thus serving the interests of the lay society, too.

Dedication to Quality

Each Frontiers article is a landmark of the highest quality, thanks to genuinely collaborative interactions between authors and review editors, who include some of the world's best academicians. Research must be certified by peers before entering a stream of knowledge that may eventually reach the public - and shape society; therefore, Frontiers only applies the most rigorous and unbiased reviews.
Frontiers revolutionizes research publishing by freely delivering the most outstanding research, evaluated with no bias from both the academic and social point of view. By applying the most advanced information technologies, Frontiers is catapulting scholarly publishing into a new generation.

What are Frontiers Research Topics?

Frontiers Research Topics are very popular trademarks of the Frontiers Journals Series: they are collections of at least ten articles, all centered on a particular subject. With their unique mix of varied contributions from Original Research to Review Articles, Frontiers Research Topics unify the most influential researchers, the latest key findings and historical advances in a hot research area! Find out more on how to host your own Frontiers Research Topic or contribute to one as an author by contacting the Frontiers Editorial Office: frontiersin.org/about/contact

BIORESPONSIVE NANOMATERIALS FOR MULTIMODALITY IMAGING AND THERAPY

Topic Editors:
Dalong Ni, Shanghai Jiao Tong University, China
Hyung-Jun Im, Seoul National University, South Korea
Dawei Jiang, Huazhong University of Science and Technology, China

Citation: Ni, D., Im, H.-J., Jiang, D., eds. (2021). Bioresponsive Nanomaterials for Multimodality Imaging and Therapy. Lausanne: Frontiers Media SA. doi: 10.3389/978-2-88971-650-0

Table of Contents

frontiers in Chemistry

REVIEW
published: 20 March 2020
doi: 10.3389/fchem.2020.00203

Recent Advances of Bioresponsive Nano-Sized Contrast Agents for Ultra-High-Field Magnetic Resonance Imaging

Hailong Hu [1,2]*

[1] School of Aeronautics and Astronautics, Central South University, Changsha, China, [2] Research Center in Intelligent Thermal Structures for Aerospace, Central South University, Changsha, China

The ultra-high-field magnetic resonance imaging (MRI) nowadays has been receiving enormous attention in both biomaterial research and clinical diagnosis. MRI contrast agents are generally comprising of T_1-weighted and T_2-weighted contrast agent types, where T_1-weighted contrast agents show positive contrast enhancement with brighter images by decreasing the proton's longitudinal relaxation times and T_2-weighted contrast agents show negative contrast enhancement with darker images by decreasing the proton's transverse relaxation times. To meet the incredible demand of MRI, ultra-high-field T_2 MRI is gradually attracting the attention of research and medical needs owing to its high resolution and high accuracy for detection. It is anticipated that high field MRI contrast agents can achieve high performance in MRI imaging, where parameters of chemical composition, molecular structure and size of varied contrast agents show contrasted influence in each specific diagnostic test. This review firstly presents the recent advances of nanoparticle contrast agents for MRI. Moreover, multimodal molecular imaging with MRI for better monitoring is discussed during biological process. To fasten the process of developing better contrast agents, deep learning of artificial intelligent (AI) can be well-integrated into optimizing the crucial parameters of nanoparticle contrast agents and achieving high resolution MRI prior to the clinical applications. Finally, prospects and challenges are summarized.

Keywords: nano-sized, contrast agents, magnetic resonance imaging, multimodal imaging, artificial intelligence

OPEN ACCESS

Edited by:
Dalong Ni,
Shanghai Jiao Tong University, China

Reviewed by:
Weiyu Chen,
Stanford University, United States
Meiying Wu,
Sun Yat-sen University, China

***Correspondence:**
Hailong Hu
hailonghu@csu.edu.cn

Specialty section:
This article was submitted to Nanoscience, a section of the journal Frontiers in Chemistry

Received: *16 February 2020*
Accepted: *04 March 2020*
Published: *20 March 2020*

Citation:
Hu H (2020) Recent Advances of Bioresponsive Nano-Sized Contrast Agents for Ultra-High-Field Magnetic Resonance Imaging. Front. Chem. 8:203. doi: 10.3389/fchem.2020.00203

INTRODUCTION

As one of the most attractive and useful techniques for non-invasive imaging, magnetic resonance imaging (MRI) shows its great superiority in the practical application of clinic diagnosis, as well as the biomedical research (Zhao et al., 2001, 2013, 2015; Werner et al., 2008; Kim et al., 2009; Lee et al., 2012; Bao et al., 2018; Pellico et al., 2019; Liu et al., 2020). It is well-acknowledged that spatial resolution can be promoted by high magnetic field over 3 T, demonstrating a high signal-to-noise ratio (Vaughan et al., 2009; Rosenberg et al., 2010; Zhou et al., 2015b; Ni et al., 2016; Zhang et al., 2016). This result is usually evidenced by the MRI study on small animals under the applied high field (over 7 T) (Nakada, 2007; Werner et al., 2008; Faucher et al., 2012; Ni et al., 2016). Moreover, compared with 1.5 or 3.0 T MRI, ultra-high-field MRI shows its unique advantage in medical imaging, especially in the field neuroscience, where functional brain responses can be

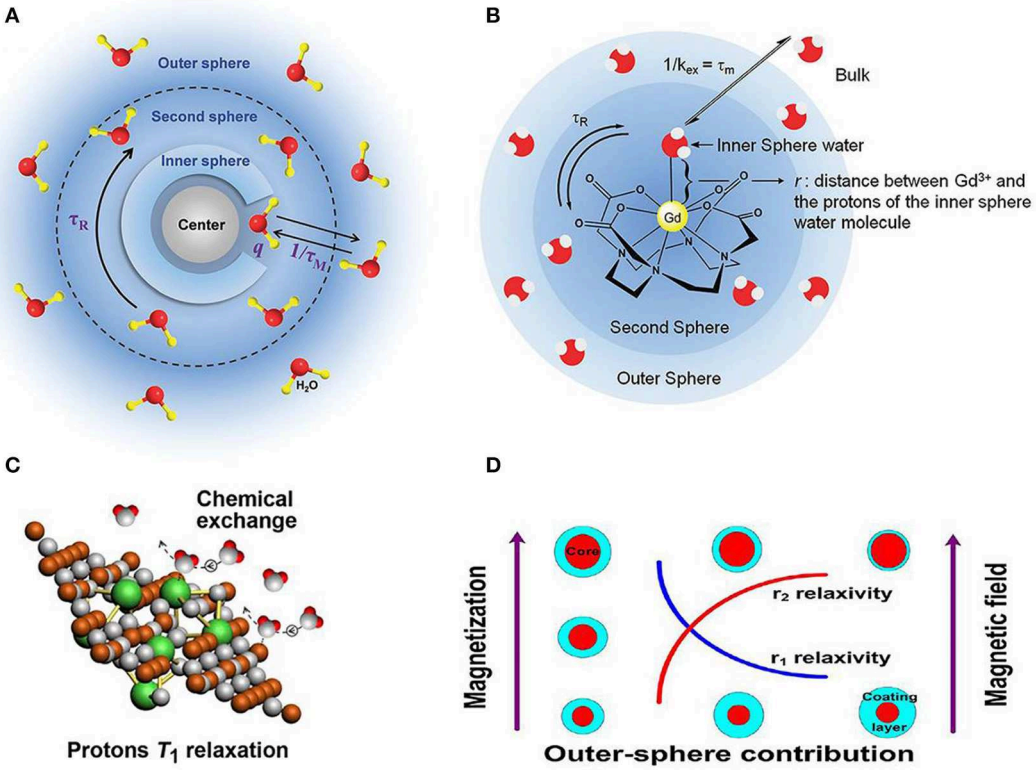

FIGURE 1 | Relationship between structure and relaxivity of nanoparticle contrast agent for MRI. **(A)** Schematic diagram of mechanism for contrast agents (Ni et al., 2017); Copyright 2017, reproduced with permission from The Royal Society of Chemistry **(B)** factors illustrated for affecting contrast agent's relaxivity (Verwilst et al., 2015); Copyright 2015, reproduced with permission from The Royal Society of Chemistry. **(C)** Efficient chemical exchange for protons to accelerate T_1 relaxation (Zhou et al., 2015a); Copyright 2015, reproduced with permission from American Chemical Society **(D)** surface modification of nanoparticles contributing to MRI T_2 contrast agents (Zhang et al., 2016); Copyright 2016, reproduced with permission from American Chemical Society.

non-invasively measured with increasing sensitivity and greater spatial resolution under ultra-high-field MRI (de Martino et al., 2018). However, much more effort should be devoted to exploring the ultra-high-field MRI to eventually achieve the enhanced solution and sensitivity for clinical imaging diagnosis (Duyn, 2012; Zhao et al., 2013; Chang et al., 2016; Gautam et al., 2019; Harris et al., 2019; Rajamanickam, 2019).

The lanthanide ions such as Dy^{3+} and Ho^{3+} contrast agent ions are generally used for high magnetic field MRI (Das et al., 2011, 2012; Harris et al., 2016; Ni et al., 2016; Zhang et al., 2016). Signal intensity of MRI is affected by the relaxation rate of *in vivo* water protons. By using the contrast agent with varied contents, the MRI signal intensity can be changed, where paramagnetic metal ion in contrast agent with different concentrations will positively alter the relaxation rate of nearby water proton spins (Idisi et al., 2019; Kubíčková et al., 2019). The contrast agent for MRI has been illustrated in **Figure 1**, where several factors affecting the MRI have been clearly indicated with the listed examples. **Figure 1A** shows the general mechanism of contrast agent, where the change of hydrogen atom's magnetization in water plays a predominant role in deciding the capability of generated contrast for contrast agent. For the atomic structure of paramagnetic contrast agent, paramagnetic center, inner sphere, secondary sphere and outer sphere are included. The relaxation contribution is quantitatively determined by the location between water protons and contrast agent. Water molecules coordinated to paramagnetic center will contribute to the inner sphere relaxation contribution and bulk water molecules will be responsible for the outer sphere relaxation (Ni et al., 2017; Marasini et al., 2020).

Moreover, take the gadolinium ions based contrast agent as another case, surface modification of organic ligands will be tightly binding to gadolinium ion avoid the toxicity for clinical diagnosis (Csajbok et al., 2005; Bridot et al., 2007). For this case, the hydrogen are bonded to the ligand instead of water molecules bounding to gadolinium ion, forming the second sphere in **Figure 1B** (Verwilst et al., 2015). Other crucial factors to the relaxation mechanism of contrast agent, such as chemical structure and surface modification (Zhu et al., 2016; Wang et al., 2018; Jin et al., 2019; Yin et al., 2019; Zhang et al., 2019) are also illustrated (**Figures 1C,D**), where efficient chemical exchange for protons accelerates relaxation and surface modification of nanoparticles contributes to MRI T_2 contrast agents, respectively (Zhou et al., 2015a; Zhang et al., 2016). Specifically, the effect of particle size and magnetic field on influencing relaxivities of r_1 and r_2 has been investigated based on the out-sphere theory,

showing the increased r_2 contributed by the increasing core size, decreasing coating layer thickness or increasing magnetic field.

When employing contrast agents for MRI, contrast agent shall possess the following distinct features for better imaging (Zhou et al., 2019): (a) Nano-size, achieve the maximum recognition; (b) diagnosis with high accuracy; (c) Compatibility, non-cytotoxic and biocompatible; (d) Stability, both chemical and photochemical stable; (e) Metabolism; renal excretion from body (Qin et al., 2007; Huang et al., 2010; Botar et al., 2020).

In addition, the recent progress of emerging artificial intelligence (AI) has advanced the exploration of ultra-high-field MRI, where AI in conjunction with MRI is supposed to be prevalently used in many cases, ranging from imaging reconstruction to the final clinical decision support (Busch, 2019). For instance, Sheth et al. discussed the AI in interpreting breast cancer on MRI, aiming to enhance the efficacy and accuracy of diagnosis (Sheth and Giger, 2019). To bridge the current gap between virtual reality and neuropathology, AI and ultra-high-field MRI with enhanced resolution will inevitably advance the knowledge of microstructure changes in varied pathogenetic stages (O'sullivan et al., 2019).

RECENT ADVANCES OF CONTRAST AGENTS FOR ULTRA-HIGH-FIELD MRI

To reveal the efficacy of a variety of contrast agents, crucial parameters have been defined to indicate the efficiency and species of contrast agents. Transverse relaxivity (r_2), longitudinal relaxivity (r_1) and the ratio of r_2/r_1 are used to evaluate the contrast efficiency of MRI contrast agent, where a high ratio of r_2/r_1 generally results in a high contrast efficiency (Shen et al., 2017b). A more efficient T_2 contrast agent instead of T_1 contrast agent will be determined by the increasing ratio of r_2/r_1 (Das et al., 2012). Metal ion includes the electron orbital motion and electron spin motion. The electron spin magnetic moment plays a predominant role in determining the longitudinal water relaxation (r_1). The existence of electron spin angular momentum of adjacent ions contributes to an enlarged total electron angular momentum, leading to a high r_1. On the contrary, total electron angular momentum will be quite small if contribution is only from electron orbital angular momentum.

Gadolinium chelates are commonly used as contrast agents owing to its advantages of offering superior non-invasive visualization for ailments (Rogosnitzky and Branch, 2016; Marangoni et al., 2017; Rees et al., 2018; Clough et al., 2019). However, both the short circulation lifetime in the body and the relatively low proton relaxation efficiency substantially limit its wide application. Moreover, to achieve the high proton relaxation efficiency, high concentration of contrast agents is required, which will deteriorate human's body in terms of the side effect induced by Gd^{3+} ions.

Alternatively, nanoparticle with magnetic responsive atom is becoming one of the most promising candidates to be used as contrast agents, such as transition metal ions (Cu^{2+}, Fe^{2+}/Fe^{3+},Co^{2+}, and Mn^{2+}, lanthanide metal ions (Eu^{3+}, Gd^{3+}, Ho^{3+}, and Dy^{3+}) (Tromsdorf et al., 2007; Mahmoudi et al., 2011; Busquets et al., 2015; Ni et al., 2017; Sousa et al., 2017; Guo et al., 2019; Hai et al., 2019; Wahsner et al., 2019; Botar et al., 2020). Furthermore, iron-based nano-system is highly recommended as spin-spin imaging or imaging probe because of its merits of electronic, magnetic, optical properties at nano scale and the excellent *in vivo* stability as well (Li et al., 2013). On the other hand, high surface area of nanoparticle promotes the chemical reactivity and make it viable to be modified with the biological and bioactive surfactants. Therefore, owing to these superior benefits, nanoparticles have been regarded as one of the promising alternatives for imaging contrast agents in future (Bobo et al., 2016; Chen et al., 2016; Shen et al., 2017c).

It is well-recognized that ultra-high-field MRI has achieved the increasing prevalence in both fundamental research and clinical applications (Dyke et al., 2017; Huelnhagen et al., 2017; Lehericy et al., 2017; Hametner et al., 2018). A bimodal contrast agent of Dy^{3+}(DOTA)/Cy7.5-conjugated tobacco mosaic virus (TMV) was developed for ultra-high-field MRI, confirming its high transverse relaxivity r_2 and suitable for both NIRF imaging and T_2 MRI in cancel cells diagnosis (Hu et al., 2017). **Figures 2A,B** show the relaxivity of contrast agent under ultra-high-magnetic of 7.0 and 9.4 T. Both high r_2 and high ratio of r_2/r_1 are obtained, showing the high efficiency of T_2 contrast agent for ultra-high-field MRI application. To further confirm the feasibility of this contrast agent, experiments are performed on concentration dependent phantom images (T_2-mapping) of contrast agent in water solutions at 7.0 and 9.4 T, showing a pronounced negative contrast gradient as a function of contrast agent concentration (**Figure 2C**). Till now, this kind of contrast agent demonstrates its great potential for ultra-high-field MRI. Furthermore, this contrast agent is to target tumors of mouse models by *in vivo* T_2-mapping MRI to check its ability. The impact of targeted and untargeted nanoparticles on local tissues is determined based on the relaxation times. **Figure 2D** shows a much stronger signal enhancement after contrast agent postinjection for a certain of hours (6 h) and the recovery is achieved after T_2 relaxation of 24 h. The biodistribution of nanoparticle contrast agent in organs and tumors are also determined (**Figure 2E**), showing more targeted nanoparticles accumulated in the tumors of mice than that of control nanoparticles, which is well-consistent with *in vivo* MRI images. Moreover, a certain number of nanoparticles are expected to stay in the liver owing to circulation of mononuclear phagocytic system. Consequently, the *in vivo* MRI results of nanoparticle confirm its efficiency as contrast agent.

Ni et al. prepared the $NaHoF_4$ nanoparticles via surface modification and studied the size effect of nanoparticles on MRI contrast agent performance under varied magnetic fields (**Figure 3**) (Ni et al., 2016, 2017). The optimal size of nanoparticles has been eventually achieved to test ultra-high-field MRI, showing an excellent biocompatibility and great promising candidate for future high field MRI. Moreover, as the size change of nanoparticles will bring alterable performance to MRI, whose detailed mechanism are also investigated, demonstrating

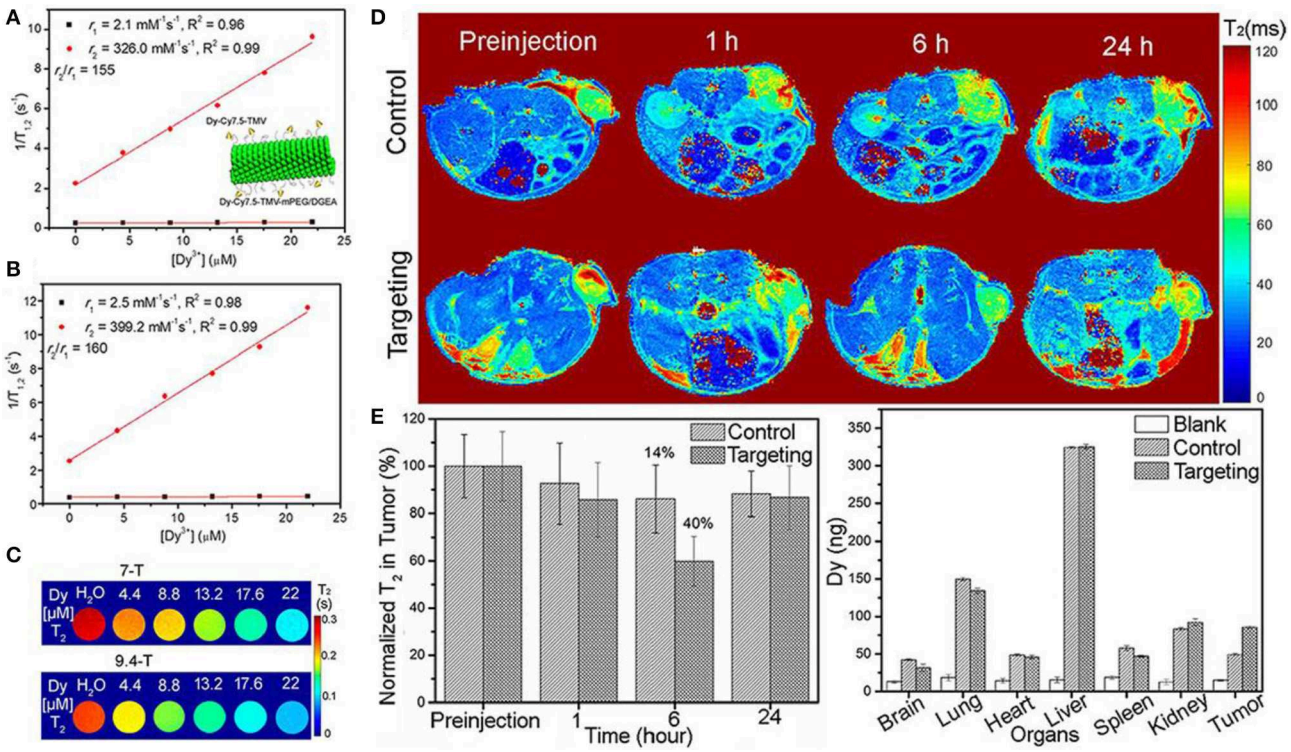

FIGURE 2 | Plots of water proton relaxation times of longitudinal r_1 and transversal r_2 as a function of Dy^{3+} content (Dy-Cy7.5-TMV-mPEG) under magnetic field of **(A)** 7 T (The insert shows the schematic diagram of modified Dy-Cy7.5-TMV-mPEG/DGEA nanoparticles); **(B)** 9 T; **(C)** T_2 mapping phantoms at different contents of Dy^{3+} under magnetic field of 7 T and 9.4 T; **(D)** *in vivo* MRI mapping as a function of time after intravenous injection of control and targeting group Dy-Cy7.5-TMV-mPEG/DGEA; **(E)** Analysis of T_2 as a function of time and distribution of Dy^{3+} in organs after 24 h injection (Hu et al., 2017); Copyright 2017, reproduced with permission from American Chemical Society.

the predominant curie mechanism for size below 7 nm and the main contribution of dipolar mechanism for size over 7 nm. Both rod-like $NaDyF_4$ and $NaHoF_4$ nanoparticles were prepared via a high temperature synthesis process and they are the promising candidate as T_2 contrast agents under the high field of 9.4 T MRI. Simulation results indicate the increase of 100 times for relaxivity when magnetic field increases from 1 to 10 T. Parameter such as the size was also studied and showed an increase of 30 times for both r_1 and r_2 when nanoparticle core size increases from 5 to 15 nm (Zhang et al., 2016).

Except the contrast agent developed for T_2-weighted MRI, the attempts into developing dual-mode T_1/T_2 contrast agents are also reported. Biju et al. reported a new type of contrast agent which can be used in either ultra-high magnetic field or multimodal imaging of MRI and optical imaging (Biju et al., 2018). This kind of contrast agent NP-PAA-FA is designed with core-shell structure with an average size of about 24 nm, and surface modification/functionalization is applied to enhance the contrast agent's biocompatibility. Both MRI and proton nuclear magnetic relaxation dispersion studies confirm the contrast agent's feasibility of behaving as a dual-weighted contrast agent at 3 T, and acting as a highly efficient T_2 weighted MRI contrast agent. **Figure 4A** shows the core-shell structure of prepared NP-PAA-FA contrast agent, and the obtained high values of ratio r_2/r_1 at ultra-high- field indicate its ability for MRI contrast agent (**Figure 4B**). To confirm the dual-modal character of NP-PAA-FA contrast agent for MRI, phantom images of concentration dependent of NP-PAA-FA water solution are compared to that commercially available Dotarem or Fe_3O_4 contrast agent, showing the pronounced alterable contrast in both T_1 and T_2 images as a function of concentration (**Figure 4C**). Therefore, great potential of NP-PAA-FA as a multimodal constant agent has been demonstrated, which will pave the way for studying more, novel and suitable contrast agent for ultra-high-field MRI.

Despite the efficient of surface modification technique to improve the biocompatibility, nanobiointerface in conjunction with surface structure engineering provides another possibility to develop high performance dual-modal MRI contrast agent (Zhou et al., 2015a). Small molecules of sodium citrate and zwitterionic dopamine sulfonate are individually exploited as surface and interface modifier to realize the superior water-dispersibility. The surface chemical exchange has been carried out through a ligand exchange process via hydrothermal technique. The exposed iron and gadolinium ions of GdIOPs surface in promoting the T_1 relaxation are illustrated in **Figure 5A**, which is attributed to the efficient chemical exchange for protons provided by the

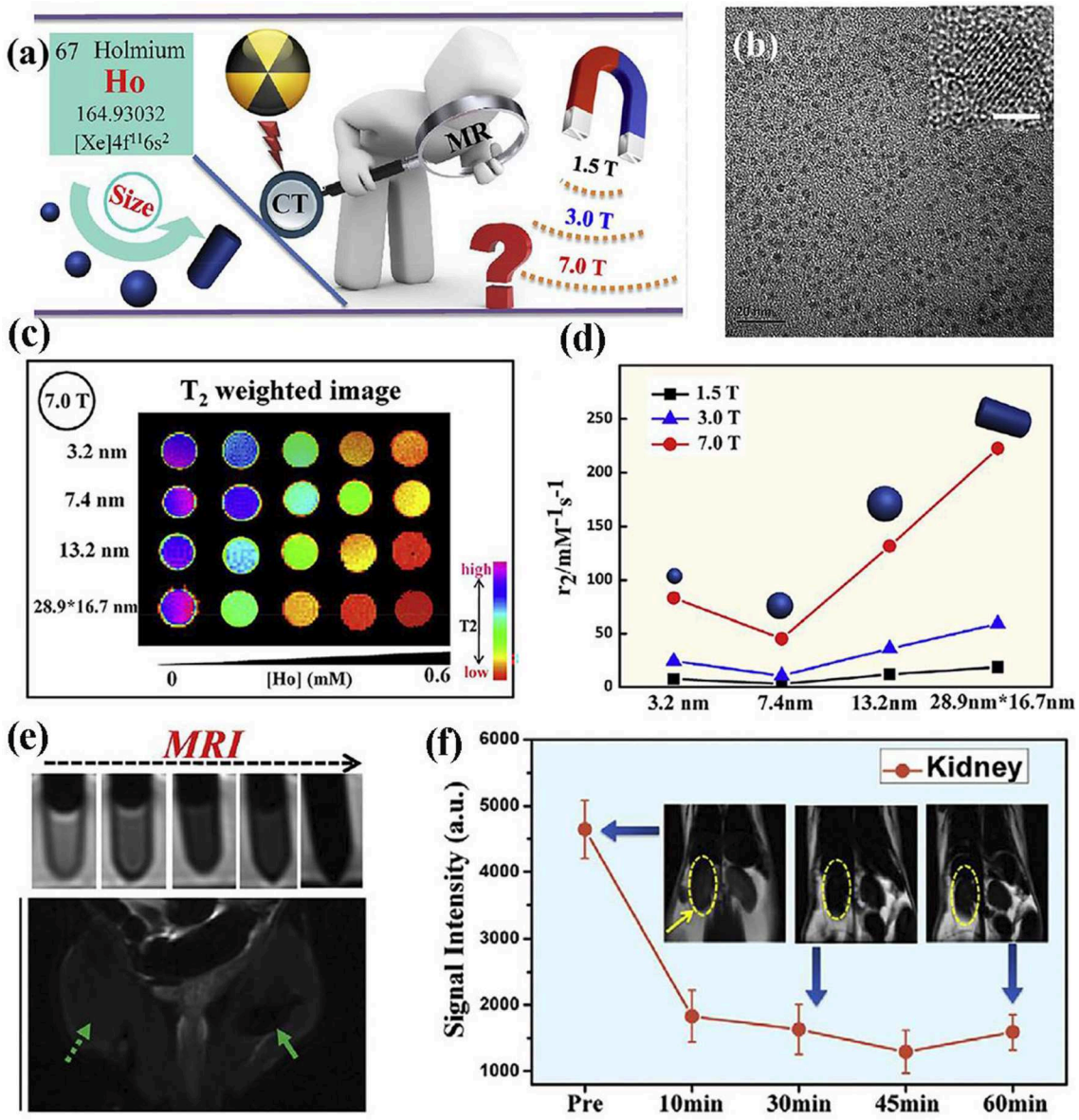

FIGURE 3 | (a) Schematic diagram of nanoparticle for high field MRI; **(b)** TEM image of nanoparticle (The scale bar of inset image is 2 nm); **(c)** nanoparticles with varied size at 7.0 T; **(d)** transverse relaxivity r_2 of nanoparticles with varied size at magnetic fields of 1.5, 3.0, and 7.0 T, respectively; **(e)** MRI of nanoparticles at different contents; **(f)** *in vivo* ultra-high-field MRI of kidney form mice after the intravenous injection of nanoparticles (Ni et al., 2016); Copyright 2016, reproduced with permission from Elsevier.

surface exposed ions (Zhou et al., 2015b; Shen et al., 2018). *In vivo* MRI performance has been performed at an ultra-high-field of 7.0 T to confirm the efficacy of dual-modal contrast agent served for liver imaging. **Figures 5B–E** show GdIOPs acting as T_1-T_2 dual-modal MRI contrast agent at an ultra-high-field of 7.0 T. MRI T_1 and T_2 images have been acquired at the targeted liver, showing both coronal and transverse plane images of liver at preinjection and each certain time postinjection. After 20 min injection, a rapid accumulation of contrast agent nanoparticles is reflected by the brighter contrast in T_1 imaging and a darker contrast in T_2 imaging results. Signal to noise ratio changes (ΔSNR) reach to the maximum value for both T_1 and T_2 images at 60 min. Subsequently, the values rapidly drop at 240 min. This demonstrates the good metabolism of nanoparticle contrast agent in liver. Consequently, this kind of nanoparticles achieved through surface and interfacial engineering demonstrates its great promising as an ultra-high-field dual-modal MRI contrast agent for accurate diagnosis (Zheng et al., 2016; Kim et al., 2017). Moreover, recent advances of the relaxivity of nanoparticle contrast agents are summarized in **Table 1**, showing the great potential for ultra-high-field MRI.

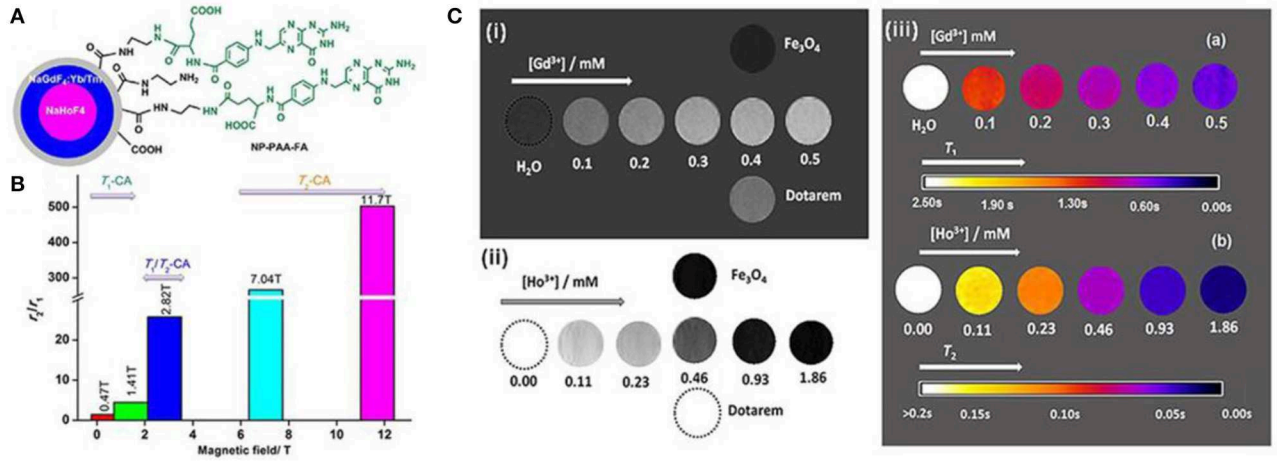

FIGURE 4 | (A) Atomic structure of prepared NP-PAA-FA; **(B)** the varied r_2/r_1 as a function of magnetic field; **(C)** (i) shows the T_1-weighted MRI; (ii) shows the T_2-weighted MRI; (iii) shows the maps of solution with NP-PAA-FA at magnetic field of 3.0 T (Biju et al., 2018); Copyright 2018, reproduced with permission from John Wiley and Sons.

BIORESPONSIVE NANO-PLATFORMS MRI-BASED MULTIMODAL MOLECULAR IMAGING

Multimodal imaging is also highly desired to provide complementary information to improve the diagnosis accuracy (Sosnovik et al., 2007; Lee et al., 2012; Li et al., 2016, 2017; Anwaier et al., 2017; Kim et al., 2017). With the emerging the ultra-high-field T_2 MRI, molecular imaging capable of performing the characterization and measurement of biological process at cellular and molecular levels is highly demonstrated *in vivo* (Shin et al., 2015; Li and Meade, 2019). To realize molecular imaging, specific contrast agent and high sensitive instrument are both required to fulfill the scans with high resolution under high magnetic field (Chen et al., 2014). A variety of MRI contrast agents have been developed till now, which are non-specific contrast agent lacking the ability to reach specific target, targeted contrast agent, smart contrast agent, and the final labeled cells, respectively (Kim et al., 2017; Chang et al., 2020).

Multimodal molecular imaging is tremendously desired in recent years because of the limited resolution and inadequate information provided by each imaging modality. To achieve the high sensitivity and quantitative analysis in clinical diagnosis, multiple imaging modalities with nanoparticle contrast agents can be integrated to make up the complementary information. For instance, MRI possesses the advantages of relative high resolution ($25 \sim 100\,\mu m$) and superior tissue penetration depth, while its sensitivity requires substantial improvement compared with the direct optical imaging technique. CT has the benefits of high resolution ($30 \sim 400\,\mu m$) and 3D visual graphing; however, the low sensitivity also becomes the obstacle for its further wide application. Near-infrared fluorescence (NIRF) imaging share the benefit of high sensitivity, while it is constricted by the low spatial resolution. Computed tomography (CT) and MRI can provide the unparalleled structural information, while CT and positron emission tomography (PET) can offer provide the insight into exploring the morphological and functional behaviors. Moreover, other combinations of multimodalities have been also attempted to resolve different upcoming issues in clinics., such as PET/MRI system into the dynamics of brain (Cho et al., 2008, 2013), MRI and CT (Ni et al., 2016), MRI and optical imaging to explore the evolution from single molecule to nanostructures (Harris et al., 2019), triple-modal imaging of NIRF/CT/MRI (Pansare et al., 2012; Hu et al., 2013; Liu et al., 2020), and dual-modality of MRI and single-photon emission computed tomography (SPECT), etc., (Dong et al., 2017; Li et al., 2019).

Figure 6A shows the schematic procedures of preparing hybrid nanoparticles. This kind of nanoparticles are used in tumor tissues to perform the diagnosis. The triple-modal NIRF/CT/MRI imaging results demonstrate the efficacy of nanoparticle contrast agent, showing the accuracy of targeting, low body residues. Interestingly, when the content is lowered to $2.1\,\mu M$, contrasted signals of NIRF/CT/MRI can be revealed by the contrast agent (**Figure 6B**). Therefore, the synergistic effect of NIRF/CT/MRI triple-modal imaging has been indicated, showing the complementary information of structural and functional imaging for tumor tissue (Hu et al., 2013). In addition, dual-modality of MRI and SPECT imaging has been endeavored to assist the detection of gene reporters to track viable cells *in vivo*. **Figures 6C,D** shows the individual MRI image and SPECT image after injecting each specific contrast agent. When MRI and SPECT are integrated for diagnosis, the combined image of dual-modality is shown in **Figure 6E**, which paves the way for further investigation of cells and gene patterns in gene expression with the multimodal molecular imaging technique (Jung et al., 2020; Song et al., 2020).

On the other hand, nanoparticle functionalization in contrast agent is playing a significant role in monitoring and revealing

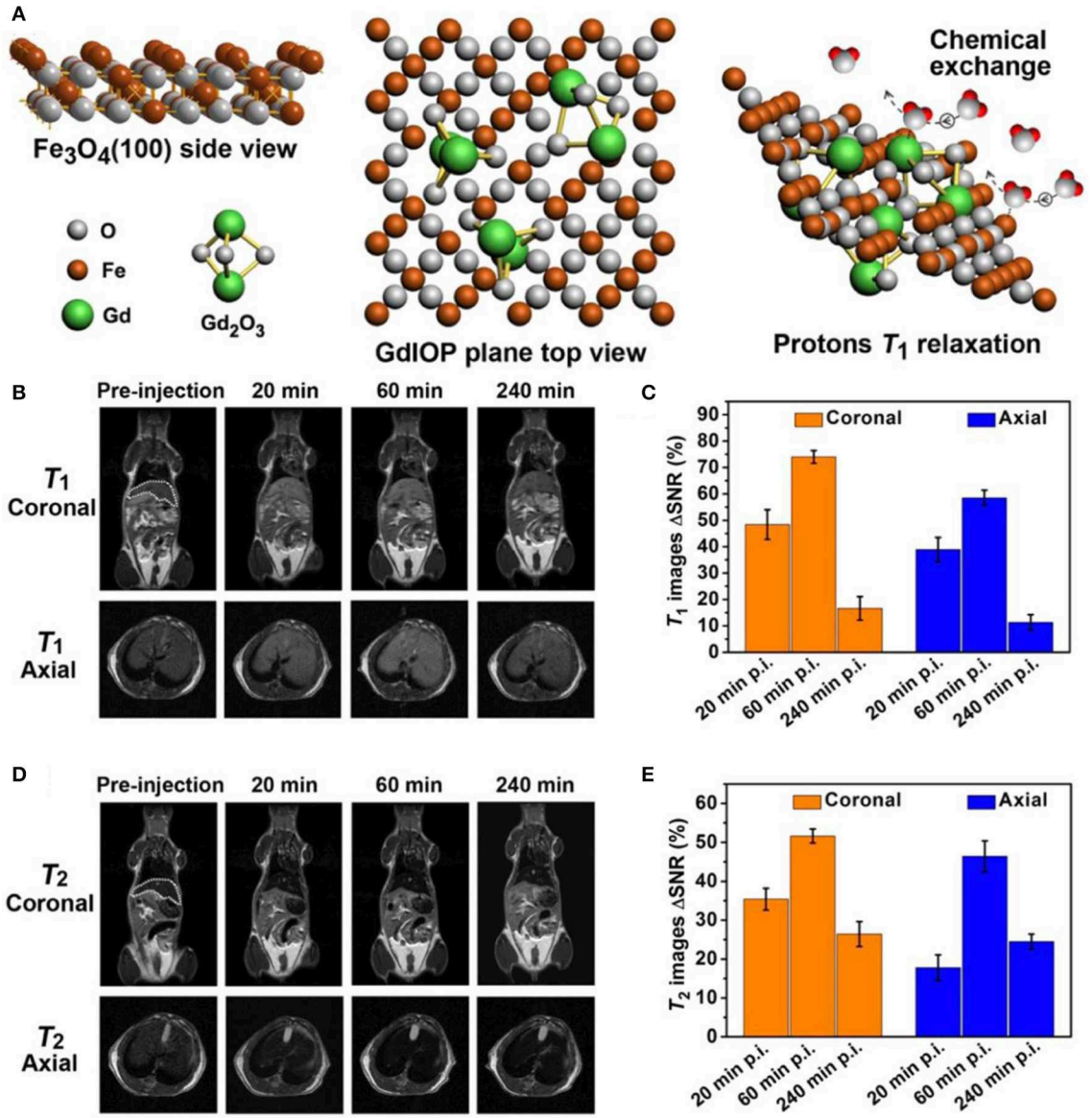

FIGURE 5 | T_1-T_2 dual-modal MRI at ultra-high-field of 7.0 T: **(A)** Atomic structure of GdIOPs, including the top view of Fe_3O_4, plane to view of GdIOP and chemical exchange in promoting protons T_1 relaxation. **(B–E)** GdIOPs acting as T_1-T_2 dual-modal MRI contrast agents (Zhou et al., 2015a); Copyright 2015, reproduced with permission from American Chemical Society.

the diagnosis information at the molecule level, which is accomplished through the combination of dual-modality or tri-modality imaging. Nanoparticle functionalization is performed via indirect or direct surface modification of nanoparticles, where folic acid, oligo nucleotides and peptides, etc., can be exploited as the surfactants (Zhou et al., 2012; Huang et al., 2015; Gao et al., 2017; Thiruppathi et al., 2017). After the functionalization of nanoparticles, these contrast agents are embraced with the advantages of good physical properties, non-invasive, well-dispersed, and homogenous, eventually to achieve the improved efficiency, and abundant modality.

Figure 7A shows the functionalized nanoparticles capable of dual-modal imaging, where strategy of linking various diagnosis molecules to nanoparticle contrast agents is illustrated through a variety of secondary linkers (Thiruppathi et al., 2017). To further verify this kind of developed strategy, magnetic nanoparticles are specifically functionalized with polymer linkers and then NIR dye for optical and magnetic resonance imaging (**Figure 7B**), demonstrating the efficacy of using functionalized nanoparticles for multi-modal imaging (Yen et al., 2013). Moreover, nanoparticles modified with two ligands demonstrate the enhanced targeting efficiency and promote the better clearing of tumor growth at large level, which are ascribed to the

TABLE 1 | Comparison of the relaxivity of bioresponsive nano-sized contrast agents for ultra-high-field MRI.

Nanoparticles	Size (nm)	Magnetic field (T)	r_1 ($mM^{-1}s^{-1}$)	r_2 ($mM^{-1}s^{-1}$)	r_2/r_1	References
DEG-Gd_2O_3	4.6	7.0	4.4	28.9	6.6	Bridot et al., 2007
PEG-Gd_2O_3	1.3	11.7	10.4	17.2	1.65	Faucher et al., 2012
$MnFe_2O_4$	7.6	9.4	18.6	227.6	12.2	Kim et al., 2009
$CoFe_2O_4$	8.0	9.4	6.3	392.5	62.3	Kim et al., 2009
PEG-$ZnFe_2O_4$	5.9	9.4	0.60	49	82	Banerjee et al., 2017
Fe_3O_4	20	7.0		679		Zhao et al., 2013
Dy_2O_3	60/70	17.6/7.0		675/190		Norek et al., 2008
Fe_3O_4 sphere	65	7.0		249		Huang et al., 2010
Fe_3O_4 brick-like	64.0	7.0	4.3	599	139	Worden et al., 2015
$NaDyF_4$ sphere	20.3	9.4		101		Das et al., 2012
PMAO-PEG/ $NaDyF_4$	25×35	9.4	0.50	204.4	410	Zhang et al., 2016
$NaHoF_4$	13.2	7.0	0.35	131.7	376	Ni et al., 2016
PMAO-PEG/$NaHoF_4$	17	9.4	0.17	130.6	768	Zhang et al., 2016
QD-CAAKA-DOTA-Dy	5.5	21.1	0.08	57.4	718	Rosenberg et al., 2010
GdIOPs	12	7.0/9.4	6.8/4.3	158.8/167.6	23.4/38.9	Zhou et al., 2015a
NP-PAA-FA	24	7.04/11.7	0.32/0.29	85/146	266/503	Biju et al., 2018

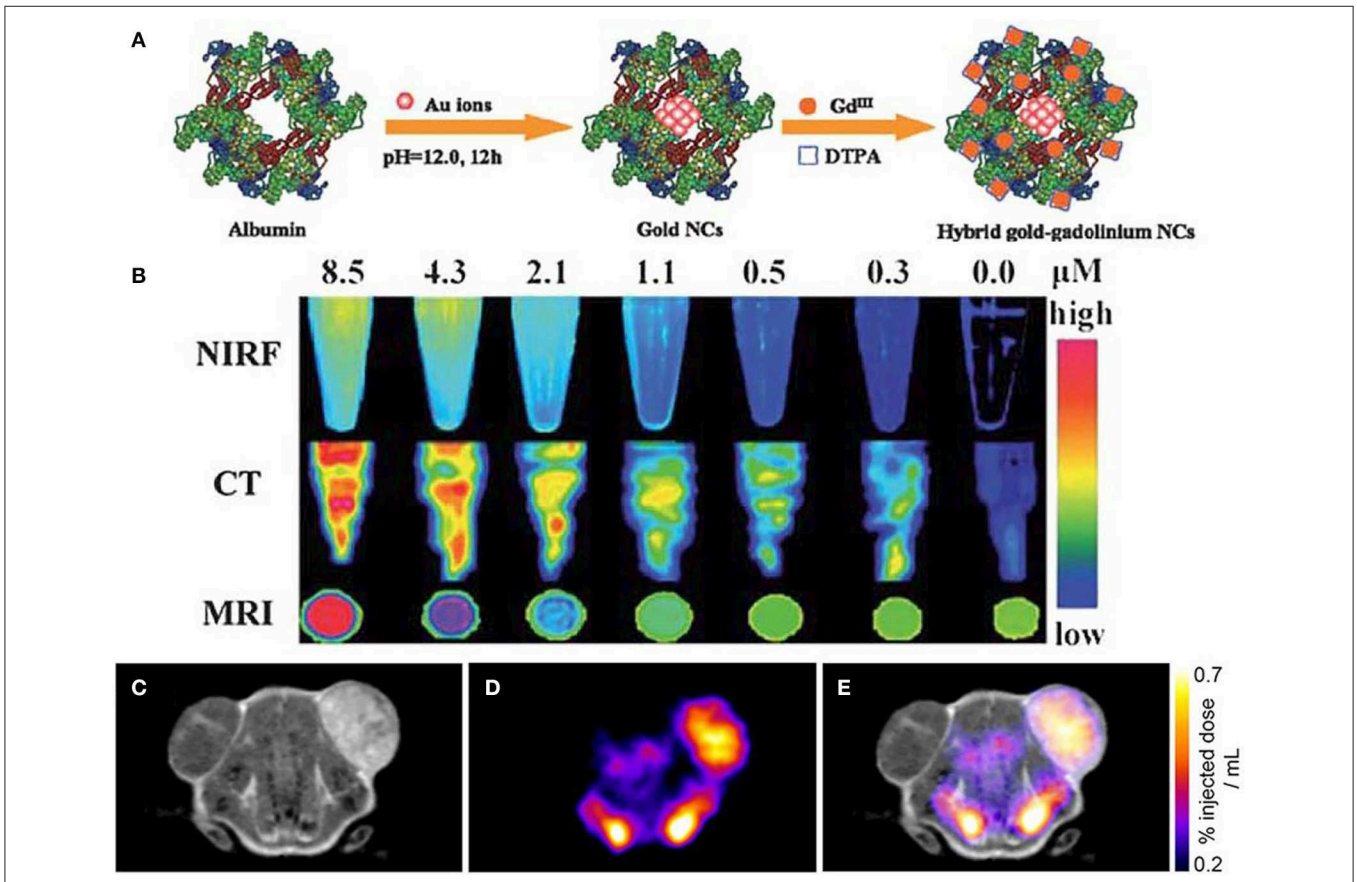

FIGURE 6 | Multimodal molecular imaging: **(A)** schematic procedures of fabricated nanoparticles; **(B)** triple-modal imaging of nanoparticles by using NIRF/CT/MRI (Hu et al., 2013); Copyright 2013, reproduced with permission from The Royal Society of Chemistry. **(C–E)** Dual-modality for *in vivo* imaging via using MRI and SPECT (Patrick et al., 2014); Copyright 2014, reproduced with permission from National Academy of Sciences.

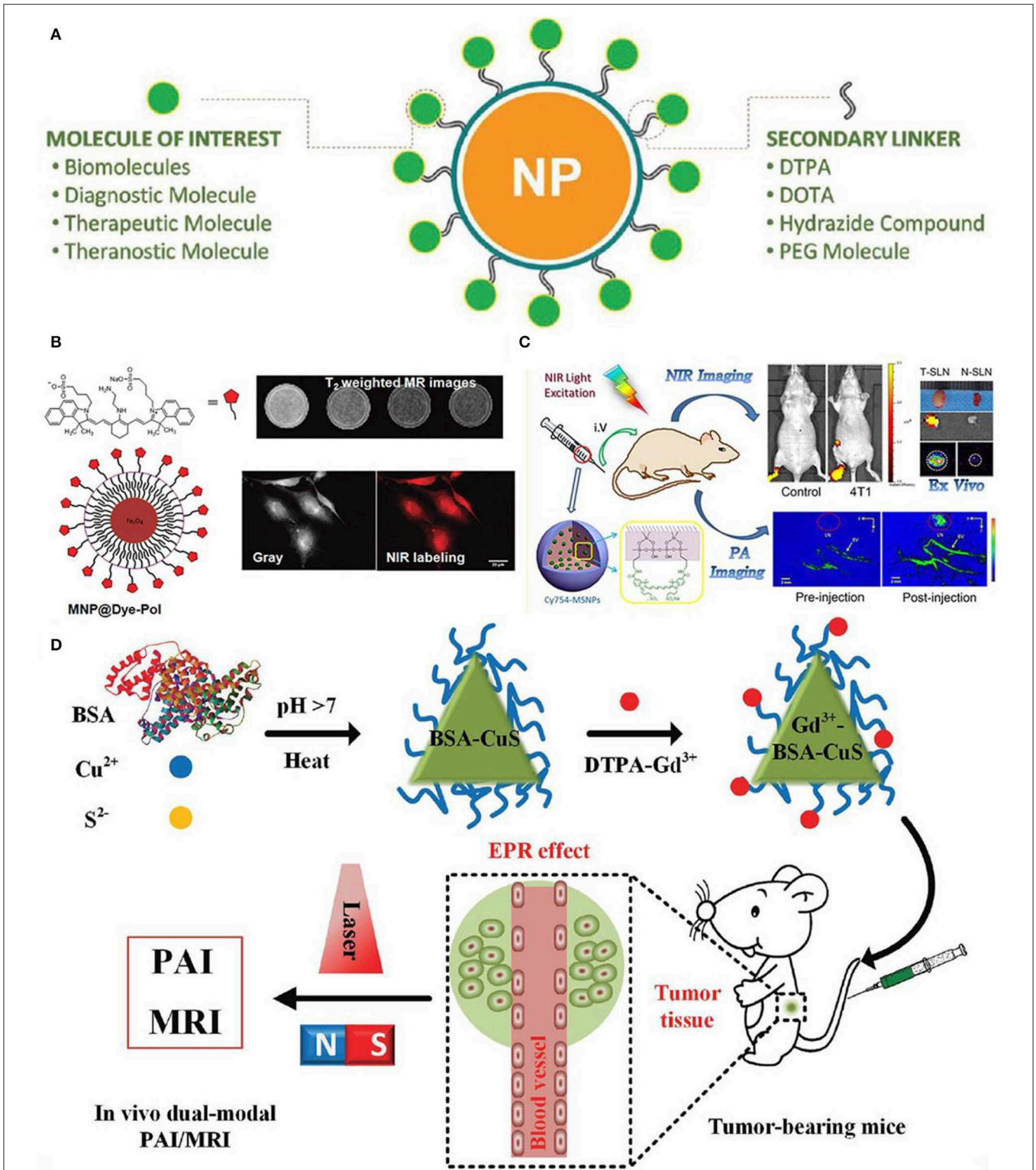

FIGURE 7 | Nanoparticle functionalization enables dual-modal imaging: **(A)** Strategy of linking various diagnosis molecules to nanoparticle agents through a variety of secondary linkers (Thiruppathi et al., 2017); Copyright 2017, reproduced with permission from John Wiley and Sons. **(B)** Magnetic nanoparticle agents functionalized with polymers used for optical and magnetic resonance dual modality imaging (Yen et al., 2013); Copyright 2013, reproduced with permission from American Chemical Society. **(C)** Mapping of sentinel lymph node by photoacoustic (PAI) and near-infrared fluorescent (NIR) (Liu et al., 2015); Copyright 2015, reproduced with permission from American Chemical Society, **(D)** *in vivo* dual-modality of tumor through both PAI and MRI (Gao et al., 2017); Copyright 2017, reproduced with permission from John Wiley and Sons.

enormously increasing uptake of functionalized nanoparticle contrast agents.

In addition, **Figure 7C** shows the mapping of sentinel lymph node by dual-modality of photoacoustic (PAI) and near-infrared fluorescent (NIR), where fluorescent dye-loaded mesoporous silica nanoparticles imaging contrast are employed to study the tumor metastasis model as well as the underlying molecular level mechanism of dual-modality imaging (Liu et al., 2015). As shown in **Figure 7C**, surface functionalized nanoparticles in conjunction with dual-modality imaging are used to visualize sentinel lymph nodes up to 2 weeks based on the tumor metastatic model. Moreover, differences of uptake rate and contrast between normal sentinel lymph nodes and metastasized sentinel lymph nodes are compared, showing the feasibility of functionalized nanoparticles in identifying tumor metastasis based on dual-modality imaging results.

Interestingly, water-soluble functionalized nanoparticle contrast agent has been showing its great significance in detecting cancer at early stage. For instance, **Figure 7D** shows the protein-modified hydrophilic copper sulfide (CuS) used as dual-modality nanoprobe, which opens a new avenue for both photoacoustic imaging and MRI in cancer diagnosis (Gao et al., 2017). This kind of functionalized nanoparticles possess the following advantages: good biocompatible and water-soluble, controllable small size with good stability, feasibly functionalized (Gao et al., 2018). *In vivo* test has been conducted in a subcutaneous tumor mouse with this functionalized nanoparticle contrast agents, showing the improved accuracy in both resolution and contrast. Therefore, with the unique properties of this protein-modified nanostructures, nanoplatform aiming for dual-modality imaging can be designed to target disease diagnosis.

Except for dual-modality imaging, the tri-modality imaging with functionalized nanoparticles has also been endeavored by researchers. Surface-enhanced Raman spectroscopy (SERS) is proposed as a sensitive and non-invasive technique, which provides precise and specific identification of signals in combination with nanoparticle contrast agents. Iterative coating approach is used to reach the rational design and synthesis of core/shell magnetic nanoflower contrast agent (Huang et al., 2015). Thus, remarkable SERS enhancement, superior PA signals, improved relaxivity, and the effective photothermal effect are achieved with this contrast agent. The combination of MRI/PA/SERS techniques has been put forward to achieve the synergistic tri-modality imaging, where MRI is responsible for the contour and localization of tumor diagnosis, PA for deep localizaiton and anatomical and SERS is for margin identification (**Figure 8A**. In addition, functional biomarker of water-soluble melanin nanoparticle is to target for melanoma imaging (**Figure 8B**). After conjugating surfactants of $\alpha_v\beta_3$ integrins and cyclic peptide to melanin nanoparticle, the U87MG tumor accumulation is observed owing to the synergistic effect of enhanced permeability and retention (Fan et al., 2014). With the combinations of different modalities of PET/MRI/PAI techniques, it is anticipated to provide guidance for localizing both superficial and deep tumor surgery. As a result, this kind of water-soluble melanin nanoparticle contrast agent after biomolecules modification shows the tremendous feasibility in multimodal imaging and can be also used as nanoplatform for potential therapeutic applications.

Therefore, through the proof-of-concept design in functionalized nanoparticle contrast agents, a general and versatile strategy can be developed to realize the multimodal imaging with functional molecular probes.

TARGETED MOLECULAR IMAGING AGENTS

Targeted molecular imaging agents in combination with imaging probe are proposed to non-invasively identify cellular processes in varied stages of disease, which generally include metabolic targeted, anti-body targeted, peptide, and activity-based probes (Zhao et al., 2012; Galluzzi et al., 2013; Chen et al., 2014; Craig et al., 2016; Dearling et al., 2016; Lee et al., 2016; Zhang et al., 2017; Mulder et al., 2018; Dammes and Peer, 2020). Peptide shows the advantages of good selectivity and specificity, which belongs to a class of ligand used for MRI (Lee et al., 2010; Craig et al., 2016). Moreover, with the surface modification of targeted molecular imaging agents, the pronounced improvement of targeting efficacy is achieved compared to that of anti-body agents, which is attributed to the controlled size of agent and its large number of ligands (Cai and Chen, 2007). To be eventually exploited as the desired targeted molecular imaging agents, a number of crucial factors need to be considered based on the agent-specific basis principle, such as the toxicity, extent of resection (EOR), the efficient and efficacy of delivery to target issue and the induced side effect. With the targeted imaging agents and probes, studies covering from imaging of breast cancer, cardiovascular disease and neurodegenerative disease has been conducted. However, much remains to be resolved before the practical *in vivo* applications, which includes the aspects of *in vivo* kinetics, efficacy, diagnostic accuracy and sensitivity, biocompatibility, chronic toxicity and the cost.

To predict and assess the metabolic alternation in tumor tissues, a non-invasive quantitative MRI approach has been exploited, where the Dixon-based MRI acts as the biomarker to predict the tumor aggressiveness before surgical intervention. **Figure 9A** shows the metabolic targeted molecular imaging agents, where tissue-based analysis has been performed with MRI quantitative parameters in anatomical coregistration. After undergoing MRI for patients, the Dixon-based MRI-derived quantitative analysis for *in vivo* fat quantification can be proceeded, showing the role of *in vivo* biomarker of metabolic targeted agents in clear cell renal carcinoma (ccRCC) (Zhang et al., 2017). To evaluate the efficacy of anti-body targeted agents, research work has been conducted to detect the colitis in a mouse model via using the imaging probe. The FIB504.64 shows a pronounced specific uptake, which is revealed by the evident observed colitis (**Figure 9B**), showing its capability as a promising disease-specific imaging agent (Dearling et al., 2016).

A variety of peptide receptors capable of targeting tumor tissues are reported in molecular biology, such as $\alpha_v\beta_3$, glucagon-like peptide-1, somatostatin and gastrin-releasing peptide. The

strategy of integrating multiple ligands into tumor tissues has been adopted to harvest more potential binding sites and *in vivo* ultrasound intensity. For instance, hyaluronic acid ceramide folic acid nanoparticles (HACE-FA NPs) are reported to target both CD44 and folate receptor (FR) (**Figure 9C**), showing their synergistic effect to increase affinity of agents to receptors (Lee et al., 2016; Ko et al., 2019). Moreover, to achieve the specific diseased sites imaging, monoclonal antibodies are prevalently used owing to their merits of specificity, affinity and serum stability.

Given the significance of β-glycosidases in human body, a set of β-glycosidase-specific activity-based probes (ABPs) are specifically studied to detect enzymatic activity over a range of glycosidases, demonstrating its role of tracking pathological relevant enzymes and its great potential in discovering the structural and biochemical

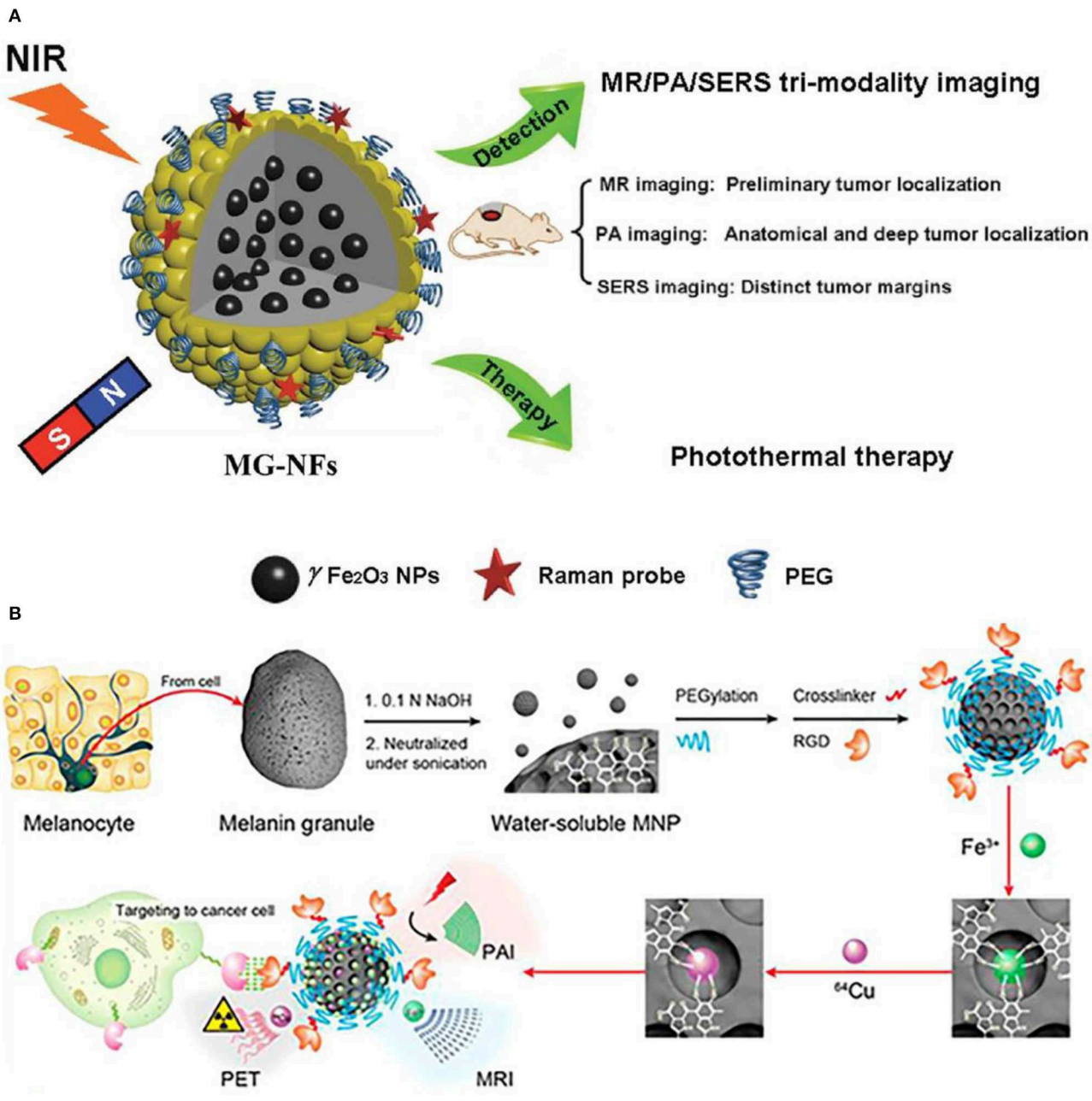

FIGURE 8 | Nanoparticle functionalization enables tri-modality imaging: **(A)** Schematic illustration of surface-enhanced magnetic resonance (MR)/Raman spectroscopy (SERS)/photoacoustic (PA) (MR/SERS/PA) tri-modality imaging of tumor (Huang et al., 2015); Copyright 2015, reproduced with permission from John Wiley and Sons. **(B)** PET/MRI/PAI tri-modality nanoplatform (Fan et al., 2014); Copyright 2014, reproduced with permission from American Chemical Society.

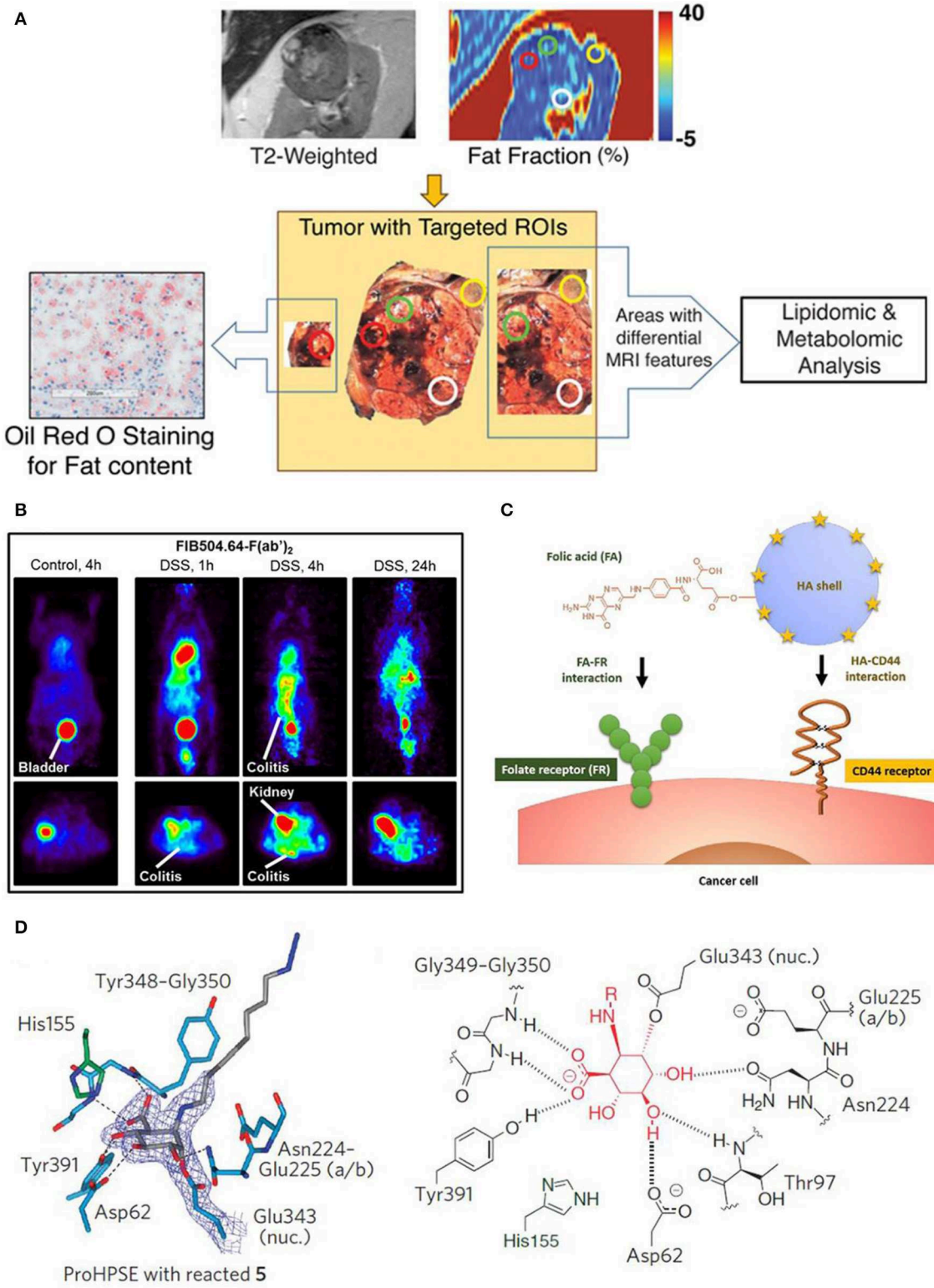

FIGURE 9 | Targeted molecular imaging agents: **(A)** Metabolic targeted agents to proceed the tissue-based analysis with MRI quantitative parameters in anatomical coregistration (Zhang et al., 2017); Copyright 2017, reproduced with permission from Clinical Medicine. **(B)** Anti-body targeted agents (Dearling et al., 2016); Copyright 2016, reproduced with permission from Crohn's & Colitis Foundation of America. **(C)** Schematic diagram of peptide targeted HACE-FA NPs to tumor tissues (Lee et al., 2016); Copyright 2016, reproduced with permission from Elsevier. **(D)** Activity based targeted agents (Zhao et al., 2012); Copyright 2017, reproduced with permission from Nature Chemical Biology.

functionality (Wu et al., 2017). **Figure 7D** shows the active site interaction with ABPs, where hydrogen bonding interactions identical to that of mature enzyme are illustrated in **Figure 9D**. Therefore, this activity based targeted agent offers a powerful tool in characterizing enzyme activities.

Upon further improvement of target molecular imaging agents for ultra-high-field MRI, specific molecular therapy with tremendously enhanced accuracy and sensitivity will profoundly impact future clinical diagnosis.

THE ROLE OF ARTIFICIAL INTELLIGENCE FOR DEVELOPING NOVEL/BIORESPONSIVE NANO AGENTS FOR MRI

One of the innovative clinical applications of AI lies in medical imaging, which includes the following aspects: image acquisition, removing the unwanted artifacts, improving the image quality, reducing the contrast agent dose, and shortening the diagnose period (Gong et al., 2018; Shan et al., 2018; Zaharchuk et al., 2018; Codari et al., 2019; Zhu et al., 2019).

For biomedical imaging, the image reconstruction can be improved by exploiting machine learning or deep learning of AI, where powerful graphical processing units and neural networks formed in computer will assist the reconstruction processing (Gong et al., 2018; Shan et al., 2018; Zaharchuk et al., 2018). Alternatively, after accessing to large amount of information, the deep learning of AI will be processed and form an algorithm based on these inputs. **Figure 10** shows the whole process of biological neural network, where receptor receives a cat as inputting information, after learning process, cat has been reconstructed at the effector side. Moreover, convolutional neural network is another type of learning method of AI, where the algorithm will be configurated to proceed further analysis based on the previous inputs (Bernal et al., 2019). Therefore, deep

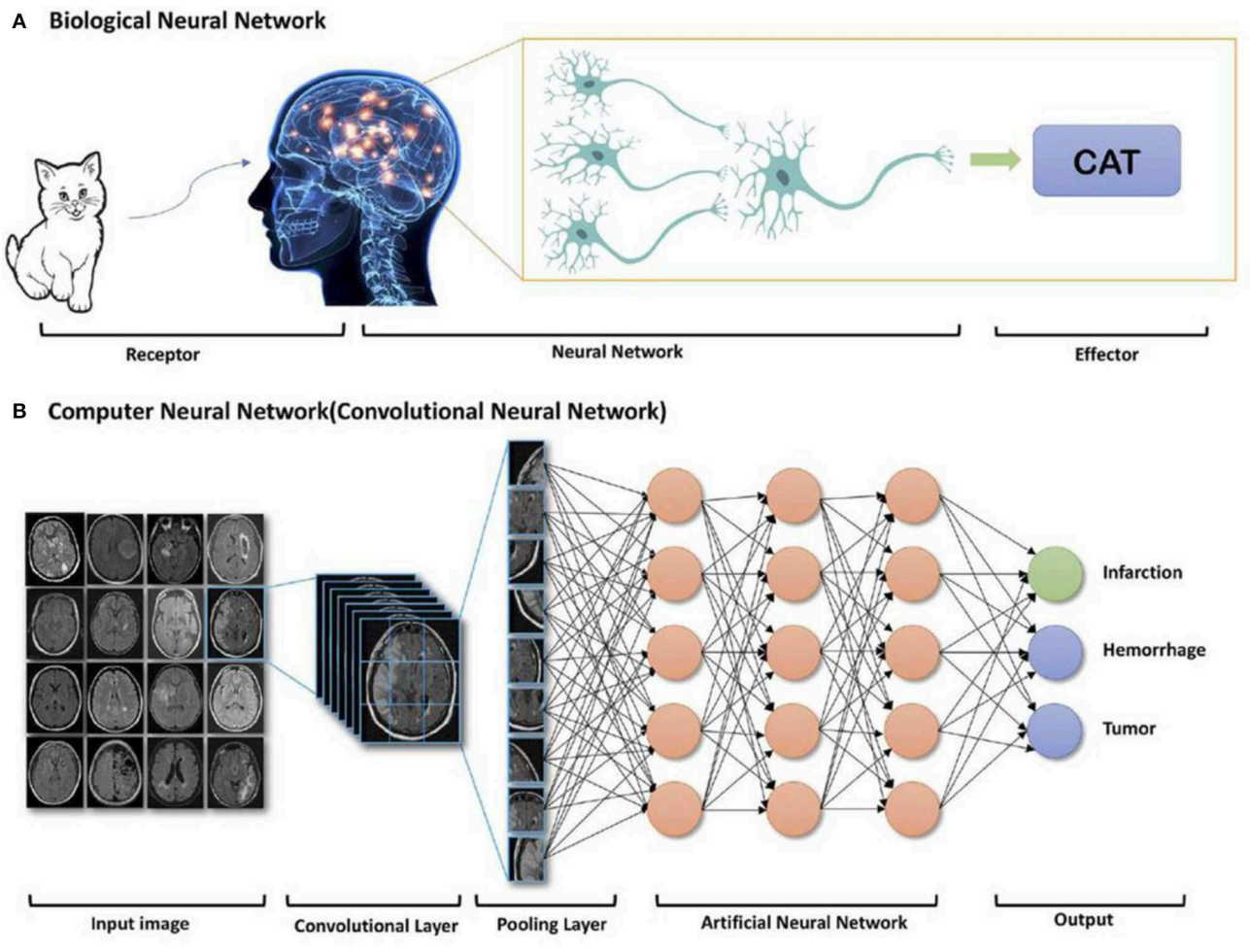

FIGURE 10 | AI deep learning example: components of **(A)** biological neural network and **(B)** computer neural network (Zaharchuk et al., 2018); Copyright 2018, reproduced with permission from American Journal of Neuroradiology.

learning of AI can assist MRI scans to acquire images with enhanced quality.

To maintain the diagnostic quality, it is also aimed to reduce the MRI contrast agent dose. As heavy metal gadolinium is indispensably used as MRI contrast agent and can remain in human body after scans, researchers are trying to improve the safety of patients after keeping the achieved scan information. Therefore, deep machine learning of AI can be implemented based on designed experiments, that is contrast agent experiment of less dose by comparing with that of no dose and full dose (Gong et al., 2018). For instance, Gong et al. performed an attempt on contrast enhanced MRI with low dose of contrast agent through deep learning of AI (**Figure 11**). By employing the non-contrast MRI and low-contrast MRI as inputs for deep learning, simulated model/algorithm will be predicted based on the obtained signal difference between non-contrast MRI and low-contrast MRI (Raval et al., 2017). Subsequently, this algorithm will be used to synthesize a full does contrast enhanced MRI to verify the formerly set-up full dose MRI. These results indicate that much useful clinical information can be obtained through using the enormously reduced dose of contrast agent based on the deep learning of AI.

On the other hand, the shortened diagnosis time is enormously expected in high field MRI with the aid of AI. To obtain a high or super-resolution MRI, ultra-high magnetic field (over 7 T) is generally required to perform the scan with contrast agent, which will inevitably induce high cost of equipment purchase and high operational cost of long-tern scanning, and the unexpected unsafety issue owing to the high magnetic field. Until now, many attempts have been devoted to exploiting machine learning of AI to replace the high field scan process, where high resolution MRI can be obtained through AI deep learning of low-resolution MRI (Shen et al., 2017a; Mahmud et al., 2018; Wegmayr et al., 2018; Mostapha and Styner, 2019; Nalepa et al., 2020). For instance, Chaudhari et al. developed a super-resolution approach to generate MRI information of thin-slice knee from thicker ones through the configurated convolutional neural networks of AI deep learning (**Figure 12**) (Chaudhari et al., 2018). Furthermore, Lyu et al. adapted two latest neural network models to realize super-resolution MRI, showing a 2-fold enhancements of resolution in MRI (Lyu et al., 2018). Therefore, with the emerging of AI, it is promising to achieve high resolution MRI without the expensive high field instrument and long-term scanning.

PROSPECTS AND CHALLENGES

With the aim of developing contrast agents with good compatibility, biodegradability, high relaxivity for MRI and ultra-high-field MRI, continuous efforts have been devoted to exploring and searching for better contrast agents for MRI. To improve the imaging sensitivity of nanoparticle contrast agents, geometry of size, surface, shape of nanoparticles can be designed, and tuned via surface modification approaches, or other

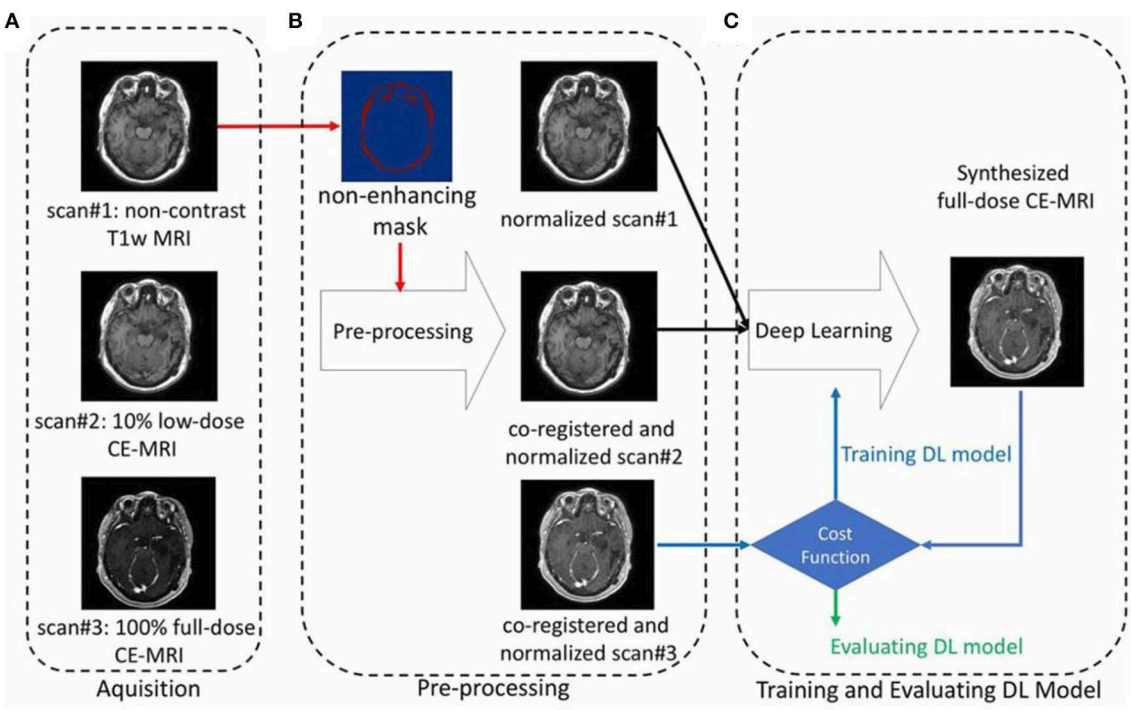

FIGURE 11 | An example showing the contrast enhanced MRI via using the reduced dose of contrast agent through deep learning of AI, including the processes of **(A)** aquisition, **(B)** pre-processing, and **(C)** training and evaluating (Gong et al., 2018); Copyright 2018, reproduced permission from International Society for Magnetic Resonance in Medicine.

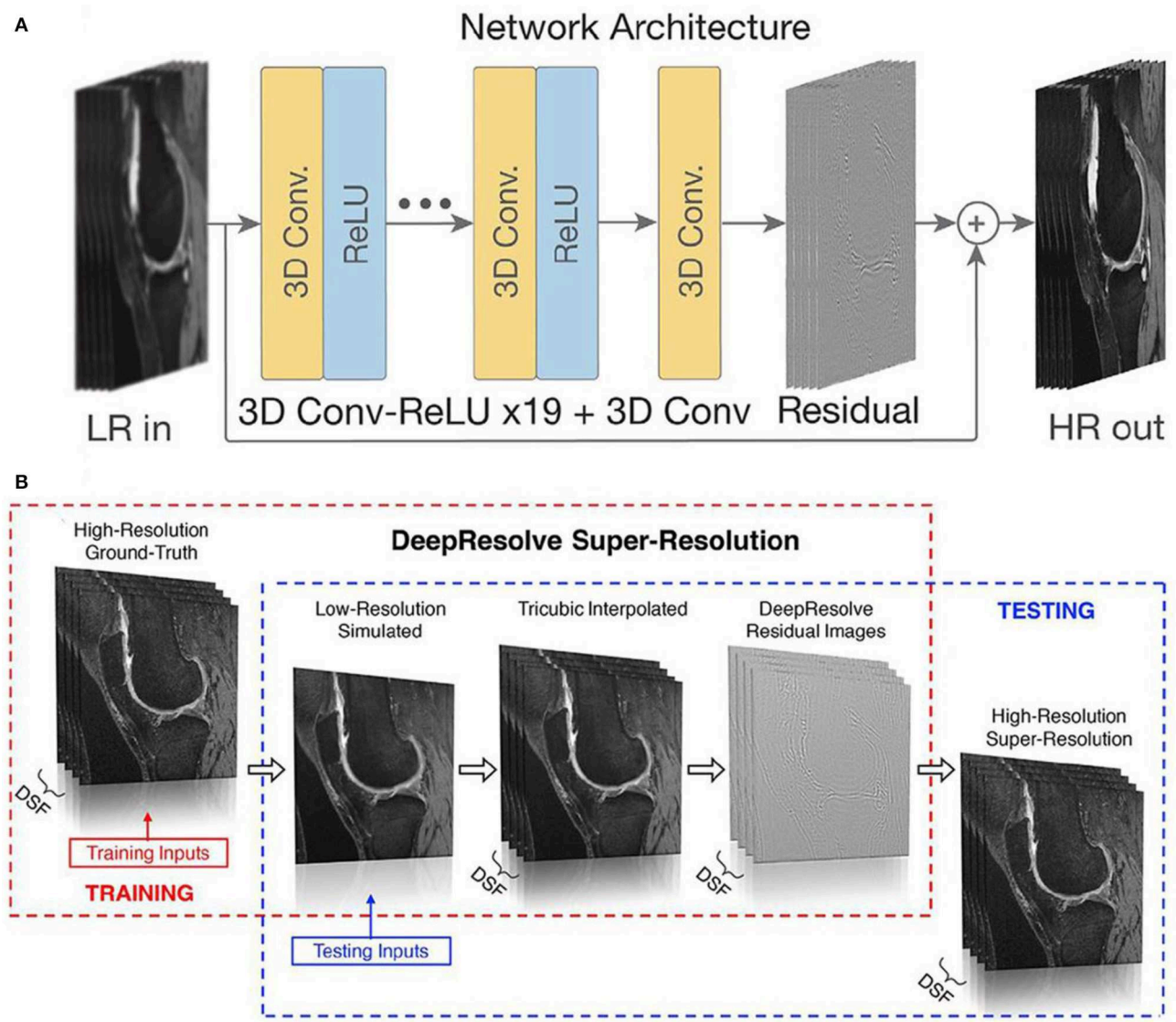

FIGURE 12 | (A) An input low-resolution (LR) image computes a high-resolution (HR) image through the deep learning of network; **(B)** schematic diagram of producing high-resolution/super resolution slices (Chaudhari et al., 2018). DSF represents the downsampling factor, where illustrates the ratio between the thickness of ground-truth slice thickness and the downsampled low-resolution slice thickness. Copyright 2018, reproduced with permission from International Society for Magnetic Resonance in Medicine.

techniques (Zhou et al., 2019). Cutting-edge interdisciplinary subjects of chemistry, physical, biological, and engineering shall also be included to resolve the current limitations of developing nanoparticle contrast agents. After implementing the rational design and surface modification of nanoparticles, this will inevitably promote MRI capable of molecular imaging for better monitoring during biological process (Zhu and Moser, 2017; Basal and Allen, 2018). For instance, **Figure 13** shows a representative example about the functionalized nanoparticle contrast agents ranging from the initial design to the final multimodal imaging applications, where doping technique has been adopted to functionalize a variety of nanoparticles with the employed various surfactants, such as poly(allylamine hydrochloride) (PAH), polyacrylic acid, and polyethylene glycol (PEG). Meanwhile, nanoparticle contrast agents are not just limited to Fe^{2+}, Fe^{3+}, Mn^{2+} based nanoparticles (Zhu et al., 2015). Other bioresponsive nano-sized contrast agents used for high field magnetic resonance imaging can also be employed for the surface functionalization, eventually to act as the molecular probes for multimodal imaging of photoacoustic (PA) imaging and MRI imaging, etc. (He et al., 2018). Consequently, wide applications of high field MRI, multimodal imaging, and theragnostic technique into MRI will be also promoted by the synergistic effect of both molecular probes and a variety of imaging techniques.

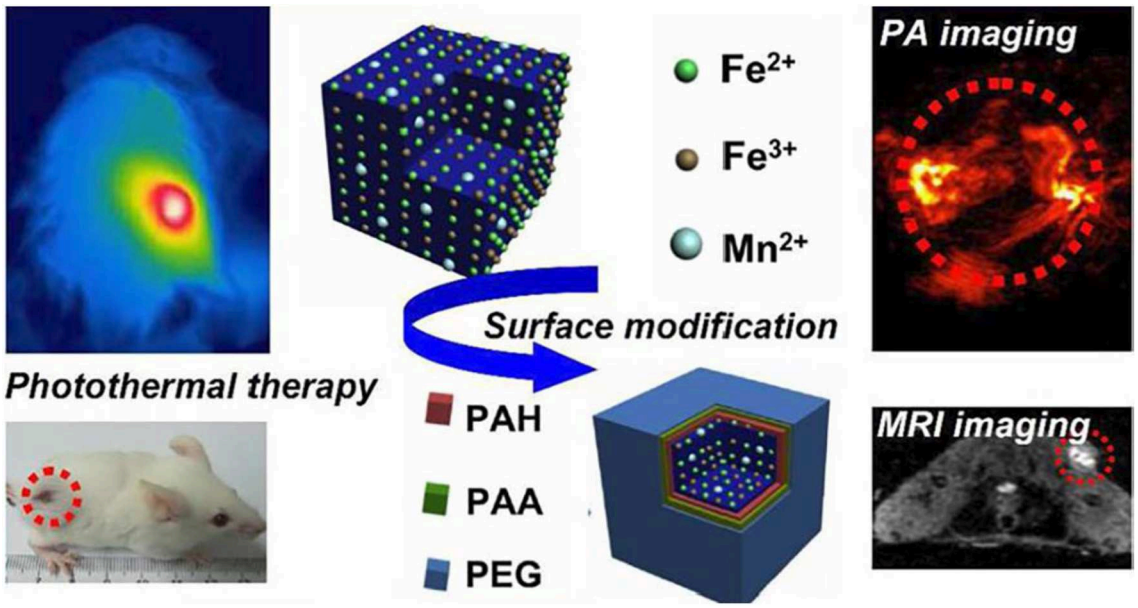

FIGURE 13 | Multimodal probes: from design to biology applications (Zhu et al., 2015); Copyright 2015, reproduced with permission from American Chemical Society.

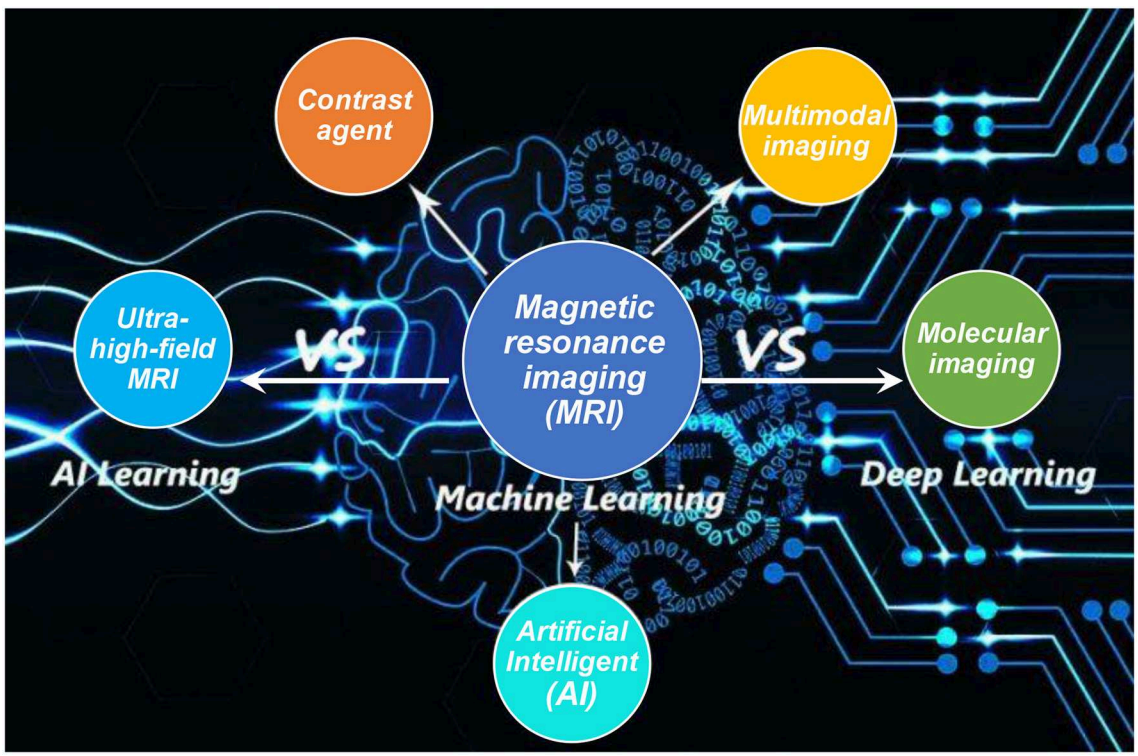

FIGURE 14 | MRI and AI to varies of imaging development.

In addition, based on the design principles of nanoparticle contrast agents, crucial aspects in terms of easy-processable and low cost are considered to meet the large-scale demands, which can be resolved with the assistance of AI technology. As the fabrications of nanoparticle contrast agents focus on optimizing a variety of parameters, with the emerging of AI, the algorithm based on the deep learning will complete all these tasks prior to perform the final optimized experiments

for verification, which will save substantial time, efforts and achieve the high resolution MRI (Moser et al., 2017; Raval et al., 2017). Furthermore, for future MRI, it is suggested to employ the convolutional neural networks in AI deep learning to get the multimodal imaging information with high resolution (**Figure 14**), where the conventional MRI can only achieve single information with the applied high magnetic field (over 7 T) (Donatelli et al., 2018; Henning, 2018; Turing, 2019).

Molecular imaging enables the quantitative characterization and measurement of biological diagnosis at the cellular and molecular level, which will inevitably advance the modern and future medical imaging and diagnosis (Wu and Shu, 2018; Li and Meade, 2019). However, the current critical issue lies in developing novel and appropriate contrast agents to meet the biological compatibility for different species (Basal et al., 2017). MRI with nanoparticle contrast agent offers one desired solution to realize molecular imaging. However, the poor sensitivity of MRI limits its wide application in clinics. Efforts can be made toward integrating the varied modalities/strengths of different instruments to avoid the problems existed in an individual instrument. Alternatively, interdisciplinary cooperation among different subjects should be strengthened to resolve the limited resolution of imaging, because molecular imaging requires the joint research of radiology, materials science and ultrasonic medicine.

To sum it up, multimodal molecular imaging agents and specific targeted molecular imaging agent will be both expected in the molecular imaging in future clinic application. With the aid of AI, a major breakthrough can be expected in multimodal molecular imaging for molecular biology clinics, despite molecular imaging combined with AI learning is still at the initial stage.

AUTHOR CONTRIBUTIONS

The author confirms being the sole contributor of this work and has approved it for publication.

FUNDING

The research was supported by the Start-up funds for outstanding talents in Central South University through project 202 045007.

REFERENCES

Anwaier, G., Chen, C., Cao, Y., and Qi, R. (2017). A review of molecular imaging of atherosclerosis and the potential application of dendrimer in imaging of plaque. *Int. J. Nanomed.* 12, 7681–7693. doi: 10.2147/IJN.S142385

Banerjee, A., Blasiak, B., Pasquier, E., Tomanek, B., and Trudel, S. (2017). Synthesis, characterization, and evaluation of PEGylated first-row transition metal ferrite nanoparticles as T2 contrast agents for high-field MRI. *RSC Adv.* 7, 38125–38134. doi: 10.1039/C7RA05495E

Bao, Y., Sherwood, J. A., and Sun, Z. (2018). Magnetic iron oxide nanoparticles as T1 contrast agents for magnetic resonance imaging. *J. Mater. Chem. C* 6, 1280–1290. doi: 10.1039/C7TC05854C

Basal, L. A., and Allen, M. J. (2018). Synthesis, characterization, and handling of Eu(II)-containing complexes for molecular imaging applications. *Front. Chem.* 6:65. doi: 10.3389/fchem.2018.00065

Basal, L. A., Yan, Y., Shen, Y., Haacke, E. M., Mehrmohammadi, M., and Allen, M. J. (2017). Oxidation-responsive, Eu(II/III)-based, multimodal contrast agent for magnetic resonance and photoacoustic imaging. *ACS Omega* 2, 800–805. doi: 10.1021/acsomega.6b00514

Bernal, J., Kushibar, K., Asfaw, D. S., Valverde, S., Oliver, A., Marti, R., et al. (2019). Deep convolutional neural networks for brain image analysis on magnetic resonance imaging: a review. *Artif. Intell. Med.* 95, 64–81. doi: 10.1016/j.artmed.2018.08.008

Biju, S., Gallo, J., Banobre-Lopez, M., Manshian, B. B., Soenen, S. J., Himmelreich, U., et al. (2018). A magnetic chameleon: biocompatible lanthanide fluoride nanoparticles with magnetic field dependent tunable contrast properties as a versatile contrast agent for low to ultrahigh field MRI and optical imaging in biological window. *Chemistry Eur. J.* 24, 7388–7397. doi: 10.1002/chem.201800283

Bobo, D., Robinson, K. J., Islam, J., Thurecht, K. J., and Corrie, S. R. (2016). Nanoparticle-based medicines: a review of FDA-approved materials and clinical trials to date. *Pharm. Res.* 33, 2373–2387. doi: 10.1007/s11095-016-1958-5

Botar, R., Molnar, E., Trencsenyi, G., Kiss, J., Kalman, F. K., and Tircso, G. (2020). Stable and inert Mn(II)-based and pH-responsive contrast agents. *J. Am. Chem. Soc.* 142, 1662–1666. doi: 10.1021/jacs.9b09407

Bridot, J. L., Laurent, A.C., Rivieire, C., Billotey, C., Hiba, B., Janier, M., et al. (2007). Hybrid gadolinium oxide nanoparticles: multimodal contrast agents for *in vivo* imaging. *J. Am. Chem. Soc.* 129, 5076–5084. doi: 10.1021/ja068356j

Busch, H. V. (2019). Artifical intelligence for MRI. *Product News-Magnetom Flash* 74, 94–97. Available online at: https://www.siemens-healthineers.com/en-au/magnetic-resonance-imaging/news/artificial-intelligence-for-mri.html

Busquets, M. A., Estelrich, J., and Sánchez-Martín, M. J. (2015). Nanoparticles in magnetic resonance imaging: from simple to dual contrast agents. *Int. J. Nanomed.* 10, 1727–1741. doi: 10.2147/IJN.S76501

Cai, W., and Chen, X. (2007). Nanoplatforms for targeted molecular imaging in living subjects. *Small* 3, 1840–1854. doi: 10.1002/smll.200700351

Chang, C., Raven, E. P., and Duyn, J. H. (2016). Brain-heart interactions: challenges and opportunities with functional magnetic resonance imaging at ultra-high field. *Philos. Trans. A Math. Phys. Eng. Sci.* 374:20150188. doi: 10.1098/rsta.2015.0188

Chang, X., Zhang, M., Wang, C., Zhang, J., Wu, H., and Yang, S. (2020). Graphene oxide/BaHoF5/PEG nanocomposite for dual-modal imaging and heat shock protein inhibitor-sensitized tumor photothermal therapy. *Carbon* 158, 372–385. doi: 10.1016/j.carbon.2019.10.105

Chaudhari, A. S., Fang, Z., Kogan, F., Wood, J., Stevens, K. J., Gibbons, E. K., et al. (2018). Super-resolution musculoskeletal MRI using deep learning. *Magn. Reson. Med.* 80, 2139–2154. doi: 10.1002/mrm.27178

Chen, G., Roy, I., Yang, C., and Prasad, P. N. (2016). Nanochemistry and nanomedicine for nanoparticle-based diagnostics and therapy. *Chem. Rev.* 116, 2826–2885. doi: 10.1021/acs.chemrev.5b00148

Chen, Z. Y., Wang, Y. X., Lin, Y., Zhang, J. S., Yang, F., Zhou, Q. L., et al. (2014). Advance of molecular imaging technology and targeted imaging agent in imaging and therapy. *Biomed. Res. Int.* 2014:819324. doi: 10.1155/2014/819324

Cho, Z. H., Son, Y. D., Choi, E. J., Kim, H. K., Kim, J. H., Lee, S. Y., et al. (2013). *In-vivo* human brain molecular imaging with a brain-dedicated PET/MRI system. *Magn. Reson. Mater. Phy.* 26, 71–79. doi: 10.1007/s10334-012-0329-4

Cho, Z. H., Son, Y. D., Kim, H. K., Kim, K. N., Oh, S. H., Han, J. Y., et al. (2008). A fusion PET-MRI system with a high-resolution research tomograph-PET and ultra-high field 7.0 T-MRI for the molecular-genetic imaging of the brain. *Proteomics* 8, 1302–1323. doi: 10.1002/pmic.200700744

Clough, T. J., Jiang, L., Wong, K. L., and Long, N. J. (2019). Ligand design strategies to increase stability of gadolinium-based magnetic resonance imaging contrast agents. *Nat. Commun.* 10:1420. doi: 10.1038/s41467-019-09342-3

Codari, M., Schiaffino, S., Sardanelli, F., and Trimboli, R. M. (2019). Artificial intelligence for breast MRI in 2008-2018: a systematic mapping review. *AJR Am. J. Roentgenol.* 212, 280–292. doi: 10.2214/AJR.18.20389

Craig, S. E. L., Wright, J., Sloan, A. E., and Brady-Kalnay, S. M. (2016). Fluorescent-guided surgical resection of glioma with targeted molecular imaging agents: a literature review. *World Neurosurg.* 90, 154–163. doi: 10.1016/j.wneu.2016.02.060

Csajbok, E., Banyai, I., Vander Elst, L., Muller, R. N., Zhou, W., and Peters, J. A. (2005). Gadolinium(III)-loaded nanoparticulate zeolites as potential high-field MRI contrast agents: relationship between structure and relaxivity. *Chemistry* 11, 4799–4807. doi: 10.1002/chem.200500039

Dammes, N., and Peer, D. (2020). Monoclonal antibody-based molecular imaging strategies and theranostic opportunities. *Theranostics* 10, 938–955. doi: 10.7150/thno.37443

Das, G. K., Johnson, N. J., Cramen, J., Blasiak, B., Latta, P., Tomanek, B., et al. (2012). $NaDyF_4$ nanoparticles as T_2 contrast agents for ultrahigh field magnetic resonance imaging. *J. Phys. Chem. Lett.* 3, 524–529. doi: 10.1021/jz201664h

Das, G. K., Zhang, Y., D'silva, L., Padmanabhan, P., Heng, B. C., Chye Loo, J. S., et al. (2011). Single-phase Dy_2O_3: Tb^{3+}nanocrystals as dual-modal contrast agent for high field magnetic resonance and optical imaging. *Chem. Mater.* 23, 2439–2446. doi: 10.1021/cm2003066

de Martino, F., Yacoub, E., Kemper, V., Moerel, M., Uludag, K., de Weerd, P., et al. (2018). The impact of ultra-high field MRI on cognitive and computational neuroimaging. *Neuroimage* 168, 366–382. doi: 10.1016/j.neuroimage.2017.03.060

Dearling, J. L., Daka, A., Veiga, N., Peer, D., and Packard, A. B. (2016). Colitis immunoPET: defining target cell populations and optimizing pharmacokinetics. *Inflamm. Bowel Dis.* 22, 529–538. doi: 10.1097/MIB.0000000000000677

Donatelli, G., Ceravolo, R., Frosini, D., Tosetti, M., Bonuccelli, U., and Cosottini, M. (2018). Present and future of ultra-high field MRI in neurodegenerative disorders. *Curr. Neurol. Neurosci. Rep.* 18:31. doi: 10.1007/s11910-018-0841-7

Dong, L., Zhang, P., Lei, P., Song, S., Xu, X., Du, K., et al. (2017). PEGylated GdF_3:Fe nanoparticles as multimodal T_1/T_2-weighted MRI and X-ray CT imaging contrast agents. *ACS Appl. Mater. Interfaces* 9, 20426–20434. doi: 10.1021/acsami.7b04438

Duyn, J. H. (2012). The future of ultra-high field MRI and fMRI for study of the human brain. *Neuroimage* 62, 1241–1248. doi: 10.1016/j.neuroimage.2011.10.065

Dyke, K., Pepes, S. E., Chen, C., Kim, S., Sigurdsson, H. P., Draper, A., et al. (2017). Comparing GABA-dependent physiological measures of inhibition with proton magnetic resonance spectroscopy measurement of GABA using ultra-high-field MRI. *Neuroimage* 152, 360–370. doi: 10.1016/j.neuroimage.2017.03.011

Fan, Q., Cheng, K., Hu, X., Ma, X., Zhang, R., Yang, M., et al. (2014). Transferring biomarker into molecular probe: melanin nanoparticle as a naturally active platform for multimodality imaging. *J. Am. Chem. Soc.* 136, 15185–15194 doi: 10.1021/ja505412p

Faucher, L., Tremblay, M., Lagueux, J., Gossuin, Y., and Fortin, M. A. (2012). Rapid synthesis of PEGylated ultrasmall gadolinium oxide nanoparticles for cell labeling and tracking with MRI. *ACS Appl. Mater. Interfaces* 4, 4506–4515. doi: 10.1021/am3006466

Galluzzi, L., Kepp, O., Vander Heiden, M. G., and Kroemer, G. (2013). Metabolic targets for cancer therapy. *Nat. Rev. Drug Discov.* 12, 829–846. doi: 10.1038/nrd4145

Gao, D., Sheng, Z., Liu, Y., Hu, D., Zhang, J., Zhang, X., et al. (2017). Protein-modified CuS nanotriangles: a potential multimodal nanoplatform for *in vivo* tumor photoacoustic/magnetic resonance dual-modal imaging. *Adv. Healthc Mater.* 6:1601094. doi: 10.1002/adhm.201601094

Gao, D., Zhang, P., Liu, Y., Sheng, Z., Chen, H., and Yuan, Z. (2018). Protein-modified conjugated polymer nanoparticles with strong near-infrared absorption: a novel nanoplatform to design multifunctional nanoprobes for dual-modal photoacoustic and fluorescence imaging. *Nanoscale* 10, 19742–19748 doi: 10.1039/C8NR06197A

Gautam, A., Komal, P., and Singh, R. S. (2019). Future demands for high field MRI diagnostic. *J. Chem. Sci.* 131:89. doi: 10.1007/s12039-019-1668-8

Gong, E., Pauly, J. M., Wintermark, M., and Zaharchuk, G. (2018). Deep learning enables reduced gadolinium dose for contrast-enhanced brain MRI. *J. Magn. Reson. Imaging* 48, 330–340. doi: 10.1002/jmri.25970

Guo, S., Xiao, X., Wang, X., Luo, Q., Zhu, H., Zhang, H., et al. (2019). Reductive microenvironment responsive gadolinium-based polymers as potential safe MRI contrast agents. *Biomater. Sci.* 7, 1919–1932. doi: 10.1039/C8BM01103F

Hai, Z., Ni, Y., Saimi, D., Yang, H., Tong, H., Zhong, K., et al. (2019). γ-lutamyltranspeptidase-triggered intracellular gadolinium nanoparticle formation enhances the T_2-weighted MR contrast of tumor. *Nano Lett.* 19, 2428–2433. doi: 10.1021/acs.nanolett.8b05154

Hametner, S., Dal Bianco, A., Trattnig, S., and Lassmann, H. (2018). Iron related changes in MS lesions and their validity to characterize MS lesion types and dynamics with ultra-high field magnetic resonance imaging. *Brain Pathol.* 28, 743–749. doi: 10.1111/bpa.12643

Harris, M., Biju, S., and Parac-Vogt, T. N. (2019). High-field MRI contrast agents and their synergy with optical imaging: The evolution from single molecule probes towards nano-architectures. *Chemistry Eur. J.* 25, 13838–13847. doi: 10.1002/chem.201901141

Harris, M., Vander Elst, L., Laurent, S., and Parac-Vogt, T. N. (2016). Magnetofluorescent micelles incorporating Dy(III)-DOTA as potential bimodal agents for optical and high field magnetic resonance imaging. *Dalton Trans.* 45, 4791–4801. doi: 10.1039/C5DT04801J

He, S., Song, J., Qu, J., and Cheng, Z. (2018). Crucial breakthrough of second near-infrared biological window fluorophores: design and synthesis toward multimodal imaging and theranostics. *Chem. Soc. Rev.* 47, 4258–4278 doi: 10.1039/C8CS00234G

Henning, A. (2018). Proton and multinuclear magnetic resonance spectroscopy in the human brain at ultra-high field strength: a review. *Neuroimage* 168, 181–198. doi: 10.1016/j.neuroimage.2017.07.017

Hu, D. H., Sheng, Z. H., Zhang, P. F., Yang, D. Z., Liu, S. H., Gong, P., et al. (2013). Hybrid gold-gadolinium nanoclusters for tumor-targeted NIRF/CT/MRI triple-modal imaging *in vivo*. *Nanoscale* 5, 1624–1628. doi: 10.1039/c2nr33543c

Hu, H., Zhang, Y., Shukla, S., Gu, Y., Yu, X., and Steinmetz, N. F. (2017). Dysprosium-modified tobacco mosaic virus nanoparticles for ultra-high-field magnetic resonance and near-infrared fluorescence imaging of prostate cancer. *ACS Nano* 11, 9249–9258. doi: 10.1021/acsnano.7b04472

Huang, J., Bu, L., Xie, J., Chen, K., Cheng, Z., Li, X., et al. (2010). Effects of nanoparticle size on cellular uptake and liver MRI with polyvinylpyrrolidone-coated iron oxide nanoparticles. *ACS Nano* 4, 7151–7160. doi: 10.1021/nn101643u

Huang, J., Guo, M., Ke, H., Zong, C., Ren, B., Liu, G., et al. (2015). Rational design and synthesis of γFe_2O_3 @Au magnetic gold nanoflowers for efficient cancer theranostics. *Adv. Mater.* 27, 5049–5056 doi: 10.1002/adma.201501942

Huelnhagen, T., Paul, K., Ku, M.-C., Serradas Duarte, T., and Niendorf, T. (2017). Myocardial T_2^* mapping with ultrahigh field magnetic resonance: physics and frontier applications. *Front. Phys.* 5:22. doi: 10.3389/fphy.2017.00022

Idisi, D. O., Oke, J. A., Sarma, S., Moloi, S. J., Ray, S. C., Pong, W. F., et al. (2019). Tuning of electronic and magnetic properties of multifunctional r-GO-ATA-Fe_2O_3-composites for magnetic resonance imaging (MRI) contrast agent. *J. Appl. Phys.* 126:035301. doi: 10.1063/1.5099892

Jin, S. M., Lee, H. S., Haque, M. R., Kim, H. N., Kim, H. J., Oh, B. J., et al. (2019). Multi-layer surface modification of pancreatic islets for magnetic resonance imaging using ferumoxytol. *Biomaterials* 214:119224. doi: 10.1016/j.biomaterials.2019.119224

Jung, S. -Y., Gwak, G. -H., Park, J. K., and Oh, J. -M. (2020). Finely crafted quasi-core–shell gadolinium/layered double hydroxide hybrids for switching on/off bimodal CT/MRI contrasting nanodiagnostic platforms. *RSC Adv.* 10, 5838–5844. doi: 10.1039/C9RA08159C

Kim, D.-H., Zeng, H., Ng, T. C., and Brazel, C. S. (2009). T_1 and T_2 relaxivities of succimer-coated $MFe_2^{3+}O_4$ (M = Mn^{2+}, Fe^{2+} and Co^{2+}) inverse spinel ferrites for potential use as phase-contrast agents in medical MRI. *J. Magn. Magn. Mater.* 321, 3899–3904. doi: 10.1016/j.jmmm.2009.07.057

Kim, J., Lee, N., and Hyeon, T. (2017). Recent development of nanoparticles for molecular imaging. *Phil. Trans. R Soc. A Math. Phys. Eng. Sci.* 375:20170022. doi: 10.1098/rsta.2017.0022

Ko, Y. J., Kim, W. J., Kim, K., and Kwon, I. C. (2019). Advances in the strategies for designing receptor-targeted molecular imaging probes for cancer research. *J. Control. Release* 305, 1–17. doi: 10.1016/j.jconrel.2019.04.030

Kubíčková, L., Brázda, P., Veverka, M., Kaman, O., Herynek, V., Vosmanská, M., et al. (2019). Nanomagnets for ultra-high field MRI: magnetic properties

and transverse relaxivity of silica-coated ε-Fe_2O_3. *J. Magn. Magn. Mater.* 480, 154–163. doi: 10.1016/j.jmmm.2019.02.067

Lee, J. Y., Termsarasab, U., Park, J. H., Lee, S. Y., Ko, S. H., Shim, J. S., et al. (2016). Dual CD44 and folate receptor-targeted nanoparticles for cancer diagnosis and anticancer drug delivery. *J. Control. Release* 236, 38–46. doi: 10.1016/j.jconrel.2016.06.021

Lee, N., Cho, H. R., Oh, M. H., Lee, S. H., Kim, K., Kim, B. H., et al. (2012). Multifunctional Fe_3O_4/TaO_x core/shell nanoparticles for simultaneous magnetic resonance imaging and X-ray computed tomography. *J. Am. Chem. Soc.* 134, 10309–10312. doi: 10.1021/ja3016582

Lee, S., Xie, J., and Chen, X. (2010). Peptide-based probes for targeted molecular imaging. *Biochemistry* 49, 1364–1376. doi: 10.1021/bi901135x

Lehericy, S., Vaillancourt, D. E., Seppi, K., Monchi, O., Rektorova, I., Antonini, A., et al. (2017). The role of high-field magnetic resonance imaging in parkinsonian disorders: pushing the boundaries forward. *Mov. Disord.* 32, 510–525. doi: 10.1002/mds.26968

Li, D.-Z., Chen, H.-D., Bi, F., and Wang, Z.-X. (2016). Progress of multimodal molecular imaging technology in diagnosis of tumor. *Chinese J. Anal. Chem.* 44, 1609–1618. doi: 10.1016/S1872-2040(16)60966-0

Li, H., and Meade, T. J. (2019). Molecular magnetic resonance imaging with Gd(III)-based contrast agents: challenges and key advances. *J. Am. Chem. Soc.* 141, 17025–17041. doi: 10.1021/jacs.9b09149

Li, H., Parigi, G., Luchinat, C., and Meade, T. J. (2019). Bimodal fluorescence-magnetic resonance contrast agent for apoptosis imaging. *J. Am. Chem. Soc.* 141, 6224–6233. doi: 10.1021/jacs.8b13376

Li, L., Jiang, W., Luo, K., Song, H., Lan, F., Wu, Y., et al. (2013). Superparamagnetic iron oxide nanoparticles as MRI contrast agents for non-invasive stem cell labeling and tracking. *Theranostics* 3, 595–615. doi: 10.7150/thno.5366

Li, X., Kim, J., Yoon, J., and Chen, X. (2017). Cancer-associated, stimuli-driven, turn on theranostics for multimodality imaging and therapy. *Adv. Mater.* 29:1606857. doi: 10.1002/adma.201606857

Liu, Y., Wu, S., Liu, Y., Zhang, H., Zhang, M., Tang, Z., et al. (2020). Cathodic protected Mn^{2+} by Na_xWO_3 nanorods for stable magnetic resonance imaging-guided tumor photothermal therapy. *Biomaterials* 234:119762. doi: 10.1016/j.biomaterials.2020.119762

Liu, Z., Rong, P., Yu, L., Zhang, X., Yang, C., Guo, F., et al. (2015). Dual-modality non-invasive mapping of sentinel lymph node by photoacoustic and near-infrared fluorescent imaging using dye-loaded mesoporous silica nanoparticles. *Mol. Pharm.* 12, 3119–3128. doi: 10.1021/mp500698b

Lyu, Q., You. C., Shan, H., and Wang, G. (2018). Super-resolution MRI through deep learning. *arXiv Prepr.* arXiv181006776.

Mahmoudi, M., Hosseinkhani, H., Hosseinkhani, M., Boutry, S., Simchi, A., Journeay, W. S., et al. (2011). Magnetic resonance imaging tracking of stem cells *in vivo* using iron oxide nanoparticles as a tool for the advancement of clinical regenerative medicine. *Chem. Rev.* 111, 253–280. doi: 10.1021/cr,1001832

Mahmud, M., Kaiser, M. S., Hussain, A., and Vassanelli, S. (2018). Applications of deep learning and reinforcement learning to biological data. *IEEE Trans. Neural. Netw. Learn. Syst.* 29, 2063–2079. doi: 10.1109/TNNLS.2018.2790388

Marangoni, V. S., Neumann, O., Henderson, L., Kaffes, C. C., Zhang, H., Zhang, R., et al. (2017). Enhancing T_1 magnetic resonance imaging contrast with internalized gadolinium(III) in a multilayer nanoparticle. *Proc. Natl. Acad. Sci. U. S. A.* 114, 6960–6965. doi: 10.1073/pnas.1701944114

Marasini, R., Thanh Nguyen, T.D., and Aryal, S. (2020). Integration of gadolinium in nanostructure for contrast enhanced-magnetic resonance imaging. *WIREs Nanomed. Nanobiotechnol.* 12:e1580. doi: 10.1002/wnan.1580

Moser, E., Laistler, E., Schmitt, F., and Kontaxis, G. (2017). Ultra-high field NMR and MRI—the role of magnet technology to increase sensitivity and specificity. *Front. Phys.* 5:33. doi: 10.3389/fphy.2017.00033

Mostapha, M., and Styner, M. (2019). Role of deep learning in infant brain MRI analysis. *Magn. Reson. Imaging* 64, 171–189. doi: 10.1016/j.mri.2019.06.003009

Mulder, M. P. C., Merkx, R., Witting, K. F., Hameed, D. S., El Atmioui, D., Lelieveld, L., et al. (2018). Total chemical synthesis of SUMO and SUMO-based probes for profiling the activity of SUMO-specific proteases. *Angew. Chem. Int. Ed. Engl.* 57, 8958–8962. doi: 10.1002/anie.201803483

Nakada, T. (2007). Clinical application of high and ultra high-field MRI. *Brain Dev.* 29, 325–335. doi: 10.1016/j.braindev.2006.10.005

Nalepa, J., Ribalta Lorenzo, P., Marcinkiewicz, M., Bobek-Billewicz, B., Wawrzyniak, P., Walczak, M., et al. (2020). Fully-automated deep learning-powered system for DCE-MRI analysis of brain tumors. *Artif. Intell. Med.* 102:101769. doi: 10.1016/j.artmed.2019.101769

Ni, D., Bu, W., Ehlerding, E. B., Cai, W., and Shi, J. (2017). Engineering of inorganic nanoparticles as magnetic resonance imaging contrast agents. *Chem. Soc. Rev.* 46, 7438–7468. doi: 10.1039/C7CS00316A

Ni, D., Zhang, J., Bu, W., Zhang, C., Yao, Z., Xing, H., et al. (2016). PEGylated $NaHoF_4$ nanoparticles as contrast agents for both X-ray computed tomography and ultra-high field magnetic resonance imaging. *Biomaterials* 76, 218–225. doi: 10.1016/j.biomaterials.2015.10.063

Norek, M., Kampert, E., Zeitler, U., and Peters, J. A. (2008). Tuning of the size of Dy_2O_3 nanoparticles for optimal performance as an MRI contrast agent. *J. Am. Chem. Soc.* 130, 5335–5340. doi: 10.1021/ja711492y

O'sullivan, S., Heinsen, H., Grinberg, L. T., Chimelli, L., Amaro, E. Jr., Do Nascimento Saldiva, P. H., et al. (2019). The role of artificial intelligence and machine learning in harmonization of high-resolution post-mortem MRI (virtopsy) with respect to brain microstructure. *Brain Inf.* 6:3. doi: 10.1186/s40708-019-0096-3

Pansare, V. J., Hejazi, S., Faenza, W. J., and Prud'homme, R. K. (2012). Review of long-wavelength optical and NIR imaging materials: contrast agents, fluorophores, and multifunctional nano carriers. *Chem. Mater.* 24, 812–827. doi: 10.1021/cm2028367

Patrick, P. S., Hammersley, J., Loizou, L., Kettunen, M. I., Rodrigues, T. B., Hu, D. E., et al. (2014). Dual-modality gene reporter for *in vivo* imaging. *Proc. Natl. Acad. Sci. U. S. A.* 111, 415–420. doi: 10.1073/pnas.1319000111

Pellico, J., Ellis, C. M., and Davis, J. J. (2019). Nanoparticle-based paramagnetic contrast agents for magnetic resonance imaging. *Contrast Media. Mol. Imaging* 2019, 1–13. doi: 10.1155/2019/1845637

Qin, J., Laurent, S., Jo, Y. S., Roch, A., Mikhaylova, M., Bhujwalla, Z. M., et al. (2007). A high-performance magnetic resonance imaging T_2 contrast agent. *Adv. Mater.* 19, 1874–1878. doi: 10.1002/adma.200602326

Rajamanickam, K. (2019). Multimodal molecular imaging strategies using functionalized nano probes. *J. Nanotechnol. Res.* 1, 119–135. doi: 10.26502/jnr.2688-85210010

Raval, S. B., Britton, C. A., Zhao, T., Krishnamurthy, N., Santini, T., Gorantla, V. S., et al. (2017). Ultra-high field upper extremity peripheral nerve and non-contrast enhanced vascular imaging. *PLoS ONE* 12:e0175629. doi: 10.1371/journal.pone.0175629

Rees, J. A., Deblonde, G. J., An, D. D., Ansoborlo, C., Gauny, S. S., and Abergel, R. J. (2018). Evaluating the potential of chelation therapy to prevent and treat gadolinium deposition from MRI contrast agents. *Sci. Rep.* 8:4419. doi: 10.1038/s41598-018-22511-6

Rogosnitzky, M., and Branch, S. (2016). Gadolinium-based contrast agent toxicity: a review of known and proposed mechanisms. *Biometals* 29, 365–376. doi: 10.1007/s10534-016-9931-7

Rosenberg, J. T., Kogot, J. M., Lovingood, D. D., Strouse, G. F., and Grant, S. C. (2010). Intracellular bimodal nanoparticles based on quantum dots for high-field MRI at 21.1 T. *Magn. Reson. Med.* 64, 871–882. doi: 10.1002/mrm.22441

Shan, H., Zhang, Y., Yang, Q., Kruger, U., Kalra, M. K., Sun, L., et al. (2018). 3-D convolutional encoder-decoder network for low-dose CT via transfer learning from a 2-D trained network. *IEEE Trans. Med. Imaging* 37, 1522–1534. doi: 10.1109/TMI.2018.2832217

Shen, D., Wu, G., and Suk, H. I. (2017a). Deep learning in medical image analysis. *Annu. Rev. Biomed. Eng.* 19, 221–248. doi: 10.1146/annurev-bioeng-071516-044442

Shen, Z., Chen, T., Ma, X., Ren, W., Zhou, Z., Zhu, G., et al. (2017b). Multifunctional theranostic nanoparticles based on exceedingly small magnetic iron oxide nanoparticles for T_1-weighted magnetic resonance imaging and chemotherapy. *ACS Nano* 11, 10992–11004. doi: 10.1021/acsnano.7b04924

Shen, Z., Song, J., Zhou, Z., Yung, B. C., Aronova, M. A., Li, Y., et al. (2018). Dotted core-shell nanoparticles for T_1 -weighted MRI of tumors. *Adv. Mater.* 30:e1803163. doi: 10.1002/adma.201803163

Shen, Z., Wu, A., and Chen, X. (2017c). Iron oxide nanoparticle based contrast agents for magnetic resonance imaging. *Mol. Pharm.* 14, 1352–1364. doi: 10.1021/acs.molpharmaceut.6b00839

Sheth, D., and Giger, M. L. (2019). Artificial intelligence in the interpretation of breast cancer on MRI. *J. Magn. Reson. Imaging*. doi: 10.1002/jmri.26878

Shin, T. H., Choi, Y., Kim, S., and Cheon, J. (2015). Recent advances in magnetic nanoparticle-based multi-modal imaging. *Chem. Soc. Rev.* 44, 4501–4516. doi: 10.1039/C4CS00345D

Song, G., Kenney, M., Chen, Y.S., Zheng, X., Deng, Y., Chen, Z., et al. (2020). Carbon-coated FeCo nanoparticles as sensitive magnetic-particle-imaging tracers with photothermal and magnetothermal properties. *Nat. Biomed. Eng.* 4, 325–334. doi: 10.1038/s41551-019-0506-0

Sosnovik, D. E., Nahrendorf, M., and Weissleder, R. (2007). Molecular magnetic resonance imaging in cardiovascular medicine. *Circulation* 115, 2076–2086. doi: 10.1161/CIRCULATIONAHA.106.658930

Sousa, F., Sanavio, B., Saccani, A., Tang, Y., Zucca, I., Carney, T. M., et al. (2017). Superparamagnetic nanoparticles as high efficiency magnetic resonance imaging T_2 contrast agent. *Bioconjug. Chem.* 28, 161–170. doi: 10.1021/acs.bioconjchem.6b,00577

Thiruppathi, R., Mishra, S., Ganapathy, M., Padmanabhan, P., and Gulyas, B. (2017). Nanoparticle functionalization and its potentials for molecular imaging. *Adv. Sci.* 4:1600279. doi: 10.1002/advs.201600279

Tromsdorf, U. I., Bigall, N. C., Kaul, M. G., Bruns, O. T., Nikolic, M. S., Mollwitz, B. et al. (2007). Size and surface effects on the MRI relaxivity of manganese ferrite nanoparticle contrast agents. *Nano Lett.* 7, 2422–2427. doi: 10.1021/nl071099b

Turing, A. (2019). The journey begins—100daysml. *Mach. Learn. Stat.* Available online at: https://100daysml.com/2019/08/31/the-journey-begins/

Vaughan, J. T., Snyder, C. J., Delabarre, L. J., Bolan, P. J., Tian, J., Bolinger, L., et al. (2009). Whole-body imaging at 7T: preliminary results. *Magn. Reson. Med.* 61, 244–248. doi: 10.1002/mrm.21751

Verwilst, P., Park, S., Yoon, B., and Kim, J. S. (2015). Recent advances in Gd-chelate based bimodal optical/MRI contrast agents. *Chem. Soc. Rev.* 44, 1791–1806. doi: 10.1039/C4CS00336E

Wahsner, J., Gale, E. M., Rodriguez-Rodriguez, A., and Caravan, P. (2019). Chemistry of MRI contrast agents: current challenges and new frontiers. *Chem. Rev.* 119, 957–1057. doi: 10.1021/acs.chemrev.8b,00363

Wang, F. H., Bae, K., Huang, Z. W., and Xue, J. M. (2018). Two-photon graphene quantum dot modified Gd_2O_3 nanocomposites as a dual-mode MRI contrast agent and cell labelling agent. *Nanoscale* 10, 5642–5649. doi: 10.1039/C7NR08068A

Wegmayr, V,. Aitharaju, S., and Buhmann, J. (2018). "Classification of brain MRI with big data and deep 3D convolutional neural networks. Medical imaging 2018," in Computer-Aided Diagnosis, Vol. 10575 (Houston, TX). doi: 10.1117/12.2293719

Werner, E. J., Datta, A., Jocher, C. J., and Raymond, K. N. (2008). High-relaxivity MRI contrast agents: where coordination chemistry meets medical imaging. *Angew. Chem. Int. Ed. Engl.* 47, 8568–8580. doi: 10.1002/anie.200800212

Worden, M., Bruckman, M. A., Kim, M. H., Steinmetz, N. F., Kikkawa, J. M., Laspina, C., et al. (2015). Aqueous synthesis of polyhedral "brick-like" iron oxide nanoparticles for hyperthermia and T_2 MRI contrast enhancement. *J. Mater. Chem. B* 3, 6877–6884. doi: 10.1039/C5TB01138H

Wu, L., Jiang, J., Jin, Y., Kallemeijn, W. W., Kuo, C. L., Artola, M., et al. (2017). Activity-based probes for functional interrogation of retaining β-glucuronidases. *Nat. Chem. Biol.* 13, 867–876. doi: 10.1038/nchembio.2395

Wu, M., and Shu, J. (2018). Multimodal molecular imaging: current status and future directions. *Contrast Media Mol. Imaging* 2018:1382183. doi: 10.1155/2018/1382183

Yen, S. K. Janczewski, D., Lakshmi, J. L., Dolmanan, S. B., Tripathy, S., Ho, V. H. B., et al. (2013). Design and synthesis of polymer-functionalized NIR fluorescent dyes-magnetic nanoparticles for bioimaging. *ACS Nano* 7, 6796–6805. doi: 10.1021/nn401734t

Yin, J., Yin, G., Pu, X., Huang, Z., and Yao, D. (2019). Preparation and characterization of peptide modified ultrasmall superparamagnetic iron oxides used as tumor targeting MRI contrast agent. *RSC Adv.* 9, 19397–19407. doi: 10.1039/C.9R.A.02636C

Zaharchuk, G., Gong, E., Wintermark, M., Rubin, D., and Langlotz, C. P. (2018). Deep learning in neuroradiology. *AJNR Am. J. Neuroradiol.* 39, 1776–1784. doi: 10.3174/ajnr.A5543

Zhang, J., Yuan, Y., Gao, M., Han, Z., Chu, C., Li, Y., et al. (2019). Carbon dots as a new class of diamagnetic chemical exchange saturation transfer (diaCEST) MRI contrast agents. *Angew. Chem. Int. Ed. Engl.* 58, 9871–9875. doi: 10.1002/anie.201904722

Zhang, X., Blasiak, B., Marenco, A. J., Trudel, S., Tomanek, B., and van Veggel, F. C. J. M. (2016). Design and regulation of $NaHoF_4$ and $NaDyF_4$ nanoparticles for high-field magnetic resonance imaging. *Chem. Mater.* 28, 3060–3072. doi: 10.1021/acs.chemmater.6b00264

Zhang, Y., Udayakumar, D., Cai, L., Hu, Z., Kapur, P., Kho, E. Y., et al. (2017). Addressing metabolic heterogeneity in clear cell renal cell carcinoma with quantitative dixon MRI. *JCI Insight* 2:e94278. doi: 10.1172/jci.insight.94278

Zhao, M., Beauregard, D.A., Loizou, L., Davletov, B., and Brindle, K. M. (2001). Non-invasive detection of apoptosis using magnetic resonance imaging and a targeted contrast agent. *Nat. Med.* 7, 1241–1244. doi: 10.1038/nm1101-1241

Zhao, Y., Liu, H., Riker, A. I., Fodstad, O., Ledoux, S. P., Wilson, G. L., et al. (2012). Emerging metabolic targets in cancer therapy. *Front. Biosci.* 16:3816. doi: 10.2741/3826

Zhao, Z., Wang, X., Zhang, Z., Zhang, H., Liu, H., Zhu, X., et al. (2015). Real-time monitoring of arsenic trioxide release and delivery by activatable T_1 imaging. *ACS Nano* 9, 2749–2759. doi: 10.1021/nn506640h

Zhao, Z., Zhou, Z., Bao, J., Wang, Z., Hu, J., Chi, X., et al. (2013). Octapod iron oxide nanoparticles as high-performance T_2 contrast agents for magnetic resonance imaging. *Nat. Commun.* 4:2266. doi: 10.1038/ncomms3266

Zheng, X., Wang, Y., Sun, L., Chen, N., Li, L., Shi, S., et al. (2016). TbF_3 nanoparticles as dual-mode contrast agents for ultrahigh field magnetic resonance imaging and X-ray computed tomography. *Nano Res.* 9, 1135–1147. doi: 10.1007/s12274-016-1008-y

Zhou, T., Wu, B., and Xing, D. (2012). Bio-modified Fe_3O_4 core/Au shell nanoparticles for targeting and multimodal imaging of cancer cells. *J. Mater. Chem.* 22, 470–477. doi: 10.1039/C1JM13692E

Zhou, Z., Changqiang, W., Liu, H., Zhu, X., Zhao, Z., Wang, L., et al. (2015a). Surface and interfacial engineering of iron oxide nanoplates for highly efficient magnetic resonance angiography. *ACS Nano* 9, 3012–3022. doi: 10.1021/nn507193f

Zhou, Z., Liu, H., Chi, X., Chen, J., Wang, L., Sun, C., et al. (2015b). A protein-corona-free T_1-T_2 dual-modal contrast agent for accurate imaging of lymphatic tumor metastasis. *ACS Appl. Mater. Interfaces* 7, 28286–28293. doi: 10.1021/acsami.5b08422

Zhou, Z., Yang, L., Gao, J., and Chen, X. (2019). Structure-relaxivity relationships of magnetic nanoparticles for magnetic resonance imaging. *Adv. Mater.* 31:1804567. doi: 10.1002/adma.201804567

Zhu, G., Jiang, B., Tong, L., Xie, Y., Zaharchuk, G., and Wintermark, M. (2019). Applications of deep learning to neuro-imaging techniques. *Front. Neurol.* 10:869. doi: 10.3389/fneur.2019.00869

Zhu, H., and Moser, E. (2017). Editorial: *in vivo* magentic resonance at ultra high field. *Fornt. Phys.* 5:45. doi: 10.3389/fphy.2017.00045

Zhu, L., Yang, Y., Farquhar, K., Wang, J., Tian, C., Ranville, J., et al. (2016). Surface modification of Gd nanoparticles with pH-responsive block copolymers for use as smart MRI contrast agents. *ACS Appl. Mater. Interfaces* 8, 5040–5050. doi: 10.1021/acsami.5b12463

Zhu, W., Liu, K., Sun, X., Wang, X., Li, Y., Cheng, L., et al. (2015). Mn^{2+}-doped prussian blue nanocubes for bimodal imaging and photothermal therapy with enhanced performance. *ACS Appl. Mater. Interfaces* 7, 11575–11582. doi: 10.1021/acsami.5b02510

Conflict of Interest: The author declares that the research was conducted in the absence of any commercial or financial relationships that could be construed as a potential conflict of interest.

frontiers in Chemistry

MINI REVIEW
published: 09 April 2020
doi: 10.3389/fchem.2020.00257

Bioresponsive Nanomedicine: The Next Step of Deadliest Cancers' Theranostics

Yuqiang Mao[1] *and Xiaoying Liu*[2]*

[1] Department of Thoracic Surgery, Shengjing Hospital, China Medical University, Shenyang, China, [2] Department of Breast Surgery, The First Affiliated Hospital of China Medical University, Shenyang, China

Among all cancers, lung, breast, and prostate carcinoma are the three most fatal cancers. Although general therapeutic strategies and existent nanomedicine have been applied in relating cancer treatments, the side effects and potential damage induced by the off-target effect greatly lower the therapeutic efficiency. Recently, an increasing number of bioresponsive nanomaterials is recruited in fighting these deadliest cancers. Therefore, these latest bioresponsive nanomedicine are summarized in the current review. More specifically, the various novel nano-agents that could selectively respond to specific bio-conditions in malignant areas (e.g., pH, temperature, enzyme, Redox, elevated copper ion, etc.) are discussed in detail for their applications in cancer imaging (e.g., fluorescence, NIR, and MRI, etc.) and therapy (e.g., antiangiogenesis, chemotherapy, photothermal, and chemodynamic therapy, etc.). The development of next-generation of bioresponsive nanomedicine and challenges involved are further discussed for future design.

Keywords: bioresponsive nanomedicine, nanoparticles, theranostics, breast cancer, lung cancer, prostate cancer

OPEN ACCESS

Edited by:
Dawei Jiang,
Huazhong University of Science and Technology, China

Reviewed by:
Zunyu Xiao,
Stanford University, United States
Weiyu Chen,
Stanford University, United States

***Correspondence:**
Xiaoying Liu
54190693@qq.com

Specialty section:
This article was submitted to Nanoscience, a section of the journal Frontiers in Chemistry

Received: *06 March 2020*
Accepted: *17 March 2020*
Published: *09 April 2020*

Citation:
Mao Y and Liu X (2020) Bioresponsive Nanomedicine: The Next Step of Deadliest Cancers' Theranostics. Front. Chem. 8:257. doi: 10.3389/fchem.2020.00257

INTRODUCTION

Cancer is a disease caused by gene mutation, leading to an uncontrolled cell division. These abnormal cells could easily generate malignant lesions and even metastasize to other organs, greatly threatening the patient's health. As the second leading cause of deaths, cancer contributed to around 10 million deaths in 2018 globally, with about 18.1 million new cases (Bray et al., 2018). Among all the cancer types, lung, breast, and prostate cancer are the deadliest carcinomas for people, contributing to 18.4, 11.6, and 7.1% of all the cancer-related deaths, respectively (Bray et al., 2018). With the support of various diagnosis technologies including positron emission tomography (PET), magnetic resonance imaging (MRI), and computed tomography (CT), surgery, radiotherapy, chemotherapy, and hormone therapy are generally applied to treat patients with cancer, including those three deadliest carcinomas. However, most strategies fail to detect and eliminate the cancerous cells efficiently, which could lead to tumor occurrence and threat to the patient's life. In addition, accompanying side effects can not be completely avoided, causing various adverse effects ranging from vomiting to asthenia (Oun et al., 2018). Although immunotherapy could be the best choice for preventing these situations, the high cost could be only afforded by a small portion of patients.

With the development of nanotechnology, functional agents could be uniformly synthesized at nano-size, showing great potential in the biomedical application as nanomedicine. These nanomaterials could perform as anti-cancer agents by carrying effective cargos (e.g., anti-cancer

drugs or monoclonal antibody, etc.) and processing directly therapeutic effects (e.g., photothermal and photodynamic therapy, etc.). Compared with general treatments, nanomedicines greatly increase the efficiency of therapy (e.g., the increased loading compacity, prolonged circulation of drug and combined therapies, etc.) and limit side effects (e.g., encapsulated anti-cancer drugs and specific tumor targeting, etc.). To date, various nanomedicines have been approved by the FDA for cancer therapy, such as paclitaxel albumin-bound nanoparticles (Abraxane) and liposomal irinotecan (Onivyde) (Ventola, 2017). Although these nano-agents exhibit desirable anti-cancer function, the constantly active cytotoxicity would potentially cause indiscriminate damage to normal tissues due to the off-target effect. Recently, a growing number of novel nanomaterials that are specifically responded to biological factors (e.g., acidity, enzyme, redox, temperature, and copper ion, etc.) within tumor area are recruited for fighting these deadliest cancers via imaging (e.g., fluorescence, near infrared (NIR), and MRI, etc.) and therapy (e.g., antiangiogenesis, chemotherapy, photothermal, and chemodynamic therapy, etc.). Therefore, these recent bioresponsive nano-platforms that have been investigated in lung, breast, and prostate cancer theranostics are highlighted in the current review. Meanwhile, the future direction and challenges involved are discussed as well, aiming to offer an overview of the development of smart nanomedicine in treating these deadliest carcinomas.

CURRENT SITUATION OF LUNG, BREAST AND PROSTATE CANCER

As the essential organ for body function, the lung is strongly associated with other systems, which make it very vulnerable to illness, such as cancer. The lung carcinoma is a life-threating disease, especially those metastasized from another part of the body, which generally indicated the late stage of cancer, such as advanced breast and prostate cancer. Normally, the 5-year life expectancy of patients with distant lung cancer is only about 5% (Torre et al., 2016). As another major carcinoma, breast cancer is the most common cancer among females. In 2020, there are an estimated 325,000 females who will be diagnosed with invasive or non-invasive breast cancer. Comparatively, prostate cancer contributes to around 366,000 men deaths and 1.6 million new cases annually (Pernar et al., 2018). Although the people with increased risks (e.g., aging and family histology) will be easier to develop these fatal cancers, there is an increasing trend of young patients diagnosed with lung and prostate cancer overall the world (Salinas et al., 2014; Liu et al., 2019a).

GENERAL THERAPEUTIC STRATEGIES

To deal with these deadliest cancers, general treatments such as surgery, chemotherapy, and radiotherapy have been recruited as routine strategies for years. Although current clinical diagnosis could promote outcomes of these treatments in the early stage, the efficiency of most therapies is limited for late-stage or advanced cancer. Recent years, the precision medicine based on individual genetic information provide effective therapy for patient via specific targeting such as the blockage of certain growth factor receptor (Dienstmann et al., 2017 #189). Although these precision therapies could work well in most cancers with general targets, its feasibility in mutated cancer types such as non-small-cell lung cancer of adenocarcinoma with EGFR mutation (∼29.3% of all) or triple-negative breast cancer (11.2% of all) is strongly restricted by the availability of small molecular or monoclonal antibody (Midha et al., 2015 #190, Tan and Dent, 2018 #191). Due to these, there is an urgent need of a novel therapeutic approach for treating developed and mutated cancers.

CURRENT STATUS OF NANOMEDICINE FOR LUNG, BREAST, AND PROSTATE CANCER THERAPY

Nanomedicine, as an advanced technique has been gradually applied in fighting cancer, especially lung, breast, and prostate cancers. Since 2018, more than 20 nano-sized medicine have been parenteral in the market, while seven of them are designed for cancer therapy (Flühmann et al., 2019). Currently, there are about 27 clinical trials associating with the nanoparticles based breast cancer therapy are active. These studies focus on imaging and treating various breast carcinoma ranging from triple-negative breast cancer (TNBC) to metastatic breast cancer. A series of nanomedicines including FDA-approved paclitaxel albumin-bound nanoparticles (Abraxane), lipid nanoparticles (mRNA-2752), curcumin/doxorubicin encapsulating nanoparticles (Imx-110), quantum dots and silica nanoparticle (cRGDY-PEG-Cy5.5-C dots) have been recruited in clinic studies, showing the great potential of nanomedicine in dealing breast cancer. In comparison, there are about 13 and 9 active clinical trials related to lung and prostate cancer, respectively. Notably, either the mostly-applied Abraxane or newly-designed cyclodextrin-based polymer (CRLX101) is constantly functional that will potentially damage the normal cells. Therefore, more efficient and safe cancer therapy could be provided by the novel nano-platforms with therapeutic functions that could smartly be activated by specific conditions, such as bioresponsive nanomedicine.

BIORESPONSIVE NANOMEDICINE

Certain biological factors including acidic extracellular environment, specific enzymes, elevated redox and cooper ion, etc. are well-identified in the tumor micro-environment (TME). Base on these factors, a series of advanced nanoplatforms with TME-activated functions have been successfully developed for treating these three fatal cancers (**Table 1**). In a comparison of current nanomedicines that generally exhibit constantly-activating functions (e.g., cytotoxicity of anti-cancer drugs), the therapeutic effects of bioresponsive nano-agents could be smartly triggered in TME, which efficiently avoids most of the adverse influence caused by miss-targeting.

TABLE 1 | Recent advanced bioresponsive nanomedicine used in treating lung, breast, and prostate cancer.

Bioresponsive factor	Type of nanomaterial	Nanomedicine	Size (nm)	Application	Cancer	References
Acidity	Polymer	PWMs	19.9 ± 1.9 × 50–200	siRNA delivery	Breast cancer with lung metastasis	(He et al., 2016 #152)
Acidity	Polymer	NP15	<100	siRNA delivery	Breast cancer	(Saw et al., 2019 #157)
Acidity	Silica	TPZ@HHSN-C/P-mAb	142.5 ± 1.3	USI and MRI—SDT and BRT	Prostate cancer	(Wang et al., 2019 #159)
Redox and acidity	Polymer	P-RUB micelles	49 ± 0.26	Chemo	Taxane resistant prostate cancer	(Lin et al., 2019 #163)
Redox and acidity	Silica	ECMI	220.0 ± 3.5	PDT and Chemo	Erlotinib-resistant EGFR-mutated NSCLC	(Zhang et al., 2019 #164)
Redox	Nanozyme	Lipo-OGzyme-AIE	122.5	PDT	Breast cancer with lung metastasis	(Gao et al., 2020 #168)
Enzyme and Redox	Gold NCs	mCAuNCs@HA	150	PDT and Chemo and Immuno	Breast cancer with lung metastasis	(Yu et al., 2019 #174)
Enzyme	Polymer	HACE	132	NIRF and PAI—PDT	Lung cancer	(Li et al., 2016 #173)
Enzyme	Polymer	WINNER	16	mAbs delivery	Lung cancer	(Li et al., 2019 #178)
Enzyme	Polymer	Self-assembled polymer	93	Chemo	Lung cancer	(Yang et al., 2016 #179)
Copper and acidity	Polymer	RPTDH	200	Antiangiogenic and Immuno	Metastatic breast cancer	(Zhou et al., 2019 #181)
Copper	Silica	Imi-OSi	<6	Antiangiogenic and TVO	Breast and lung cancer	(Yang et al., 2019a #182)
Thermal and acidity	Polymer	mPEG-PAAV	174.5	NIRF and PAI—PTT and Chemo	Breast cancer with lung metastasis	(Yang et al., 2018 #184)

USI, ultrasound imaging; MRI, magnetic resonance imaging; SDT, sonodynamic therapy; BRT, bioreductive therapy; Chemo, chemotherapy; PDT, photodynamic therapy; Immuno, immunotherapy; NIRF, near infrared fluorescence; PAI, photoacoustics imaging; TVO, tumor vascular obstructing.

pH-RESPONSIVE NANOMEDICINE

With excessive aerobic glycolysis, the extracellular area around cancerous cells is packed with lactic acid, showing an acidic environment with pH ranging from 6.5 to 6.9 (Kato et al., 2013). As the major tumor feature, various nanomaterials including polymer (Kato et al., 2013; He et al., 2016; Xu et al., 2017; Zhao et al., 2017; Shen et al., 2018; Saw et al., 2019), silica (Wang et al., 2018, 2019) and upconversion (Qiao et al., 2017) nanoparticles were designed for smart drug delivery via pH-response. With excellent pH-responsive features (e.g., via structural or solubility change), polymer-based nano-platforms demonstrate a great advantage in pH-triggered drug release (Kocak et al., 2017). By coating with pH-sensitive mPEG-b–$PDPA_{20}$, succinobucol (SCB), vascular cell adhesion molecule-1 (VCAM-1) inhibitor could efficiently escape from micelles (PWMs) at TME, and inhibit the lung metastasis of breast cancer tumors for around ∼6.25 and 4.5 times, respectively, in comparison with saline and SCB groups (He et al., 2016). Besides, by combing enzyme-induced feature (esterase), Saw et al. successfully synthesized an N15 polymer nanoparticle (<100 nm) consisting of a core (siRNA and amphiphilic cationic mitoxantrone, MTO) and pH-responsive PEG shell (Saw et al., 2019) (**Figure 1A**). The siRNA of Polo-like kinase 1 (PLK1) (more than 90%) would be only released after a two-step decomposition caused by acidic pH and esterase in the tumor area, which efficiently inhibited ∼70% of PLK1 expression and around 2-fold of MDA-MB-231 tumor growth within 18 days (**Figure 1B**). Meanwhile, a silica based multi-module theranostic platform (HHSN-C/P-mAb) was developed by Wang et al. for imaging (US and MRI) and treating (sonodynamic and bioreductive therapy) prostate cancer (Wang et al., 2019). This acidic-degraded silica nanomedicine was able to target PC3 tumors (via modified monoclonal antibody of prostate stem cell antigen) and smartly release tirapazamine (TPZ) at TME, eventually inhibiting more than 91.5% tumor growth with US irradiation.

REDOX-RESPONSIVE NANOMEDICINE

As other major factors, the concentrations of reactive oxygen species (ROS) and glutathione (GSH) are extremely higher in TME (Cook et al., 2004), which allow different nano-agents to be applied for treating aggressive cancers including taxane resistant prostate cancer, erlotinib-resistant EGFR-mutated NSCLC cells and TNBC via redox-induced therapeutic functions (He et al., 2018; Dai et al., 2019; Hu et al., 2019; Lin et al., 2019; Liu et al., 2019b; Yang et al., 2019a; Zhang et al., 2019; Gao et al., 2020). In the combination of acidic and GSH sensitive features, a novel P-RUB micelle was designed for co-delivering docetaxel (DTX) and rubone (RUB) in fighting taxane resistant prostate cancer (PC3-TXR) (Lin et al., 2019). As-prepared nanomedicine (49 ± 0.26 nm) could quickly release both cargos (∼100%) at acidic conditions (pH = 5) when GSH (10 mM) was presented.

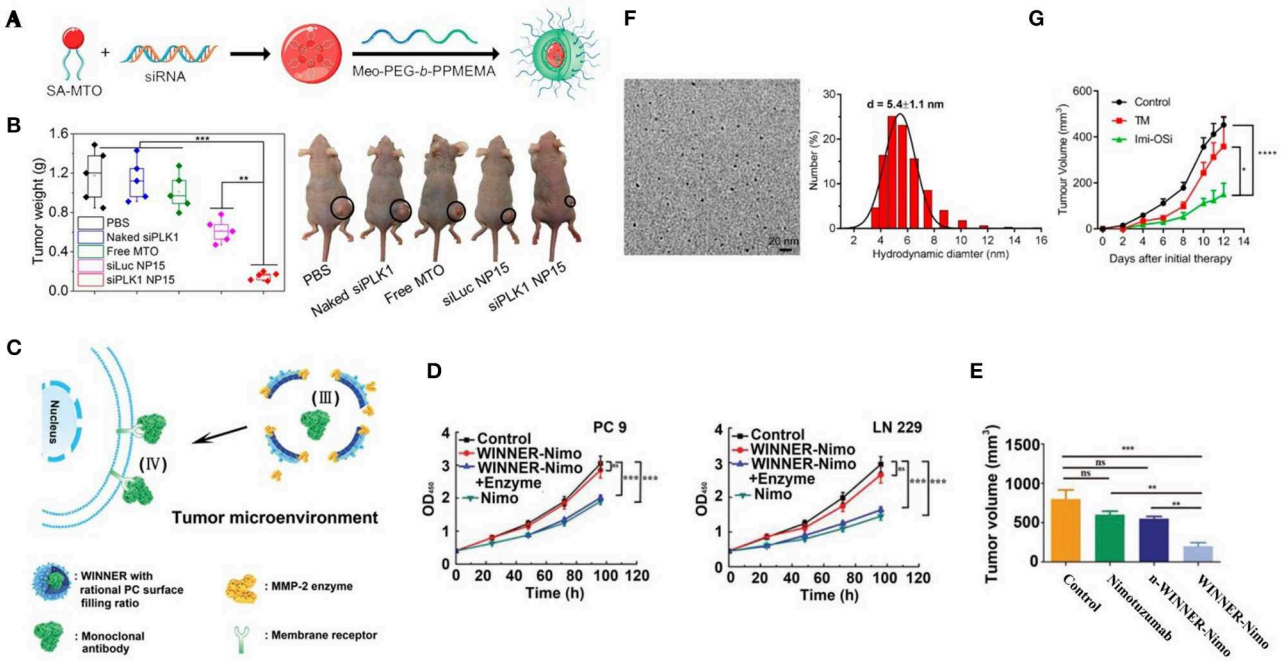

FIGURE 1 | Bioresponsive nanomedicine for lung, breast, and prostate cancer therapy. **(A)** Scheme of synthesis of SA-MTO (NP15); **(B)** MDA-MB-231 tumor weights from nude mice xenograft model that were treated with different groups and representative photograph tumor-bearing mice at day 18 [(Saw et al., 2019) #157] (Copyright 2019, reproduced with permission from American Chemical Society). **(C)** Schematic illustration of WINNER coating with PC ratio for extracellular delivery of mAb; **(D)** The antitumor efficacy of WINNER-Nimo in LN 229 and PC 9 cells; **(E)** Tumor volume from different treatment groups [(Li et al., 2019) #178] (Copyright 2019, reproduced with permission from Wiley). **(F)** TEM image and DLS of Imi-OSi; **(G)** 4T1 tumor inhibition efficiency of TM (copper chelator) and Imi-OSi (Yang et al., 2019b #182) (Copyright 2019, reproduced with permission from American Chemical Society).

With two-step triggered therapy, the proliferation of PC3-TXR tumors was efficiently suppressed for ∼50% compared to other groups. Similarly, pH-responsive zinc oxide quantum dots (ZnO QDs) and disulfide bond linked chitosan (Cs) were employed as triggers in ECMI silica nanoparticles for lung cancer therapy (Zhang et al., 2019). ECMI carrying ICG and erlotinib exhibited specific distribution and effective inhibition for EGFR mutated NSCLC tumors with the NIR irradiation. Most recently, Gao et al. developed a hypoxia-tropic nanozymes as theranostic nanomedicine for suppressing orthotopic breast cancer growth and lung metastasis (Gao et al., 2020). Significantly, the MnO_2 core inside ferritin nanocages (FTn) catalase the H^+ and H_2O_2 into O_2 that could be generated into toxic ROS by AIE modules under the irradiation. These reactions could effectively alter the TME (e.g., neutralization of hypoxic environment, with ∼51.9 ± 8.5% reduction of hypoxic tissue) and prohibit the proliferation and metastasis of breast cancer with only ∼5% metastasis compared to PBS group.

ENZYME-RESPONSIVE NANOMEDICINE

Besides, various enzymes are strongly associated with cancerous cells. It has been found that the excess hyaluronidase could be found within malignant tissues including lung, prostate, and breast carcinoma (Mcatee et al., 2014). More importantly, the presentation of hyaluronidase could accelerate the development of cancer progression. Li et al. were inspired by this tumor-related enzyme and developed a hyaluronidase-activated theranostic micelles (HACE NPs) with hyaluronic acid (HA) and chlorin e6 (Ce6) (Li et al., 2016). This polymer (132 nm) could produce both A549 tumor imaging (including NIR fluorescence and photoacoustic imaging) and photodynamic therapy (PDT) via the Ce6 that was released by hyaluronidase. Similarly, a HA- and ROS-responsive nano-agent (mCAuNCs@HA) was successfully recruited in treating breast cancer and lung metastasis via PDT and the blockage of checkpoint (Yu et al., 2019).

Matrix metalloproteinase (MMP) is another type of tumor-specific enzyme. Notably, a significant difference could be observed between malignant and normal lung tissues in terms of the expression of MMPs (Merchant et al., 2017), showing great potential of MMPs as the bioresponsive factor for lung cancer theranostics. Recently, a series of MMPs-responsive (especially MMP2/9) nanomedicines were developed in therapy against lung cancer (Van Rijt et al., 2015; Yang et al., 2016; Battistella et al., 2019; Li et al., 2019). For instance, Yang et al. prepared self-assembled nano drugs by conjugating an MMP-2-cleavable peptide, which allowed this nanomedicine selectively to deliver camptothecin (CP) and trans-retinoic acid (RA) antitumor drugs to cancerous cells with high expression of MMP-2 (Yang et al., 2016). In the comparison of typical intracellular drug delivery, Li et al. designed a novel nano-vehicle (WINNER)

for specific extracellular delivery (**Figure 1C**). With MMP-2-responsive peptides and controlled surface filling ratio (50.5–58.3%) of phosphorylcholine (PC), WINNER could efficiently protect and release loading nimotuzumab to the lung tumor (PC-9 and LN-229) extracellular area, showing highest antitumor effect in compared with free nimotuzumab (**Figures 1D,E**).

OTHER BIO-RESPONSIVE NANOMEDICINE

An increasing number of studies have found that elevated serum copper ion was associated with various cancers and strongly related to the stage and progression of carcinoma, such as breast cancer (Denoyer et al., 2015). As a promising tumor stimulus, copper ion also plays a key role in tumor angiogenesis. In most recent, two copper-chelator based nanomedicines have been synthesized for lung and breast cancer therapy (Yang et al., 2019b; Zhou et al., 2019) (**Figure 1F**). In addition to the anti-angiogenesis induced by chelation of Cu^{2+}, these smart nanoparticles caused further anti-tumor effects via tumor vessel obstruction (e.g., aggregation of nanochelators) and TLR-mediated immune cells stimulation (with TLR7 and TLR8 agonist), respectively (**Figure 1G**).

Meanwhile, several temperature-responsive nanomedicines were also developed for prostate and breast carcinoma therapy (Wadajkar et al., 2013; Yang et al., 2018). These nano-composites are sensitive to the change of temperature (40–43°) and will release the cargos at lower or upper critical solution temperature, eventually triggering the anti-cancer effects via chemotherapy or combined therapy.

CONCLUSION AND FUTURE OUTLOOK

The deadliest cancers, lung, breast, and prostate cancers cause thousands of deaths annually, while the efficiency of general strategies is limited, especially for those with drug resistance or genetic mutations. In comparison, the bioresponsive nanomedicine has shown great potential in treating deadliest cancers via the smartly-triggered (e.g., pH, Redox, Enzyme, Copper ion, temperature) functions. Since now, a series of these nano-agents have been successfully developed and shown promising outcomes. Undeniably, the bioresponsive nanomedicine would be the next step of theranostics for these deadliest cancers. For future development, we believe there are several issues could be considered. (1) In consideration of the different TME, specific designs of bioresponsive nanomedicine are highly recommended. For instance, with significantly elevated MMPs, the MMP-activated nanomedicine is more promising and feasible in lung cancer compared with others. (2) The novel direction such as extracellular delivery could be further designed for treating TME. (3) Plural triggers (e.g., pH and Redox, pH and Enzyme) for function activation could be achieved by incorporating functional nanomaterials, such as polymers, which would provide more precision therapy. (4) Meanwhile, multiple functions (e.g., image-guided surgery and therapy) are demanded for the future bioresponsive nanomedicine. (5) Although bioresponsive nanomedicines are more smarted and precise compared with general therapy, specific training of handling this type of novel medicine (e.g., the pH- and Redox-responsive nanomedicine) during manufacture, delivery, storage, and therapeutic process may be required, which may potentially increase the cost for treatment. Therefore, the re-design of current nanomedicine as bioresponsive agents or collaboration between industry and research and could be options for reducing the expense in the quality control and further training.

AUTHOR CONTRIBUTIONS

YM wrote the manuscript with the help and guidance of XL.

REFERENCES

Battistella, C., Callmann, C. E., Thompson, M. P., Yao, S., Yeldandi, A. V., Hayashi, T., et al. (2019). Delivery of immunotherapeutic nanoparticles to tumors via enzyme-directed assembly. *Adv. Healthcare Mater.* 8:1901105. doi: 10.1002/adhm.201901105

Bray, F., Ferlay, J., Soerjomataram, I., Siegel, R. L., Torre, L. A., and Jemal, A. (2018). Global cancer statistics 2018: GLOBOCAN estimates of incidence and mortality worldwide for 36 cancers in 185 countries. *CA Cancer J Clin.* 68, 394–424. doi: 10.3322/caac.21492

Cook, J. A., Gius, D., Wink, D. A., Krishna, M. C., Russo, A., and Mitchell, J. B. (2004). "Oxidative stress, redox, and the tumor microenvironment," in *Seminars in Radiation Oncology* (Elsevier), 14, 259–266. doi: 10.1016/j.semradonc.2004.04.001

Dai, L., Li, X., Duan, X., Li, M., Niu, P., Xu, H., et al. (2019). A pH/ROS cascade-responsive charge-reversal nanosystem with self-amplified drug release for synergistic oxidation-chemotherapy. *Adv. Sci.* 6:1801807. doi: 10.1002/advs.201801807

Denoyer, D., Masaldan, S., La Fontaine, S., and Cater, M. A. (2015). Targeting copper in cancer therapy:'copper that cancer'. *Metallomics* 7, 1459–1476. doi: 10.1039/C5MT00149H

Dienstmann, R., Vermeulen, L., Guinney, J., Kopetz, S., Tejpar, S., and Tabernero, J. (2017). Consensus molecular subtypes and the evolution of precision medicine in colorectal cancer. *Nat Rev Cancer.* 17:79. doi: 10.1038/nrc.2016.126

Flühmann, B., Ntai, I., Borchard, G., Simoens, S., and Mühlebach, S. (2019). Nanomedicines: the magic bullets reaching their target? *Eur. J. Pharm. Sci.* 128, 73–80. doi: 10.1016/j.ejps.2018.11.019

Gao, F., Wu, J., Gao, H., Hu, X., Liu, L., Midgley, A. C., et al. (2020). Hypoxia-tropic nanozymes as oxygen generators for tumor-favoring theranostics. *Biomaterials* 230:119635. doi: 10.1016/j.biomaterials.2019.119635

He, X., Cai, K., Zhang, Y., Lu, Y., Guo, Q., Zhang, Y., et al. (2018). Dimeric prodrug self-delivery nanoparticles with enhanced drug loading and bioreduction responsiveness for targeted Cancer therapy. *ACS Appl. Mater. Interfaces* 10, 39455–39467. doi: 10.1021/acsami.8b09730

He, X., Yu, H., Bao, X., Cao, H., Yin, Q., Zhang, Z., et al. (2016). pH-responsive wormlike micelles with sequential metastasis targeting inhibit lung metastasis of breast cancer. *Adv. Healthcare Mater.* 5, 439–448. doi: 10.1002/adhm.201500626

Hu, D., Zhong, L., Wang, M., Li, H., Qu, Y., Liu, Q., et al. (2019). Perfluorocarbon-loaded and redox-activatable photosensitizing agent with oxygen supply for enhancement of fluorescence/photoacoustic imaging guided tumor photodynamic therapy. *Adv. Funct. Mater.* 29:1806199. doi: 10.1002/adfm.201806199

Kato, Y., Ozawa, S., Miyamoto, C., Maehata, Y., Suzuki, A., Maeda, T., et al. (2013). Acidic extracellular microenvironment and cancer. *Cancer Cell Int.* 13:89. doi: 10.1186/1475-2867-13-89

Kocak, G., Tuncer, C., and Bütün, V. (2017). pH-responsive polymers. *Polym. Chem.* 8, 144–176. doi: 10.1039/C6PY01872F

Li, S., Chen, L., Huang, K., Chen, N., Zhan, Q., Yi, K., et al. (2019). Tumor microenvironment-tailored weakly cell-interacted extracellular delivery platform enables precise antibody release and function. *Adv. Funct. Mater.* 29:1903296. doi: 10.1002/adfm.201970301

Li, W., Zheng, C., Pan, Z., Chen, C., Hu, D., Gao, G., et al. (2016). Smart hyaluronidase-actived theranostic micelles for dual-modal imaging guided photodynamic therapy. *Biomaterials* 101, 10–19. doi: 10.1016/j.biomaterials.2016.05.019

Lin, F., Wen, D., Wang, X., and Mahato, R. I. (2019). Dual responsive micelles capable of modulating miRNA-34a to combat taxane resistance in prostate cancer. *Biomaterials* 192, 95–108. doi: 10.1016/j.biomaterials.2018.10.036

Liu, B., Quan, X., Xu, C., Lv, J., Li, C., Dong, L., et al. (2019a). Lung cancer in young adults aged 35 years or younger: a full-scale analysis and review. *J. Cancer* 10:3553. doi: 10.7150/jca.27490

Liu, C., Wang, D., Zhang, S., Cheng, Y., Yang, F., Xing, Y., et al. (2019b). Biodegradable biomimic copper/manganese silicate nanospheres for chemodynamic/photodynamic synergistic therapy with simultaneous glutathione depletion and hypoxia relief. *ACS Nano* 13, 4267–4277. doi: 10.1021/acsnano.8b09387

Mcatee, C. O., Barycki, J. J., and Simpson, M. A. (2014). "Emerging roles for hyaluronidase in cancer metastasis and therapy," in *Advances in Cancer Research* (Elsevier), 123, 1–34. doi: 10.1016/B978-0-12-800092-2.00001-0

Merchant, N., Nagaraju, G. P., Rajitha, B., Lammata, S., Jella, K. K., Buchwald, Z. S., et al. (2017). Matrix metalloproteinases: their functional role in lung cancer. *Carcinogenesis* 38, 766–780. doi: 10.1093/carcin/bgx063

Midha, A., Dearden, S., and McCormack, R. (2015). EGFR mutation incidence in non-small-cell lung cancer of adenocarcinoma histology: a systematic review and global map by ethnicity (mutMapII). *Am J Cancer Res*. 5, 2892.

Oun, R., Moussa, Y. E., and Wheate, N. J. (2018). The side effects of platinum-based chemotherapy drugs: a review for chemists. *Dalton Trans.* 47, 6645–6653. doi: 10.1039/C8DT00838H

Pernar, C. H., Ebot, E. M., Wilson, K. M., and Mucci, L. A. (2018). The epidemiology of prostate cancer. *Cold Spring Harbor Perspect. Med.* 8:a030361. doi: 10.1101/cshperspect.a030361

Qiao, H., Cui, Z., Yang, S., Ji, D., Wang, Y., Yang, Y., et al. (2017). Targeting osteocytes to attenuate early breast cancer bone metastasis by theranostic upconversion nanoparticles with responsive plumbagin release. *ACS Nano* 11, 7259–7273. doi: 10.1021/acsnano.7b03197

Salinas, C. A., Tsodikov, A., Ishak-Howard, M., and Cooney, K. A. (2014). Prostate cancer in young men: an important clinical entity. *Nat. Rev. Urol.* 11, 317–323. doi: 10.1038/nrurol.2014.91

Saw, P. E., Yao, H., Lin, C., Tao, W., Farokhzad, O. C., and Xu, X. (2019). Stimuli-responsive polymer–prodrug hybrid nanoplatform for multistage siRNA delivery and combination cancer therapy. *Nano Lett.* 19, 5967–5974. doi: 10.1021/acs.nanolett.9b01660

Shen, S., Wu, Y., Li, K., Wang, Y., Wu, J., Zeng, Y., et al. (2018). Versatile hyaluronic acid modified AQ4N-Cu (II)-gossypol infinite coordination polymer nanoparticles: multiple tumor targeting, highly efficient synergistic chemotherapy, and real-time self-monitoring. *Biomaterials* 154, 197–212. doi: 10.1016/j.biomaterials.2017.11.001

Tan, T., and Dent, R. (2018). Triple-Negative Breast Cancer: Clinical Features. *Triple-Negative Breast cancer* (Cham: Springer), 23–32. doi: 10.1007/978-3-319-69980-6_2

Torre, L. A., Siegel, R. L., and Jemal, A. (2016). "Lung cancer statistics," in *Lung Cancer and Personalized Medicine* (Cham: Springer), 893, 1–19. doi: 10.1007/978-3-319-24223-1_1

Van Rijt, S. H., BÃ¡LÃKbas, D. A., Argyo, C., Datz, S., Lindner, M., Eickelberg, O., et al. (2015). Protease-mediated release of chemotherapeutics from mesoporous silica nanoparticles to *ex vivo* human and mouse lung tumors. *ACS Nano* 9, 2377–2389. doi: 10.1021/nn5070343

Ventola, C. L. (2017). Progress in nanomedicine: approved and investigational nanodrugs. *Pharm. Ther.* 42:742.

Wadajkar, A. S., Menon, J. U., Tsai, Y.-S., Gore, C., Dobin, T., Gandee, L., et al. (2013). Prostate cancer-specific thermo-responsive polymer-coated iron oxide nanoparticles. *Biomaterials* 34, 3618–3625. doi: 10.1016/j.biomaterials.2013.01.062

Wang, Y., Liu, X., Deng, G., Sun, J., Yuan, H., Li, Q., et al. (2018). Se@ SiO_2-FA–CuS nanocomposites for targeted delivery of DOX and nano selenium in synergistic combination of chemo-photothermal therapy. *Nanoscale* 10, 2866–2875. doi: 10.1039/C7NR09237G

Wang, Y., Liu, Y., Wu, H., Zhang, J., Tian, Q., and Yang, S. (2019). Functionalized holmium-doped hollow silica nanospheres for combined sonodynamic and hypoxia-activated therapy. *Adv. Funct. Mater.* 29:1805764. doi: 10.1002/adfm.201805764

Xu, X., Saw, P. E., Tao, W., Li, Y., Ji, X., Yu, M., et al. (2017). Tumor microenvironment-responsive multistaged nanoplatform for systemic RNAi and cancer therapy. *Nano Lett.* 17, 4427–4435. doi: 10.1021/acs.nanolett.7b01571

Yang, X., Hu, C., Tong, F., Liu, R., Zhou, Y., Qin, L., et al. (2019a). Tumor microenvironment-responsive dual drug dimer-loaded PEGylated bilirubin nanoparticles for improved drug delivery and enhanced immune-chemotherapy of breast cancer. *Adv. Funct. Mater.* 29:1901896. doi: 10.1002/adfm.201901896

Yang, Y., Tang, J., Zhang, M., Gu, Z., Song, H., Yang, Y., et al. (2019b). Responsively aggregatable sub-6 nm nanochelators induce simultaneous antiangiogenesis and vascular obstruction for enhanced tumor vasculature targeted therapy. *Nano Lett.* 19, 7750–7759. doi: 10.1021/acs.nanolett.9b02691

Yang, Y., Yue, C., Han, Y., Zhang, W., He, A., Zhang, C., et al. (2016). Tumor-responsive small molecule self-assembled nanosystem for simultaneous fluorescence imaging and chemotherapy of lung cancer. *Adv. Funct. Mater.* 26, 8735–8745. doi: 10.1002/adfm.201601369

Yang, Z., Cheng, R., Zhao, C., Sun, N., Luo, H., Chen, Y., et al. (2018). Thermo-and ph-dual responsive polymeric micelles with upper critical solution temperature behavior for photoacoustic imaging-guided synergistic chemo-photothermal therapy against subcutaneous and metastatic breast tumors. *Theranostics* 8:4097. doi: 10.7150/thno.26195

Yu, W., He, X., Yang, Z., Yang, X., Xiao, W., Liu, R., et al. (2019). Sequentially responsive biomimetic nanoparticles with optimal size in combination with checkpoint blockade for cascade synergetic treatment of breast cancer and lung metastasis. *Biomaterials* 217:119309. doi: 10.1016/j.biomaterials.2019.119309

Zhang, Y., Zhang, L., Lin, X., Ke, L., Li, B., Xu, L., et al. (2019). Dual-responsive nanosystem for precise molecular subtyping and resistant reversal of EGFR targeted therapy. *Chem. Eng. J.* 372, 483–495. doi: 10.1016/j.cej.2019.04.140

Zhao, K., Li, D., Xu, W., Ding, J., Jiang, W., Li, M., et al. (2017). Targeted hydroxyethyl starch prodrug for inhibiting the growth and metastasis of prostate cancer. *Biomaterials* 116, 82–94. doi: 10.1016/j.biomaterials.2016.11.030

Zhou, P., Qin, J., Zhou, C., Wan, G., Liu, Y., Zhang, M., et al. (2019). Multifunctional nanoparticles based on a polymeric copper chelator for combination treatment of metastatic breast cancer. *Biomaterials* 195, 86–99. doi: 10.1016/j.biomaterials.2019.01.007

Conflict of Interest: The authors declare that the research was conducted in the absence of any commercial or financial relationships that could be construed as a potential conflict of interest.

frontiers in Chemistry

REVIEW
published: 22 April 2020
doi: 10.3389/fchem.2020.00326

Nanomedicine Particles Associated With Chemical Exchange Saturation Transfer Contrast Agents in Biomedical Applications

Yanlong Jia[1], *Kuan Geng*[2], *Yan Cheng*[1], *Yan Li*[1], *Yuanfeng Chen*[1] *and Renhua Wu*[1]*

[1] *Department of Radiology, Second Affiliated Hospital, Shantou University Medical College, Shantou, China,* [2] *Department of Radiology, The First People's Hospital of Honghe Prefecture, Mengzi, China*

Theranostic agents are particles containing both diagnostic and medicinal agents in a single platform. Theranostic approaches often employ nanomedicine because loading both imaging probes and medicinal drugs onto nanomedicine particles is relatively straightforward, which can simultaneously provide diagnostic and medicinal capabilities within a single agent. Such systems have recently been described as nanotheranostic. Currently, nanotheranostic particles incorporating medicinal drugs are being widely explored with multiple imaging methods, including computed tomography, positron emission tomography, single-photon emission computed tomography, magnetic resonance imaging, and fluorescence imaging. However, most of these particles are metal-based multifunctional nanotheranostic agents, which pose potential toxicity or radiation risks. Hence, alternative non-metallic and biocompatible nanotheranostic agents are urgently needed. Recently, nanotheranostic agents that combine medicinal drugs and chemical exchange saturated transfer (CEST) contrast agents have shown good promise because CEST imaging technology can utilize the frequency-selective radiofrequency pulse from exchangeable protons to indirectly image without requiring metals or radioactive agents. In this review, we mainly describe the fundamental principles of CEST imaging, features of nanomedicine particles, potential applications of nanotheranostic agents, and the opportunities and challenges associated with clinical transformations.

Keywords: chemical exchange saturation transfer (CEST), drug delivery systems, magnetic resonance imaging, nanomedicine, nanoparticles, theranostic

OPEN ACCESS

Edited by:
Dalong Ni,
Shanghai Jiao Tong University School of Medicine, China

Reviewed by:
Zhongmin Tang,
Shenzhen University, China
Zhiwei Shen,
Philips Healthcare, China

***Correspondence:**
Renhua Wu
rhwu@stu.edu.cn

Specialty section:
This article was submitted to Nanoscience, a section of the journal Frontiers in Chemistry

Received: *22 February 2020*
Accepted: *31 March 2020*
Published: *22 April 2020*

Citation:
Jia Y, Geng K, Cheng Y, Li Y, Chen Y and Wu R (2020) Nanomedicine Particles Associated With Chemical Exchange Saturation Transfer Contrast Agents in Biomedical Applications. Front. Chem. 8:326. doi: 10.3389/fchem.2020.00326

INTRODUCTION

Cancer remains one of the most threatening diseases to human health. Currently, the standard therapeutic regimens for cancer include surgery, radiation therapy, and adjuvant chemotherapy (Allhenn et al., 2012). Among these, adjuvant chemotherapy forms a significant part of medicinal strategies, even in cases that are considered unresectable (Li et al., 2016). However, the clinical outcome of chemotherapeutic drugs is discouraging due to their severe side effects, multidrug resistance, and insufficient drug delivery to the tumor areas (Chan et al., 2014a). Creating a platform that can overcome the disadvantages of chemotherapeutic drugs and improve their tumor curative effects is therefore essential.

Nanoparticles (NPs), with their advantages of high surface-area-to-volume ratio, high drug payload capacity, high sensitivity, multimodal signaling capacity, unique size, and fewer adverse effects, are an ideal platform for improving the medicinal effect of drugs on cancer treatment (Pan et al., 2009; Jokerst and Gambhir, 2011; Mao et al., 2016). Additionally, encapsulating medicinal drugs and imaging contrast agents (CAs) into a single platform can enable providing real-time feedback on the pharmacokinetics, monitoring location, and biodistribution of the target site, which can help to predict treatment responses (Lammers et al., 2011). NPs have shown remarkable success as both medicinal and diagnostic agents, thereby showing potential as a single platform capable of combining active or passive drug delivery targeting, environmentally receptive drug release, molecular imaging, and other medicinal functions (Yue et al., 2017). Such systems have collectively been described as nanotheranostics, which is an emerging field that uses nanoscale materials to collect diagnostic information for well-informed cancer therapy, which is especially vital for establishing personalized treatment routines that improve outcomes and reduce side effects (Janib et al., 2010). To develop effective multifunctional nanotheranostic agents, the imaging sensitivity, target accuracy, and drug release control need to be considered. Presently, nanotheranostic particles incorporating medicinal drugs are being extensively explored with multiple imaging methods, including computed tomography (CT), positron emission tomography (PET), single-photon emission computed tomography (SPECT), magnetic resonance imaging (MRI), and fluorescence imaging (Janib et al., 2010). However, each imaging method and theranostic agent have advantages and disadvantages. For example, metal-based (namely, Gd, Fe, or Mn) nanotheranostic agents possess multifunctional features but also increase the potential risks of toxicity. MRI provides limited physiological or biochemical information (Kato and Artemov, 2009; Choi et al., 2011), whereas PET and SPECT can provide early-stage tumor metabolic information but require the injection of high-cost radioactive agents, thus limiting their broad application (Medricka et al., 2019). Furthermore, the intrinsic depth limitation of fluorescence imaging hinders its broad application, despite its high sensitivity (Lian et al., 2019). Hence, alternative non-metallic and biocompatible nanotheranostic agents are urgently needed.

Recently, nanotheranostic agents combining medicinal drugs and chemical exchange saturated transfer (CEST) contrast agents have shown good promise. CEST is a new MRI approach based on the theory of magnetization transfer (MT) and chemical exchange that utilizes a selective radiofrequency (RF) irradiation pulse on exchangeable protons, thus resulting in a loss of the bulk water proton signal intensity (Mao et al., 2016). When detected, the bulk water signal change indirectly reveals information about solute protons. Since Ward and Balaban first proposed it in 2000 (Ward et al., 2000), the CEST approach has gained popularity, because it enables the amplified detection of low-concentration molecules and can be turned "on" and "off" when required by changing the frequency-selective RF irradiation pulses. It can also concurrently identify multiple agents with distinct exchangeable protons because each resonates with a specific frequency (Winter, 2012). Notably, CEST MRI has the potential to supply information on metabolites in biological tissues as well as anatomical features. Furthermore, CEST contrast agents can be precisely adapted to react to a given stimulus (e.g., pH, enzymes, temperature, and metabolite levels) (Langereis et al., 2009; Liu et al., 2012; Daryaei et al., 2017; Zhang et al., 2017; Sinharay et al., 2018), which provides benefits for imaging sensitivity and specificity. Most importantly, CEST contrast agents represent an attractive alternative to metals or radioactive agents, and they show unaltered pharmacokinetic and safety profiles, which are essential for nanotheranostic agent development.

In this review, we mainly described CEST imaging fundamental principles, features of nanomedicine particles, potential application of nanotheranostic agents, and clinical opportunities and challenges.

BASIC PRINCIPLES OF CEST IMAGING

The basic principles of CEST imaging are principally based on the phenomenon of MT and chemical exchange between exchangeable protons and bulk water protons (Dou et al., 2019). A dual pool model is often used to analyze the CEST imaging mechanism (Van Zijl and Yadav, 2011). Typically, pool A represents a solute containing exchangeable protons with a specific frequency offset, and pool B represents a solvent that provides bulk water protons (**Figure 1**). When a frequency-selective RF saturated pulse is applied to pool A, the saturated solute protons in pool A transfer to the bulk water protons of pool B via the chemical exchange process, resulting in the loss of the bulk water signal, which in turn enhances the MRI contrast. Notable, when the solvent concentration in pool B is about 110 M (molar), which is much higher than the pool A solute concentration (in the micromolar or millimolar range), a single saturation transfer would be inadequate to show any perceptible effect on the bulk water protons. However, if the solute protons have a suitably fast exchange rate and lengthy saturation time, this process continually repeats, thus serving as an amplification and eventually becoming evident on the water signal (Mao et al., 2016). That is why CEST imaging enables the indirect amplification of detectable solutes at low concentration. Additionally, this mechanism of CEST allows turning the CEST signal "on" and "off" by simply changing the RF saturation pulse parameters.

Naturally, not all solute protons provide the CEST effect, which requires certain conditions. When pool A is saturated by an RF pulse, a positive exchange rate (K_{AB}) and a reverse exchange rate (K_{BA}) exist in the two pools. Typically, for CEST to occur efficiently, the following condition must be met: $\mathbf{K}_{AB} < \Delta\boldsymbol{\omega}_{AB}$, where $\Delta\boldsymbol{\omega}_{AB}$ is the chemical shift differential between the exchangeable pool A and pool **B** (expressed by $\Delta\boldsymbol{\omega}_{AB} = \boldsymbol{\omega}_A - \boldsymbol{\omega}_B$) (Castelli et al., 2013; Mcmahon and Bulte, 2018). Another condition is $K_{AB} \geq R_{1A}$, that is, the positive exchange rate must be faster than the longitudinal relaxation rate (R_{1A}) of the exchangeable protons. In short, $K_{AB} \geq R_{1A}$ achieves effective saturation, and $\mathbf{K}_{AB} < \Delta\boldsymbol{\omega}_{AB}$ ensures better resolution (Zhou et al., 2004; Zhou and Van Zijl, 2006). Earlier studies showed that

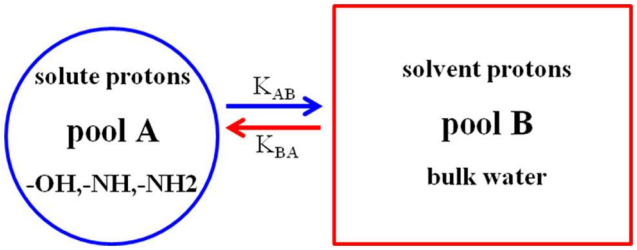

FIGURE 1 | The basic principle of CEST experiment (dual pool model). Pool A (solute) is in exchange with pool B (solvent).

the CEST mechanism is affected by many factors but primarily by the (i) exchange rate; (ii) number of exchangeable protons or concentration; (iii) saturation time and RF pulse power; (iv) pH and temperature; and (v) field strength (Castelli et al., 2013; Daryaei et al., 2017; Mao et al., 2019). Among these factors, the exchange rate most involved in determining the CEST efficiency. A higher exchange rate increases the CEST signal sensitivity. However, if the exchange rate of solute protons is too high or too low, then no CEST signal will appear (Soesbe et al., 2013). When the exchange rate is too high ($\mathbf{K}_{AB} > \Delta\boldsymbol{\omega}_{AB}$), the K_{BA} is increased, and the resolution is insufficient to display the CEST signal. If the exchange rate is too low ($\mathbf{K}_{AB} < \Delta\boldsymbol{\omega}_{AB}$), fewer saturation exchangeable protons transfer to the bulk water protons in a given time, and thus, the CEST signal is too weak for observation. Zhou et al. (2004) reported that as the main magnetic field strength (B_0) increases, both $\Delta\boldsymbol{\omega}$ and the exchange rate increase, while R_{1A} decreases. Enhancing the magnetic field strength may be an effective way to increase the sensitivity of the CEST. Unfortunately, the higher field strength not only dramatically increases the MT effect but also increases the chance of reaching the specific absorption rate (SAR) safety limitation (Simegn et al., 2019). Hence, the effectiveness of a CEST agent may be improved by maximizing both the exchange rate and frequency shift ($\Delta\boldsymbol{\omega}$).

According to the MT ratio asymmetry (MTR_{asym}), the CEST contrast scale can be quantified using the following formula (Wang et al., 2019):

$$\mathrm{MTRasym} = (S - \Delta\omega - S + \Delta\omega)/S_0$$

Where $S -\Delta\boldsymbol{\omega}$ and $S +\Delta\boldsymbol{\omega}$ are the signal intensities obtained by saturation at the negative and positive sides of the CEST spectrum, also called the Z-spectrum, respectively. S_0 is the signal intensity of bulk water without saturation. The Z-spectrum is often used to provide insights into the interpretation of the exchange mechanism and the physics phenomenon. In the Z-spectrum, 0 ppm represents the bulk water maximum saturation point. Typically, most values are offset from water, and those marked as having a positive frequency are situated on the left side of the Z-spectrum, while negative frequencies are situated on the right side. As mentioned above, the uniformity of the B_0 magnetic field is important for CEST imaging. An inhomogeneous B_0 field shifts the Z-spectrum relative to the zero frequency of water, thereby weakening the CEST effect. Therefore, using the water saturation shift reference (WASSR) approach is essential for the shimming correction before scans (Kim et al., 2009).

FEATURES OF NANOMEDICINE PARTICLES

Image-guided drug delivery is essential for personalized medicinal routines. Several studies have shown that some anticancer drugs have CEST effects, while others do not. For example, Li et al. reported that more than 22 anticancer drugs have CEST effects (Li et al., 2016). However, anticancer drugs directly injected into the body for CEST imaging and treatment were limited by the high dose requirements, highly toxic side effects on normal tissues, and the possible CEST signal reduction by physiological or pathological factors. Therefore, a single platform that can combine both CEST contrast agents and medicinal drugs is urgently required. NPs may be an ideal platform owing to several unique features: (i) Their high surface-area-to-volume ratio, which enables the incorporation of various functionalities to reduce adverse effects on the surface, minimal disruption of the drug itself, prolonged drug circulation times, enhanced tumor targeting, and improvement of the medicinal efficacy of drugs. (ii) Their unique small size tends to be selective toward tumor sites, where they rapidly accumulate. This is known as the enhanced permeability and retention (EPR) effect (including leaky vasculature and decreased lymphatic drainage) and provides a higher signal-to-noise ratio in tumors. Further, they offer a (iii) high drug payload capacity and large numbers of exchange protons conjugated on the surface, which allow detecting the amplified CEST signal even at low dosages of contrast agent, and (iv) high biocompatibility and biodegradability without toxic byproducts (Wu et al., 2010; Jokerst and Gambhir, 2011; Mao et al., 2016; Reessing and Szymanski, 2019). In short, NPs offer a promising platform not only to further enhance CEST imaging sensitivity but also to improve the medicinal effect of the drug, while having various other biomedical applications.

POTENTIAL APPLICATIONS OF NANOTHERANOSTIC AGENTS

Nanotheranostic agents offer advantages by combining disease diagnosis and therapy within a single nanoparticle formulation to provide real-time information on the pharmacokinetics, as well as the location and distribution of target sites, but challenges are inevitable. Because nanotheranostics is highly interdisciplinary, involving fields including biomedicine, imaging, chemistry, pharmaceutical sciences, and nanotechnology, its development has been relatively slow compared to that of single diagnostic or medicinal agents (**Figure 2**) (Lammers et al., 2011). Nonetheless, metal-based nanotheranostic agents have been successfully used in pre-clinical and clinical research (Lacerda and Toth, 2017). For example, drug-loaded superparamagnetic NPs and Gd- or Mn-conjugated nanomedicine enable monitoring not only drug delivery but also drug release by observing the change in T_1 and

T_2/T_2^* relaxation times after the drugs were released (Choi et al., 2011; Liu et al., 2019; Ruan et al., 2019). Although metal-based nanotheranostic agents have shown promise for cancer therapy, metal deposition, and potential toxicity risks hinder their future development in clinical use. Furthermore, indirectly detectable MRI signals reflect only the drug carriers rather than the drug itself, and it remains unknown whether the pharmacokinetic profiles of the contrast agents and the liberated drugs correspond well. Therefore, alternative novel contrast methods based on the natural properties of tissues without employing metal or other lanthanides are urgently needed. Non-metal-based CEST MRI contrast agents are promising for monitoring the drug delivery process. Consequently, drug delivery systems, including liposomes, metal, mesoporous silica, and virus NPs, dendrimers or dendritic polymers, micelles, and scaffolds are being co-loaded with medicinal and CEST agents for pre-clinical and clinical research (**Table 1**).

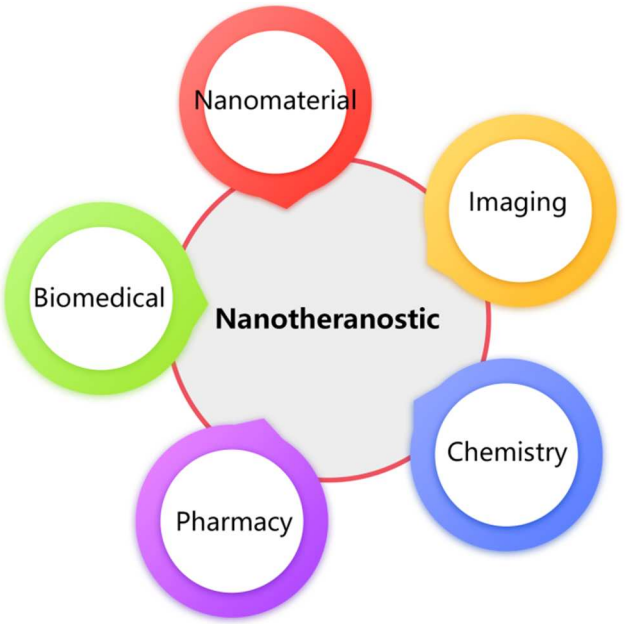

FIGURE 2 | Schematic represent that nanotheranostic was a highly interdisciplinary field, including the biomedical, imaging, chemistry, pharmaceutical sciences, and nanotechnology.

Liposomes

Liposomes are the most versatile particles for delivering nanotheranostic agents, and they have been successfully embedded with medicinal drugs and CEST contrast agents for preclinical and clinical studies. For example, Chan et al. (2014b) loaded the diamagnetic CEST (diaCEST) contrast agent barbituric acid (BA) and the medicinal drug doxorubicin (Dox) into liposomes, which were intravenously injected into the tail of mice to target and treat CT26 colon tumors. They successfully observed an increased nanotheranostic agent accumulation within the tumor areas by CEST MRI (Chan et al., 2014b). Their results showed that the co-treatment with tumor necrosis factor-alpha (TNF-α) had higher treatment potency based on synergistic effects (with an average CEST contrast of 1.5%) than co-treatment without TNF-α (with an average CEST contrast

TABLE 1 | Nanotheranostic agents with the diaCEST effects in preclinical applications.

Nanotheranostic	Parameters (*in vivo*)	Results	Chemical shift	Models	References
BA/DOX-liposome	11.7 T, TR = 5.0 s, TE = 21. 6 ms, B_1 = 4.7 μT T_{sat} = 3 s	Liposomes+ TNF-α group (1.5%) was higher than liposomes (0.4%) group	5.0 ppm	CT26 tumor	(Chan et al., 2014b)
BA/MPP-liposome	11.7 T, TR = 5.0 s, TE = 21. 6 ms, B_1 = 4.7 μT T_{sat} = 3 s	BA/MPP-liposome group was ∼4% (peak at post- 90 min), and liposomal MPP group was ∼1% (peak at post- 30 min)	5.0 ppm	Vaginal mucus	(Yu et al., 2015)
Citicoline-liposome	11.7 T, TR = 5.0 s, TE = 6 ms, B_1 = 2.7 μT Tsat = 3 s, total time = 5 min	Citicoline-liposomal delivery could be directly monitored and quantified via CEST MRI	2.0 ppm	Ischemic stroke	(Liu et al., 2016)
PEG-PAM-PAN@Dox	7.0 T, TR = 6.0 s, TE = 27.6 ms, B_1 = 1.5 μT Tsat = 5 s, total time = 13 min 13 s	Nanomedicine both have the CEST effect and therapy; MTR_{asym} was ∼2.17 vs. ∼0.09% (post-injection vs. pre-)	0.5 ppm	Breast cancer	(Jia et al., 2019)
Olsa-RVRR NPs	11.7 T, TR = 5 s, TE = 3.7 ms, B_1 = 3.6 μT, Tsat = 4 s, total time = 9 min 20 s	Furin-mediated intracellular self-assembly; Olsa-NPs have a good antic-cancer effect and CEST was pH independence	9.8 ppm	HCT116 LoVo	(Yuan et al., 2019)
SA-Dendrimer	11.7 T, TR = 5.5 s, TE = 4.8 ms, B_1 = 3.4 μT, T_{sat} = 2.2 s, time = 6 min 19 s	SA-dendrimers present a promising new nanoplatform for medical applications	9.4 ppm	U87 glioma	(Lesniak et al., 2016)
Dextran-polymers	11.7 T, TR = 5s, TE = 5 ms, B1 = 1.8 μT, T_{sat} = 3 s, total time = 20.7 min	MTR_{asym} of dextran+ TNF-α group was higher than dex150 alone (∼4.2 vs. ∼0%)	1.0 ppm	CT26 tumor	(Chen et al., 2019)
Pem-hydrogels	11.7 T, TR = 5 s, TE = 6 ms, B1 = 3.6 μT, T_{sat} = 3 s	Pem-peptide hydrogels have the potential of monitoring drug distribution and release	5.2 ppm	GL261	(Lock et al., 2017)
PS-PPF scaffold	11.7 T, TR = 6 s, TE = 16.5 ms, B_1 = 4.7 μT, T_{sat} = 4 s	PS-coated 3D-PPF have the potential to monitor drug delivery and drug release	1.8 ppm 3.6 ppm	PC12 cells	(Choi et al., 2011)

BA, Barbituric acid; MPP, mucus-penetrating particles; PEG-b-P(AM-co-AN), polyethylene glycol-polyacrylamide-polyacetonitrile; Dox, doxorubicin; NPs, Nanoparticles; Olsa, Olsalazine; SA, Salicylic acid; Pem, pemetrexed; PS, protamine sulfate; PPF, poly(propylene fumarate); IONP, iron oxide nanoparticles; MONP, manganese oxide nanoparticles.

of 0.4%). BA was very well-suited to be a diaCEST contrast agent due to its large frequency offset from water (peak at 5.0 ppm), high loading into liposomes, and good biocompatibility. In addition, these liposomes were developed based on the formulation of the clinically used DOXIL® and therefore hold potential for clinical translation. Thus, they have implications for future clinical trials on liposomes and other NPs. Recently, Yu et al. designed liposomal-based mucus-penetrating particles (MPPs) loaded with BA to monitor their vaginal distribution and retention by CEST imaging (Yu et al., 2015). Their results demonstrated that the liposomal-based MPPs co-loaded with medicinal drugs could overcome the mucus barrier and provided a uniform distribution and sustained delivery of mucosal drug, thus exhibiting immense potential to improve the monitoring and treatment of diseases. Liu et al. also packaged citicoline in liposomes as a theranostic agent, and citicoline maintained its inherent CEST effect (2 ppm) to image-guide the treatment of ischemic stroke tissue (Liu et al., 2016). Citicoline is a natural supplement used to treat neurodegenerative diseases and possesses good neuroprotective properties. Their results showed that the delivery of liposomal citicoline to the ischemic stroke tissue could be monitored in real time and quantified using CEST MRI without the need for chemical labeling or any extra imaging agents. This not only facilitates rapid clinical translation for citicoline but also provides a useful method for monitoring the effectiveness of citicoline delivery in individual patients to achieve personalized medicine.

As previously mentioned, although liposome-based paramagnetic (PARA) CEST agents have great potential for molecular imaging and drug delivery, their clinical application is limited owing to the potential toxicity of metallic ions. Pan et al. recently developed lipid-encapsulated perfluorocarbon (PFC) NPs carrying PARACEST contrast agents and medicinal drugs, making them an extremely useful platform for molecular imaging and drug delivery and release (Pan et al., 2009). Lipid-encapsulated PFC-based nanoemulsions have high sensitivity and specificity, thus avoiding interference from the surrounding background. The combined application of PFC and the diaCEST contrast agent conjugate as a promising theranostic agent currently being further explored.

Nanoparticles

NPs are promising as nanocarriers that avoid the drawbacks of traditional chemotherapy drugs and enhance their curative effects using image guidance. For example, our research team successfully synthesized a NP [polyethylene glycol-polyacrylamide-polyacetonitrile, PEG-*b*-P (AM-co-AN)] with an inherent CEST MRI signal at 0.5 ppm for treating breast cancer (Jia et al., 2019). The results showed that the nanomedicine loaded with Dox (PEG-PAM-PAN@DOX) could not only treat breast cancer but also enabled monitoring its accumulation in the tumor areas using CEST MRI (**Figure 3**). Additionally, the surface of the PEG-PAM-PAN@DOX prolonged drug exposure time, which is important for improving medicinal indices. However, the frequency offset of PEG-PAM-PAN@DOX was too small and easily confused with the surrounding background. Moreover, the NP had no target and was limited by the drug-load capacity. Recently, Yuan et al. demonstrated that the furin-mediated intracellular self-assembly of Olsalazine (Olsa) NPs enhanced both the CEST MRI signal and the tumor therapy efficacy (Yuan et al., 2019). They conjugated the anticancer drug Olsa with the cell-penetrating peptide RVRR to create a single small-molecule probe Olsa-RVRR for CEST imaging with a large frequency shift (at 9.8 ppm) relative to that of water. Subsequently, Olsa-RVRR enters intracellularly during the furin-mediated self-assembly of Olsa-NPs, which then inhibit the DNA methylation for tumor therapy. *In vitro* and *in vivo* findings show that Olsa-NPs provide a good anti-cancer effect, long drug circulation time, and a pH-independent OlsaCEST signal. The advantage of pH independence would enable applying Olsa in different furin-expressing tumor models without considering the interference of endogenous tumor-derived pH changes. Finally, it is our hope that this study will inspire further attempts to effectively design enzyme-responsive agents that could be also used as a theranostic platform for CEST imaging and cancer therapy.

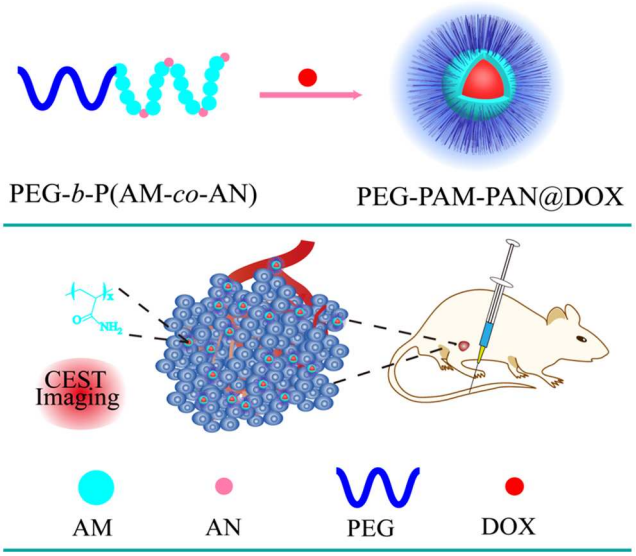

FIGURE 3 | Schematic diagram of the fabrication of PEG-PAM-PAN@DOX for chemotherapy and CEST imaging. Reproduced from Jia et al. (2019) under a Creative Commons Attribution (CC BY) license.

Dendrimers or Dendritic Polymers

Dendritic polymers serve as classical compounds with immense biomedical application potential because of their specific properties (including low polydispersity and rigidity), and their surfaces can be easily modified, making them particularly well-suited for CEST imaging and medicinal agents (Gonawala and Ali, 2017; Mcmahon and Bulte, 2018). Ali et al. reported the feasibility of using dendritic PARACEST agents to simultaneously track the pharmacokinetics of two differently sized NPs *in vivo* (Ali et al., 2009). Snoussi et al. observed that polyuridylic acid [poly(rU)], as single-stranded RNA, could be used for both treatment and CEST imaging (frequency offset

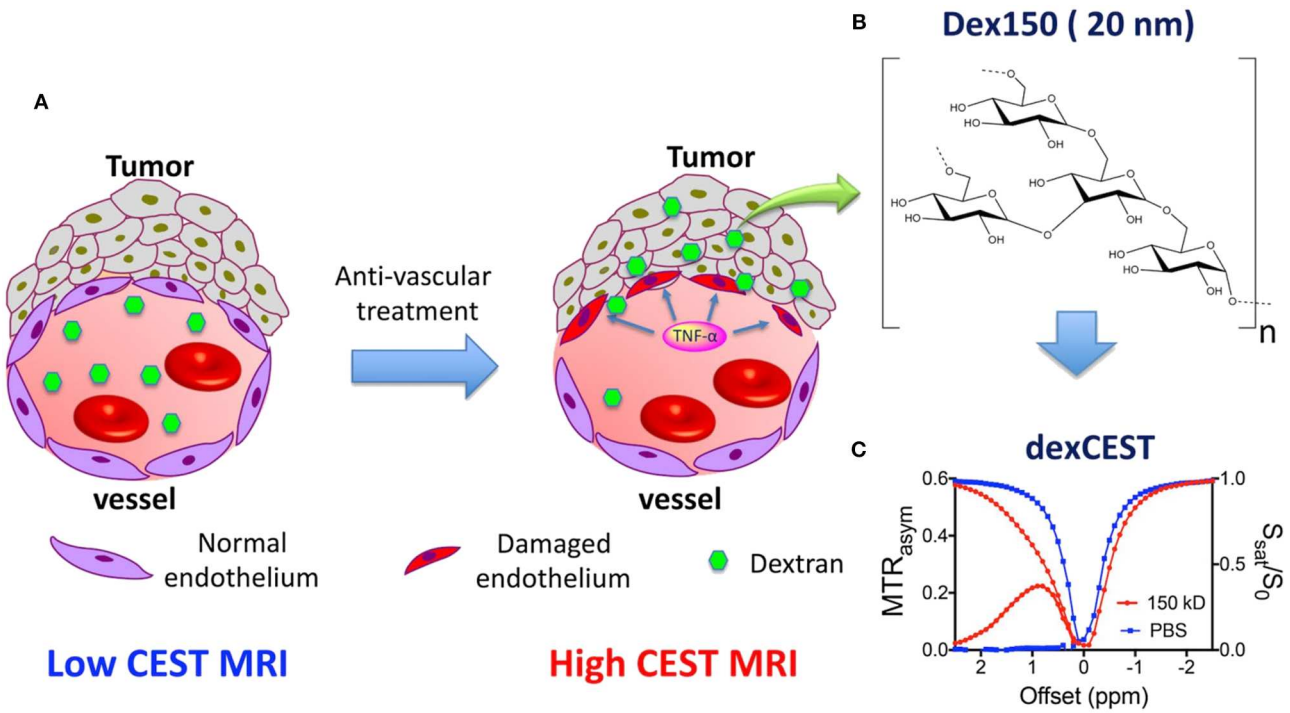

FIGURE 4 | Illustration of using dexCEST MRI to monitor the tumor responses to antivascular therapies. **(A)** Schematic of the effect of antivascular therapies such as TNF-α on the extravasation of dextran molecules. The picture on the left shows a "normal" vessel around tumor cells, consisting of endothelial cells but lacking pericyte coverage. While it has greater permeability than healthy vessels, molecules larger than the pore size cannot easily pass. Upon TNF-α treatment, as shown in the picture on right, tumor endothelial cells are selectively damaged by TNF-α, resulting in an enormous augmentation of vessel permeability and strong extravasation of large molecules in the tumor. **(B)** Chemical structure of Dex150. **(C)** CEST characteristics of Dex150 in PBS as shown by the Z spectrum and MTRasym plot of 3.6 mg/mL mM Dex150 (20 mM per glucose unit or 24 μM per dextran molecule, in 10 mM PBS, pH = 7.3). CEST MRI was performed using a 4-s-long CW radiofrequency pulse (B 1 = 3.6 μT) at 37°C. Reproduced from Chen et al. (2019) with permission from Copyright 2019 John Wiley & Sons.

from water at 6 ppm) (Snoussi et al., 2003). If it associates with cationic dendrimers that could easily cross the anionic barrier of cell membranes, it could provide insights into a detection model for gene therapy and would open a novel avenue for future research that may contribute to designing an ideal *in vivo* gene delivery vehicle. Salicylic acid (SA), a metabolite of aspirin, serves as an anti-inflammatory drug that is widely used in clinics. Most importantly, SA derivatives possess large chemical shifts from water (peak at 9.4 ppm) and can be conjugated to poly(amidoamine) (PAMAM) dendrimers to form a theranostic agent. Lesniak et al. successfully developed SA conjugated to PAMAM dendrimers as a versatile platform for tunable, high performance CEST imaging to monitor its distribution in mice carrying U87 glioblastoma (Lesniak et al., 2016). In the future, SA-based PAMAM dendrimers co-loaded with medicinal drugs that target the specific proteins of brain tumors [e.g., integrins and epidermal growth factor receptor (EGFR)], have the potential to improve drug retention within tumors and to augment the medicinal effects.

Recently, sugar-based polymers have been investigated for CEST MRI detection and theranostic systems (Li et al., 2018; Han and Liu, 2019). Dextran has a well-proven safety profile and is widely used in clinics without the risk of accumulation and toxicity, even at very high doses. Chen et al. demonstrated that dextran, with an inherent CEST signal at 1.0 ppm, can be used to observe tumor permeability changes in response to a vascular-disrupting agent (**Figure 4**) (Chen et al., 2019). By simply monitoring the changes in the dextran CEST signal in the tumor at various time intervals, the beginning of vascular disruption can be determined. The future of nanotheranostic research using dextran-based polymers conjugated with medicinal drugs is very promising. Future research should aim to optimize the time frame for vascular-disrupting agents, which can enhance the tumor uptake of chemotherapeutic agents.

Micelles

Micellar formations are an attractive structure for diagnostic imaging and drug delivery owing to their uniform size, high stability, ease of formation, and good biocompatibility and biodegradation. Further, they enable integrating various functionalities into a single structure. Lock et al. reported a supramolecular strategy to convert pemetrexed (Pem)-peptide to a molecular hydrogelator with an inherent CEST effect at 5.2 ppm for nanotheranostic use in a mouse glioma model (**Figure 5**) (Lock et al., 2017). The concept of self-assembling drug-peptide conjugates permits precisely controlling a high drug load at the molecular design level. Uniform distribution in the tumor was observed by CEST MRI 2 h post-injection. CEST imaging 4 days post-injection still detected the Pem-peptide hydrogel and indicated a larger, more uniform distribution. All these results

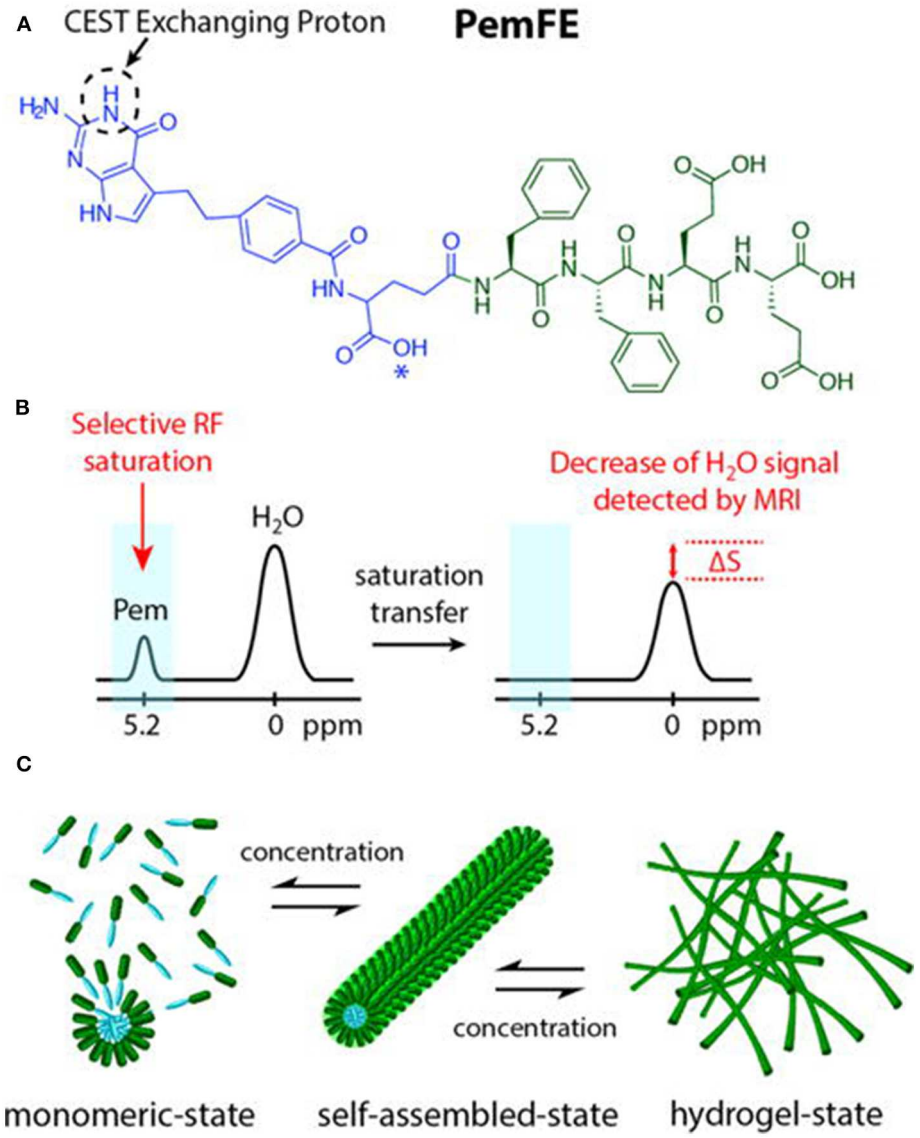

FIGURE 5 | (A) Chemical structure of the studied PemFE molecule with the CEST MRI signal originating from the aromatic amine exchangeable proton on Pem (blue). A possible PemFE structural isomer conjugation site is indicated by an asterisk (*). **(B)** CEST contrast is measured by a decrease in water signal when the selectively saturated 5.2 ppm exchangeable proton is within supramolecular filaments and hydrogels. **(C)** Schematic illustration of the self-assembly of PemFE monomers into filamentous nanostructures that can further entangle into a 3D network for formation of self-supporting hydrogels under suitable conditions (pH, concentration, and ionic strength). Reprinted with permission from Lock et al. (2017). Copyright (2017) American Chemical Society.

demonstrated Pem-peptide nanofiber hydrogels enabled the *in vivo*, non-invasive monitoring of the drug release, drug location, and distribution. This whole hydrogel approach only comprises the designed drug conjugate and water, thus affording a single label-free theranostic platform.

Tissue engineering is a novel biomedical technology offering great advantages for tissue replacement and restoration. Furthermore, it has the potential for loading gene therapy agents into the target cells because of its good biocompatibility and biodegradability. Most importantly, engineered tissues, such as hyaluronic acid (HA) hydrogels and poly(amido amines) (PAA) polyamide materials, contain more mobile exchange protons and can potentially be applied *in vivo* for CEST imaging. Therefore, drug delivery and tissue regeneration based on engineered tissues show great promise in both imaging guidance and disease treatment. HA, as a major component of extracellular matrices, has been used for drug delivery, tissue regeneration, and CEST imaging (Varghese et al., 2009; Shazeeb et al., 2018). Recently, Dou et al. successfully crafted novel HA hydrogels and PAA polymers with unique CEST signals that enabled guidance during the hydrogel optimization process for regenerative medicine, drug delivery applications, or both (Dou et al., 2019). Although the research on CEST properties in engineered tissues is still in its initial stages, the first *in vivo* evidence obtained is essential

for further developing and optimizing these biomaterials and achieving clinical translation.

Scaffold

Using biodegradable 3D poly(propylene fumarate) (PPF) scaffolds as the matrix for drug release is relatively new, but incorporating water-soluble drugs into PPF is challenging because of its hydrophobicity. Nevertheless, Choi et al. successfully used porous PPF scaffolds to load Dox-coated iron oxide nanoparticles (IONPs) and manganese oxide nanoparticles (MONPs) as vehicles for prolonged anti-cancer drug release (Choi et al., 2011). The observed changes in the T_1 and T_2 values caused by Dox-coated IONPs and MONPs indicated the drug release. Interestingly, protamine sulfate (PS), as a small cationic protein with inherent CEST signals at 1.8 ppm (guanidine proton) and 3.6 ppm (amide proton), can be coated on the 3D-PPF scaffold surface to directly monitor the bio-polymer release (e.g., proteins, polypeptides) using CEST MRI without the need for intermediate metallic compounds. These findings indicate a novel system that can monitor drug release, growth factors, and cytokines, which is particularly important for tailoring personalized treatments. Additionally, PS has two relatively large labile groups that cause a chemical shift, which make PS very suitable for use in the ratiometric CEST approach, as it reduces the compounding effects derived from the concentration of the contrast agent. PS thus has good prospects for wide application (Chen et al., 2017).

Virus Nanoparticles

The architecture of virus NPs contains interior and exterior areas, which are easily modified, either chemically or genetically, to attach differentiated specific targeting groups. The natural cell-targeting capability of virus NPs enables carrying CEST MRI contrast agents and chemotherapeutic drugs to diseased tissues by altering the virus biology (Wu et al., 2010). For example, Vasalatiy et al. successfully designed viral-based PARACEST agents for molecular targeted imaging (Vasalatiy et al., 2008). As viral-based CEST NPs develop in the future, they are expected to potentially conjugate medicinal genes or targeted drugs for gene- or cell-level therapy. They could thus become an interesting platform for nanotheranostic agents.

Mesoporous Silica Nanoparticles

Mesoporous silica nanoparticles (MSNs), which have uniform mesopores, good biocompatibility, and large surface areas, can

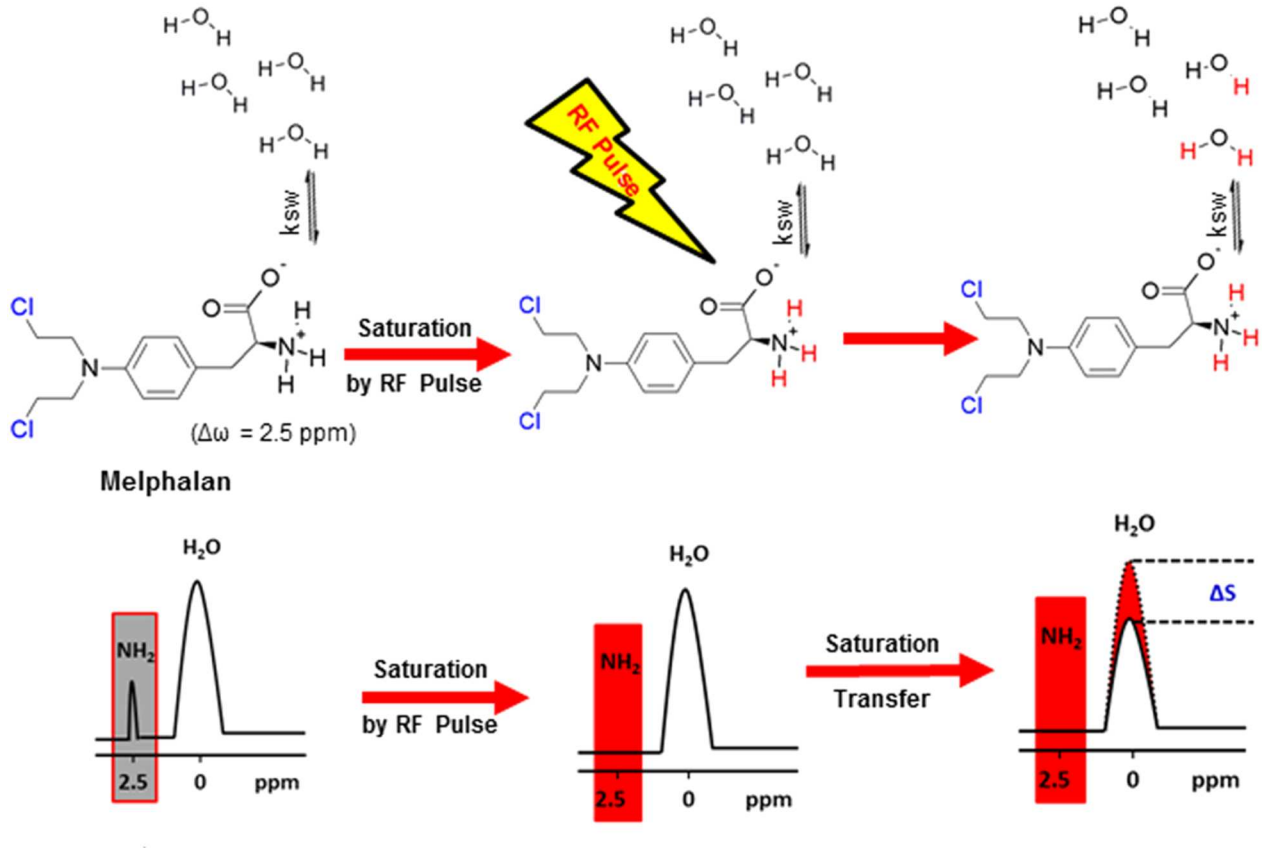

FIGURE 6 | Mechanism of CEST MRI contrast generation by melphalan. Saturated melphalan amine protons are highlighted in red. The biologically active site of melphalan is highlighted in blue (the Cl -leaves for DNA alkylation by the activated carbocation to occur). Ksw is the exchange rate constant of the labile melphalan protons with exchangeable protons of endogenous biological molecules represented by bulk water protons. Reprinted with permission from Ngen et al. (2016). Copyright (2016) American Chemical Society.

serve as a nanocarrier for ion complexes, and MSNPs have been extensively used in preclinical applications. Ferrauto et al. demonstrated that PARACEST agents anchored on the surface of MSNs had a higher sensitivity than those anchored on dendrimers or micelles (Ferrauto et al., 2014). However, these findings were demonstrated only in *in vitro* studies. Thus far, *in vivo* applications have been constrained by the complex synthesis of the PARACEST agents and the potential toxic effects of metal. Undeniably, however, the outer surface and inner pores of the silica framework afford large spaces that can potentially attach specific drug payloads and imaging probes. Thus, MSNs could finally fulfill the multimodal functions of drug release and imaging diagnosis in the future.

Drugs With CEST Effects

As mentioned above, drugs have inherent CEST effects. For example, Ngen et al. demonstrated that the DNA alkylating anti-cancer agent (melphalan) could be directly monitored by CEST MRI to observe its *in vitro* medicinal response without the need to conjugate or modify the drug (Ngen et al., 2016). This is extremely important because even a small modification can significantly reduce drug activity or change its target. Their results demonstrated that melphalan had an inherent CEST signal at 2.5 ppm, which was pH-dependent and peaked at a pH of 6.2 (**Figure 6**). Upon cell death, the cellular pH decreased from 7.4 to 6.4, thus amplifying the melphalan CEST signal, making melphalan very suitable for the CEST MRI monitoring of its medicinal response. Additionally, 24 h after treatment with melphalan, the CEST signal peak at 3.3 ppm broadened. It was speculated that this broadening was caused by melphalan entering the cells and interacting with the DNA to form melphalan-DNA adducts. However, direct *in vivo* application of melphalan is still limited and needs further study.

OPPORTUNITIES AND CHALLENGES

Opportunities

Feasibly, nanotheranostic agents containing both CEST imaging contrast agents and medicinal drugs on a single platform can enable early disease detection and improving the treatment efficacy. They can provide the ability to rapidly assess and modify treatments to address the requirements of individual patients, while also prompting the further development nanotheranostic agents. Concurrently, many nanocarriers (e.g., liposomes and micelles) have been approved for clinical trials, and CEST MRI has been successfully transferred to clinical applications (Mao et al., 2016; Lin et al., 2018). All these findings indicate that nanotheranostic agents are a very promising way to improve people's health. In addition, in excess of 45 nanoparticulate drug formulations have gained clinical approval, and Phase I–III clinical trials are currently being conducted on at least 200 products (Davis et al., 2008). Tailoring some of these formulations into nanotheranostic systems using the CEST MRI approach will enable directly using this approach in clinical practice to prioritize patients and facilitate personalized medicine.

Challenges

Although nanotheranostic agents show promise in both CEST imaging and therapy, they still present various challenges: (i) Metal-based nanotheranostic agents are toxic, are easily recognized by the reticuloendothelial system (RES), and are rapidly cleared out. (ii) The dosage and circulation time for *in vivo* application must be reasonably weighted because imaging diagnosis has a short duration and a low-dosage design, while medicinal applications require a longer circulation duration and higher dosage. (iii) The pharmacokinetic profiles of the imaging agents and the liberated drugs currently do not match. (iv) Theoretically, nanotheranostic agents are biodegradable, but the potential hazards of long-duration body retention are unknown. (v) Finally, the detailed interpretation of the CEST signal and its clinical application may be affected by many factors, such as B_1 and B_0 inhomogeneities, long scan duration, and high power deposition, thus highlighting the need for a unified standard (Van Zijl and Yadav, 2011; Vinogradov et al., 2013; Ferrauto et al., 2016). Hence, these issues must be addressed to further develop nanotheranostic agents and to realize their clinical transformation.

CONCLUSIONS

Nanotheranostic agents combining the complementary advantages of CEST MRI and NPs have great potential for transformation into clinical applications. Although the exact nanotheranostic mechanisms are still not completely understood, and although various challenges must still be resolved, improving the MRI hardware, image acquisition schemes, and nanotechnology may lead to a promising future for nanotheranostics. Undeniably, future advancements require multidisciplinary cooperation in the fields of chemistry, nanotechnology, pharmaceutical sciences, and biomedical imaging. Medicinal drugs using real-time imaging-guided visualization play an important role in individualized treatment and appear to be a promising approach to completely understanding the disease components, processes, dynamics, and therapies at the molecular level. In summary, in the near future, interest in possible applications of this method is very likely to increase, and its further development will expand its applicability.

AUTHOR CONTRIBUTIONS

YJ and RW conceived and designed the project. YJ contributed to the writing and editing of the final review. KG, YCheng, YL, and YChen conducted the literature research. Renhua Wu critically revised the manuscript. All the authors approved the final draft.

FUNDING

This work was supported by the National Natural Science Foundation of China (Grant no. 31870981), Grant for Key Disciplinary Project of Clinical Medicine under the Guangdong High-level University Development Program (Grant no. 002-18119101).

REFERENCES

Ali, M. M., Yoo, B., and Pagel, M. D. (2009). Tracking the relative *in vivo* pharmacokinetics of nanoparticles with PARACEST MRI. *Mol. Pharm.* 6, 1409–1416. doi: 10.1021/mp900040u

Allhenn, D., Boushehri, M. A., and Lamprecht, A. (2012). Drug delivery strategies for the treatment of malignant gliomas. *Int. J. Pharm.* 436, 299–310. doi: 10.1016/j.ijpharm.2012.06.025

Castelli, D. D., Terreno, E., Longo, D., and Aime, S. (2013). Nanoparticle-based chemical exchange saturation transfer (CEST) agents. *NMR Biomed.* 26, 839–849. doi: 10.1002/nbm.2974

Chan, K. W., Bulte, J. W., and Mcmahon, M. T. (2014a). Diamagnetic chemical exchange saturation transfer (diaCEST) liposomes: physicochemical properties and imaging applications. *Wiley Interdiscip. Rev. Nanomed. Nanobiotechnol.* 6, 111–124. doi: 10.1002/wnan.1246

Chan, K. W., Yu, T., Qiao, Y., Liu, Q., Yang, M., Patel, H., et al. (2014b). A diaCEST MRI approach for monitoring liposomal accumulation in tumors. *J. Control. Release* 180, 51–59. doi: 10.1016/j.jconrel.2014.02.005

Chen, H., Liu, D., Li, Y., Xu, X., Xu, J., Yadav, N. N., et al. (2019). CEST MRI monitoring of tumor response to vascular disrupting therapy using high molecular weight dextrans. *Magn. Reson. Med.* 82, 1471–1479. doi: 10.1002/mrm.27818

Chen, M. M., Chen, C. Y., Shen, Z. W., Zhang, X. L., Chen, Y. Z., Lin, F. F., et al. (2017). Extracellular pH is a biomarker enabling detection of breast cancer and liver cancer using CEST MRI. *Oncotarget* 8, 45759–45767. doi: 10.18632/oncotarget.17404

Choi, J., Kim, K., Kim, T., Liu, G., Bar-Shir, A., Hyeon, T., et al. (2011). Multimodal imaging of sustained drug release from 3-D poly(propylene fumarate) (PPF) scaffolds. *J. Control. Release* 156, 239–245. doi: 10.1016/j.jconrel.2011.06.035

Daryaei, I., Jones, K. M., and Pagel, M. D. (2017). Detection of DT-diaphorase enzyme with a ParaCEST MRI contrast agent. *Chemistry* 23, 6514–6517. doi: 10.1002/chem.201700721

Davis, M. E., Chen, Z. G., and Shin, D. M. (2008). Nanoparticle therapeutics: an emerging treatment modality for cancer. *Nat. Rev. Drug. Discov.* 7, 771–782. doi: 10.1038/nrd2614

Dou, W., Lin, C. E., Ding, H., Shen, Y., Dou, C., Qian, L., et al. (2019). Chemical exchange saturation transfer magnetic resonance imaging and its main and potential applications in pre-clinical and clinical studies. *Quant. Imaging. Med. Surg.* 9, 1747–1766. doi: 10.21037/qims.2019.10.03

Ferrauto, G., Carniato, F., Tei, L., Hu, H., Aime, S., and Botta, M. (2014). MRI nanoprobes based on chemical exchange saturation transfer: Ln(III) chelates anchored on the surface of mesoporous silica nanoparticles. *Nanoscale* 6, 9604–9607. doi: 10.1039/C4NR02753A

Ferrauto, G., Delli Castelli, D., Di Gregorio, E., Terreno, E., and Aime, S. (2016). LipoCEST and cellCEST imaging agents: opportunities and challenges. *Wiley Interdiscip. Rev. Nanomed. Nanobiotechnol.* 8, 602–618. doi: 10.1002/wnan.1385

Gonawala, S., and Ali, M. M. (2017). Application of dendrimer-based nanoparticles in glioma imaging. *J. Nanomed. Nanotechnol.* 8:444. doi: 10.4172/2157-7439.1000444

Han, Z., and Liu, G. (2019). Sugar-based biopolymers as novel imaging agents for molecular magnetic resonance imaging. *Wiley Interdiscip. Rev. Nanomed. Nanobiotechnol.* 11:e1551. doi: 10.1002/wnan.1551

Janib, S. M., Moses, A. S., and Mackay, J. A. (2010). Imaging and drug delivery using theranostic nanoparticles. *Adv. Drug. Deliv. Rev.* 62, 1052–1063. doi: 10.1016/j.addr.2010.08.004

Jia, Y., Wang, C., Zheng, J., Lin, G., Ni, D., Shen, Z., et al. (2019). Novel nanomedicine with a chemical-exchange saturation transfer effect for breast cancer treatment *in vivo*. *J. Nanobiotechnol.* 17:123. doi: 10.1186/s12951-019-0557-0

Jokerst, J. V., and Gambhir, S. S. (2011). Molecular imaging with theranostic nanoparticles. *Acc. Chem. Res.* 44, 1050–1060. doi: 10.1021/ar200106e

Kato, Y., and Artemov, D. (2009). Monitoring of release of cargo from nanocarriers by MRI/MR spectroscopy (MRS): significance of T2/T2* effect of iron particles. *Magn. Reson. Med.* 61, 1059–1065. doi: 10.1002/mrm.21939

Kim, M., Gillen, J., Landman, B. A., Zhou, J. Y., and Van Zijl, P. C. M. (2009). Water Saturation Shift Referencing (WASSR) for Chemical Exchange Saturation Transfer (CEST) experiments. *Magn. Reson. Med.* 61, 1441–1450. doi: 10.1002/mrm.21873

Lacerda, S., and Toth, E. (2017). Lanthanide complexes in molecular magnetic resonance imaging and theranostics. *ChemMedChem* 12, 883–894. doi: 10.1002/cmdc.201700210

Lammers, T., Aime, S., Hennink, W. E., Storm, G., and Kiessling, F. (2011). Theranostic nanomedicine. *Acc. Chem. Res.* 44, 1029–1038. doi: 10.1021/ar200019c

Langereis, S., Keupp, J., Van Velthoven, J. L., De Roos, I. H., Burdinski, D., Pikkemaat, J. A., et al. (2009). A temperature-sensitive liposomal 1H CEST and 19F contrast agent for MR image-guided drug delivery. *J. Am. Chem. Soc.* 131, 1380–1381. doi: 10.1021/ja8087532

Lesniak, W. G., Oskolkov, N., Song, X., Lal, B., Yang, X., Pomper, M., et al. (2016). Salicylic acid conjugated dendrimers are a tunable, high performance CEST MRI nanoplatform. *Nano. Lett.* 16, 2248–2253. doi: 10.1021/acs.nanolett.5b04517

Li, Y., Chen, H., Xu, J., Yadav, N. N., Chan, K. W., Luo, L., et al. (2016). CEST theranostics: label-free MR imaging of anticancer drugs. *Oncotarget* 7, 6369–6378. doi: 10.18632/oncotarget.7141

Li, Y., Qiao, Y., Chen, H., Bai, R., Staedtke, V., Han, Z., et al. (2018). Characterization of tumor vascular permeability using natural dextrans and CEST MRI. *Magn. Reson. Med.* 79, 1001–1009. doi: 10.1002/mrm.27014

Lian, X., Wei, M. Y., and Ma, Q. (2019). Nanomedicines for near-infrared fluorescent lifetime-based bioimaging. *Front. Bioeng. Biotechnol.* 7:386. doi: 10.3389/fbioe.2019.00386

Lin, G., Zhuang, C., Shen, Z., Xiao, G., Chen, Y., Shen, Y., et al. (2018). APT weighted MRI as an effective imaging protocol to predict clinical outcome after acute ischemic stroke. *Front. Neurol.* 9:901. doi: 10.3389/fneur.2018.00901

Liu, C. Y., Ewert, K. K., Wang, N., Li, Y. L., Safinya, C. R., and Qiao, W. H. (2019). A multifunctional lipid that forms contrast-agent liposomes with dual-control release capabilities for precise MRI-guided drug delivery. *Biomaterials* 221:119412. doi: 10.1016/j.biomaterials.2019.119412

Liu, G., Moake, M., Har-El, Y. E., Long, C. M., Chan, K. W., Cardona, A., et al. (2012). *In vivo* multicolor molecular MR imaging using diamagnetic chemical exchange saturation transfer liposomes. *Magn. Reson. Med.* 67, 1106–1113. doi: 10.1002/mrm.23100

Liu, H., Jablonska, A., Li, Y., Cao, S., Liu, D., Chen, H., et al. (2016). Label-free CEST MRI detection of citicoline-liposome drug delivery in ischemic stroke. *Theranostics* 6, 1588–1600. doi: 10.7150/thno.15492

Lock, L. L., Li, Y., Mao, X., Chen, H., Staedtke, V., Bai, R., et al. (2017). One-component supramolecular filament hydrogels as theranostic label-free magnetic resonance imaging agents. *ACS. Nano* 11, 797–805. doi: 10.1021/acsnano.6b07196

Mao, X., Xu, J., and Cui, H. (2016). Functional nanoparticles for magnetic resonance imaging. *Wiley Interdiscip. Rev. Nanomed. Nanobiotechnol.* 8, 814–841. doi: 10.1002/wnan.1400

Mao, Y., Zhuang, Z., Chen, Y., Zhang, X., Shen, Y., Lin, G., et al. (2019). Imaging of glutamate in acute traumatic brain injury using chemical exchange saturation transfer. *Quant. Imaging. Med. Surg.* 9, 1652–1663. doi: 10.21037/qims.2019.09.08

Mcmahon, M. T., and Bulte, J. W. M. (2018). Two decades of dendrimers as versatile MRI agents: a tale with and without metals. *Wiley Interdiscip. Rev. Nanomed. Nanobiotechnol.* 10:e1496. doi: 10.1002/wnan.1496

Medricka, M., Janeckova, J., Koranda, P., Buriankova, E., and Bachleda, P. (2019). ^{18}F-FDG PET/CT and (99m)Tc-HMPAO-WBC SPECT/CT effectively contribute to early diagnosis of infection of arteriovenous graft for hemodialysis. *Biomed. Pap. Med. Fac. Univ. Palacky. Olomouc. Czech. Repub.* 163, 341–348. doi: 10.5507/bp.2019.025

Ngen, E. J., Bar-Shir, A., Jablonska, A., Liu, G., Song, X., Ansari, R., et al. (2016). Imaging the DNA alkylator melphalan by CEST MRI: an advanced approach to theranostics. *Mol. Pharm.* 13, 3043–3053. doi: 10.1021/acs.molpharmaceut.6b00130

Pan, D., Lanza, G. M., Wickline, S. A., and Caruthers, S. D. (2009). Nanomedicine: perspective and promises with ligand-directed molecular imaging. *Eur. J. Radiol.* 70, 274–285. doi: 10.1016/j.ejrad.2009.01.042

Reessing, F., and Szymanski, W. (2019). Following nanomedicine activation with magnetic resonance imaging: why, how, and what's next? *Curr. Opin. Biotechnol.* 58, 9–18. doi: 10.1016/j.copbio.2018.10.008

Ruan, L. P., Chen, W., Wang, R. N., Lu, J., and Zink, J. I. (2019). Magnetically stimulated drug release using nanoparticles capped by self-assembling peptides. *ACS. Appl. Mater. Interfaces* 11, 43835–43842. doi: 10.1021/acsami.9b13614

Shazeeb, M. S., Corazzini, R., Konowicz, P. A., Fogle, R., Bangari, D. S., Johnson, J., et al. (2018). Assessment of *in vivo* degradation profiles of hyaluronic acid hydrogels using temporal evolution of chemical exchange saturation transfer (CEST) MRI. *Biomaterials* 178, 326–338. doi: 10.1016/j.biomaterials.2018.05.037

Simegn, G. L., Van Der Kouwe, A. J. W., Robertson, F. C., Meintjes, E. M., and Alhamud, A. (2019). Real-time simultaneous shim and motion measurement and correction in glycoCEST MRI using double volumetric navigators (DvNavs). *Magn. Reson. Med.* 81, 2600–2613. doi: 10.1002/mrm.27597

Sinharay, S., Randtke, E. A., Howison, C. M., Ignatenko, N. A., and Pagel, M. D. (2018). Detection of enzyme activity and inhibition during studies in solution, *in vitro* and *in vivo* with CatalyCEST MRI. *Mol. Imaging. Biol.* 20, 240–248. doi: 10.1007/s11307-017-1092-8

Snoussi, K., Bulte, J. W., Gueron, M., and Van Zijl, P. C. (2003). Sensitive CEST agents based on nucleic acid imino proton exchange: detection of poly(rU) and of a dendrimer-poly(rU) model for nucleic acid delivery and pharmacology. *Magn. Reson. Med.* 49, 998–1005. doi: 10.1002/mrm.10463

Soesbe, T. C., Wu, Y., and Dean Sherry, A. (2013). Advantages of paramagnetic chemical exchange saturation transfer (CEST) complexes having slow to intermediate water exchange properties as responsive MRI agents. *NMR Biomed.* 26, 829–838. doi: 10.1002/nbm.2874

Van Zijl, P. C., and Yadav, N. N. (2011). Chemical exchange saturation transfer (CEST): what is in a name and what isn't? *Magn. Reson. Med.* 65, 927–948. doi: 10.1002/mrm.22761

Varghese, O. P., Sun, W., Hilborn, J., and Ossipov, D. A. (2009). *In situ* cross-linkable high molecular weight hyaluronan-bisphosphonate conjugate for localized delivery and cell-specific targeting: a hydrogel linked prodrug approach. *J. Am. Chem. Soc.* 131, 8781–8783. doi: 10.1021/ja902857b

Vasalatiy, O., Gerard, R. D., Zhao, P., Sun, X., and Sherry, A. D. (2008). Labeling of adenovirus particles with PARACEST agents. *Bioconjug. Chem.* 19, 598–606. doi: 10.1021/bc7002605

Vinogradov, E., Sherry, A. D., and Lenkinski, R. E. (2013). CEST: from basic principles to applications, challenges and opportunities. *J. Magn. Reson.* 229, 155–172. doi: 10.1016/j.jmr.2012.11.024

Wang, R., Wang, C., Dai, Z., Chen, Y., Shen, Z., Xiao, G., et al. (2019). An amyloid-beta targeting chemical exchange saturation transfer probe for *in vivo* detection of Alzheimer's disease. *ACS. Chem. Neurosci.* 10, 3859–3867. doi: 10.1021/acschemneuro.9b00334

Ward, K. M., Aletras, A. H., and Balaban, R. S. (2000). A new class of contrast agents for MRI based on proton chemical exchange dependent saturation transfer (CEST). *J. Magn. Reson.* 143, 79–87. doi: 10.1006/jmre.1999.1956

Winter, P. M. (2012). Magnetic resonance chemical exchange saturation transfer imaging and nanotechnology. *Wiley Interdiscip. Rev. Nanomed. Nanobiotechnol.* 4, 389–398. doi: 10.1002/wnan.1167

Wu, Y., Evbuomwan, M., Melendez, M., Opina, A., and Sherry, A. D. (2010). Advantages of macromolecular to nanosized chemical-exchange saturation transfer agents for MRI applications. *Future. Med. Chem.* 2, 351–366. doi: 10.4155/fmc.09.152

Yu, T., Chan, K. W., Anonuevo, A., Song, X., Schuster, B. S., Chattopadhyay, S., et al. (2015). Liposome-based mucus-penetrating particles (MPP) for mucosal theranostics: demonstration of diamagnetic chemical exchange saturation transfer (diaCEST) magnetic resonance imaging (MRI). *Nanomedicine* 11, 401–405. doi: 10.1016/j.nano.2014.09.019

Yuan, Y., Zhang, J., Qi, X., Li, S., Liu, G., Siddhanta, S., et al. (2019). Furin-mediated intracellular self-assembly of olsalazine nanoparticles for enhanced magnetic resonance imaging and tumour therapy. *Nat. Mater.* 18, 1376–1383. doi: 10.1038/s41563-019-0503-4

Yue, L., Wang, J., Dai, Z., Hu, Z., Chen, X., Qi, Y., et al. (2017). pH-responsive, self-sacrificial nanotheranostic agent for potential in vivo and in vitro dual modal MRI/CT imaging, real-time, and in situ monitoring of cancer therapy. *Bioconjug. Chem.* 28, 400–409. doi: 10.1021/acs.bioconjchem.6b00562

Zhang, L., Martins, A. F., Zhao, P., Wu, Y., Tircso, G., and Sherry, A. D. (2017). Lanthanide-based T2ex and CEST complexes provide insights into the design of pH sensitive MRI agents. *Angew. Chem. Int. Ed. Engl.* 56, 16626–16630. doi: 10.1002/anie.201707959

Zhou, J. Y., and Van Zijl, P. C. M. (2006). Chemical exchange saturation transfer imaging and spectroscopy. *Prog. Nucl. Magn. Reson. Spectrosc.* 48, 109–136. doi: 10.1016/j.pnmrs.2006.01.001

Zhou, J. Y., Wilson, D. A., Sun, P. Z., Klaus, J. A., and Van Zijl, P. C. M. (2004). Quantitative description of proton exchange processes between water and endogenous and exogenous agents for WEX, CEST, and APT experiments. *Magn. Reson. Med.* 51, 945–952. doi: 10.1002/mrm.20048

Conflict of Interest: The authors declare that the research was conducted in the absence of any commercial or financial relationships that could be construed as a potential conflict of interest.

frontiers in Chemistry

MINI REVIEW
published: 21 August 2020
doi: 10.3389/fchem.2020.00732

Reactive Oxygen Species (ROS)-Responsive Nanomedicine for Solving Ischemia-Reperfusion Injury

Weiyu Chen[1,2] *and Deling Li*[3]*

[1] The Fourth Affiliated Hospital, Zhejiang University School of Medicine, Yiwu, China, [2] Molecular Imaging Program at Stanford, Department of Radiology, Stanford University, Stanford, CA, United States, [3] Department of Neurosurgery, Beijing Tiantan Hospital, Capital Medical University, Beijing, China

Ischemia-reperfusion injury (IRI) is a severe condition for most organs, which could occur in various tissues including brain, heart, liver, and kidney, etc. As one of the major hazards, reactive oxygen species (ROS) is excessively generated after IRI, which causes severe damage inside tissues and further induces the following injury via inflammatory response. However, current medical strategies could not thoroughly diagnose and prevent this disease, eventually leading to severe sequelae by missing the best time point for therapy. In the past decade, various nanoparticles that could selectively respond to ROS have been developed and applied in IRI. These advanced nanomedicines have shown efficient performance in detecting and treating a series of IRI (e.g., acute kidney injury, acute liver injury, and ischemic stroke, etc.), which are well-summarized in the current review. In addition, the nano-platforms (e.g., anti-IL-6 antibody, rapamycin, and hydrogen sulfide delivering nanoparticles, etc.) for preventing IRI during organ transplantation have also been included. Moreover, the development and challenges of ROS-responsive nanomedicine are systematically discussed for guiding the future direction.

Keywords: bioresponsive nanomedicine, ischemia-reperfusion injury, reactive oxygen species, organ transplantation, nanoparticles

OPEN ACCESS

Edited by:
Dawei Jiang,
Huazhong University of Science and Technology, China

Reviewed by:
Zhilei Ge,
Shanghai Jiao Tong University, China
Weijun Wei,
University of Wisconsin-Madison, United States

***Correspondence:**
Deling Li
ttyyneuroli@126.com

Specialty section:
This article was submitted to Nanoscience, a section of the journal Frontiers in Chemistry

Received: *25 June 2020*
Accepted: *15 July 2020*
Published: *21 August 2020*

Citation:
Chen W and Li D (2020) Reactive Oxygen Species (ROS)-Responsive Nanomedicine for Solving Ischemia-Reperfusion Injury. Front. Chem. 8:732. doi: 10.3389/fchem.2020.00732

INTRODUCTION

Instead of restoring and saving tissues from hypoxic conditions, the reperfusion of blood would cause severe damage to those ischemic organs via oxidative stress, which is referred as ischemia-reperfusion injury (IRI). Normally, IRI is strongly associated with a series of diseases, such as the infraction of organs, including stroke, renal infraction, and trauma, etc. Notably, the concern of IRI often affects the best timing of reperfusion, the most effective therapy for treating ischemic disease, for example, the acute myocardial infarction (AMI) (Benjamin et al., 2017). Moreover, the acute myocardial IRI can lead to coronary heart disease (CHD) that accounts for over 366,800 deaths per year and more cases with disability (Benjamin et al., 2018).

In addition to the interruption of cellular homeostasis that could damage cells via apoptotic and autophagic pathways, ischemia-reperfusion would bring great oxidative stress and further injure organs via the generation of redox free radicals, for instance, reactive oxygen species (ROS) (Zhang et al., 2007). Although appropriate ROS is essential for intracellular signaling and immune response against pathogens, the excessive ROS can not be entirely scavenged by cellular antioxidants, which would mediate the severe damage on cells by destroying organelle, cell membrane, and nuclei DNA (Nita and Grzybowski, 2016). To protect injured tissues and prevent further damage of organs during transplantation, the administration of antioxidant reagents for scavenging ROS has been

widely applied, such as edaravone (Fu et al., 2020). However, the usage of edaravone is generally accompanied by a series of side effects ranging from bruising to skin inflammation or rash, leading to many concerns and demands of new types of antioxidant reagents.

In the comparison of traditional drugs, the novel nanomedicine has been gifted with more functional features including high cargos loading, specific targeting, and *in-situ* theranostics (Chen et al., 2018a,b; Qiao et al., 2020). With these highly controllable functions, precision therapy could be achieved. As a representative, paclitaxel albumin-bound nanoparticles (Abraxane), the FDA-approved nanomedicine has been widely employed for fighting cancer. More importantly, various nanoparticles demonstrate excellent redox activity by trapping free radicals or self-oxidation (Ni et al., 2019). Notably, an increasing number of nano-antioxidants [e.g., Mo-based polyoxometalate nanoclusters (POM), framework nucleic acid (FNA), hydrophobic ceria nanoparticles (NPs), etc.] were recruited as ROS scavenger in dealing with various diseases associate with IRI (e.g., acute kidney injury, acute liver injury, and ischemic stroke, etc.). Here, those advanced ROS-responsive nanoparticles along with antioxidants delivering nano-platforms, have been summarized in the current review to highlight the recent innovation of nanomedicine in dealing with IRI associated diseases. Moreover, the perspective of future development and facing challenges are systemically discussed.

IRI AND ITS THREATS

Organs will become ischemic if related vasculars were blockaged, which could induce irreservable damage inside the organs. However, the acute reperfusion for ischemics would cause IRI in some patients, which has been widely observed in various diseases including acute coronary syndrome, hepatic/renal acute injury and organ transplantation (Varadarajan et al., 2004). Eventrually, this unexpected complication, IRI will directly lead to a series pathological changes that manifests in brain edema, infarct progression, hemorrhagic transformation, and worsening neurologic system (Zhai et al., 2013; Prabhakaran et al., 2015). More importantly, the severe IRI may further induce systemic diseases including the inflammatory response syndrome (SIRS) and multiple organ dysfunction syndrome (MODS), and increase the mortality of patients, especially for those from the intensive care unit (Cryer, 2000).

GENERAL STRATEGIES FOR DEALING IRI

How to deal with the IRI is of clinical importance, therefore arousing the interests of diverse scientific communities. From the aspect of clinical view, three key factors have been focused on improving the efficiency and safety of reperfusion treatment, including developing different generation thrombectomy devices, lowering the time to reperfusion and applying potential imaging techniques for enrolling suitable patients (Prabhakaran et al., 2015). However, the reality of the synergistic role of various biological mechanisms in IRI made it challenging to prevent or treat. Indeed, some medications with predicted benefits to IRI have not been proved with a definite role in prevention or treatment, likely vitamin C (Hill et al., 2019), morphine (Le Corvoisier et al., 2018), etc. In the field of liver transplantation, nearly all randomized clinical trials have ultimately failed to ameliorate liver IRI in patients (Zhai et al., 2013). Therefore, innovative strategies with smart features for targeting local environmental factor, such as ROS would be an exciting direction for IRI treatment in the future.

NANOMEDICINE APPLIED IN IRI THERAPY

Ischemia could be induced via physical conditions (e.g., elevated blood pressure and diabetes, etc.) or damage, which can further trigger following IRI in various organs, ranging from cerebral to renal system. Notably, the elevated ROS after reperfusion mainly contributes to cellular and tissue damage. Recently, a series of novel nanomedicine (e.g., POM and Ceria NPs, etc.) has been designed for treating affected tissues via the smartly ROS-responsive scavenge and imaging of redox in the ischemic area (**Table 1**).

NANOMEDICINE FOR CEREBRAL IRI

Cerebral ischemia that generally caused by stroke is associated with high mortality and disability rate. More importantly, ROS produced by cerebral ischemia-reperfusion can further damage brain tissues via neurodegeneration. To overcome this severe disease, various of nanomaterials including polymer NPs (Reddy and Labhasetwar, 2009; Petro et al., 2016; Ghosh et al., 2017; Mei et al., 2019; Mukherjee et al., 2019), ceria NPs (Zhang et al., 2018), polyoxometalate (POM) nanoclusters (Li et al., 2019a), and Framework Nucleic Acids (Li et al., 2019b) have been applied as protective agents, indicating the high efficiency in saving cerebral tissue via ROS scavenging. Notably, the high biocompatibility allows the polymer to be widely recruited for delivering antioxidant reagents [i.e., superoxide dismutase (Reddy and Labhasetwar, 2009), antioxidants catalas (Petro et al., 2016), and curcumin (Mukherjee et al., 2019), etc]. Besides, a dual functional polymer NPs, t-PA@iRNP was successfully employed to induce thrombolytic and antioxidant therapies in cerebral tissue (Mei et al., 2019). With the encapsulation of tissue plasminogen activator (t-PA) and conjugation of 4-amino-2,2,6,6-tetramethylpiperidine-1-oxyl (4-amino-TEMPO), self-assemble t-PA@iRNP (∼50 nm) demonstrated an acidic-triggered (pH = 6.2) thrombolytic activity and a significant decrease of ROS production in middle cerebral artery occlusion (MCAO) model mice. More importantly, the antioxidant effect of t-PA@iRNP efficiently avoided the subarachnoid hemorrhage induced by t-PA, releasing a great potential of this dual therapy via synergistic effect.

In addition, novel bio-responsive nanomaterials containing the different status of metal ion (i.e., Mo^{5+} and Mo^{6+}) or oxygen-sensitive bio-structure (i.e., DNA) showed excellent capabilities as antioxidants (Li et al., 2019a,b). For instance, a

TABLE 1 | The representatives of novel nanomedicine for treating various IRI via ROS savaging.

Application	Type of materials	Nanomedicine	Size (nm)	Mechanism	Investigation	References
Cerebral IRI	FNA	aC5a-FNA	10	Antioxidant (FNA)/C5a-blocking	Protection for cerebral I/R	Li et al., 2019b
Cerebral IRI	Polyoxometalate	POM	∼1	Antioxidant	Protection for cerebral I/R	Li et al., 2019a
Cerebral IRI	Polymer	t-PA@iRNP	48 ± 2	Antioxidant (LMW nitroxide)/Thrombolysis	Protection for Middle cerebral artery occlusion	Mei et al., 2019
Cardiac IRI	Polymer	PEG-b-PPS	∼100	Antioxidant (ginsenoside Rg3)	Protection for Myocardial IRI	Li et al., 2020
Cardiac IRI	Polymer	CLP NPs	150 ± 18	Enhanced FL signal via oxidative stress	IVIS imaging of Myocardial IRI	Ziegler et al., 2019
Cardiac IRI	Polymer	MCTD-NPs	95	Antioxidant (TPP)	Protection for Myocardial IRI	Cheng et al., 2019
Hepatic IRI	Ceria	Ceria NPs	4.48 ± 0.8	Antioxidant	Protection for Partial hepatic IRI	Ni et al., 2019
Hepatic IRI	Ceria	CeO_2	10–30	Antioxidant	Protection for Partial hepatic IRI	Manne et al., 2017
Hepatic IRI	Polymer	BRNPs	100	Antioxidant (Bilirubin)	Protection for Partial hepatic IRI	Kim et al., 2017
Hepatic IRI	Polymeric	PVO	550	Antioxidant (peroxalate esters)/Gas generation	Protection for and US imaging Partial hepatic IRI	Kang et al., 2016
Renal IRI	Carbon QDs	SeCQDs	40	Antioxidant (doping selenium)	Protection for Glycerol/Cisplatin-induced AKI Models	Rosenkrans et al., 2020
Renal IRI	FNA	DONs	90, 120, 400	Antioxidant	Protection for Glycerol-induced AKI Model	Jiang et al., 2018
Renal IRI	Melanin	MMPP NPs	4.5	Antioxidant	Protection for Glycerol-induced AKI Model	Sun et al., 2019
Cardiac IRI	Silica	DATS-MIONs	230 ± 35	H_2S delivery (DATS)	Protection for Myocardial IRI	Wang et al., 2019
Organ transplant	Polymer	Anti–IL-6–PLGA-NPs	100	Anti-IL-6 delivery	Protection for Heart allograft	Solhjou et al., 2017
Organ transplant	Micelles	TRaM	15.3 ± 2.3	Rapamycin delivery	Protection for Aortic interposition allografts	Zhu et al., 2018

FNA, Framework nucleic acid; DONs, DNA origami nanostructures; FL, Fluorescence; TPP, Triphenylphosphine; LMW, Low molecular weight; IVIS, in vivo fluorescence imaging system; AKI, Acute kidney injury; PEG, Poly ethylene glycoland; PPS, Poly propylene sulfide.

POM nanocluster was developed and employed as an ROS-responsive agent in treating rats with cerebral I/R injury (Li et al., 2019a). After intrathecal injection, POM could efficiently accumulate in the brain and reduce the oxidative pressure, eventually suppressing the apoptosis of cerebral cells, edema, and infarct volume within the brain (for about 40∼50% decrease). Accompanied by IRI, excessive inflammation plays as another key factor for neuronal damage. Recently, a framework nucleic acids (FNA) conjugating with anti-C5a aptamer (aC5a) was applied in the therapy against IRI in the brain (**Figure 1A**) (Li et al., 2019b). More specifically, the aC5a-FNA could effectively reduce the C5a receptor on polymorphonuclear neutrophils (PMNs) and microglia, eventually bringing down the chemotaxis induced by C5a. Meanwhile, the concentrations of C5a (within plasma and penumbra) and detrimental ROS in cerebral issues were well-scavenged by aC5a-FNA administration, which efficiently protects brain cells from IRI, with a much smaller infarct volume of 17.0 ± 5.6% in comparison with that in control group (41.6 ± 7.1%).

NANOMEDICINE FOR CARDIAC IRI

Among the leading causes of death, cardiovascular disease (CVD), especially the myocardial infarction, is extremely dangerous for any patient. As the biggest challenge, the prevention of IRI greatly affects the outcome of therapy for myocardial infarction. To date, several ROS-responsive nanomaterials have been recruited in cardiac IRI therapy via the delivery of antioxidants (i.e., resveratrol and Ginsenoside Rg3, etc.) (Bae et al., 2016; Cheng et al., 2019; Li et al., 2020). This year, a self-assemble nanoparticle poly ethylene glycol-b-poly propylene sulfide (PEG-b-PPS) that smartly responses to ROS was successfully synthesized and used for ginsenoside Rg3 (Rg3) delivery (Li et al., 2020). PEG-b-PPS-Rg3 exhibited a ROS-dependent release of Rg3 (80% release of Rg3 within 1 day when 1.0 mM ROS was presented) and induced antioxidative stress effects by a strong interaction with FoxO3a (−6.0 kcal/mol). More importantly, the administration of PEG-b-PPS-Rg3 successfully increased the survival rate of I/R rat (90%) in comparison with the group injected with Free Rg3 (40%), indicating its high efficiency in responding to and scavenging cardiac-generated ROS. It is notable that precision targeting may increase therapeutic efficiency. To achieve that, Cheng et al. further modified Szeto-Schiller (SS)-31 and ischemic myocardium targeted peptide (IMTP) for preventing myocardial IRI via mitochondria-targeted antioxidant effect (Cheng et al., 2019). As-prepared MCTD-NPs specifically deliver resveratrol into cardiac tissues, reducing

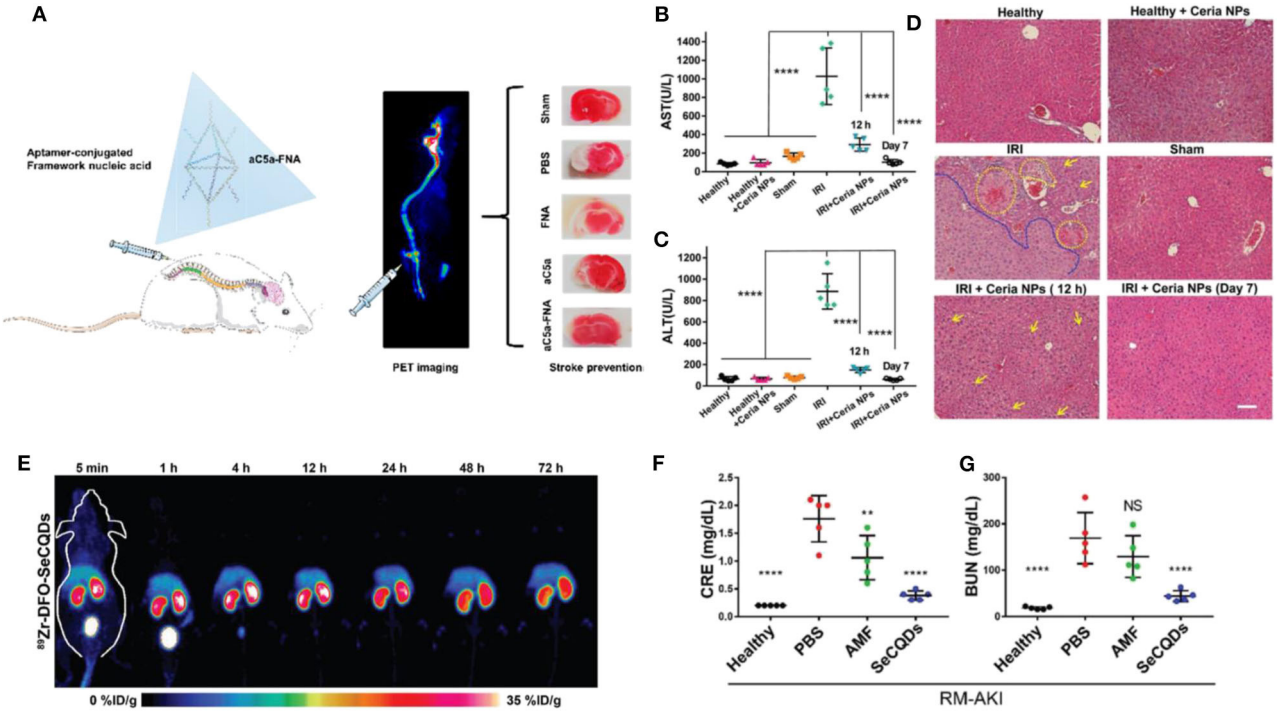

FIGURE 1 | Advanced ROS-responsive nanomedicine for various IRI therapy. **(A)** The aptamer-conjugated FNA for cerebral IRI therapy. Reproduced with permission from Li et al. (2019b). Copyright 2019, American Chemical Society. The therapeutic effects mediated by Ceria NPs in liver IRI. The level of AST **(B)** and ALT **(C)** in serum after different treatments (****$p < 0.0001$); **(D)** The HandE staining of liver harvested from different groups. The damage of hepatic cells (i.e., hemorrhage, cytolysis, and necrosis) and severely damaged tissue areas are labeled by yellow and blue dash lines, respectively. Lipid droplets formed are indicated by yellow arrows. Scale bar: 100 μm. Reproduced with permission from Ni et al. (2019). Copyright 2019, Wiley. The application of SeCQDs in treating AKI for protecting kidney from renal IRI. **(E)** The time-dependent bio-distribution of ^{89}Zr-DFO-SeCQDs in healthy ICR mice via MIP-PET images; The CRE **(F)** and BUN **(G)** concentration in serum among groups after various treatments (**$P < 0.01$, ****$P < 0.0001$, NS: no significant difference). Reproduced with permission from Rosenkrans et al. (2020). Copyright 2020, Wiley.

sizes of the infraction and protecting cardiomyocyte from ROS damage.

Notably, the elevated intracellular Ca^{2+} is strongly associated with the ROS generation in cardiac cells, which provides another therapeutic strategy via the intervention of Ca^{2+} influx (via anti-L-Type Ca^{2+} Peptide and CaMKII inhibitor) (Hardy et al., 2015; Wongrakpanich et al., 2017). However, the efficiency of channel blockage is relatively lower. Thus, the combination of antioxidant (i.e., curcumin) reagents and mitochondria-targeting functionalization (i.e., TPP) are required for improving the therapeutic effect.

Besides, several ROS-responsive nano-platforms were also developed for monitoring the status of IRI during the therapy (Yang et al., 2016; Ziegler et al., 2019). Specifically, Peter Lab developed CLP nanoparticles that could smartly light up the ROS-generated myocardium area after ischemic/reperfusion (Ziegler et al., 2019). The presentation of ROS could restore the fluorescent intensity of Ce6 that was attenuated by the aggregation-induced fluorescence quenching. By this strategy, damaged cardiac areas could be real-time detected and monitored throughout the first day after reperfusion.

NANOMEDICINE FOR HEPATIC IRI

Liver, one of the major organs has played a key role in metabolisms and been involved in various functions, which demands a lot of blood supply. Hepatic ischemia and IRI, a serious complication caused by liver diseases or transplantation would directly trigger irreversible damage in liver tissue. In comparison with other organs, especially the brain, the liver is able to actively "uptake" foreign agents from blood, which allows a series of therapeutic agents to accumulate inside. Thus, antioxidant gene delivery (i.e., expression genes of extracellular superoxide dismutase, catalase or TLR-4 siRNA) (He et al., 2006; Jiang et al., 2011), antioxidant prodrug (i.e., BRAP, etc.) (Lee et al., 2015), and nanoparticles (CeO_2 and platinum NP_S, etc.) (Katsumi et al., 2014; Kang et al., 2016; Li et al., 2016; Kim et al., 2017; Manne et al., 2017; Ni et al., 2019) were recruited in treating herpetic IRI. For example, a nanoparticle was designed to release p-hydroxybenzyl alcohol (HBA) when H_2O_2 or LPS was presented, which could remove ROS and decrease the level of pro-inflammation factors (i.e., NO and TNF-α) (Lee et al., 2015). Moreover, Kang et al. (2016) developed smartly bio-responsive nanoparticles that could provide ultrasound (US) imaging signal

during H_2O_2 scavenge. As-prepared PVO nanoparticles could quickly react with ROS and generate CO_2 in liver tissue with IRI, offering detectable US signals as early as 25 min post injection.

Additionally, metal nanomaterials exhibiting high reducibility were used as therapeutic agents for hepatic IRI. Among all, CeO_2 NP_S demonstrated high biocompatibility and efficiency. More specifically, a uniform-sized ceria NPs (∼4.5 nm) was synthesized, containing two valences of Ce (32.01% of Ce^{3+} and 67.99% of Ce^{4+}) (Ni et al., 2019). Administration of CeO_2 NP_S greatly attenuated the IRI in liver tissue as early as 12 h post reperfusion (**Figures 1B–D**). It is crucial that the ROS scavenge mediated by CeO_2 NP_S efficiently inhibits the pro-inflammation cytokine secretion (i.e., IL-12, IL-1, and TNF-α, etc.) and an influx of immune cells (i.e., monocyte and neutrophils). Meanwhile, CeO_2 NP_S also illustrated a high quality in preventing intestinal cells from ROS-based IRI (Gubernatorova et al., 2017).

NANOMEDICINE FOR RENAL IRI

Acute kidney injury (AKI) that is triggered by diseases or physical damage could lead to renal disorder/failure. In addition to general therapies like dialysis, ROS-responsive nanomedicine may provide another approach for AKI treatment. Mainly, the functional incapacitation of kidney will directly result in passive accumulation of "waste" inside, including nanomedicine injected. By taking this shortcut, advanced nanomaterials with additional functions such as acid-activated (Yoshitomi et al., 2011) or magnetic resonance imaging (MRI) (Sun et al., 2019) were designed for dealing AKI via ROS reduction. Moreover, Minami et al. also synthesized a nanomedicine (e.g., APP-103) that could effectively accumulate in non-functional kidneys and protect them from IRI during AKI or transplantation (Minami et al., 2020).

In comparison, Cai's lab successfully developed two nanomedicines specifically targeting to the kidney. Both nanoparticles, SeCQDs and DONs (DNA origami nanostructures) predominantly accumulated in the health murine kidney with ∼10 and ∼27%ID/g, respectively, while the kidney after AKI further enhanced the accumulation of nanoparticles (**Figure 1E**) (Jiang et al., 2018; Rosenkrans et al., 2020). With oxidant-sensitive structures (e.g., doped selenium and nuclei acid), SeCQDs and DONs efficiently removed excessive ROS from renal cells (**Figures 1F,G**).

ALTERNATIVE STRATEGIES FOR IRI THERAPY AND ORGAN TRANSPLANTATION

In addition to an active reduction of cellular ROS, cytoprotective reagents such as hydrogen sulfide (H_2S) are also applied as an anti-inflammation agent in various medical situations associated with ischemic diseases. It is notable that various smart nanomedicines have been prepared for H_2S delivery, showing promising efficiency (Chen et al., 2019). More specifically, as-designed mesoporous iron oxide and silica nanoparticles could effectively carry and deliver H_2S donor diallyl trisulfide (DATS) to ischemic organs (i.e., heart and aortic graft endothelium), eventually reducing the flowing injury caused by reperfusion (Wang et al., 2016, 2019).

Meanwhile, nano-platforms conjugating with immune-modulators could mediate desirable protection for injured or transplanted organs as well. For instance, the modification of antibodies on PLGA NPs successfully moderated the chronic rejection of transplanted heart by targeting IL-6 secreted by allograft-derived dendritic cells (ADDCs) (Solhjou et al., 2017). Furthermore, the endothelial cell inflammation and pro-inflammatory cytokines secretion following tracheal or aortic allografts could be greatly attenuated by the pre-treatment of rapamycin (Nadig et al., 2015; Zhu et al., 2018).

CONCLUSION/FUTURE DIRECTIONS

ROS generated by ischemic reperfusion plays a crucial role in the following tissue injury. In other words, this also provides an efficient approach for dealing and preventing IRI via the reduction of ROS. Novel nanoparticles that smartly respond or consume ROS have been designed and proved for their promising performance. However, several directions and challenges should be aware for the future design of ROS-responsive nanomedicine. (a) A combination of multiple functions (i.e., imaging and therapy) in single nanomedicine is highly recommended for monitoring and treating IRI diseases; (b) Desirable IRI therapy may be achieved via dual therapy of ROS scavenge and immune-repress (i.e., H_2S delivery); (c) Although alternative strategies, such as antioxidant gene delivery, may provide another direction for IRI therapy, the quick response and antioxidant effects are still the key issues for the future design of ROS-responsive nano-platforms; (d) Tissue-depended design is strongly recommended as well. For example, the antioxidant capability is more important than tissue targeting in AKI model (e.g., passive accumulation in AKI); (e) Sub-organ/cell-targeting for IRI therapy is highly suggested (i.e., antibody-induced cell targeting). Specifically, the most of antioxidant nanoparticles would be internalized by Kupffer cells during the liver IRI, which may lower the therapeutic effect of nanomedicine in major hepatic cells such as liver sinusoidal endothelial cells; (f) The antioxidant efficiency and biocompatibility should be balanced. Thus, advanced ROS-responsive nanomedicine have shown high-performance in dealing with various IRI, which exhibits a great potential in clinical translation, especially organ transplantation.

AUTHOR CONTRIBUTIONS

WC planned and wrote this review with the help of DL. All authors contributed to the article and approved the submitted version.

FUNDING

This work was supported by the National Natural Science Foundation of China (81971668).

REFERENCES

Bae, S., Park, M., Kang, C., Dilmen, S., Kang, T. H., Kang, D. G., et al. (2016). Hydrogen peroxide-responsive nanoparticle reduces myocardial ischemia/reperfusion injury. *J. Am. Heart Assoc.* 5:e003697. doi: 10.1161/JAHA.116.003697

Benjamin, E. J., Blaha, M. J., Chiuve, S. E., Cushman, M., Das, S. R., Deo, R., et al. (2017). Heart disease and stroke statistics-2017 update: a report from the American Heart Association. *Circulation* 135, e146–e603. doi: 10.1161/CIR.0000000000000485

Benjamin, E. J., Virani, S. S., Callaway, C. W., Chamberlain, A. M., Chang, A. R., Cheng, S., et al. (2018). Heart disease and stroke statistics-—2018 update: a report from the American Heart Association. *Circulation* 137, e67–e492. doi: 10.1161/CIR.0000000000000558

Chen, W., Ni, D., Rosenkrans, Z. T., Cao, T., and Cai, W. (2019). Smart H2S-triggered/therapeutic system (SHTS)-based nanomedicine. *Adv. Sci.* 6:1901724. doi: 10.1002/advs.201901724

Chen, W., Zuo, H., Li, B., Duan, C., Rolfe, B., Zhang, B., et al. (2018a). Clay nanoparticles elicit long-term immune responses by forming biodegradable depots for sustained antigen stimulation. *Small* 14:1704465. doi: 10.1002/smll.201704465

Chen, W., Zuo, H., Zhang, E., Li, L., Henrich-Noack, P., Cooper, H., et al. (2018b). Brain targeting delivery facilitated by ligand-functionalized layered double hydroxide nanoparticles. *ACS Appl. Mater. Interfaces* 10, 20326–20333. doi: 10.1021/acsami.8b04613

Cheng, Y., Liu, D.-Z., Zhang, C.-X., Cui, H., Liu, M., Mei, Q.-B., et al. (2019). Mitochondria-targeted antioxidant delivery for precise treatment of myocardial ischemia–reperfusion injury through a multistage continuous targeted strategy. *Nanomed. Nanotechnol. Biol. Med.* 16, 236–249. doi: 10.1016/j.nano.2018.12.014

Cryer, H. G. (2000). "Ischemia and reperfusion as a cause of multiple organ failure," in *Multiple Organ Failure*, eds A. E. Baue, E. Faist, and D. E. Fry (New York, NY: Springer), 108–113. doi: 10.1007/978-1-4612-1222-5_12

Fu, Z.-Y., Wu, Z.-J., Zheng, J.-H., Li, N., Lu, J.-Y., and Chen, M.-H. (2020). Edaravone ameliorates renal warm ischemia-reperfusion injury by downregulating endoplasmic reticulum stress in a rat resuscitation model. *Drug Des. Devel. Ther.* 14:175. doi: 10.2147/DDDT.S211906

Ghosh, S., Sarkar, S., Choudhury, S. T., Ghosh, T., and Das, N. (2017). Triphenyl phosphonium coated nano-quercetin for oral delivery: neuroprotective effects in attenuating age related global moderate cerebral ischemia reperfusion injury in rats. *Nanomed. Nanotechnol. Biol. Med.* 13, 2439–2450. doi: 10.1016/j.nano.2017.08.002

Gubernatorova, E. O., Liu, X., Othman, A., Muraoka, W. T., Koroleva, E. P., Andreescu, S., et al. (2017). Europium-doped cerium oxide nanoparticles limit reactive oxygen species formation and ameliorate intestinal ischemia–reperfusion injury. *Adv. Healthcare Mater.* 6:1700176. doi: 10.1002/adhm.201700176

Hardy, N., Viola, H. M., Johnstone, V. P., Clemons, T. D., Cserne Szappanos, H., Singh, R., et al. (2015). Nanoparticle-mediated dual delivery of an antioxidant and a peptide against the L-type Ca2+ channel enables simultaneous reduction of cardiac ischemia-reperfusion injury. *ACS Nano* 9, 279–289. doi: 10.1021/nn5061404

He, S. Q., Zhang, Y. H., Venugopal, S. K., Dicus, C. W., Perez, R. V., Ramsamooj, R., et al. (2006). Delivery of antioxidative enzyme genes protects against ischemia/reperfusion–induced liver injury in mice. *Liver Transpl.* 12, 1869–1879. doi: 10.1002/lt.21001

Hill, A., Clasen, K. C., Wendt, S., Majoros, A. G., Stoppe, C., Adhikari, N. K. J., et al. (2019). Effects of vitamin C on organ function in cardiac surgery patients: a systematic review and meta-analysis. *Nutrients* 11:2103. doi: 10.3390/nu11092103

Jiang, D., Ge, Z., Im, H.-J., England, C. G., Ni, D., Hou, J., et al. (2018). DNA origami nanostructures can exhibit preferential renal uptake and alleviate acute kidney injury. *Nat. Biomed. Eng.* 2, 865–877. doi: 10.1038/s41551-018-0317-8

Jiang, N., Zhang, X., Zheng, X., Chen, D., Zhang, Y., Siu, L., et al. (2011). Targeted gene silencing of TLR4 using liposomal nanoparticles for preventing liver ischemia reperfusion injury. *Am. J. Transpl.* 11, 1835–1844. doi: 10.1111/j.1600-6143.2011.03660.x

Kang, C., Cho, W., Park, M., Kim, J., Park, S., Shin, D., et al. (2016). H2O2-triggered bubble generating antioxidant polymeric nanoparticles as ischemia/reperfusion targeted nanotheranostics. *Biomaterials* 85, 195–203. doi: 10.1016/j.biomaterials.2016.01.070

Katsumi, H., Fukui, K., Sato, K., Maruyama, S., Yamashita, S., Mizumoto, E., et al. (2014). Pharmacokinetics and preventive effects of platinum nanoparticles as reactive oxygen species scavengers on hepatic ischemia/reperfusion injury in mice. *Metallomics* 6, 1050–1056. doi: 10.1039/C4MT00018H

Kim, J. Y., Lee, D. Y., Kang, S., Miao, W., Kim, H., Lee, Y., et al. (2017). Bilirubin nanoparticle preconditioning protects against hepatic ischemia-reperfusion injury. *Biomaterials* 133, 1–10. doi: 10.1016/j.biomaterials.2017.04.011

Le Corvoisier, P., Gallet, R., Lesault, P. F., Audureau, E., Paul, M., Ternacle, J., et al. (2018). Intra-coronary morphine versus placebo in the treatment of acute ST-segment elevation myocardial infarction: the MIAMI randomized controlled trial. *BMC Cardiovasc. Disord.* 18:193. doi: 10.1186/s12872-018-0936-8

Lee, D., Park, S., Bae, S., Jeong, D., Park, M., Kang, C., et al. (2015). Hydrogen peroxide-activatable antioxidant prodrug as a targeted therapeutic agent for ischemia-reperfusion injury. *Sci. Rep.* 5:16592. doi: 10.1038/srep16592

Li, H., Sun, J.-J., Chen, G.-Y., Wang, W.-W., Xie, Z.-T., Tang, G.-F., et al. (2016). Carnosic acid nanoparticles suppress liver ischemia/reperfusion injury by inhibition of ROS, caspases and NF-κB signaling pathway in mice. *Biomed. Pharmacother.* 82, 237–246. doi: 10.1016/j.biopha.2016.04.064

Li, L., Wang, Y., Guo, R., Li, S., Ni, J., Gao, S., et al. (2020). Ginsenoside Rg3-loaded, reactive oxygen species-responsive polymeric nanoparticles for alleviating myocardial ischemia-reperfusion injury. *J. Control. Release* 317, 259–272. doi: 10.1016/j.jconrel.2019.11.032

Li, S., Jiang, D., Ehlerding, E. B., Rosenkrans, Z. T., Engle, J. W., Wang, Y., et al. (2019a). Intrathecal administration of nanoclusters for protecting neurons against oxidative stress in cerebral ischemia/reperfusion injury. *ACS Nano* 13, 13382–13389. doi: 10.1021/acsnano.9b06780

Li, S., Jiang, D., Rosenkrans, Z. T., Barnhart, T. E., Ehlerding, E. B., Ni, D., et al. (2019b). Aptamer-conjugated framework nucleic acids for the repair of cerebral ischemia-reperfusion injury. *Nano Lett.* 19, 7334–7341. doi: 10.1021/acs.nanolett.9b02958

Manne, N. D., Arvapalli, R., Graffeo, V. A., Bandarupalli, V. V., Shokuhfar, T., Patel, S., et al. (2017). Prophylactic treatment with cerium oxide nanoparticles attenuate hepatic ischemia reperfusion injury in sprague dawley rats. *Cell. Physiol. Biochem.* 42, 1837–1846. doi: 10.1159/000479540

Mei, T., Kim, A., Vong, L. B., Marushima, A., Puentes, S., Matsumaru, Y., et al. (2019). Encapsulation of tissue plasminogen activator in pH-sensitive self-assembled antioxidant nanoparticles for ischemic stroke treatment–synergistic effect of thrombolysis and antioxidant. *Biomaterials* 215:119209. doi: 10.1016/j.biomaterials.2019.05.020

Minami, K., Bae, S., Uehara, H., Zhao, C., Lee, D., Iske, J., et al. (2020). Targeting of intragraft reactive oxygen species by APP-103, a novel polymer product, mitigates ischemia/reperfusion injury and promotes the survival of renal transplants. *Am. J. Transpl.* 20, 1527–1537. doi: 10.1111/ajt.15794

Mukherjee, A., Sarkar, S., Jana, S., Swarnakar, S., and Das, N. (2019). Neuro-protective role of nanocapsulated curcumin against cerebral ischemia-reperfusion induced oxidative injury. *Brain Res.* 1704, 164–173. doi: 10.1016/j.brainres.2018.10.016

Nadig, S. N., Dixit, S. K., Levey, N., Esckilsen, S., Miller, K., Dennis, W., et al. (2015). Immunosuppressive nano-therapeutic micelles downregulate endothelial cell inflammation and immunogenicity. *RSC Adv.* 5, 43552–43562. doi: 10.1039/C5RA04057D

Ni, D., Wei, H., Chen, W., Bao, Q., Rosenkrans, Z. T., Barnhart, T. E., et al. (2019). Ceria nanoparticles meet hepatic ischemia-reperfusion injury: the perfect imperfection. *Adv. Mater.* 31:1902956. doi: 10.1002/adma.201902956

Nita, M., and Grzybowski, A. (2016). The role of the reactive oxygen species and oxidative stress in the pathomechanism of the age-related ocular diseases and other pathologies of the anterior and posterior eye segments in adults. *Oxid. Med. Cell. Longev.* 2016:3164734. doi: 10.1155/2016/3164734

Petro, M., Jaffer, H., Yang, J., Kabu, S., Morris, V. B., and Labhasetwar, V. (2016). Tissue plasminogen activator followed by antioxidant-loaded nanoparticle delivery promotes activation/mobilization of progenitor cells in infarcted rat brain. *Biomaterials* 81, 169–180. doi: 10.1016/j.biomaterials.2015.12.009

Prabhakaran, S., Ruff, I., and Bernstein, R. A. (2015). Acute stroke intervention: a systematic review. *JAMA* 313, 1451–1462. doi: 10.1001/jama.2015.3058

Qiao, Y., He, J., Chen, W., Yu, Y., Li, W., Du, Z., et al. (2020). Light-activatable synergistic therapy of drug-resistant bacteria-infected cutaneous chronic wounds and nonhealing keratitis by cupriferous hollow nanoshells. *ACS Nano* 14, 3299–3315. doi: 10.1021/acsnano.9b08930

Reddy, M. K., and Labhasetwar, V. (2009). Nanoparticle-mediated delivery of superoxide dismutase to the brain: an effective strategy to reduce ischemia-reperfusion injury. *FASEB J.* 23, 1384–1395. doi: 10.1096/fj.08-116947

Rosenkrans, Z. T., Sun, T., Jiang, D., Chen, W., Barnhart, T. E., Zhang, Z., et al. (2020). Selenium-doped carbon quantum dots act as broad-spectrum antioxidants for acute kidney injury management. *Adv. Sci.* 7:2000420. doi: 10.1002/advs.202000420

Solhjou, Z., Uehara, M., Bahmani, B., Maarouf, O. H., Ichimura, T., Brooks, C. R., et al. (2017). Novel application of localized nanodelivery of anti–interleukin-6 protects organ transplant from ischemia–reperfusion injuries. *Am. J. Transpl.* 17, 2326–2337. doi: 10.1111/ajt.14266

Sun, T., Jiang, D., Rosenkrans, Z. T., Ehlerding, E. B., Ni, D., Qi, C., et al. (2019). A melanin-based natural antioxidant defense nanosystem for theranostic application in acute kidney injury. *Adv. Funct. Mater.* 29:1904833. doi: 10.1002/adfm.201904833

Varadarajan, R., Golden-Mason, L., Young, L., Mcloughlin, P., Nolan, N., Mcentee, G., et al. (2004). Nitric oxide in early ischaemia reperfusion injury during human orthotopic liver transplantation. *Transplantation* 78, 250–256. doi: 10.1097/01.TP.0000128188.45553.8C

Wang, W., Liu, H., Lu, Y., Wang, X., Zhang, B., Cong, S., et al. (2019). Controlled-releasing hydrogen sulfide donor based on dual-modal iron oxide nanoparticles protects myocardial tissue from ischemia–reperfusion injury. *Int. J. Nanomed.* 14:875. doi: 10.2147/IJN.S186225

Wang, W., Sun, X., Zhang, H., Yang, C., Liu, Y., Yang, W., et al. (2016). Controlled release hydrogen sulfide delivery system based on mesoporous silica nanoparticles protects graft endothelium from ischemia–reperfusion injury. *Int. J. Nanomed.* 11:3255. doi: 10.2147/IJN.S104604

Wongrakpanich, A., Morris, A. S., Geary, S. M., Mei-Ling, A. J., and Salem, A. K. (2017). Surface-modified particles loaded with CaMKII inhibitor protect cardiac cells against mitochondrial injury. *Int. J. Pharm.* 520, 275–283. doi: 10.1016/j.ijpharm.2017.01.061

Yang, L., Ren, Y., Pan, W., Yu, Z., Tong, L., Li, N., et al. (2016). Fluorescent nanocomposite for visualizing cross-talk between microRNA-21 and hydrogen peroxide in ischemia-reperfusion injury in live cells and *in vivo*. *Anal. Chem.* 88, 11886–11891. doi: 10.1021/acs.analchem.6b03701

Yoshitomi, T., Hirayama, A., and Nagasaki, Y. (2011). The ROS scavenging and renal protective effects of pH-responsive nitroxide radical-containing nanoparticles. *Biomaterials* 32, 8021–8028. doi: 10.1016/j.biomaterials.2011.07.014

Zhai, Y., Petrowsky, H., Hong, J. C., Busuttil, R. W., and Kupiec-Weglinski, J. W. (2013). Ischaemia-reperfusion injury in liver transplantation—from bench to bedside. *Nat. Rev. Gastroenterol. Hepatol.* 10, 79–89. doi: 10.1038/nrgastro.2012.225

Zhang, T., Li, C.-Y., Jia, J.-J., Chi, J.-S., Zhou, D., Li, J.-Z., et al. (2018). Combination therapy with LXW7 and ceria nanoparticles protects against acute cerebral ischemia/reperfusion injury in rats. *Curr. Med. Sci.* 38, 144–152. doi: 10.1007/s11596-018-1858-5

Zhang, W., Wang, M., Xie, H., Zhou, L., Meng, X., Shi, J., et al. (2007). Role of reactive oxygen species in mediating hepatic ischemia-reperfusion injury and its therapeutic applications in liver transplantation. *Transpl. Proc.* 39, 1332–1337. doi: 10.1016/j.transproceed.2006.11.021

Zhu, P., Atkinson, C., Dixit, S., Cheng, Q., Tran, D., Patel, K., et al. (2018). Organ preservation with targeted rapamycin nanoparticles: a pre-treatment strategy preventing chronic rejection *in vivo*. *RSC Adv.* 8, 25909–25919. doi: 10.1039/C8RA01555D

Ziegler, M., Xu, X., Yap, M. L., Hu, H., Zhang, J., and Peter, K. (2019). A self-assembled fluorescent nanoprobe for imaging and therapy of cardiac ischemia/reperfusion injury. *Adv. Ther.* 2:1800133. doi: 10.1002/adtp.201800133

Conflict of Interest: The authors declare that the research was conducted in the absence of any commercial or financial relationships that could be construed as a potential conflict of interest.

The handling editor declared a past co-authorship with one of the authors WC.

frontiers in Chemistry

MINI REVIEW
published: 08 September 2020
doi: 10.3389/fchem.2020.00804

Tumor Immune Microenvironments (TIMEs): Responsive Nanoplatforms for Antitumor Immunotherapy

Xueqing Sui[1†], Teng Jin[2†], Tonghui Liu[3], Shiman Wu[4], Yue Wu[4], Zhongmin Tang[5], Yan Ren[4], Dalong Ni[6], Zhenwei Yao[4*] and Hua Zhang[1*]*

[1] Department of Radiology, The Affiliated Hospital of Qingdao University, Qingdao, China, [2] Department of Radiology, Union Hospital, Tongji Medical College, Huazhong University of Science and Technology, Wuhan, China, [3] Department of Neurology, The Affiliated Hospital of Qingdao University, Qingdao, China, [4] Department of Radiology, Huashan Hospital, Fudan University, Shanghai, China, [5] State Key Laboratory of High-Performance Ceramics and Superfine Microstructure, Shanghai Institute of Ceramics, Chinese Academy of Sciences, Shanghai, China, [6] Departments of Radiology, Medical Physics, and Pharmaceutical Sciences, University of Wisconsin - Madison, Madison, WI, United States

OPEN ACCESS

Edited by:
Steve Suib,
University of Connecticut,
United States

Reviewed by:
Kelong Ai,
Central South University, China
Hu Ping,
Shanghai Institute of Ceramics
(CAS), China

***Correspondence:**
Dalong Ni
Dni2@wisc.edu
Zhenwei Yao
zwyao@fudan.edu.cn
Hua Zhang
wozhanghua@126.com

[†] These authors have contributed equally to this work

Specialty section:
This article was submitted to Nanoscience, a section of the journal Frontiers in Chemistry

Received: 28 May 2020
Accepted: 30 July 2020
Published: 08 September 2020

Citation:
Sui X, Jin T, Liu T, Wu S, Wu Y, Tang Z, Ren Y, Ni D, Yao Z and Zhang H (2020) Tumor Immune Microenvironments (TIMEs): Responsive Nanoplatforms for Antitumor Immunotherapy. Front. Chem. 8:804. doi: 10.3389/fchem.2020.00804

Interest in cancer immunotherapy has rapidly risen since it offers many advantages over traditional approaches, such as high efficiency and prevention of metastasis. Efforts have primarily focused on two major strategies for regulating the body's antitumor immune response mechanisms: "enhanced immunotherapy" that aims to amplify the immune activation, and "normalized immunotherapy" that corrects the defective immune mechanism in the tumor immune microenvironments (TIMEs), which returns to the normal immune trajectory. However, due to the complexity and heterogeneity of the TIMEs, and lack of visualization research on the immunotherapy process, cancer immunotherapy has not been widely used in clinical setting. Recently, through the design and modification of nanomaterials, intelligent TIME-responsive nanoplatforms were developed from which encouraging results in many aspects of immunotherapy have been achieved. In this mini review, the status of designed nanomaterials for nanoplatform-based immune regulation of TIMEs has been emphasized, particularly with respect to the aforementioned approaches. It is envisaged that future prospects will focus on a combination of multiple immunotherapies for more efficient cancer inhibition and elimination.

Keywords: cancer, nanomaterials, enhanced immunotherapy, normalized immunotherapy, tumor immune microenvironment

INTRODUCTION

Immunotherapy, a fast-growing tumor treatment strategy, restarts and maintains the tumor-immunity cycle to restore the body's antitumor immune response, thereby controlling and eliminating tumors (Liu et al., 2019). However, many patients have experienced minimal or no clinical benefits in response to this strategy. This has been attributed to evaded and tolerant antitumor immune responses (Gajewski et al., 2013) *via* the following mechanisms: (i) resistance to an immune attack through dominant inhibitory effects of the immune system, including suppressive pathways in infiltrated-inflamed (I-I) tumor immune microenvironments (TIMEs), brought about by programmed death-ligand 1 (PD-L1) (Gadiot et al., 2011) and tumor-associated macrophage 2 (TAM2)-type macrophages (Goswami et al., 2017), and (ii) resistance to an immune attack through immune system exclusion or ignorance in

infiltrated-excluded (I-E) TIMEs in which the immune system is unable to recognize or respond to a pathogen or malignancy (Evans et al., 2016). Thus, these tumors are considered to be poorly immunogenic or "cold" (Spranger, 2016). The core of this immunosuppressive environment established in tumors is oncogenes and abnormal pathway signals, which leads to the production of potent cytokines, chemokines, and numerous immunosuppressive immune cells, finally forming the TIMEs. Broad effects of factors directly affect the quality and character of the TIMEs, such as diet (Julia et al., 2015), adiposity, the microbiome and sex, and systemic inflammatory state of an individual.

Currently, TIMEs are divided into three classes according to recent human and mouse data, helping us understand how the immune composition and immune state affect cancer cells and immunotherapy. I-E TIMEs are flooded with immune cells, but relatively lacking in cytotoxic lymphocytes (CTL) in the core of the tumor. I-E TIMEs place CTLs at the invasion boundary of tumor tissue or cause them to sink into the fibrous nest. I-I TIMEs are characterized by the high infiltration of CTLs expressed by PD-1 and cancer cells expressed by PD-1 inhibitory ligand PD-L1. Tertiary lymphoid structures (TLSs)-TIME contains a large number of lymphocytes including naive and activated conventional T cells, regulatory T cells, B cells, and protruding cells. TLS-TIMEs are usually found in the margins and stroma of aggressive tumors (Binnewies et al., 2018). Analysis of the unique classes and subclasses of TIMEs can predict and guide immunotherapeutic responsiveness and reveal new therapeutic targets (Binnewies et al., 2018). According to different treatment principles, two strategies are available, namely, normalized and enhanced tumor immunity. The former aims to reduce the suppression signal of the immune system, while the latter induces the immune system's ability to kill heterogeneous cells (Sanmamed and Chen, 2018), thereby combating tumor immune therapeutic resistance.

Nanotechnology has been intensively investigated with respect to cancer immunotherapy. This is a key step toward creation of more effective immune responses with fewer negative implications in clinical and preclinical trials (Goldberg, 2019). Chemical modification of a nanoplatform (e.g., shape, surface charge, targeting, and responsive ability) for transport and biodistribution behavior (**Figure 1**) mainly focuses on (i) effective and precise delivery of immune drugs (immune antigens and cytokines, adjuvant) to targeted sites, and controlled drug release (Fan and Moon, 2015; Wang et al., 2020); (ii) optimization of the immune response to nano-tumor vaccines, enabling a variety of immune mechanisms to specifically attack and destroy cancer cells (Fu et al., 2018); (iii) regulation of immunosuppressive components of tumor immunity in the tumor microenvironment to normalize cancer immunotherapy for restoration of the lost antitumor immunity (Gao et al., 2019); and (iv) implementation of photothermal therapy (PTT) and photodynamic therapy (PDT), among others, to activate the body's immune system to improve the number and quality of antitumor immune responses, combined with cancer immunotherapy (Sang et al., 2019). However, TIME-responsive nanomaterials for cancer immunotherapy remain poorly investigated, and thus, there is scope for future work. In this minireview, the development of TIME-responsive nanomaterials has been assessed with respect to normalized and enhanced cancer immunotherapy, and perspectives for future applications are provided.

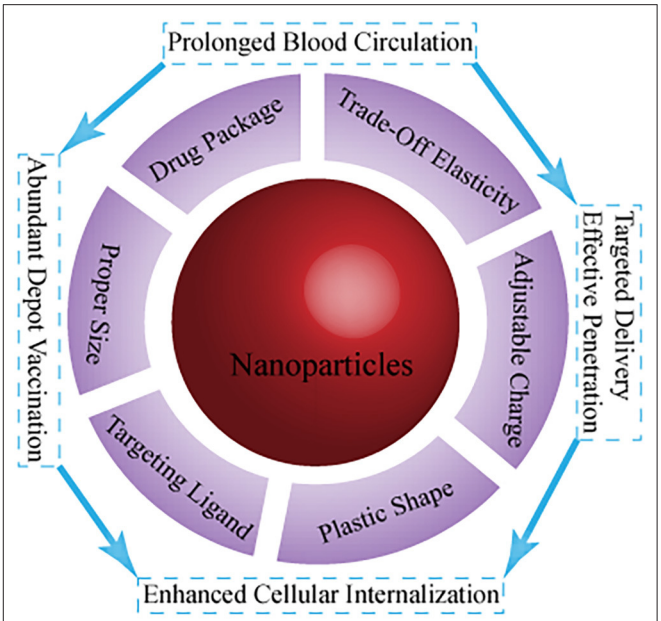

FIGURE 1 | Current main strategies on the fate of immunomodulators using nanotechnology with different parameters.

ENHANCEMENT OF CANCER IMMUNOTHERAPY

Since its inception, various types of immunotherapies have been employed to activate and increase the immune response *via* modulation of general regulatory and/or activatory mechanisms (Sanmamed and Chen, 2018), involving antigen processing, activation and expansion of naive T cells, and intensification of the effector phase of the immune response. Another approach is to use effector cells/molecules of the immune system to directly attack tumor cells, consisting of antibody therapy and its derivatives, including adoptive immune cell therapy (ACT) with genetically engineered T cells, and regulation of the phenotype of immune cells in TIMEs. With the development of drug-carrying nanotechnology, significantly more antitumor molecules such as antibodies, molecular vaccines, and cytokines can be selectively delivered to target sites for augmenting retention (Bertrand et al., 2014); this is assisted by folate-, transferrin-, mannose-, and antibody-conjugated nanomaterials (Huang et al., 2016) and is combined with the EPR effect. The discovery of new drugs such as ipilimumab has paved the way for active immunotherapy by eliminating residuals and advanced cancer with durable and long-lasting responses (Hodi et al., 2010; Baronzio et al., 2013).

The presence of TAM2 in the TIME inhibits the recruitment of effector T cells to the tumor core (Beatty et al., 2015).

Additionally, IL-10 and TGF-β that are excreted by TAM2 macrophages can suppress adaptive immune responses and drive the differentiation of regulatory T cells (Tregs) (Liu et al., 2019). Utilization of biomarkers that are overexpressed on tumor-associated macrophages (TAMs) to design specific ligands, construct nanocarriers, and modify their targets to remodel the TIMEs has attracted much attention, especially with respect to the polarization from TAM2 to antitumor TAM1 macrophages (Goswami et al., 2017). Additionally, albumin nanoparticles that are modified with mannose and encapsulated with drugs such as regorafenib, target albumin-binding proteins such as secreted protein acidic and rich in cysteine (SPARC) overexpressed in tumor cells and the protumor TAM2, serving both as a delivery and therapeutic strategy. TAM2 is "reeducated" into the antitumor TAM1 by means of the interplay of the TAMs, Treg, and effector $CD8^+$T cells, thereby reducing apoptosis (Zhao et al., 2018). Similarly, more multifunctional nanoprobes decorated with target markers and loaded with macrophage regulators have been utilized to remodel the TIMEs *via* reprogramming of TAMs and efficiently trigger macrophage-directed cancer immunotherapy (Ai et al., 2018; Nath et al., 2018). Interestingly, natural killer cell membranes that are carried with photosensitizer-embellished nanoparticles are used synergistically with photodynamic therapy and have been found to enhance M1-macrophage polarization, inhibiting the growth of primary and distant metastatic tumors (Deng et al., 2018).

ACT is an important part of cancer immunity. Nanoprobe-based regulation mainly focuses on pre-removal of tumor suppressor T cell recruitment factors such as TGF-β to activate the T cells (Zheng et al., 2017) and on normalization of tumor vasculature with vascular endothelial growth factor (VEGF) antibodies (Stephan et al., 2015). Additionally, nanoparticles have been found to enable *ex vivo* and *in vivo* T-cell proliferation, allowing the generation of effector T cells of high quality and quantity. Iron-dextran-derived artificial antigen-presenting cells (aAPCs) were used to selectively filter tumor-specific T cells from the naïve precursors by virtue of a magnetic force (Perica et al., 2015). Nanoprobes that were conjugated with fibronectin were utilized to activate T-cell proliferation, thereby increasing the T cell expansion rate (Perica et al., 2015). Furthermore, nanoprobes loaded with DNA were selectively connected to the T cells, resulting in expression of a defined leukemia-specific Chimeric Antigen Receptor (Smith et al., 2017).

However, the therapeutic effects of ACT are impaired by insufficient proliferation and inadequate T-cell activity in the immunosuppressive TIMEs (Mardiana et al., 2019). In contrast to immunotherapy in isolation, nanoplatform-based synergistic combination cancer immunotherapy allows for improved anticancer activity as it includes radiotherapy, chemotherapy, photothermal and photodynamic therapy, gene therapy (Sang et al., 2019), and magnetic hyperthermia therapy (Pan et al., 2020). In essence, this is also a measure for enhancement of immunity by means of exposing more tumor-associated antigens, promoting the recruitment and infiltration of more effector cells into tumor tissue, and generating long-term memory T cells to prevent tumor recurrence and metastasis. Additionally, switching non-T cell-inflamed into T-cell-inflamed TIMEs can contribute to subsequent effective immunological checkpoint blockade (ICB) therapy (Spranger, 2016).

NORMALIZATION OF CANCER IMMUNOTHERAPY

Compared with enhancement of cancer immunotherapy, normalized way harnesses the identification and correction of immune response deficiencies during tumor progression to further selectively restore natural antitumor immune capacity (Sanmamed and Chen, 2018). It is mainly comprised of ICB therapy, which has been widely recognized and used in clinical trials as it exhibits fewer side effects.

The B7-H1/programmed cell death-1 (PD-1) inhibitory pathway leads to the suppression of immune responses (Zou et al., 2016; Ribas and Wolchok, 2018). It has been approved for commercial use by the U.S. Food and Drug Administration (FDA) and used in clinical cancer immunotherapy (Liu et al., 2019). Accumulation and retention of checkpoint inhibitors that are encapsulated in nanoprobes within the tumor allows for enhanced efficacy (Meir et al., 2017). Furthermore, the αPD-L1 antibody combined with gold nanoparticles as the targeted marker has been harnessed to predict the benefits of anti-PD-1/PD-L1 immunotherapy through image-guided accumulation. Additionally, compared to free checkpoint inhibitors, nanomaterials loaded with PD-L1 can be decorated with tumor-targeting probes to decrease the dose while reducing side effects, and be sustainably released within the sites of interest (Teo et al., 2015; Wang C. et al., 2016). Furthermore, knockdown expression of the PD-1/PD-L1 pathway also enhances the efficacy of ICB (Shi et al., 2018). Small interfering RNA (siRNA) has been utilized to silence the PD-L1 pathway and for knockdown of PD-1 on tumor-infiltrated T cells to promote immunity against cancer and inhibit progression and metastasis of tumors (Borkner et al., 2010; Iwamura et al., 2012; Wang D. et al., 2016). Moreover, clinical trials indicate that anti-PD-1/PD-L1 combined with cytotoxic T-lymphocyte-associated protein 4 (CTLA-4) blockade exerts a synergistic antitumor effect in melanoma and lung cancer (Chae et al., 2018). Additionally, the study of inhibitory signaling pathways independence of PD-1/PD-L1 in the TIMEs will provide new strategies for nanotechnology to adjust immune normalization, such as for fibrinogen-like protein 1 (FGL1)/lymphocyte-activation gene 3 (LAG-3) (Wang et al., 2019), and the v-set immunoglobulin domain suppressor of T cell activation (VISTA) pathway (ElTanbouly et al., 2019; Mahoney and Freeman, 2020).

CONCLUSIONS AND FUTURE PERSPECTIVES

The urgent demand for effective cancer immunotherapy strategies has attracted attention in the field of biomaterials

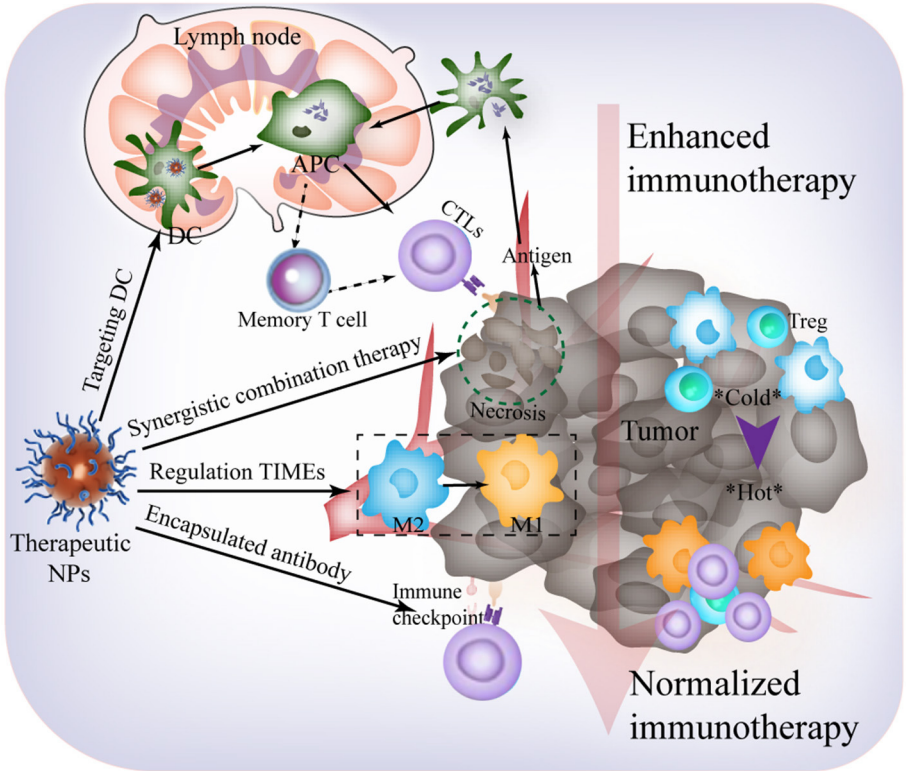

FIGURE 2 | Future outlooks for effective immunological response harnessing TIME-responsive nanomaterial.

science, immunity, and molecular imaging (Liu et al., 2019). Following decades of progress, anti-TIME responses assisted by artificial nanoplatforms have been harnessed, and this is a fundamental strategy in cancer immunotherapy. However, within the development of these artificial nanomaterials, there are still many unexplored opportunities, and technical issues and scientific challenges remain to be addressed. This minireview highlights current difficulties in cancer immunotherapy and the advantages of applying nanotechnology to address immune escape and rejection. Based on previous studies (Binnewies et al., 2018), herein, we would like to provide some key points and perspectives on nanomaterial design for an effective immunological response (**Figure 2**). These are as follows:

1) A deeper understanding of the TIMEs can better reveal advanced biomarkers for designing nanoplatforms to exert antitumor immunotherapy. The rich immunosuppression mechanism in the tumor makes it difficult for a single treatment to standalone. The development of new tumor immune escape mechanism pathways provides more immunological checkpoint blockade targets, such as FGL1/LAG-3 and VISTA. The controlled release and multidirectional carrying characteristics of targeted nanoplatforms can comprehensively inhibit multiple immune pathways, making ICB more effective. In addition, the I-E TIMEs result in poor therapeutic effect and require warming prior to combination with other therapies, providing new ideas for effective treatment.
2) Future prospects may involve rational combination of immunotherapies with other treatments for more efficient cancer inhibition and elimination. Generally, the immune system of the patient with cancer is normal, and the focus is on the mode of usage of the composite and intelligent nanomaterials to better tune the body's immune defense to eliminate the tumor. Hence, during the design of a nanomaterial, the combination of multiple treatment methods should be considered.
3) The enhanced immune strategy frequently leads to immune-related adverse events (irAEs). To promote basic to clinical conversion, safety of nanotechnology and side effects of immunity must be comprehensively evaluated (Sanmamed and Chen, 2018).

As a collaborative study, we believe that the use of nanotechnology to achieve higher objective response rates with fewer irAEs is a promising approach. Additionally, it is envisaged that the steady development of such nanomaterials will improve the quality of life for patients with cancer and certainly promote the transformation of cancer immunotherapy from a basic study to clinical application.

AUTHOR CONTRIBUTIONS

XS and TJ contributed equally this work. DN, ZY, and HZ are the corresponding authors. All the authors contribute to writing this manuscript.

FUNDING

This work was financially supported by the National Natural Science Foundation of China Research (Grant No. 81671732) and the Youth Fund of the Affiliated Hospital of Qingdao University.

ACKNOWLEDGMENTS

We would like to thank Editage (www.editage.com) for English language editing.

REFERENCES

Ai, X., Hu, M., Wang, Z., Lyu, L., Zhang, W., Li, J., et al. (2018). Enhanced cellular ablation by attenuating hypoxia status and reprogramming tumor-associated macrophages via NIR light-responsive upconversion nanocrystals. *Bioconjug. Chem*. 29, 928–938. doi: 10.1021/acs.bioconjchem.8b00068

Baronzio, G., Parmar, G., Ballerini, M., Kiselevsky, M., Cassuti, V., Irina, Zh S., et al. (2013). Update on the challenges and recent advances in cancer immunotherapy. *Immunotargets Ther*. 2:39. doi: 10.2147/itt.s30818

Beatty, G. L., Winograd, R., Evans, R. A., Long, K. B., Luque, S. L., Lee, J. W., et al. (2015). Exclusion of T cells from pancreatic carcinomas in mice is regulated by Ly6C(low) F4/80(+) extratumoral macrophages. *Gastroenterology* 149, 201–210. doi: 10.1053/j.gastro.2015.04.010

Bertrand, N., Wu, J., Xu, X., Kamaly, N., and Farokhzad, O. C. (2014). Cancer nanotechnology: the impact of passive and active targeting in the era of modern cancer biology. *Adv. Drug Deliv. Rev.* 66, 2–25. doi: 10.1016/j.addr.2013.11.009

Binnewies, M., Roberts, E. W., Kersten, K., Chan, V., Fearon, D. F., Merad, M., et al. (2018). Understanding the tumor immune microenvironment (TIME) for effective therapy. *Nat. Med*. 24, 541–550. doi: 10.1038/s41591-018-0014-x

Borkner, L., Kaiser, A., van de Kasteele, W., Andreesen, R., Mackensen, A., Haanen, J. B., et al. (2010). RNA interference targeting programmed death receptor-1 improves immune functions of tumor-specific T cells. *Cancer Immunol. Immunother*. 59, 1173–1183. doi: 10.1007/s00262-010-0842-0

Chae, Y. K., Arya, A., Iams, W., Cruz, M. R., Chandra, S., Choi, J., et al. (2018). Current landscape and future of dual anti-CTLA4 and PD-1/PD-L1 blockade immunotherapy in cancer; lessons learned from clinical trials with melanoma and non-small cell lung cancer (NSCLC). *J. Immunother. Cancer* 6:39. doi: 10.1186/s40425-018-0349-3

Deng, G., Sun, Z., Li, S., Peng, X., Li, W., Zhou, L., et al. (2018). Cell-membrane immunotherapy based on natural killer cell membrane coated nanoparticles for the effective inhibition of primary and abscopal tumor growth. *ACS Nano* 12, 12096–12108. doi: 10.1021/acsnano.8b05292

ElTanbouly, M. A., Croteau, W., Noelle, R. J., and Lines, J. L. (2019). VISTA: a novel immunotherapy target for normalizing innate and adaptive immunity. *Semin. Immunol*. 42:101308. doi: 10.1016/j.smim.2019.101308

Evans, R. A., Diamond, M. S., Rech, A. J., Chao, T., Richardson, M. W., Lin, J. H., et al. (2016). Lack of immunoediting in murine pancreatic cancer reversed with neoantigen. *JCI Insight* 1:e88328. doi: 10.1172/jci.insight.88328

Fan, Y., and Moon, J. J. (2015). Nanoparticle drug delivery systems designed to improve cancer vaccines and immunotherapy. *Vaccines* 3, 662–685. doi: 10.3390/vaccines3030662

Fu, B., Huang, X., Deng, J., Gu, D., Mei, Q., Deng, M., et al. (2018). Application of multifunctional nanomaterials in cancer vaccines (Review). *Oncol. Rep*. 39, 893–900. doi: 10.3892/or.2018.6206

Gadiot, J., Hooijkaas, A. I., Kaiser, A. D. M., van Tinteren, H., van Boven, H., and Blank, C. (2011). Overall survival and PD-L1 expression in metastasized malignant melanoma. *Cancer* 117, 2192–2201. doi: 10.1002/cncr.25747

Gajewski, T. F., Schreiber, H., and Fu, Y. X. (2013). Innate and adaptive immune cells in the tumor microenvironment. *Nat. Immunol*. 14, 1014–1022. doi: 10.1038/ni.2703

Gao, S., Yang, D., Fang, Y., Lin, X., Jin, X., Wang, Q., et al. (2019). Engineering nanoparticles for targeted remodeling of the tumor microenvironment to improve cancer immunotherapy. *Theranostics* 9, 126–151. doi: 10.7150/thno.29431

Goldberg, M. S. (2019). Improving cancer immunotherapy through nanotechnology. *Nat. Rev. Cancer* 19, 587–602. doi: 10.1038/s41568-019-0186-9

Goswami, K. K., Ghosh, T., Ghosh, S., Sarkar, M., Bose, A., and Baral, R. (2017). Tumor promoting role of anti-tumor macrophages in tumor microenvironment. *Cell. Immunol*. 316, 1–10. doi: 10.1016/j.cellimm.2017.04.005

Hodi, F. S., O'Day, S. J., McDermott, D. F., Weber, R. W., Sosman, J. A., Haanen, J. B., et al. (2010). Improved survival with ipilimumab in patients with metastatic melanoma. *N. Engl. J. Med*. 363, 711–723. doi: 10.1056/NEJMoa1003466

Huang, W.-C., Burnouf, P.-A., Su, Y.-C., Chen, B.-M., Chuang, K.-H., Lee, C.-W., et al. (2016). Engineering chimeric receptors to investigate the size- and rigidity-dependent interaction of PEGylated nanoparticles with cells. *ACS Nano* 10, 648–662. doi: 10.1021/acsnano.5b05661

Iwamura, K., Kato, T., Miyahara, Y., Naota, H., Mineno, J., Ikeda, H., et al. (2012). siRNA-mediated silencing of PD-1 ligands enhances tumor-specific human T-cell effector functions. *Gene Ther*. 19, 959–966. doi: 10.1038/gt.2011.185

Julia, V., Macia, L., and Dombrowicz, D. (2015). The impact of diet on asthma and allergic diseases. *Nat. Rev. Immunol*. 15, 308–322. doi: 10.1038/nri3830

Liu, J., Zhang, R., and Xu, Z. P. (2019). Nanoparticle-based nanomedicines to promote cancer immunotherapy: recent advances and future directions. *Small* 15, 1–21. doi: 10.1002/smll.201900262

Mahoney, K. M., and Freeman, G. J. (2020). Acidity changes immunology: a new VISTA pathway. *Nat. Immunol*. 21, 13–16. doi: 10.1038/s41590-019-0563-2

Mardiana, S., Solomon, B. J., Darcy, P. K., and Beavis, P. A. (2019). Supercharging adoptive T cell therapy to overcome solid tumor-induced immunosuppression. *Sci. Transl. Med*. 11:eaaw2293. doi: 10.1126/scitranslmed.aaw2293

Meir, R., Shamalov, K., Sadan, T., Motiei, M., Yaari, G., Cohen, C. J., et al. (2017). Fast image-guided stratification using anti-programmed death ligand 1 gold nanoparticles for cancer immunotherapy. *ACS Nano* 11, 11127–11134. doi: 10.1021/acsnano.7b05299

Nath, A., Pal, R., Singh, L. M., Saikia, H., Rahaman, H., Ghosh, S. K., et al. (2018). Gold-manganese oxide nanocomposite suppresses hypoxia and augments pro-inflammatory cytokines in tumor associated macrophages. *Int. Immunopharmacol*. 57, 157–164. doi: 10.1016/j.intimp.2018.02.021

Pan, J., Hu, P., Guo, Y., Hao, J., Ni, D., Xu, Y., et al. (2020). Combined magnetic hyperthermia and immune therapy for primary and metastatic tumor treatments. *ACS Nano* 14, 1033–1044. doi: 10.1021/acsnano.9b08550

Perica, K., Bieler, J. G., Schütz, C., Varela, J. C., Douglass, J., Skora, A., et al. (2015). Enrichment and expansion with nanoscale artificial antigen presenting cells for adoptive immunotherapy. *ACS Nano* 9, 6861–6871. doi: 10.1021/acsnano.5b02829

Ribas, A., and Wolchok, J. D. (2018). Cancer immunotherapy using checkpoint blockade. *Science* 359, 1350–1355. doi: 10.1126/science.aar4060

Sang, W., Zhang, Z., Dai, Y., and Chen, X. (2019). Recent advances in nanomaterial-based synergistic combination cancer immunotherapy. *Chem. Soc. Rev*. 48, 3771–3810. doi: 10.1039/c8cs00896e

Sanmamed, M. F., and Chen, L. (2018). A paradigm shift in cancer immunotherapy: from enhancement to normalization. *Cell* 175, 313–326. doi: 10.1016/j.cell.2018.09.035

Shi, X., Zhang, X., Li, J., Mo, L., Zhao, H., Zhu, Y., et al. (2018). PD-1 blockade enhances the antitumor efficacy of GM-CSF surface-modified bladder cancer stem cells vaccine. *Int. J. Cancer* 142, 2106–2117. doi: 10.1002/ijc.31219

Smith, T. T., Stephan, S. B., Moffett, H. F., McKnight, L. E., Ji, W., Reiman, D., et al. (2017). *In situ* programming of leukaemia-specific T cells using synthetic DNA nanocarriers. *Nat. Nanotechnol.* 12, 813–820. doi: 10.1038/nnano.2017.57

Spranger, S. (2016). Mechanisms of tumor escape in the context of the T-cell-inflamed and the non-T-cell-inflamed tumor microenvironment. *Int. Immunol.* 28, 383–391. doi: 10.1093/intimm/dxw014

Stephan, S. B., Taber, A. M., Jileaeva, I., Pegues, E. P., Sentman, C. L., and Stephan, M. T. (2015). Biopolymer implants enhance the efficacy of adoptive T-cell therapy. *Nat. Biotechnol.* 33, 97–101. doi: 10.1038/nbt.3104

Teo, P. Y., Yang, C., Whilding, L. M., Parente-Pereira, A. C., Maher, J., George, A. J. T., et al. (2015). Ovarian cancer immunotherapy using PD-L1 siRNA targeted delivery from folic acid-functionalized polyethylenimine: strategies to enhance T cell killing. *Adv. Healthc. Mater.* 4, 1180–1189. doi: 10.1002/adhm.201500089

Wang, C., Ye, Y., Hochu, G. M., Sadeghifar, H., and Gu, Z. (2016). Enhanced cancer immunotherapy by microneedle patch-assisted delivery of anti-PD1 antibody. *Nano Lett.* 16, 2334–2340. doi: 10.1021/acs.nanolett.5b05030

Wang, D., Wang, T., Liu, J., Yu, H., Jiao, S., Feng, B., et al. (2016). Acid-activatable versatile micelleplexes for PD-L1 blockade-enhanced cancer photodynamic immunotherapy. *Nano Lett.* 16, 5503–5513. doi: 10.1021/acs.nanolett.6b01994

Wang, J., Sanmamed, M. F., Datar, I., Su, T. T., Ji, L., Sun, J., et al. (2019). Fibrinogen-like protein 1 is a major immune inhibitory ligand of LAG-3. *Cell* 176, 334–347.e12. doi: 10.1016/j.cell.2018.11.010

Wang, J., Yang, T., and Xu, J. (2020). Therapeutic development of immune checkpoint inhibitors. *Adv. Exp. Med. Biol.* 1248, 619–649. doi: 10.1007/978-981-15-3266-5_23

Zhao, P., Wang, Y., Kang, X., Wu, A., Yin, W., Tang, Y., et al. (2018). Dual-targeting biomimetic delivery for anti-glioma activity via remodeling the tumor microenvironment and directing macrophage-mediated immunotherapy. *Chem. Sci.* 9, 2674–2689. doi: 10.1039/c7sc04853j

Zheng, Y., Tang, L., Mabardi, L., Kumari, S., and Irvine, D. J. (2017). Enhancing adoptive cell therapy of cancer through targeted delivery of small-molecule immunomodulators to internalizing or noninternalizing receptors. *ACS Nano* 11, 3089–3100. doi: 10.1021/acsnano.7b00078

Zou, W., Wolchok, J. D., and Chen, L. (2016). PD-L1 (B7-H1) and PD-1 pathway blockade for cancer therapy: Mechanisms, response biomarkers, and combinations. *Sci. Transl. Med.* 8:328rv4. doi: 10.1126/scitranslmed.aad7118

Conflict of Interest: The authors declare that the research was conducted in the absence of any commercial or financial relationships that could be construed as a potential conflict of interest.

The reviewer HP declared a shared affiliation, though no other collaboration, with one of the authors ZT to the handling editor.

frontiers in Chemistry

REVIEW
published: 18 September 2020
doi: 10.3389/fchem.2020.00838

Biomedical Application of Reactive Oxygen Species–Responsive Nanocarriers in Cancer, Inflammation, and Neurodegenerative Diseases

Jinggong Liu[1†], Yongjin Li[1†], Song Chen[1], Yongpeng Lin[1], Haoqiang Lai[2], Bolai Chen[1] and Tianfeng Chen[2*]*

[1] Orthopedics Department, Guangdong Provincial Hospital of Traditional Chinese Medicine, The Second Affiliated Hospital of Guangzhou University of Chinese Medicine, Guangzhou, China, [2] Department of Chemistry, Jinan University, Guangzhou, China

OPEN ACCESS

Edited by:
Dalong Ni,
Shanghai Jiao Tong University, China

Reviewed by:
Wei Tao,
Harvard Medical School, United States
Haibo Xie,
University of Wisconsin-Madison, United States
Han Zhang,
Shenzhen University, China

***Correspondence:**
Bolai Chen
chenbolai337@163.com
Tianfeng Chen
tchentf@jnu.edu.cn

[†]These authors have contributed equally to this work

Specialty section:
This article was submitted to Nanoscience, a section of the journal Frontiers in Chemistry

Received: *29 May 2020*
Accepted: *11 August 2020*
Published: *18 September 2020*

Citation:
Liu J, Li Y, Chen S, Lin Y, Lai H, Chen B and Chen T (2020) Biomedical Application of Reactive Oxygen Species–Responsive Nanocarriers in Cancer, Inflammation, and Neurodegenerative Diseases. Front. Chem. 8:838. doi: 10.3389/fchem.2020.00838

Numerous pathological conditions, including cancer, inflammatory diseases, and neurodegenerative diseases, are accompanied by overproduction of reactive oxygen species (ROS). This makes ROS vital flagging molecules in disease pathology. ROS-responsive drug delivery platforms have been developed. Nanotechnology has been broadly applied in the field of biomedicine leading to the progress of ROS-responsive nanoparticles. In this review, we focused on the production and physiological/pathophysiological impact of ROS. Particular emphasis is put on the mechanisms and effects of abnormal ROS levels on oxidative stress diseases, including cancer, inflammatory disease, and neurodegenerative diseases. Finally, we summarized the potential biomedical applications of ROS-responsive nanocarriers in these oxidative stress diseases. We provide insights that will help in the designing of new ROS-responsive nanocarriers for various applications.

Keywords: reactive oxygen species, nanocarriers, cancer, inflammation, neurodegenerative diseases

INTRODUCTION

Oxygen is necessary for aerobic respiration in living bodies. It is required in oxidative metabolism for the generation of adenosine triphosphate. However, partial reduction of molecular oxygen is mutagenic as it leads to the formation of reactive oxygen species (ROS) (Kaelin and Thompson, 2010). ROS constitutes a collective terminology referring to oxygen-derived free radicals and small molecules consisting of superoxide anion ($O_2\cdot^-$), hydroxyl free radical (·OH), hydrogen peroxide (H_2O_2), hypochlorous acid (HOCl), singlet oxygen ($^1O_2$), and so on (Bayr, 2005; Giorgio et al., 2007; Trachootham et al., 2009; Dickinson and Chang, 2011; Gligorovski et al., 2015). $O_2\cdot^-$ is the primary ROS produced by metabolic processes. Activation of oxygen with an electron from physical irradiation produces $O_2\cdot^-$, which generates ROS through a series of reactions. $O_2\cdot^-$ directly interacts with other molecules through enzymatic or metal-catalyzed processes to produce secondary ROS (Imlay, 2003; Valko et al., 2006; Hayyan et al., 2016). ROS is indispensable for normal physiological functions as they participate in cell signaling, immunity, and tissue homeostasis (Bryan et al., 2012; Ray et al., 2012; Nathan and Cunningham-Bussel, 2013; Nosaka and Nosaka, 2017).

ROS is considered as a double-edged sword playing beneficial or unavoidable toxic functions in living systems, depending on the equilibrium between ROS production and antioxidants. ROS is essential for physiological metabolism at normal concentrations. They regulate cellular response to hypoxia and resistance to infectious agents and participate in several cell-signaling systems. However, very high or low ROS levels directly or indirectly result in the pathogenesis of various diseases (Bandyopadhyay et al., 1999; Di Rosanna and Salvatore, 2012; Franceschi et al., 2018). Generally, numerous substances in cells are susceptible to the effects of ROS. ROS causes cellular damage and results in the formation of harmful by-products, such as lipid oxides and lipid peroxides. Similarly, excessive ROS causes damage proteins and DNA, blocks enzyme activity, or even leads to cancer (Kumar et al., 2008; Mouthuy et al., 2016; Kunkemoeller and Kyriakides, 2017; Franceschi et al., 2018). The imbalance in ROS generation and elimination is believed to be implicated with the oxidative stress, resulting in mitochondrial dysfunction. Oxidative stress directly or indirectly causes various diseases (Andersen, 2004; Barnham et al., 2004; Houstis et al., 2006; Ishikawa et al., 2008; Fraisl et al., 2009; Trachootham et al., 2009), including stroke (Sarmah et al., 2019), sepsis (Hoetzenecker et al., 2012), diabetes (Liang et al., 2018), hypertension (Touyz, 2003), neurodegenerative diseases (Radi et al., 2014), inflammation (Blaser et al., 2016), and cancer (Schumacker, 2015). Restoring the appropriate ROS concentration by regulating ROS production or neutralizing ROS is a potentially effective means of preventing and treating diseases related to oxidative stress (Zhou et al., 2016).

The unique redox microenvironment distinguishes the pathological area from the surrounding normal environment (Forman and Torres, 2001; Gomberg, 2020). For instance, the concentration of H_2O_2 in healthy human plasma is ∼1 to 8 μM (Lacy et al., 2000), whereas its level following activation of macrophages is as high as 1,000 μM (Droge, 2002; Yao et al., 2019). The concentration of hydrogen peroxide in respiratory lining cells is nearly 0.1 to 1 μM, but this increases by 20-fold in cases of inflammatory lung disease (Sznajder et al., 1989; Burgoyne et al., 2013). Developing ROS-responsive agents is postulated to be a promising solution to control the detrimental effects of ROS in cells (Liang and Liu, 2016; Hu et al., 2017; Zhang et al., 2019). Changes in the chemical structure, biochemical, or physical properties of ROS-responsive materials are induced by environmental stimuli (e.g., light, enzymes, pH, ionic strength, temperature, etc.) (Wang et al., 2014; Fang et al., 2015; An et al., 2016; Dou et al., 2017; Lee et al., 2018; Qiao et al., 2018; Xiang et al., 2018; Yang et al., 2020b). So far, stimuli-responsive agents have been extensively studied in biotechnology, as well as biomedicine fields (Hoffman, 2013; Grzelczak et al., 2019; Ovais et al., 2020). Redox-reactive materials hold huge promise in the design of drugs and gene delivery systems to target site-specific disease sites based on overproduction of ROS, protecting the cells against oxidative stress. This is because they can sense and eliminate active oxygen.

Nanotechnology provides numerous applications in the field of biomedicine. The development of nanotechnology has resulted in considerable progress in the design of nanoparticles (NPs) targeting ROS responses. Many researchers have studied the preparation and application of some ROS-responsive NPs (Tapeinos and Pandit, 2016; Xu et al., 2016; Saravanakumar et al., 2017; Ballance et al., 2019; Fan and Xu, 2020). Herein, we focused first on the production and physiological/pathophysiological effects of normal levels of ROS. Then the roles of ROS in cancer, inflammatory diseases, and neurodegenerative diseases were clarified. Moreover, we also focused on the latest progress of various ROS-responsive nanocarriers and highlight the mechanisms by which nanocarriers respond to changes in the oxidative microenvironment and its potential biomedical applications in three aspects, including cancer, inflammatory diseases, and neurodegenerative diseases (**Figure 1**).

ROS PRODUCTION AND PHYSIOLOGICAL/PATHOPHYSIOLOGICAL EFFECTS

The Generation of ROS

In 1954, Commoner et al. (1954) discovered free radicals in various freeze-dried biological materials. In the same year, Gerschman (1954) proposed that oxidized free radicals derived from partially reduced oxygen cause oxygen poisoning and related diseases. Harman (1956) subsequently defined these oxidizing free radicals and small molecules as ROS. ROS is produced by healthy cells during metabolism and in specific subcellular compartments (mainly mitochondria, **Figure 2A**, West et al., 2011). Activation of the nicotinamide adenine dinucleotide phosphate oxidase (NOX) complex located in the cell membrane generates ROS in some cancer cells (**Figure 2B**, Brandes et al., 2014). The endoplasmic reticulum also produces ROS; for example, flavoenzyme endoplasmic oxidoreductin-1 uses O_2 as a 2-electron receptor to produce H_2O_2 (Nathan and Cunningham-Bussel, 2013). $O_2{\cdot}^-$, as the first generated ROS, acts as a signaling molecule in aerobic organisms and regulates multiple physiological processes, including cell aging, apoptosis, and host defense (Newsholme et al., 2016). The monovalent reduction between O_2 and NADPH molecules generates $O_2{\cdot}^-$, which is converted to H_2O_2 and has a relatively short biological life span (Bhattacharjee, 2019). Notably, H_2O_2 is the most stable form of ROS and diffuses freely within and between cells. Besides direct oxidative injury, $O_2{\cdot}^-$ and its by-product H_2O_2 participate in the formation of other reactive substances (Bolduc et al., 2019). For instance, $O_2{\cdot}^-$ results in the production of highly reactive hydroxyl groups (·OH) through the Haber-Weiss cycle or a Fenton-type reaction.

HOCl is another type of ROS produced by the catalytic reaction of myeloperoxidase (MPO) and eosinophil peroxidase with H_2O_2 and Cl^- in body fluids (Freitas et al., 2009). HOCl is 100 to 1,000 times more destructive than $O_2{\cdot}^-$ and H_2O_2. Moreover, when it reacts with other biologically active molecules, it produces even more toxic effects than $O^{2\cdot-}$ and H_2O_2. HOCl promotes the production of $^1O_2$, a free radical with high reactivity with many biomolecules (Winterbourn, 2008). ·OH, HOCl, and $^1O_2$ are considered secondary ROS in comparison with the original ROS ($O_2{\cdot}^-$ and H_2O_2). They cause higher

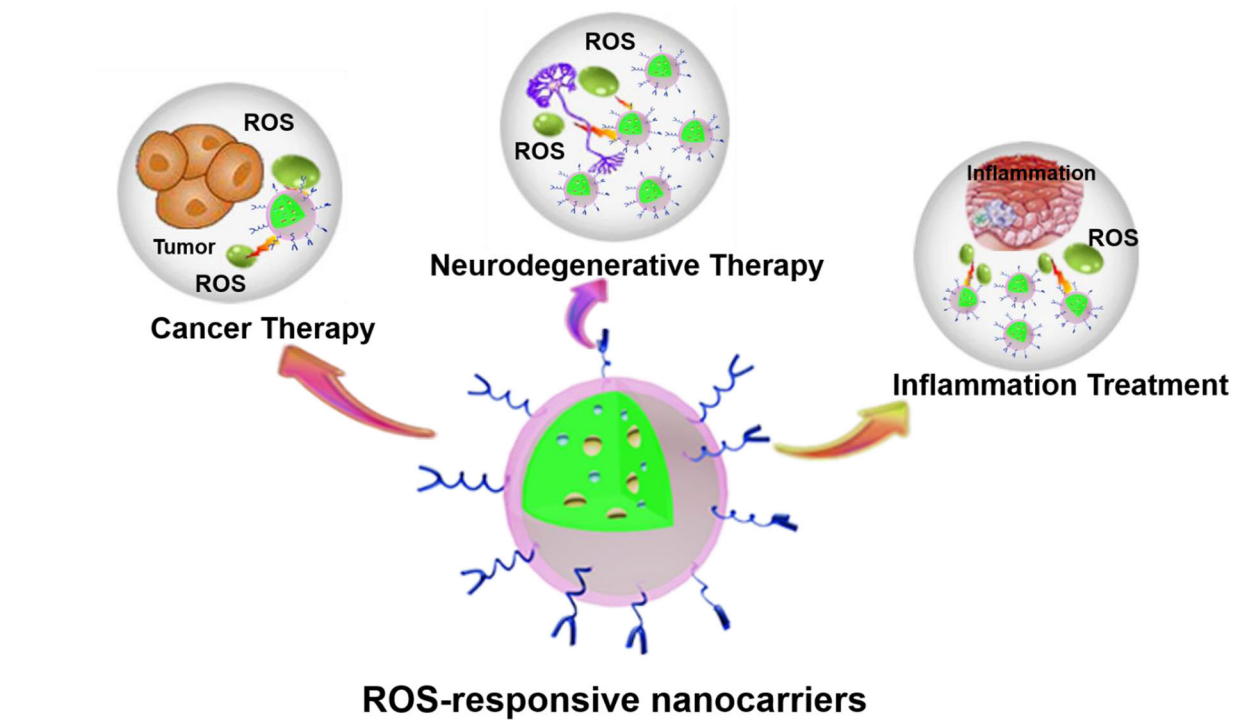

FIGURE 1 | ROS-responsive nanocarriers for various applications. The abundant material chemistry endows nanocarriers with unique ROS-responsive properties for the treatment of various pathological diseases, such as cancer, inflammation, neurodegenerative diseases, etc.

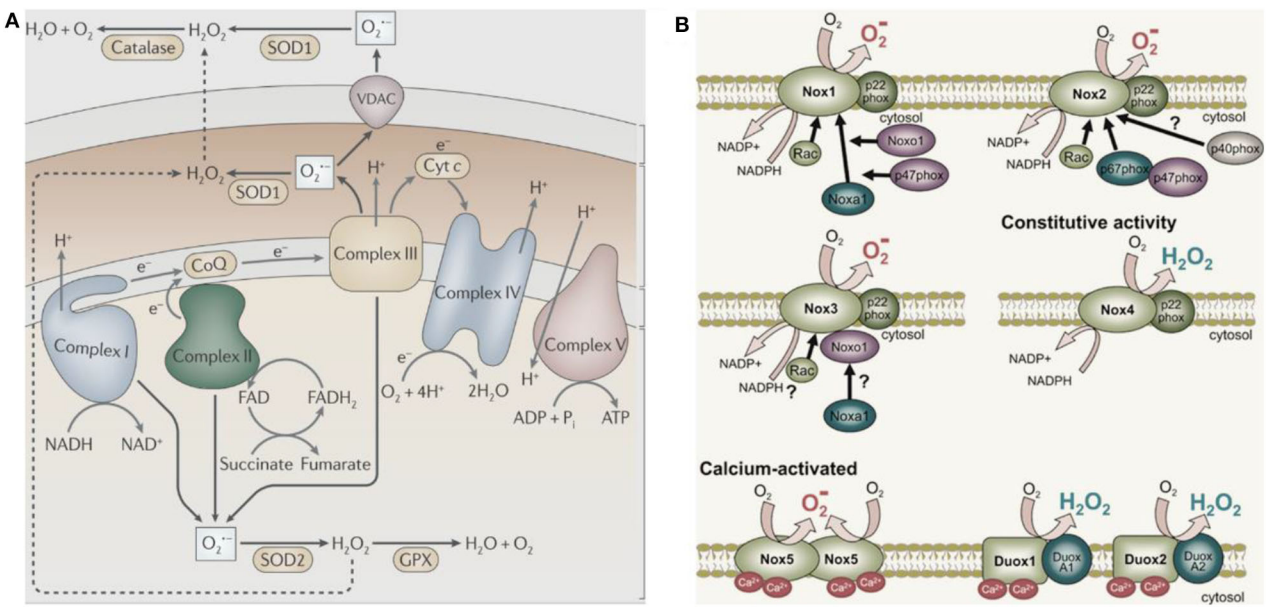

FIGURE 2 | The major cellular sources of ROS production. **(A)** The mitochondria sources of ROS (West et al., 2011) (Copyright 2011, reproduced with permission from Elsevier). **(B)** The NADPH sources of ROS (Brandes et al., 2014) (Copyright 2014, reproduced with permission from Elsevier).

oxidative damage to cells and tissues. Therefore, under stress conditions, it is crucial to prevent secondary ROS-induced oxidative damage. Unfortunately, there are no endogenous protective enzymes specific for these secondary ROS.

The Effect of Normal Levels of ROS on Physiological/Pathophysiological Process

A basal level of ROS can participate in many important physiological processes and play an important role in various signal cascades, such as the responses to growth factor stimulation or inflammation (Finkel, 2011; Le Belle et al., 2011; Beckhauser et al., 2016). ROS is involved in numerous cellular processes, including cell growth, proliferation, differentiation, apoptosis, cytoskeleton regulation, contraction, and migration. A healthy human body needs protection from the inflammatory responses, which eliminate harmful stimuli and initiate the healing process (Clark, 1999; Lamkanfi and Dixit, 2012). The NOX complex is rapidly activated by soluble factors and stimulants through interactions with cell surface receptors, leading to massive ROS oxidation (Lambeth, 2004). Numerous studies have confirmed that ROS acts as secondary messengers to regulate the production of inflammatory molecules and cytokines (Blaser et al., 2016; Missiroli et al., 2020). For instance, ROS stimulates macrophages to release tumor necrosis factor and the proinflammatory cytokine interleukin 1 (IL-1) (Hsu and Wen, 2002).

Active cellular proliferation produces H_2O_2, which influences the proliferation and differentiation of stem cells. For example, H_2O_2 is produced during proliferation of adult neural hippocampal progenitor cells, which then regulate self-renewal as well as neurogenesis via the PI3K/Akt signaling cascade. H_2O_2 augments overall proliferation of neural stem cells (NSCs) at moderate concentrations (Le Belle et al., 2011). At the same time, H_2O_2 is also considered as an intracellular signaling medium for neuronal differentiation induced by the nerve growth factor (Suzukawa et al., 2000). The rare case of hypothyroidism has revealed another example of the importance of ROS in health (Erdamar et al., 2008). H_2O_2 is an essential cofactor for thyroid peroxidase, which is involved in the production of thyroid hormone. Numerous studies have shown that dual oxidase 2 (and possibly dual oxidase 1) enzyme is required for H_2O_2 production and thyroid peroxidase function (Ameziane-El-Hassani et al., 2005). Notably, patients with congenital hypothyroidism possess dual oxidase 2 gene mutations, providing strong support for this theory (Moreno et al., 2002).

MECHANISMS AND EFFECTS OF ABNORMAL ROS LEVELS ON OXIDATIVE STRESS DISEASES

Cancer

Globally, cancer, following the cardiovascular disease, has the second highest death rate. Chemotherapy is currently among the primary clinical therapies for cancer; however, it is well-known to have relatively serious side effects. While chemotherapy drugs kill tumor cells, they additionally kill healthy cells and severely damage the immune system (Blattman and Greenberg, 2004). At the same time, multiple rounds of treatment with chemotherapeutic drugs cause cancer cells to become resistant, rendering the chemotherapy drugs ineffective (Riley et al., 2019). ROS has a critical influence on the progression of the cell cycle of malignancy cells through their role in energy metabolism, cell movement, cell state maintenance, cell proliferation, and apoptosis (Liou and Storz, 2010). Notably, ROS plays a dual function in tumors; they promote tumor proliferation, survival, and adaptation to hypoxia (Tafani et al., 2016). Cancer cells increase their metabolism and adapt to hypoxia to increase their ROS production rate to overactivate cancer-promoting signaling. On the other hand, ROS promotes antitumor signaling and triggers cancer cell death induced by oxidative stress (Reczek and Chandel, 2017). Moreover, ROS promotes tumorigenic signal transduction by overactivating the PI3K/Akt/mTOR survival cascade and by oxidation and deactivation of phosphatase and tensin homolog deleted on chromosome ten (PTEN) and protein tyrosine phosphatase 1B (PTP1B) phosphatase (negative modulators of PI3K/Akt signal transduction). The carcinogenic stimulation of Akt elevates ROS production to additionally promote cancer cell proliferation and survival (Clerkin et al., 2008; Cairns et al., 2011). Other relationships between cancer and ROS have also been elucidated. For example, ROS promote tumor cell survival by activating nuclear factor κB and Nrf2 (transcription factors that up-modulate antioxidant expression), which enable malignancy cells to escape ROS-mediated cell apoptosis (Morgan and Liu, 2011). ROS production decreases with the destruction of the mitochondrial respiratory chain, reducing the occurrence of tumors (Weinberg et al., 2010). In response to glucose and hypoxia deficiency, cancer cells undergo metabolic transformations, including AMP protein kinase activation, hypoxia-inducible factor (HIF) stabilization, and the use of a carbon metabolism axis (Denko, 2008). This raises the production of NADPH and ROS while leading to tumor angiogenesis and metastasis (Ye et al., 2014). ROS formation is additionally promoted by the release of $O_2\cdot^-$, ·OH, and H_2O_2 from the mitochondrial electron transport chain. ROS then stabilizes HIF-1α in normoxia and hypoxia (Huang et al., 1996). ROS plays an essential role in cancer cell metastasis by stimulating matrix metalloproteinases that break down constituents of the extracellular matrix to promote cancer cell invasion and infiltration (Folgueras et al., 2004). This stimulates the formation of the infiltrating foot, a membrane protrusion in cancer cells that is rich in actin, and participates in the proteolysis and invasion behavior of malignancy cells (Morry et al., 2017).

Inflammatory Diseases

Inflammation is related to many types of diseases, such as arthritis, coronary heart disease, myocardial infarction, asthma, and cystic fibrosis (Franceschi et al., 2018). Mounting research evidence shows that the overproduction of free radicals at the inflammatory area is related to the pathogenicity of associated diseases (Droge, 2002) Notably, ROS production has been reported to stimulate NLRP3 inflammatory body

assembly in a ROS-sensitive manner (Hughes and O'Neill, 2018). The primary source of ROS in response to harmful stimuli constitutes the mitochondria, which also directs inflammation by releasing mitochondrial DNA. Uncontrolled ROS production by mitochondria, hyperactivated leukocytes, and endothelial cells under chronic inflammation eventually leads to serious cell and tissue damage, further promoting and aggravating inflammatory damage. In numerous inflammatory diseases, the presently available intervention approaches have limited or no success (Hotamisligil, 2017); hence, we require new methods of treating chronic inflammatory diseases. It is assumed that the persistence of oxidative stress promotes these harmful inflammatory processes and could serve as new targets for treating chronic inflammation (Mittal et al., 2014). Rheumatoid arthritis (RA) is a systemic autoimmune disease with unknown etiology typified by chronic joint pain, macrophage invasion, and activated T-cell infiltration. The redox-sensitive signaling cascades cause abnormal expression of several adhesion molecules related to RA, which also cause monocytes and lymphocytes to migrate into the synovium in RA patients (Hitchon and El-Gabalawy, 2004). Atherosclerosis is a disease characterized by arterial wall thickening and is considered an inflammatory disease because it promotes the recruitment, expansion, and maintenance of monocytes/macrophages. This is due to the expression of endothelial cell factors constituting adhesion molecules and chemoattractants (Kinscherf et al., 1999) Oxidative stress induces overexpression of protein kinases and intercellular adhesion molecules, further promoting the infiltration of monocytes, smooth muscle cells, and macrophages (Droge, 2002). These cells bind to oxidized low-density lipoprotein, activate monocytes as well as macrophages, stimulate the Mn superoxide dismutase expression, and increase the levels of H_2O_2 (Yang et al., 2017). This high aggregation of ROS is thought to contribute to the development of atherosclerosis by causing high levels of macrophage apoptosis (Kinscherf et al., 1999).

Neurodegenerative Diseases

Diseases in which neuronal loss progresses slowly are collectively referred to as neurodegenerative diseases (Manoharan et al., 2016). The common neurodegenerative diseases include amyotrophic lateral sclerosis (ALS), Parkinson disease (PD), Huntington disease (HD), and Alzheimer disease (AD). The brain has a high requirement for oxygen and a comparatively high level of redox-active metals, e.g., iron or copper, which play catalytic roles in the production of ROS (Cheignon et al., 2018). Consequently, the brain is more susceptible to suffer from oxidative stress (Liu et al., 2017c). Additionally, as the concentration of polyunsaturated fatty acids in the cell membrane increases, the brain becomes more prone to lipid peroxidation (Youdim et al., 2000; Barnham et al., 2004). The causes of neurodegenerative diseases are closely related to oxidative stress (Uttara et al., 2009; Melo et al., 2011). Analysis of AD pathogenesis revealed that the deterioration of antioxidant status, mitochondrial deterioration, and increased apoptosis accompany poor antioxidant status (Manoharan et al., 2016). Physiologically, the brain has a low antioxidant capacity, and the glial cells and neurons have a relatively strong metabolism and higher oxidation sensitivity and are more likely to produce excessive superoxide free radicals, altogether making the brain more prone to oxidative stress, which causes AD (Nakajima and Kohsaka, 2001; Gadoth and Göbel, 2011). Similarly, oxidative stress is closely related to the pathogenesis of PD, ALS, and HD. The occurrence of diseases, such as PD, also leads to excessive ROS production. Numerous studies have shown that PD reduces the activity of the respiratory chain complex I, resulting in excessive ROS (Schapira, 1998; Guo et al., 2013). At the same time, dopamine metabolism at the site of the disease increases, causing the accumulation of toxic oxidative free radicals (Cadet and Brannock, 1998).

ROS-Responsive Nanocarriers and Their Applications

The results of our group and numerous other studies show that ROS could be used as a target or biosignature for the treatment of various diseases (Huang et al., 2017, 2020; Mei et al., 2018; Lai et al., 2019; He et al., 2020; Yang et al., 2020a,c; Zhao et al., 2020). Reactive oxygen species–responsive materials refers to materials capable of responding to those elevated ROS, such as H_2O_2, $O^{2\cdot-}$, $^1O_2$, and so on. There have been great progress in nanomedicines and responsive materials used in biomedical fields (Tao et al., 2017, 2019; Qiu et al., 2018, 2019; Luo et al., 2019; Feng et al., 2020; Hu et al., 2020; Kong et al., 2020; Tang et al., 2020; Xie et al., 2020). ROS-responsive nanocarriers have some unique advantages for therapy compared with these reported materials. ROS-reactive agents are activated by ROS *in vivo* to produce corresponding physical or chemical changes. ROS-reactive materials could be utilized as imaging agents, site-specific delivery agents, and drugs for the treatment of various diseases. They could additionally be employed to modulate the tissue microenvironment and enhance the regeneration of tissues, as well as navigating and sensing via programmed changes in material properties (Tapeinos and Pandit, 2016; Saravanakumar et al., 2017; Ballance et al., 2019). Depending on its reaction to oxidation, the mechanisms of ROS-reactive functional groups are categorized into two main classes, namely, the change of physical characteristics (solubility) and the change in chemical bonds accompanying polymer degradation. The responsiveness of these ROS-responsive functional groups under diverse conditions is dependent on the type of ROS, the structure of the polymer, the shape of the material, and the exposure time.

So far, top-down and bottom-up are the two main methods for the fabrication of NPs, including the nanocarriers (Chan and Kwok, 2011; Qiu et al., 2018). Generally, most of the ROS-responsive nanocarriers are formed by bottom-up methods. The small drug molecules or polymers can be built up into NPs with bottom-up methods, but the shape, size, and dispersity are not easily to control, while the top-down method can be used in the fabrication of NPs with well-controlled shape and uniform size (Chan and Kwok, 2011). Maruf et al. (2020) fabricated red blood cell membrane–coated ROS-responsive 5-aminolevulinic acid prodrug nanostructures with robust atheroprotection using the top-down method.

Drug carriers, in the form of NPs, which respond to ROS, are designed to release their payloads in response to high ROS levels by increasing emissions or explosions. The drug molecules contained in these particles are small compounds or biomolecules. The particles can be used with a group of chemicals that react with ROS to create a charge and change the hydrophilicity, bonding, breaking, or otherwise stimulate the reaction at the particle. Overall, these reactions cause the swelling of particles, separation of particles, or increased release of drug molecules from particles. Researchers choose specific mechanisms for particle operations and drug delivery, respectively, depending on the final target of the particles. Currently, most of the ROS-responsive nanocarriers reported show low toxicity toward their own *in vitro* and *in vivo* cell and animal evaluation models, and the loading capacity of these nanocarriers depends on the carrier itself and the interaction of between the carriers and the payloads. In this section, we will discuss NPs that respond to ROS and their use as drug delivery carriers for various applications in cancer, inflammation, and neurodegenerative diseases. Some representative ROS-responsive agents and their biomedical applications are also summarized in **Table 1**.

Application of ROS-Responsive NPs for Cancer Therapy

In cancer cells, the concentration of ROS is higher compared with the normal cells because of the constant generation of ROS as the by-products of aerobic metabolic processes resulting from oncogenic transformation (Kong and Chandel, 2020). The elevated ROS levels in malignancies are employed in the design of ROS-responsive nanoagents, which promote site-specific drug release. The most common typical groups utilized in the design of ROS-responsive components include boronic ester, thioketal, and sulfide groups (summarized in **Table 1**). These ROS-responsive components result in the design of drug carriers for the systematic delivery of chemotherapy.

Selenium (Se) is a chalcogen element widely present in some proteins capable of maintaining the cellular redox homeostasis (e.g., glutathione peroxidase, thioredoxin reductase) (Chaudhary et al., 2016). Se-containing particles can oxidize and change their hydrophilicity in response to ROS. Various Se derivatives of inorganic, organic, and amino acids have been found to exhibit biological activity primarily via antioxidant and pro-oxidant mechanisms (Lai et al., 2019; Huang et al., 2020). The different oxidation states (−2, 0, +4, +6) and forms of Se contribute to the antioxidant effects of Se. The direct antioxidant function of Se is conferred by some of the selenoproteins that directly protect against oxidative stress. Moreover, the regeneration of low-molecular-weight antioxidants (Q10, vitamins C and E, etc.) mediated by selenoproteins makes Se an indirect antioxidant (Hatfield et al., 2009; Lobanov et al., 2009). However, at elevated doses, Se typically turns into a pro-oxidant with well-established growth inhibiting properties and high cytotoxic activities. Toxicity of Se compounds is thus strictly dependent on the concentration of Se-binding chemical species and the associated redox potential (Weekley and Harris, 2013). Therefore, in addition to redox function of modified Se NMs, anticancer activity of differently modified Se NMs has also been reported (Liu et al., 2015, 2016). Epidemiological studies have shown that SeNPs can effectively prevent and treat diseases related to oxidative stress. The overproduction of ROS is an important contributor for cisplatin-induced nephrotoxicity. Our group developed a polyphenol-functionalized SeNPs (Se@TE NPs) using microwave-assisted method (Lai et al., 2019). Se@TE NPs showed renal protection activities through reducing the cisplatin-induced ROS. The facial tea polyphenols are ROS-responsive and could be consumed with the explosion to ROS, releasing the inner SeNPs. The suppressing of p53 phosphorylation and regulating of AKT and MAPKs signaling pathways of Se@TE NPs were confirmed in HK-2 cells. Further mechanistic studies suggested that Se@TE NPs showed its protective effects in the form of selenomethionine (Se-Met) and selenocystine (Se-Cys2), activating selenoenzymes and eliminating the excessive ROS (**Figure 3**). Recently, in our other Se-related work, we paid attention to the chiral nanomaterials and fabricated a chiral glutathione (GSH) SeNPs (G@SeNPs), coated with GSH on the surface of SeNPs, capable of preventing oxidation damage caused by palmitic acid (Huang et al., 2020). G@SeNPs showed ROS-responsive and clearance activities in INS-1 cells. Positron emission tomography imaging of chiral G@SeNPs *in vivo* illustrated that the ^{64}Cu-labeled L-G@SeNPs were cleared slower in organs than D-G@SeNPs because of the homologous adhesion between L-GSH and the L-phospholipid membrane. This remaining higher concentration of L-G@SeNPs contributed to the stronger antioxidant activities.

Zhang et al. (2015) developed a biocompatible ROS-responsive β-cyclodextrin (β-CD) NPs through the conjugation of 4-phenylboronic acid pinacol ester (PBAP) onto the hydroxyl groups of β-CD for upgraded drug delivery applications. Because of the sensitivity of boronic ester units to the oxidation-responsive microenvironment, the newly obtained (Ox-bCD) material is hydrolyzed into parent β-CD molecules when exposed to ROS, displaying superior biocompatibility both *in vitro* and *in vivo*. Additionally, other therapeutics, such as imaging agents and biomacromolecules, can also be transported using this ROS-triggered nanocarrier for different applications.

Proteins have also been used as carriers for ROS-responsive cancer therapy. For instance, a protein-based delivery system named RNase A-NBC is responsive to ROS designed through a convenient chemical conjugation of 4-nitrophenyl 4-(4,4,5,5-tetramethyl-1,3,2-dioxaborolan-2-yl) benzyl carbonate (NBC) with the lysine residues of RNase A. These RNase A-NBC NPs present with minor cytotoxicity against normal cells but selective inhibition cytotoxicity against tumor cells because of the high concentration of ROS in malignant cells compared with the healthy cells. The high levels of H_2O_2 react with the amide bond and induce the lysine deprotection in cancer cells, reestablishing the cytotoxicity effect of RNase A in tumor cells. These protein-based pharmaceutical products are used as a tool targeting ROS-responsive cancer therapy (Wang et al., 2014).

ROS is elevated in the tumor microenvironment and the biotin transporter; avidin is overproduced in many tumors. The cancer-targeting ROS-responsive nanocarriers release

TABLE 1 | Representative ROS-responsive materials and their biomedical applications.

ROS-responsive materials	Nanocarriers	Application	References
Selenium	Diselenide block copolymers	Oxidants and reductants dual-responsive combining radiotherapy and chemotherapy.	(Ma et al., 2010b)
	Diselenide-containing polyelectrolyte multilayer film	Combination of chemotherapy and photodynamic therapy	(Ren et al., 2013)
	Phosphate segments and selenide groups polymer	H_2O_2-triggered drug release for cancer treatment	(Liu et al., 2013)
	Selenium-containing polyphosphoester nanogels	ROS induced the release of Dox for cancer treatment	(Zhang et al., 2018)
	Selenium-containing amphiphilic block copolymer PEG-PUSe-PEG	Oxidation-responsive release of Dox	(Ma et al., 2010a)
Sulfur	Polypropylene sulfide nanoparticles	Reduce the tissue reaction to neuroprostheses	(Mercanzini et al., 2010)
	Free-blockage mesoporous Nanoparticles	ROS induced the release of Dox for cancer treatment	(Cheng et al., 2017)
	Thioether linked conjugates	GSH and ROS dual-responsive for cancer chemotherapy	(Luo et al., 2016)
	Thioketal nanoparticles (TKNs) loaded with TNF-α-siRNA	ROS-sensitive nanoparticles targeting inflammation with oral administration	(Wilson et al., 2010)
Tellurium	Coassemblies of tellurium-containing molecules and phospholipids	ROS-responsive with good biocompatibility	(Wang et al., 2015)
	Hyperbranched tellurium-containing polymers	Site-specific elimination of excess ROS	(Fang et al., 2015)
	Tellurium-containing polymer (PEG-PUTe-PEG) based nanoparticles	Near-infrared light stimuli-responsive synergistic therapy for cancer	(Li et al., 2017a)
	Tellurium-containing polymer micelle	Combination of chemo- and radio-therapies with responsive to both $H_2O_2$and 2 Gy gamma radiation	(Cao et al., 2015)
Oxalate esters	Poly(vanillin oxalate) (PVO) nanoparticles	H_2O_2-responsive nanoparticles for the treatment of ischemia–reperfusion injury	(Kang et al., 2016)
	Poly(vanillyl alcohol-co-oxalate) (PVAX) polymers	Oxidation-responsive nanoparticles for anticancer drug delivery	(Huang et al., 2018)
	Peroxalate nanoparticles	*In vivo* imaging of H_2O_2	(Lee et al., 2007)
	Hydroxybenzyl alcohol (HBA)-incorporated copolyoxalate	H_2O_2 responsive nanoparticles for detection and therapy of ischemia–reperfusion injury	(Lee et al., 2013)
	Poly(vanillin oxalate) (PVO)	H_2O_2- and acid-mediated hydrolytic degradation with anti-inflammatory activity	(Kwon et al., 2013)
Phenylboronic acid (ester)	Amphiphilic block copolymers containing aryl boronate ester-capped block	Sustained drug release combination chemotherapy with magnetic resonance (MR) imaging	(Deng et al., 2016)
	Conjugating phenylboronic acid pinacol ester (PBAP) groups onto β-CD	ROS-responsive and H_2O_2-eliminating materials for diseases associated with inflammation and oxidative stress	(Zhang et al., 2017)
	Boronic ester modified dextran polymer nanoparticles	H_2O_2 responsive nanoparticles for ischemic stroke treatment	(Lv et al., 2018)
	Poly[(2-acryloyl)ethyl(*p*-boronic acid benzyl)diethylammonium bromide] (BA-PDEAEA, BAP) modified traceable nanoparticles	H_2O_2 responsive nanoparticles for RNAi-based immunochemotherapy of intracranial glioblastoma	(Qiao et al., 2018)

the drugs into the tumor microenvironment, resulting in higher antitumor efficacy. Based on the cancer-targeting and ROS-responsive dual concepts, Lee et al. (2018) proposed new bilirubin-based NPs (BRNPs) using biotin as cancer targeting ligand and bilirubin as the ROS-responsive carrier. Additionally, doxorubicin (Dox) is loaded as a therapeutic drug. In the synthesis of this drug, bt-PEG-BR is first obtained by reacting bilirubin and biotin-PEG, and then the Dox@bt-BRNPs are prepared in a single-step self-assembly procedure, with its size ∼100 nm (**Figure 4**). Dox is released from the

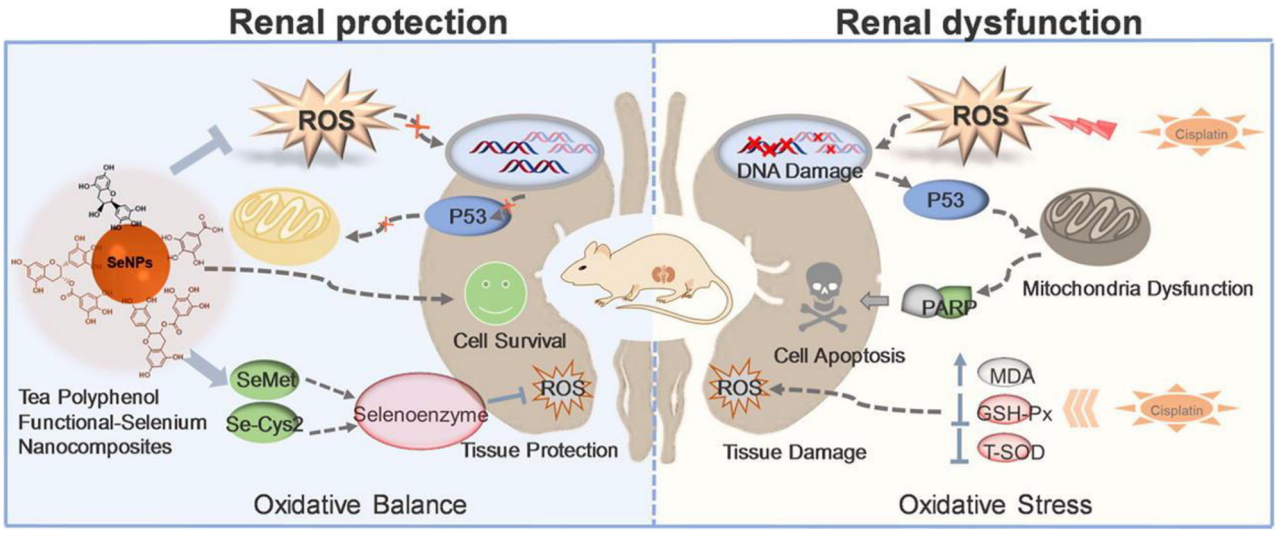

FIGURE 3 | Tea polyphenol functionalized selenium nanoparticles reversed cisplatin-induced renal injury (Lai et al., 2019) (Copyright 2019, reproduced with permission from Elsevier).

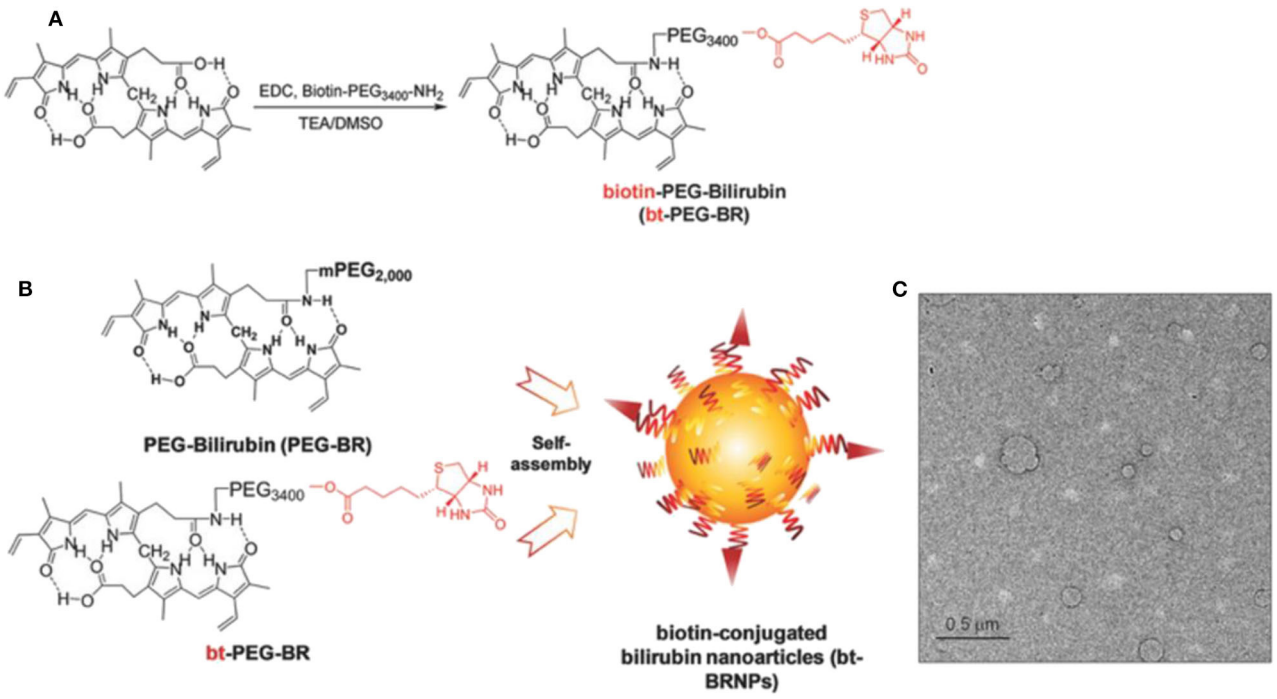

FIGURE 4 | Biotin-conjugated bilirubin nanoparticles (bt-BRNPs) are formed from biotin-PEG-bilirubin (bt-PEG-BR) and PEG-bilirubin (PEG-BR) (Lee et al., 2018) (Copyright 2018, reproduced with permission from Elsevier). **(A,B)** Scheme for the synthesis of bt-PEG-BR starting from free bilirubin and biotin-PEG **(A)** and the formation of bt-BRNPs by self-assembly from PEG-BRs and bt-PEG-BR in PBS **(B)**. **(C)** Transmission electron microscopy (TEM) images of bt-BRNPs. Scale bar: 500 nm.

BRNPs after incubation with a peroxy radical precursor, 2,2′-azobis (2-amidinopropane) dihydrochloride, exhibiting the ROS-responsive releasing activities. Dox@bt-BRNPs has superior anticancer efficacy in biotin transporter–overexpressing HeLa cells than the free Dox. Similar results have been reported in xenograft mice. More BRNPs are preferentially accumulated and distributed in tumor areas than in other organs, as reported via *in vivo* fluorescence imaging assays (Lee et al., 2018). The biodegradability and biocompatibility of the bt-BRNPs made BRNPs as

novel ROS-responsive nanocarriers for treating various tumors effectively.

ROS/GSH-Responsive Nanocarriers for Cancer Therapy

Compared with healthy cells, malignant cells have a strong reduction environment because of the excessive production of intracellular GSH. However, some cancer cells produce excessive ROS simultaneously, resulting in increased oxidative stress (Fang et al., 2009). Besides, regarding the redox potential difference, cancer cells are characteristically heterogeneous. The levels of GSH/ROS vary across different stages of tumor growth and reproduction, and excessive production of ROS and GSH is present in various cancers or different areas of the same malignancy at the same time (Marusyk and Polyak, 2010). Nanocarriers capable of a dual response to ROS/GSH have attracted broad interests because of their application prospects in controllable packaging and drug delivery in physiological environments.

Luo et al. (2016) reported a new redox dual-reaction prodrug nanosystem self-assembled from paclitaxel (PTX), oleic acid (OA), and thioether bonds. This novel prodrug nanosystem provides a solution to issues associated with the low drug loading and low-efficiency drug release of PTX hydrophobic drugs and has been used for additional drug development. PTX is released via thiolysis by GSH or oxidation by ROS and exhibits potent *in vivo* antitumor efficacy in KB-3-1 tumor mice, without non-specific toxicity to major organs and tissues (Luo et al., 2016). This redox dual-sensitive polymers or complexes offer effective anticancer drug delivery possibilities. In the work of Chen et al. (2018), a type of thioketal NPs (TKNs) with double reactivity to H_2O_2 and GSH was designed for PTX delivery. This dual-responsive nanocarrier is sensitive to biologically relevant levels of GSH, and H_2O_2, releases drugs on demand and is biodegraded into biocompatible by-products after completing drug delivery tasks, compared with other stimuli-responsive nanocarriers (**Figure 5**). Given the variability in redox potential gradients across different microenvironments *in vivo*, the TKNs loaded with PTX (PTX-TKN) respond first to extracellular ROS, followed by the intracellular GSH, to achieve the controlled release of PTX into tumor sites. Both *in vitro* and *in vivo* findings showed that PTX-TKN is selective for cancer cells with high ROS and GSH levels.

Applications of ROS-Responsive Nanocarriers in Combination Other Therapy Strategies

Chemotherapy, combined with hyperthermia, has attracted considerable research attention in disease treatment, such as cancer. Photothermal therapy (PTT) has represented an extraordinary non-invasive approach for cancer treatment, and photothermal agents are able to covert near-infrared (NIR) light into thermal energy under light irradiation. The NIR lasers most commonly used in PTT are 808 and 980 nm, and the safe power density limits are ~0.33 and ~0.726 W cm^{-2}, respectively. Precise delivery of drugs to complicated and specific pathological sites while controlling the quantitative release of drugs remains challenging. Therefore, to ensure the simultaneous delivery of chemotherapeutic drugs and photothermal agents to the tumor area and achieve their synergistic effect, Xiao et al. (2015)

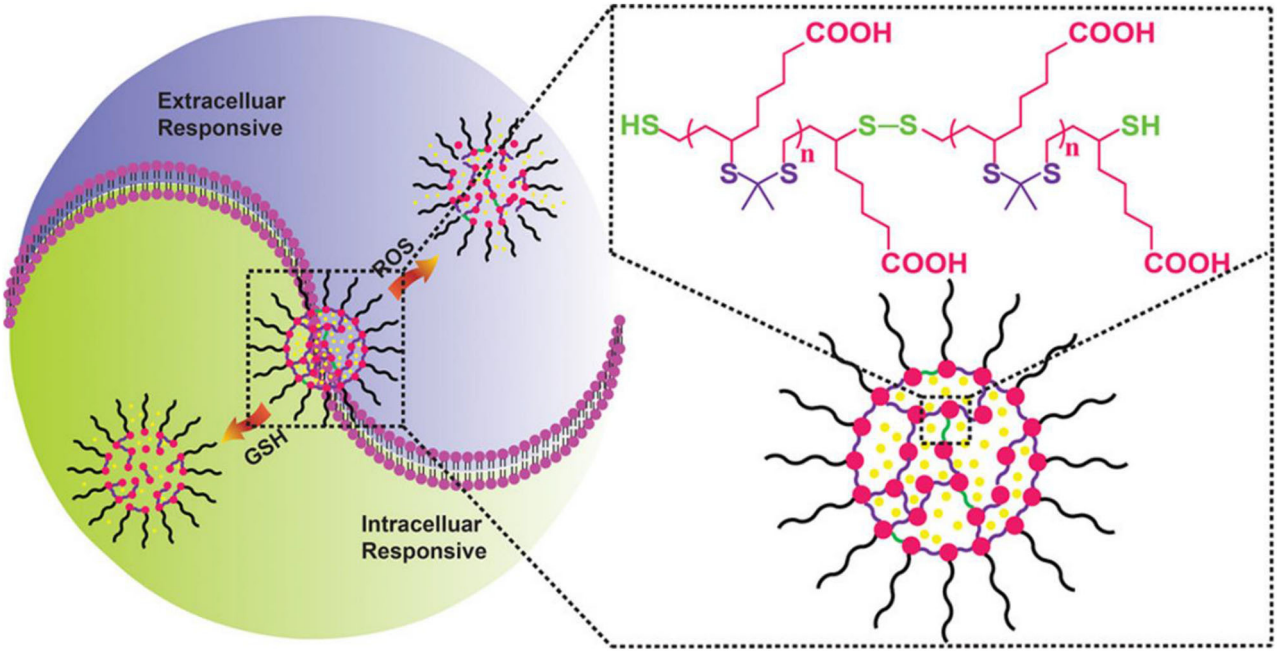

FIGURE 5 | Schematic illustration of the ROS and GSH dual-responsive nano-DDS, the structure of nano-DDSs, containing both ROS-responsive (purple) and GSH-responsive (green) motifs (Chen et al., 2018) (Copyright 2018, reproduced with permission from American Chemical Society).

developed a thermal and ROS dual-responsive polymer with an alternating structure of hydrophilic and hydrophobic links in its backbone. The triblock copolymer is easily synthesized via thiophene polymerization of the poly(ethylene glycol) (PEG) diacrylate and 1,2-ethanedithiol (EDT) monomer. Nile red is effectively encapsulated into the core of the nanocarriers at physiological temperatures and is released upon the destruction of the NP triggered by oxidation. This adjustable thermal response behavior combined with oxidizable thioether groups renders these PEG-EDT copolymers as promising ROS-reactive drug delivery system. Moreover, Wang and coworkers fabricated a NIR light and ROS dual-responsive Se-inserted copolymer (I/D-Se-NPs) for synergistic thermo-chemotherapy (Wang et al., 2017). The photothermal agent (ICG) and the chemotherapeutic drug (Dox) are loaded. A 785-nm irradiation at 1.0 W cm^{-2} is used to evaluate the photothermal conversion of I/D-Se-NPs. The ΔTm value of I/D-Se-NPs was 7.8°C when the ICG was used at a dose of 2.0 $\mu g\ mL^{-1}$, exhibiting promising photothermal conversion efficiency.

The combination of $^1O_2$-responsive nanocarriers with other treatment, such as photodynamic therapy (PDT), has remarkable synergistic therapeutic effects (Wang et al., 2016; Yang et al., 2016; Yu et al., 2016; Li et al., 2017b; Liu et al., 2017a). In PDT, non-toxic photosensitizers are activated by exogenous light of a specific wavelength to transfer their excited energy to the surrounding oxygen to produce ROS. Ce6 is extensively used in photodynamic treatment of cancer as a photosensitizer and effectively generates $^1O_2$ under light irradiation. Yang and coworkers developed a smart mesoporous silica nanorod drug delivery system with a photosensitizer chlorin e6 (Ce6) doped in a *bis*-(alkylthio) alkene (BATA) as the nanocarrier, named CMSNRs. The BATA linker is cleaved by $^1O_2$ produced by Ce6 after illumination with 660 nm light irradiation, Dox is released from this $^1O_2$-responsive CMSNRs both *in vitro* and *in vivo* (Yang et al., 2016). Furthermore, Liu et al. (2017a) developed light-controlled, $^1O_2$-responsive polymers, NCP-Ce6-DOX-PEG, through a solvothermal method with a size of about 70 nm (Liu et al., 2017a). UV-vis-NIR absorption spectrum showed that the Ce6 and Dox were loaded in this nanocarrier with the loading ratio of 80% of Ce6 (**Figure 6**). As low as 5 mW cm^{-2} light irradiates the release of $^1O_2$, breaking the BATA link. This accelerated $^1O_2$-responsive nanoscale coordination polymers in tumors are observed through computed tomography imaging, and this combination of chemophotodynamic therapy has excellent antitumor efficacy *in vitro* and *in vivo* (Liu et al., 2017a).

Sun et al. (2019) designed photoactivatable photodynamic PEG-coated drug nanoplatforms for core-shell cooperative chemotherapy and PDT. A new type of photodynamic polymer was rationally developed and synthesized through conjugation of pyropheophorbide-a (PPa) with PEG 2000 (PEG2k). In this system, PTX is encapsulated as the therapeutic drug, and PPa is utilized as the hydrophobic and photodynamic part of the amphiphilic PPa-PEG2k polymer. PPa-PEG2k is used in PDT treatment; under laser irradiation, PPa-PEG2k produces ROS and synergistically promotes endogenous ROS generation in cancer cells to promote PTX release. Nanomicelles have also been employed in the construction of a photoactivatable system. A recent study on new nanomicelles constructed long-circulating photoactivated nanocarriers via self-assembly of thioketal and a PEG-stearyl amine conjugate (PTS) (Uthaman et al., 2020). Dox and photosensitive pheophorbide A (PhA) are coloaded into the formed nanocarriers to enhance local chemical and PDT (**Figure 7**). The resulting Dox- and PhA-loaded nanocarriers exhibit ROS stimulus responsiveness after accumulating in the tumor area to release the internally loaded DOX and PhA. Moreover, after laser irradiation of the tumor area, PhA initially released into the tumor produces enhanced $^1O_2$, thereby promoting the rapid dissociation of nanocarriers and accelerating the release of DOX. ROS triggers the photoactivated PhA to release Dox, which increases local ROS levels gradually to inhibit cancer cell growth and enhance antitumor immunity synergistically. Therefore, the combination of ROS-sensitive PTS nanocarriers with local chemical PDT is a promising method for treating tumors.

Application of ROS-Responsive NPs for Inflammation Treatment

In recent years, preclinical and clinical research has demonstrated that excessive ROS at the inflammatory site accelerates disease progress. Numerous studies utilize ROS as triggers in developing ROS-responsive NPs carrying anti-inflammatory drugs (Pu et al., 2014; Feng et al., 2016; Zhang et al., 2017, 2020; Chen et al., 2019; Li et al., 2019, 2020; Ni et al., 2020). The release of loaded drugs in the inflammatory joints improves patient symptoms. Boronic esters are excellent and selective H_2O_2-responsive units and are degraded under physiologically relevant H_2O_2 levels. Furthermore, these types of boronic ester–functionalized nanomaterials possess good safety profiles. They are a promising approach for the development of ROS-responsive nanocarriers with significant potential for clinical translation. Zhang et al. (2017) designed and synthesized a series of ROS-responsive core-shell OxbCD NPs via conjugation of PBAP groups onto a β-CD with H_2O_2-eliminating profiles (**Figure 8A**). These OxbCD NPs have excellent antioxidant and anti-inflammatory activities. The anti-inflammatory mechanisms of OxbCD NPs are shown in **Figure 8B**. OxbCD NPs reverse the oxidative stress and repress cell death triggered by H_2O_2 in RAW264.7 cells. OxbCD NPs efficaciously decrease the secretion of the classic inflammatory chemokines, such as MCP-1, MIP-2, and IL-8, as well as the proinflammatory cytokines consisting of tumor necrosis factor α (TNF-α), IL-1β, and IL-6, the expression levels of which are high in H_2O_2 treatment macrophages. Additionally, neutrophil infiltration and macrophage recruitment are inhibited with the treatment of OxbCD NPs. Moreover, OxbCD NPs suppress the expression of the activation marker, MPO, and other oxidative mediators. Finally, OxbCD NPs loaded with anti-inflammatory drugs have superior efficacy as seen in an acute inflammation model of peritonitis in mice. RA is an immune-mediated inflammatory disease with higher levels of ROS. ROS in arthritis tissues leads to the overproduction of the cytokines consisting of TNF-α, IL-1β, and IL-6. The interactions between these inflammatory factors and ROS mainly

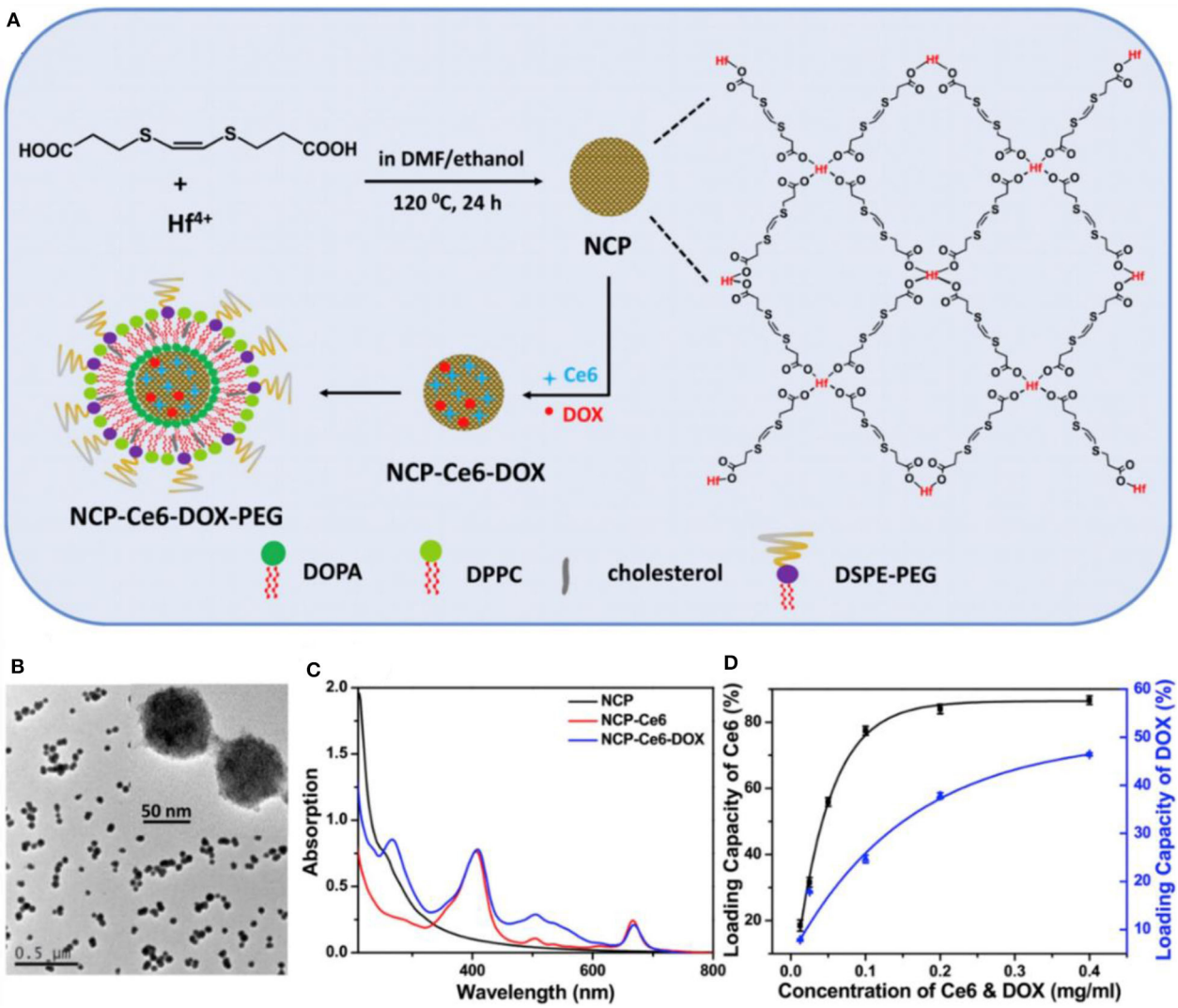

FIGURE 6 | The synthesis and characterization of NCP-Ce6-DOX-PEG nanoparticles (Liu et al., 2017a) (Copyright 2017a, reproduced with permission from Elsevier). **(A)** The schematic illustration for the synthesis of NCP-Ce6-DOX-PEG nanoparticles. **(B)** A TEM image of NCP nanoparticles. The insert is an image with higher resolution. **(C)** UV-vis-NIR spectra of NCP, NCP-Ce6, and NCP-Ce6-DOX. **(D)** Quantification of Ce6 and DOX loadings at different feeding concentrations of Ce6 and DOX in ethanol. NCP solutions with the same concentration (0.05 mg/mL) were used in this experiment.

contribute to the acceleration of RA progression. Ni et al. (2020) developed ROS-responsive dexamethasone (Dex)-loaded NPs named Dex/folic acid (FA)-Oxi-αCD using α-cyclodextrin (α-CD) as nanocarriers and FA as targeting group for the treatment of RA (**Figure 9**). Dex/FA-Oxi-αCD is sensitive to H_2O_2, and elevated levels of H_2O_2 promote the degradation of Oxi-αCD, releasing Dex. An anti-inflammatory mechanism study revealed that Dex/FA-Oxi-αCD inhibits the expression of iRhom2, TNF-α, and BAFF *in vitro* and *in vivo*. FA modification accumulates the biodistribution of Dex/FA-Oxi-αCD in the inflamed joints of RA, and the therapeutic efficacy is significantly improved compared to free Dex (Ni et al., 2020).

Chung et al. (2015) fabricated an inflammatory microenvironment ultrasensitive ROS-responsive gas-generating carrier for the treatment of osteoarthritis. In this work, the PLGA hollow microsphere (HM) carrier is functionalized with an anti-inflammatory drug, dexamethasone sodium phosphate (DEX-P); an acid precursor (composed of ethanol and $FeCl_2$); and a bubble-generating agent, sodium bicarbonate (SBC). As shown in **Figure 10**, in the inflammatory environment, the encapsulated ethanol is oxidized by H_2O_2 in the presence of Fe^{2+} by the Fenton reaction, producing an acidic milieu. The decomposition of SBC in acidic conditions generates CO_2 bubbles to disrupt the shell wall of HM, and the payload

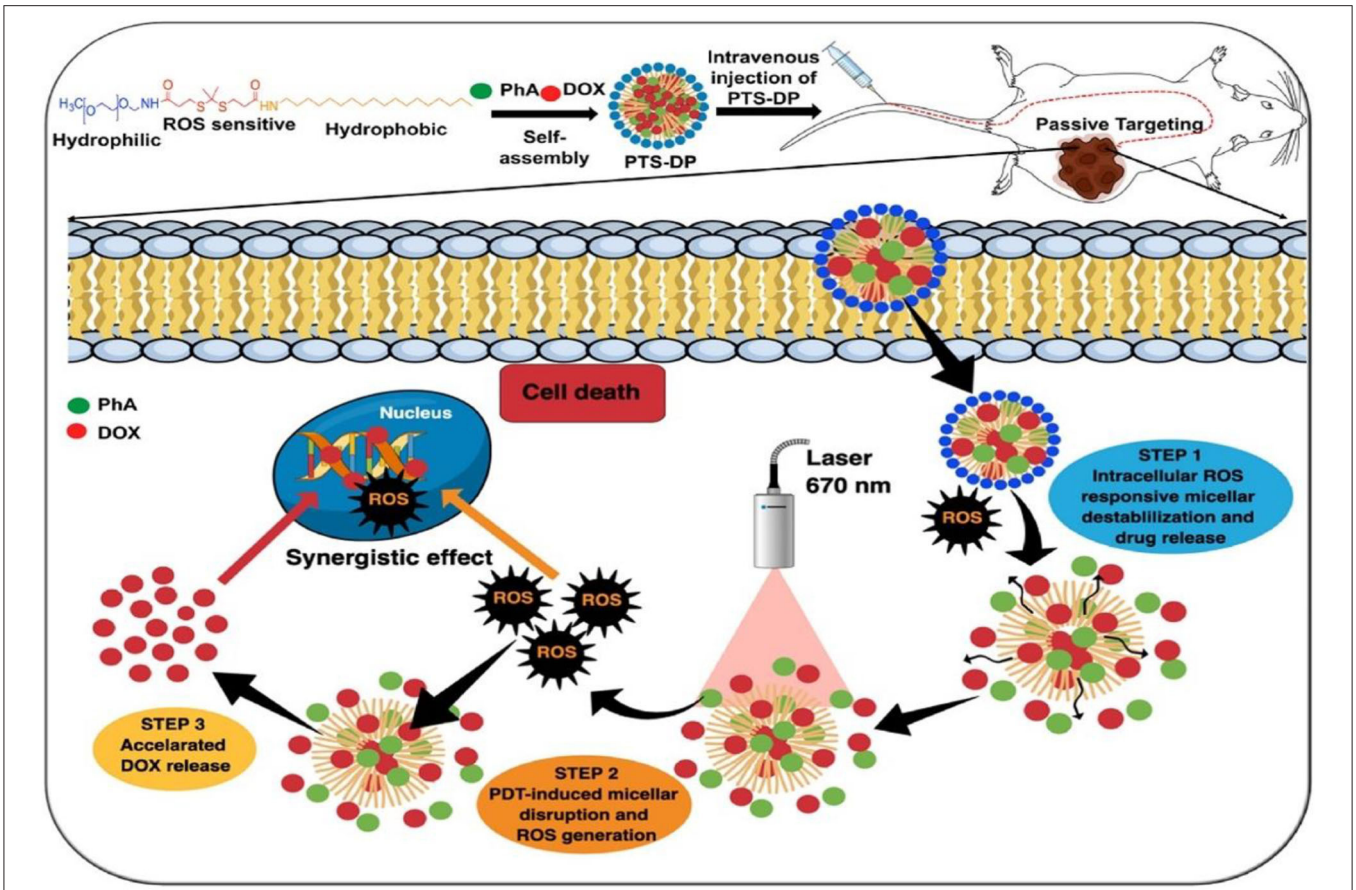

FIGURE 7 | Schematic illustration of ROS cascade–responsive drug release of PTS-DP for enhanced locoregional chemophotodynamic therapy (Uthaman et al., 2020) (Copyright 2020, reproduced with permission from Elsevier).

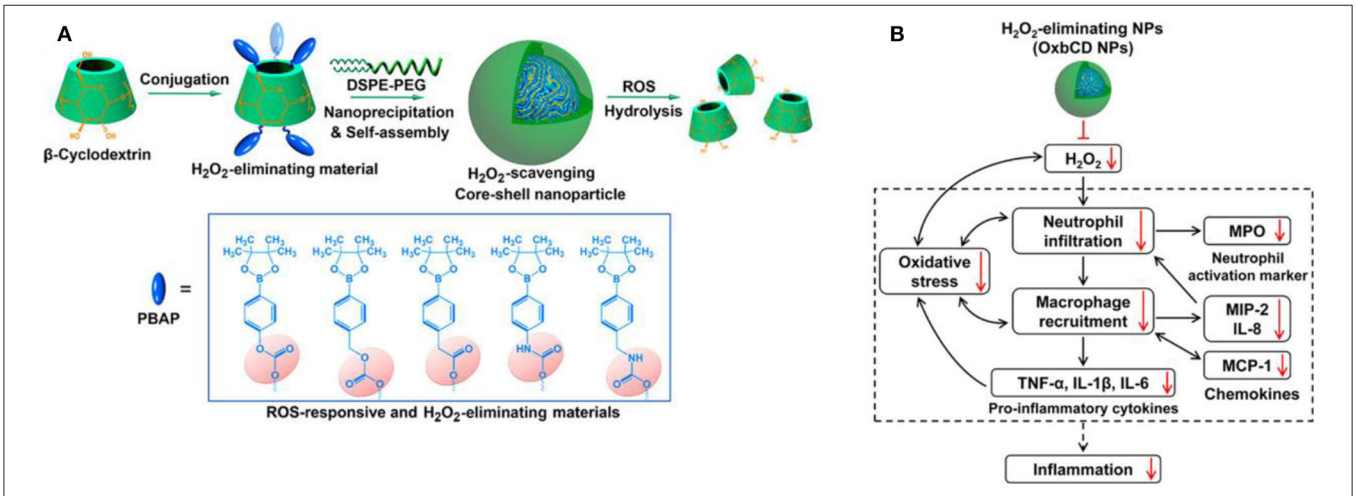

FIGURE 8 | (A) Design and synthetic routes of different H_2O_2-scavenging materials derived from β-CD, as well as engineering of anti-inflammatory nanoparticles. **(B)** Schematic illustration of anti-inflammatory mechanisms of H_2O_2-eliminating OxbCD NPs (Zhang et al., 2017) (Copyright 2017, reproduced with permission from American Chemical Society).

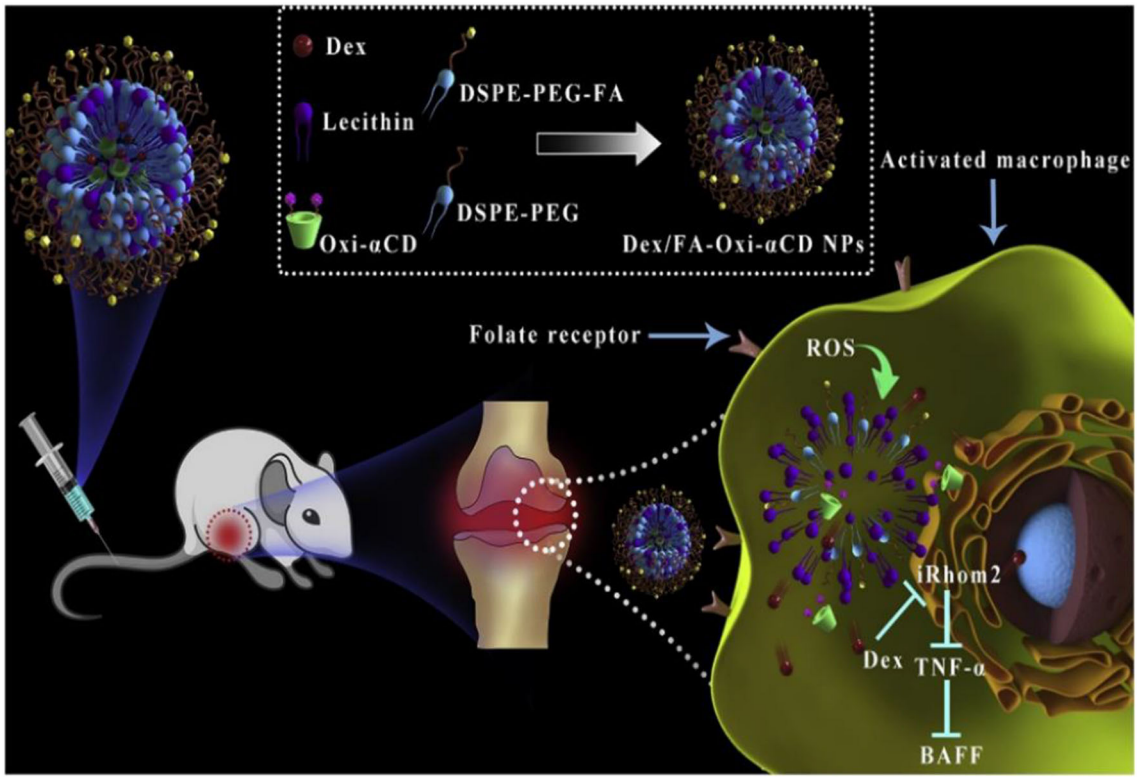

FIGURE 9 | Schematic illustration of Dex-loaded ROS-responsive NPs for targeted RA therapy. The proposed mechanisms showing a cascade of events in macrophages via the iRhom2–TNF-α-BAFF signaling pathway (Ni et al., 2020) (Copyright 2020, reproduced with permission from Elsevier).

anti-inflammatory drug DEX-P is released in high dosage with potential efficacy against joint destruction (Chung et al., 2015).

ROS/pH Response Nanocarrier for Inflammation Treatment

Where ROS is excessively produced, the pH changes. For example, compared to normal tissue/blood flow (pH ∼7.4), the tumor/inflammation area is slightly acidic (pH 5.4–7.1). Much drug development work has aimed at designing nanoplatforms that respond to multiple stimuli to enhance the performance of nanoagents through improved delivery of drugs to the target site. Physiological pH gradients and ROS levels have been extensively utilized in the design of stimuli-responsive nanosystems to deliver drugs to target sites. These delivery systems are usually based on an NP that undergoes swelling, charge conversion, membrane fusion, or bond-breaking after receiving pH and ROS signals. Actively targeted NPs that can simultaneously respond to low pH and high concentrations of ROS are potential nanocarriers for the precise delivery of therapeutic drugs to the target site. pH/ROS dual-responsive nanocarriers are constructed by combining pH-sensitive materials and oxidation-responsive materials. Through adjusting the weight ratio of the pH-sensitive materials and oxidation-responsive materials, it is possible to adjust the pH/ROS response capability, thereby providing nanocarriers with different hydrolysis characteristics in an inflammatory microenvironment. Studies have shown that pH/ROS double-reactive NPs can be used as an effective and safe nanocarrier for the precise treatment of vascular inflammatory diseases.

The inflammatory bowel disease (IBD) is characterized by high levels of ROS in the diseased sites, and oxidative stress is involved in and contributes to the pathogenesis and progression of IBD (Tian et al., 2017). Bertoni et al. (2018) synthesized phenylboronic ester–modified dextran (OxiDEX) NPs loaded with rifaximin (RIF) for targeted therapy of IBD, with a sequential responsive behavior to both pH and ROS. The permeability of OxiDEX NPs is remarkably lower compared with the traditional enteric formulation in an *in vivo* intestinal membrane mimicking the C2bbe1/HT29-MTX cell monolayer model. High amount of the drug is transported to the diseased sites, and the therapeutics efficacy is significantly improved, reducing unspecific absorption and systemic side effects. Lin et al. (2020) developed a polyadenylic acid micelle (PD-MC) based on the ROS and pH dual-sensitive block polymer PEG-P (PBEM-co-DPA). The micelles have excellent potential for improving the biocompatibility of resveratrol glycosides and effective targeted drug delivery into the liver fibrosis microenvironment. *In vitro* and *in vivo* studies show that PD-MCs inhibit inflammation and oxidative stress and reduce apoptosis of liver cells Notably, the empty micelle promotes liver ROS depletion at the pathological

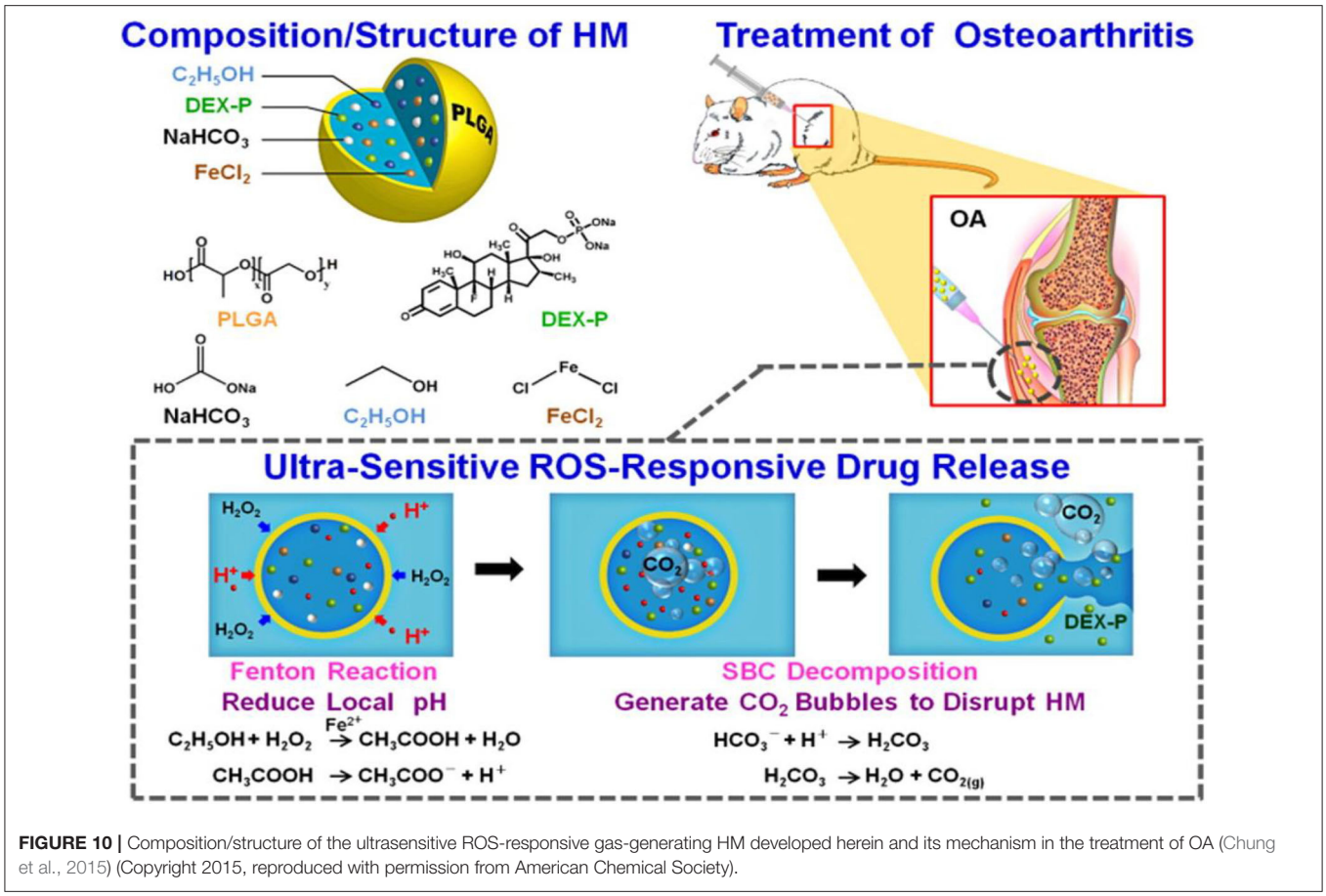

FIGURE 10 | Composition/structure of the ultrasensitive ROS-responsive gas-generating HM developed herein and its mechanism in the treatment of OA (Chung et al., 2015) (Copyright 2015, reproduced with permission from American Chemical Society).

site; hence, it has an anti-inflammatory effect. Therefore, PD-MCs have great potential for clinical use in anti–liver fibrosis drug treatment methods. More recently, Zhang et al. (2020) designed a pH-sensitive β-CD material (ACD) and a ROS-responsive β-CD material (OCD) NPs with loaded rapamycin (RAP) for targeted treatment of vascular inflammatory diseases. These NPs were constructed by the combination of a pH-sensitive unit (ACD) and an oxidation-responsive unit (OCD) facilely synthesized via acetylation of β-CD (**Figure 11**). The loaded RAP molecule is released from the RAP/AOCD NP in high levels of H_2O_2 or low pH inflammatory microenvironment. IV collagen (Col-IV) is highly expressed in the inflammation sites, by a surface decoration of AOCD NP with a Col-IV–targeting peptide (KLWVLPKGGGC); the resulting peptide-modified targeted RAP/AOCD NP efficiently accumulates in the rat vascular smooth muscle cells (VSMCs) *in vitro*, as well as in the balloon-injured arteries of rats *in vivo*, and inhibits the migration and proliferation of VSMCs and the formation of neointimal. This shows potential antirestenosis effects (Zhang et al., 2020). Finally, this constructed cascade pH/ROS dual-responsive drug targeted delivery system (AOCD NP and RAP/AOCD) is safe *in vitro* and *in vivo* in long-term treatment experiments. AOCD NP is a potential novel tool for delivering drugs to the inflammatory diseased sites utilizing the ROS microenvironment.

Application of ROS-Responsive NPs for Neurodegenerative Diseases

Most neurodegenerative diseases, including AD, PD, and ischemic stroke, are characterized by increased inflammation and ROS with cognitive decline and memory loss. Elevated ROS triggers inflammation, promoting the deterioration of diseases. Numerous studies have developed ROS-responsive drug delivery systems for treating neurodegenerative diseases by reducing the elevated levels of ROS (Li et al., 2018; Lv et al., 2018; Ballance et al., 2019; Jiang et al., 2019).

AD is among the most common neurodegenerative disorders in which high levels of ROS cause oxidative stress seen in patients with AD. ROS is an excellent therapeutic target in AD as demonstrated by experimental and clinical research findings (Behl et al., 1994; Butterfield and Lauderback, 2002; Geng et al., 2012; Li et al., 2013; Hu et al., 2015). ROS-responsive antioxidant nanotherapies with ROS-eliminating abilities have shown good clinical outcome in AD patients. Li et al. (2018) developed a self-assembled ROS-responsive positively charged polyprodrug amphiphiles by connecting poly(carboxy betaine) and simvastatin using a ROS-responsive diselenide bond (**Figure 12**). Simvastatin improves functional recovery of the spinal cord injury as seen in a rat model. It achieves this effect by upregulating the expression of brain-derived neurotrophic factors (BDNFs) leading to enhanced spatial memory recovery

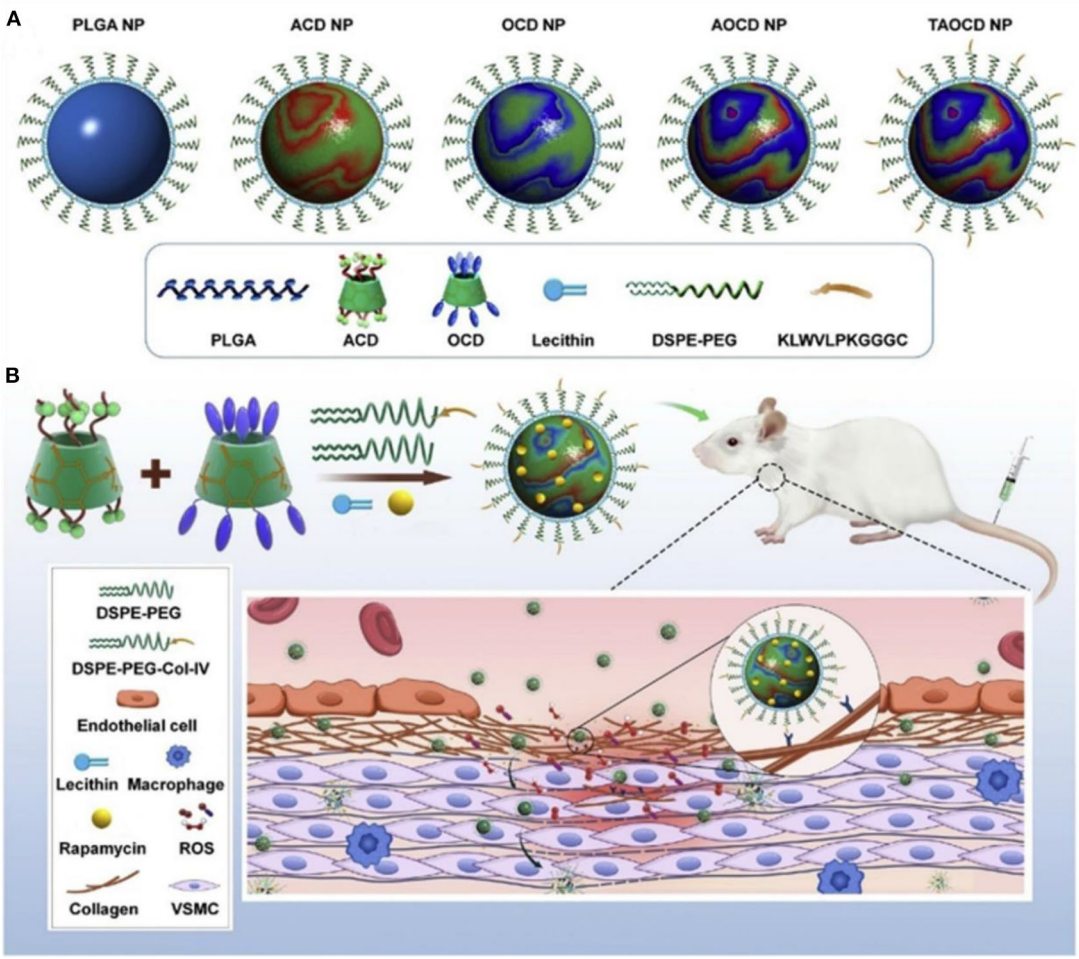

FIGURE 11 | Design and engineering of pH/ROS dual-responsive nanotherapies for targeted treatment of restenosis (Zhang et al., 2020) (Copyright 2020, reproduced with permission from Elsevier). **(A)** Schematic illustration of different NPs examined in this study. **(B)** Engineering of a dual-responsive, targeting rapamycin nanotherapy based on a pH-sensitive β-CD material (ACD) and a ROS-responsive β-CD material (OCD), as well as targeted treatment of a vascular inflammatory disease of restenosis.

(Han et al., 2011). BDNF is an important neurotrophic factor that modulates nerve cell migration and neurogenesis, as well as stabilizes the intercellular environment (Zuccato and Cattaneo, 2009; Jiang et al., 2010). A NSC differentiation–promoting negative drug molecule, a lethal-7b antisense oligonucleotide (let-7b) (Zhao et al., 2010), and hydrophobic superparamagnetic iron oxide nanocubes (SPIONs), which is used for tracking mesenchymal stem cells (Park et al., 2017), are encapsulated in this polyprodrug amphiphiles to synthesize PCB-Se–Se-Sim/SPIONs/let-7b antisense oligonucleotide NPs (CSeM/let-7b NPs). Neural stem cells treated with CSeM/let-7b NPs show a remarkable improvement in memory function as seen in 2xTg-AD mice. This NP enhances the secretion of BDNF, yielding remarkably therapeutic effects *in vivo* (Li et al., 2018). Besides, CSeM/let-7b NP helps to trace the transplantation site and the migration of exogenous NSCs because of its high r_2 value of SPIONs in magnetic resonance imaging.

Elsewhere, a spherical-like Congo red/rutin-MNPs nanotheranostic comprising a central Fe_3O_4 NP, the surface of which is coated with Congo red and rutin, was used to design a biocompatible H_2O_2-responsive magnetic nanocarrier for AD therapy (Hu et al., 2015). As illustrated in **Figure 13**, the biocompatibility of the Congo red/rutin-MNPs is improved by coating the DSPE-PEG-Congo red and DSPE-PEG-phenylboronic acid on the surface of Fe_3O_4 NPs. This carrier delivers high amount of the drug into the central nervous system using the PEGlyated modification, reducing its uptake by the reticuloendothelial system. The boronate ester bond between the vicinal diols and phenylboronic acid is cleaved using H_2O_2, and rutin is released from the Congo red/rutin-MNPs in an H_2O_2-responsive and concentration-dependent manner, thereby curtailing the effects of Aβ-induced cytotoxicity in SH-SY5Y cells and oxidative stress. Furthermore, the ultrasmall size of the Congo red/rutin-MNPs enables the detection of distribution of amyloid plaques and makes particles easier to

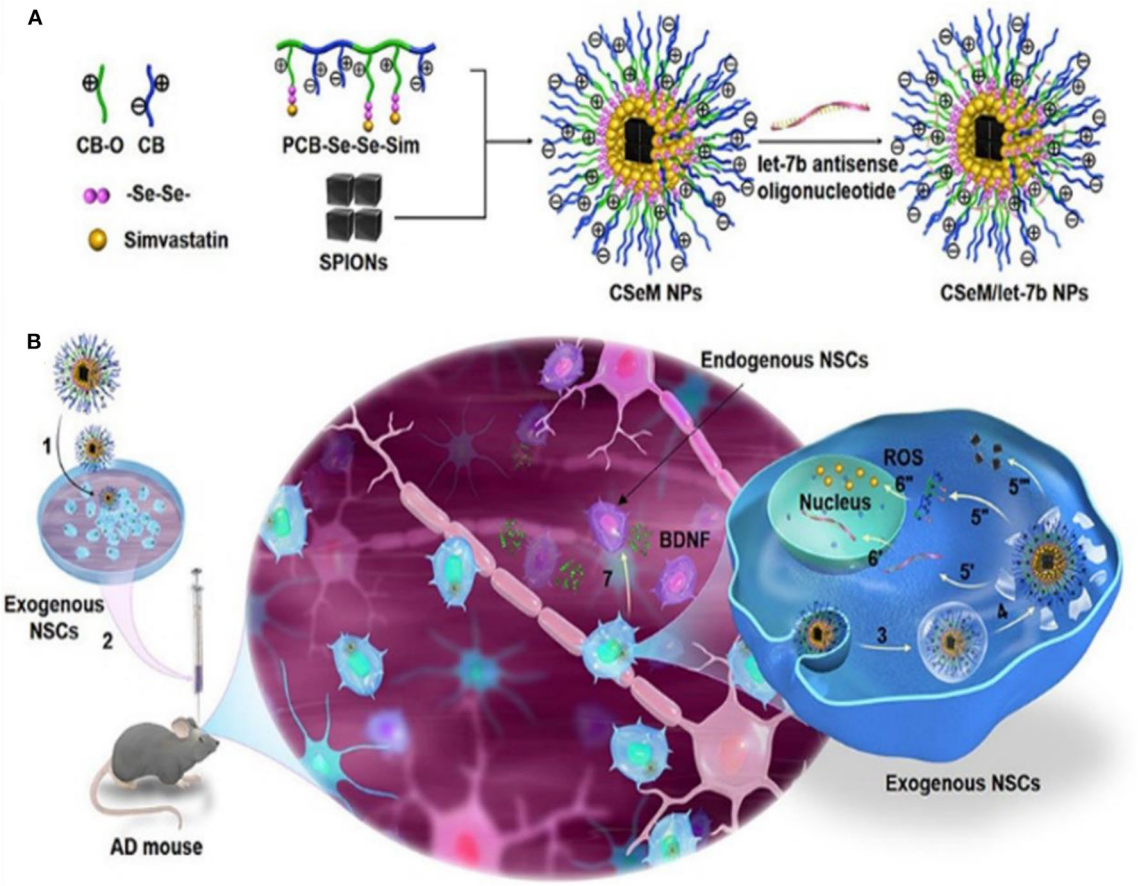

FIGURE 12 | Illustration of strategy for construction and functionalization of the traceable CSeM/let-7b NPs (Li et al., 2018) (Copyright 2018, reproduced with permission from American Chemical Society). **(A)** Preparation of the traceable CSeM/let-7b NPs. Polyprodrug amphiphiles were self-assembled to load SPIONs and absorb let-7b antisense oligonucleotide. **(B)** Schematic illustration of the mechanism of the traceable CSeM/let-7b NPs controlling exogenous NSCs as BDNF source for AD therapy.

cross the blood–brain barrier (BBB), rescuing memory deficits and neuronal loss in APPs we/PS1dE9 transgenic mice (Hu et al., 2015). The targeted delivery and controlled release properties of these Congo red/rutin-MNPs open up a new direction for application of theranostics in AD.

Ischemic stroke is another neurodegenerative disease that causes long-term disability and death worldwide due to overproduction of ROS. High levels of ROS cause detrimental effects on neurons and tissue injury at ischemic sites (Benjamin et al., 2017). Therefore, reducing oxidative stress is a prospective therapeutic approach for ischemic stroke (Panagiotou and Saha, 2015; Amani et al., 2017; Liu et al., 2017b; Lv et al., 2018; He et al., 2020; Tapeinos et al., 2020). Indeed, many ROS-responsive nanocarriers have been developed for the treatment of ischemic stroke (Lu et al., 2016, 2019; Jiang et al., 2019). Recently, we developed bifunctional nanomaterials zeolitic imidazolate framework-8-capped ceria NPs (CeO_2@ZIF-8 NPs) based on *in situ* synthesis strategy with ROS response and clearance capabilities (He et al., 2020). In this nanosystem, CeO_2 NPs was first created as the core structure of the NPs through a facile hydrothermal method, which is coated with a ZIF-8 shell, regulating the size, shape, and surface charge of CeO_2 inner core through the addition of polyvinylpyrrolidone. CeO_2@ZIF-8 NPs is decomposed by H_2O_2, releasing CeO_2 slowly, which exhibits effective ROS-scavenging activities *in vitro* and protects against tert-butyl hydroperoxide (t-BOOH)–induced PC-12 cytotoxicity (**Figure 14**). A pharmacokinetic study demonstrated that CeO_2@ZIF-8 NPs were able to across BBB and have prolonged circular behavior in the blood, which enhances its accumulation in brain tissue with better therapeutic efficacy. Furthermore, CeO_2@ZIF-8 NPs can effectively inhibit the activation of astrocytes and microglia and reduce the expression levels of inflammatory factors and lipid peroxidation in a middle cerebral artery occlusion (MCAO) injury ischemic rat model. Particularly, CeO_2@ZIF-8 reduces brain damage in ischemic stroke rats with good *in vivo* biocompatibility and biosafety.

Endogenous NSCs are ischemia-homing elements that induce the production of extracellular matrix molecules, such as

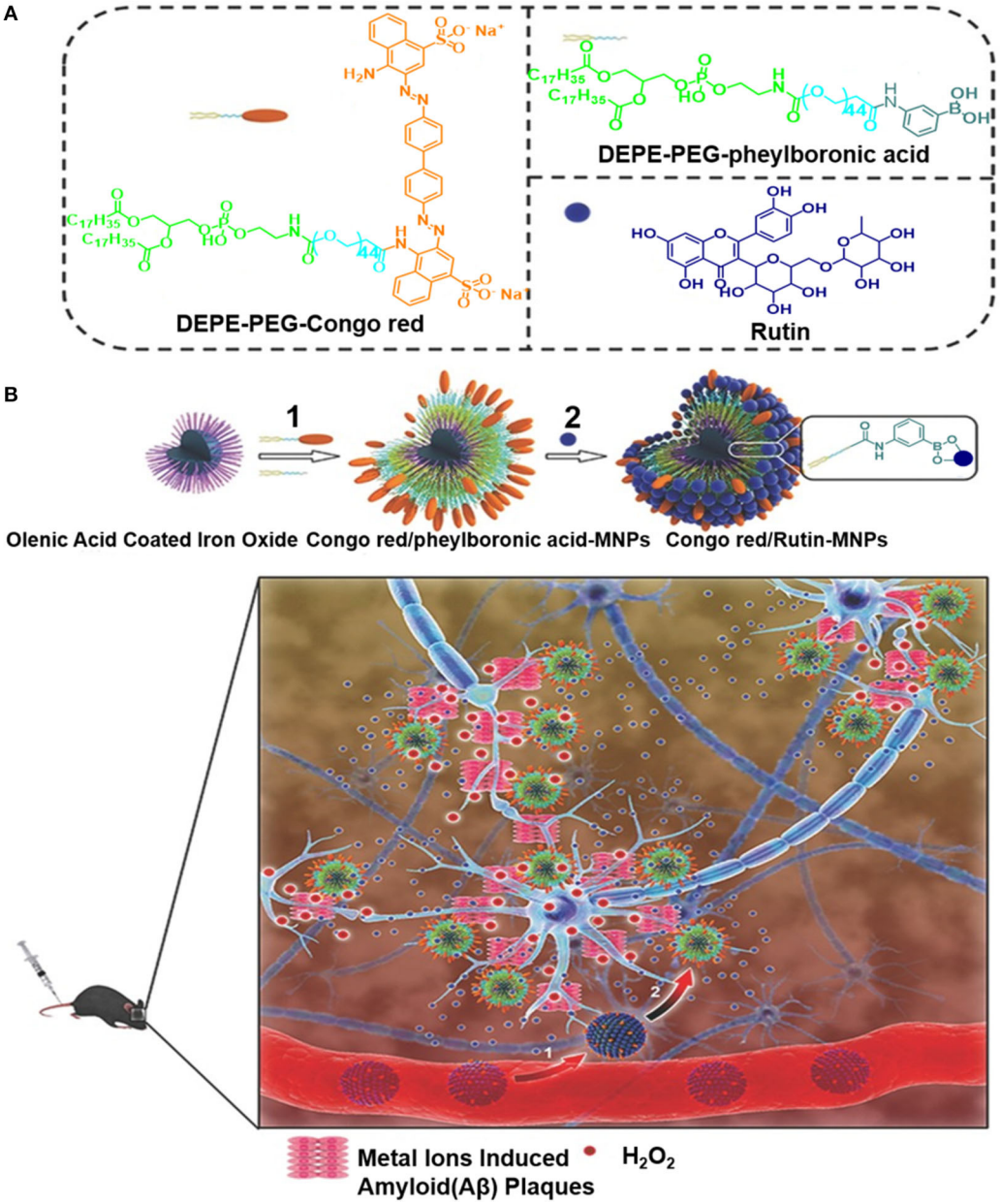

FIGURE 13 | (A) The preparation of Congo red and Rutin–loaded magnetic nanoparticles (Congo red/Rutin-MNPs): (1) DSPE-PEG-Congo red and DSPE-PEG-phenylboronic acid were used to improve the biocompatibility of magnetic nanoparticles through a micelle formation procedure. (2) Rutin was grafted onto the surface of the nanoparticles through the formation of a boronate ester bond between vicinal diols and phenylboronic acid. **(B)** Schematic interpretation of Congo red/Rutin-MNPs *in vivo*: (1) Congo red/Rutin-MNPs coinjected with mannitol penetrated the BBB. (2) Congo red/Rutin-MNPs detected amyloid plaques specifically, realized targeted delivery, and controlled release of Rutin by H_2O_2 (Hu et al., 2015) (Copyright 2015, reproduced with permission from John Wiley and Sons).

BDNFs to support neural cell growth (Aizman et al., 2009). Recently, Jiang et al. (2019) fabricated the first charge-reversal polymeric vector-transfected NSC with ROS responsiveness that homes the ischemia regions for synergistic ischemic stroke treatment (**Figure 15**). In this study, cationic poly [(2-acryloyl) ethyl (*p*-boronic acid benzyl) diethyl ammonium bromide] (B-PDEA) was first used to absorb plasmid DNA to form spherical polyplexes with excellent stability in a gel electrophoresis experiment. The newly constructed polyplexes effectively transfect NSCs via clathrin-mediated endocytosis with high gene transfection efficiency and less toxicity. After internalization into the cytosol, B-PDEA is first conversed to negatively charged polyacrylic acid by intracellular ROS. The released BDNF plasmids induce the NSCs to secret a

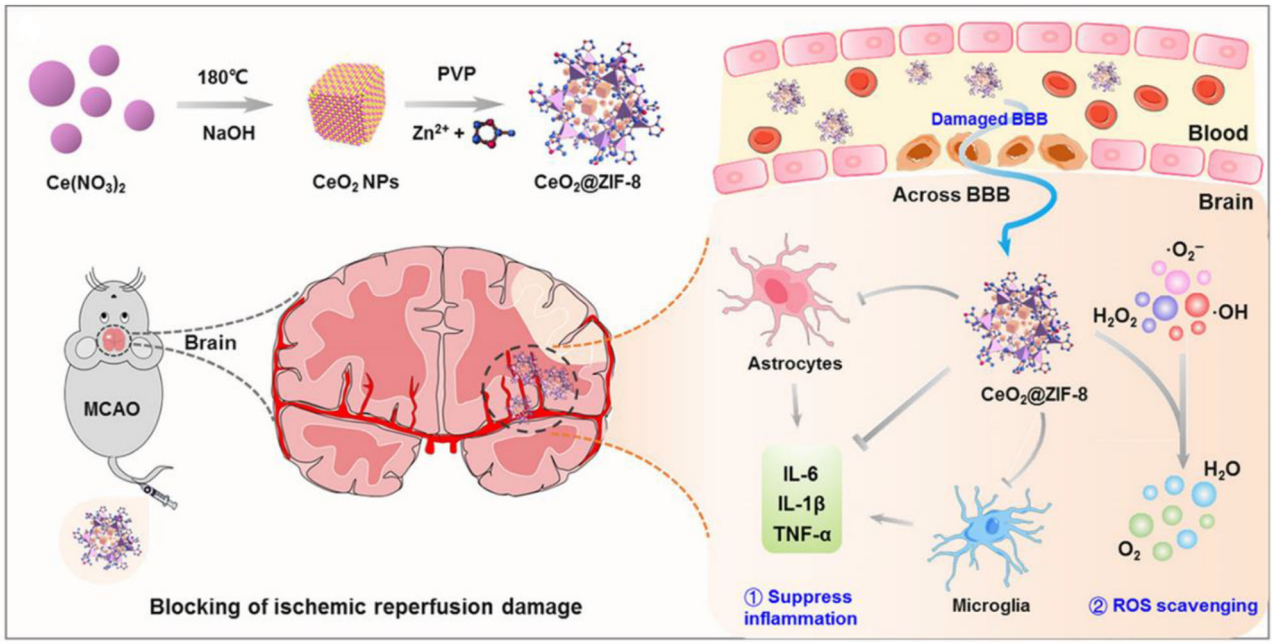

FIGURE 14 | Schematic illustration for *in situ* synthetic approach of CeO_2@ZIF-8 nanotherapeutics and its neuroprotective application mechanisms against reperfusion-induced injury in ischemic stroke (He et al., 2020) (Copyright 2020, reproduced with permission from American Association for the Advancement of Science).

high amount of BDNF into the injured ischemic cerebrum area in MCAO mice. Moreover, BDNF-NSCs eliminate the excessive ROS, resulting in the significant improvement of neurological and motor functions in MCAO mice (Jiang et al., 2019).

CONCLUSIONS AND FUTURE PERSPECTIVES

Herein, we reviewed the role of ROS in various human diseases. Although ROS is important for normal functioning of the human body, excessive levels of ROS cause oxidative stress leading to the pathogenesis of diseases. The ROS-responsive nanocarriers used in scientific research and their biomedical applications in the treatment of diseases related to oxidative stress were discussed in this review. In the past decade, the rapid development in nanotechnology has expanded the types and preparation methods of ROS-responsive nanomaterials and nanocarriers, which have been applied in multiple biological systems. However, despite the considerable achievements made in the designing of ROS-responsive nanocarriers, the delivery efficiency of current drug carriers, controlled drug release profile, and *in vivo* therapeutic effects of these drug platforms remain unsatisfactory. Our current understanding of their therapeutic function and the underlying chemical/biological relationship remains preliminary, and our research on these nanocarriers is insufficient to guarantee commercialization. We have not seen the commercialized clinical application of ROS-responsive nanocarriers due to the complexity of majority of ROS-responsive nanocarriers; the manufacturing process, reproducibility, and quality are difficult to control. Several limitations hinder further clinical translation of these nanocarriers including endosome safety and effectiveness of long-term systemic use of ROS-responsive nanocarriers because of absence of degradability or insufficient biocompatibility. It seems that we need to pay more attention to develop clinically acceptable ROS-responsive nanocarriers with simpler and easier structure if we want to put these nanocarriers forward to commercialization as soon as possible. The safety and efficacy of ROS-responsive nanocarriers will be evaluated more precisely in biosystems. Moreover, the risks of ROS-responsive nanocarriers need to be considered for therapy application. The biological mechanisms underlying the interaction between active oxygen-based nanomedicines and the human body is not well-understood. The tissue structures and physiological behaviors of experimental animals, in which the drug carriers are often tested, are very different from humans. Moreover, different patients may react differently to these ROS-responsive nanomedicines because of the variations and complexities of the biological system. The specificity of ROS-responsive nanomedicines needs to improve to the specific patients with different tumors, inflammations, or neurodegenerative diseases in order to reduce security risk to normal tissues and organs. Hence, additional rigorous safety and effectiveness assessments of these nanocarriers should be carried out before they can be administered to patients. In conclusion, ROS-responsive

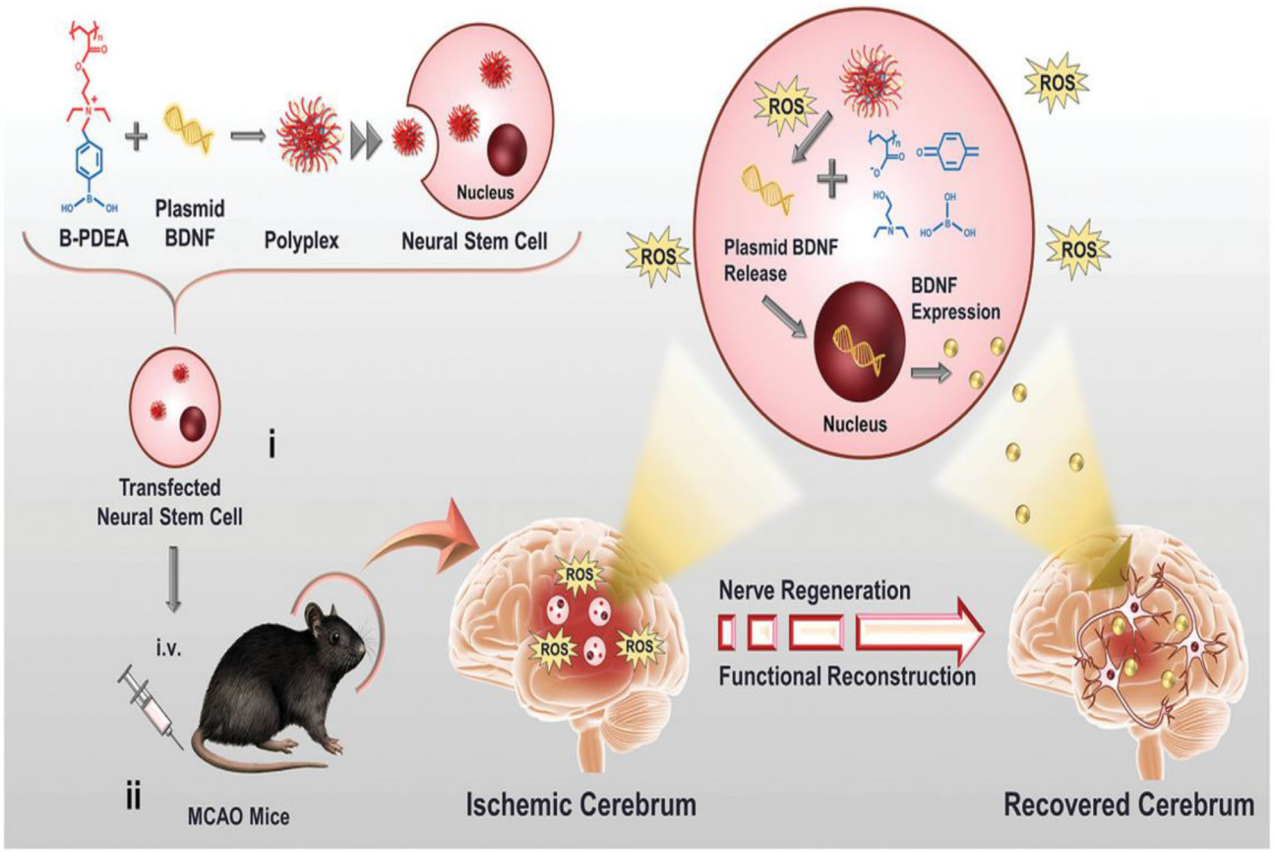

FIGURE 15 | Schematic illustration of B-PDEA–mediated BDNF transfection of NSCs for ischemic stroke treatment (Jiang et al., 2019) (Copyright 2019, reproduced with permission from John Wiley and Sons). (i) B-PDEA complexes BDNF plasmids to form polyplexes used for transfection of NSCs. (ii) The transfected NSCs i.v. transplanted to MCAO mice migrate to the injured area in the brain, whose high level of ROS efficiently triggers B-PDEA's conversion to negatively charged polyacrylate and the release of BDNF plasmids for NSCs to express and excrete BDNF. The released BDNF stimulates nerve regeneration and functional reconstruction, giving rise to a significant therapeutic effect in ischemic stroke.

nanocarriers have shown remarkable progress in preclinical studies over the past decade, and more clinical trials are needed to test their clinical utility.

AUTHOR CONTRIBUTIONS

TC and BC contributed to the design of the review. JL, YL, SC, and HL contributed to writing the paper. All authors approved the final version of the manuscript for submission.

FUNDING

This work was supported by the Natural Science Foundation of China (21877049), the Science and Technology Program of Guangzhou, China (201904010421), the Specific Research Fund for TCM Science and Technology of Guangdong Provincial Hospital of Chinese Medicine (YN2018QJ05 and YN2019MJ08), and the Medical Science and Technology Research Fund of Guangdong Provincial (A2018202).

REFERENCES

Aizman, I., Tate, C. C., McGrogan, M., and Case, C. C. (2009). Extracellular matrix produced by bonemarrow stromal cells and by their derivative, SB623 cells, supports neural cell growth. *J. Neurosci. Res.* 87, 3198–3206. doi: 10.1002/jnr.22146

Amani, H., Habibey, R., Hajmiresmail, S., Latifi, S., Pazoki-Toroudi, H., and Akhavan, O. (2017). Antioxidant nanomaterials in advanced diagnoses and treatments of ischemia reperfusion injuries. *J. Mater. Chem. B* 5, 9452–9476. doi: 10.1039/C7TB01689A

Ameziane-El-Hassani, R., Morand, S., Boucher, J.-L., Frapart, Y.-M., Apostolou, D., Agnandji, D., et al. (2005). Dual oxidase-2 has an intrinsic Ca2+-dependent H2O2-generating activity. *J. Biol. Chem.* 280, 30046–30054. doi: 10.1074/jbc.M500516200

An, X., Zhu, A., Luo, H., Ke, H., Chen, H., and Zhao, Y. (2016). Rational design of multi-stimuli-responsive nanoparticles for precise cancer therapy. *ACS Nano* 10, 5947–5958. doi: 10.1021/acsnano.6b01296

Andersen, J. K. (2004). Oxidative stress in neurodegeneration: cause or consequence? *Nat. Med.* 10, S18–S25. doi: 10.1038/nrn1434

Ballance, W. C., Qin, E. C., Chung, H. J., Gillette, M. U., and Kong, H. (2019). Reactive oxygen species-responsive drug delivery systems for

the treatment of neurodegenerative diseases. *Biomaterials* 217:119292. doi: 10.1016/j.biomaterials.2019.119292

Bandyopadhyay, U., Das, D., and Banerjee, R. K. (1999). Reactive oxygen species: oxidative damage and pathogenesis. *Curr. Sci*. 77, 658–666.

Barnham, K. J., Masters, C. L., and Bush, A. I. (2004). Neurodegenerative diseases and oxidative stress. *Nat. Rev. Drug Discov*. 3, 205–214. doi: 10.1038/nrd1330

Bayr, H. (2005). Reactive oxygen species. *Crit. Care Med*. 33, S498–S501. doi: 10.1097/01.CCM.0000186787.64500.12

Beckhauser, T. F., Francis-Oliveira, J., and de Pasquale, R. (2016). Reactive oxygen species: physiological and physiopathological effects on synaptic plasticity: supplementary issue: brain plasticity and repair. *J. Exp. Neurosci*. 10:S39887. doi: 10.4137/JEN.S39887

Behl, C., Davis, J., Lesley, R., and Schubert, D. (1994). Hydrogen peroxide mediates amyloid β protein toxicity. *Cell* 77, 817–827. doi: 10.1016/0092-8674(94)90131-7

Benjamin, E. J., Blaha, M. J., Chiuve, S. E., Cushman, M., Das, S. R., Deo, R., et al. (2017). Heart disease and stroke statistics-2017 update: a report from the American heart association. *Circulation* 135, e146–e603. doi: 10.1161/CIR.0000000000000485

Bertoni, S., Liu, Z., Correia, A., Martins, J. P., Rahikkala, A., Fontana, F., et al. (2018). pH and reactive oxygen species-sequential responsive nano-in-micro composite for targeted therapy of inflammatory bowel disease. *Adv. Funct. Mater*. 28:1806175. doi: 10.1002/adfm.201806175

Bhattacharjee, S. (ed.). (2019). "ROS and oxidative stress: origin and implication," in *Reactive Oxygen Species in Plant Biology* (New Delhi: Springer), 1–31.

Blaser, H., Dostert, C., Mak, T. W., and Brenner, D. (2016). TNF and ROS crosstalk in inflammation. *Trends Cell Biol*. 26, 249–261. doi: 10.1016/j.tcb.2015.12.002

Blattman, J. N., and Greenberg, P. D. (2004). Cancer immunotherapy: a treatment for the masses. *Science* 305, 200–205. doi: 10.1126/science.1100369

Bolduc, J. A., Collins, J. A., and Loeser, R. F. (2019). Reactive oxygen species, aging and articular cartilage homeostasis. *Free Radic. Biol. Med*. 132, 73–82. doi: 10.1016/j.freeradbiomed.2018.08.038

Brandes, R. P., Weissmann, N., and Schröder, K. (2014). Nox family NADPH oxidases: molecular mechanisms of activation. *Free Radic. Biol. Med*. 76, 208–226. doi: 10.1016/j.freeradbiomed.2014.07.046

Bryan, N., Ahswin, H., Smart, N., Bayon, Y., Wohlert, S., and Hunt, J. A. (2012). Reactive oxygen species (ROS)–a family of fate deciding molecules pivotal in constructive inflammation and wound healing. *Eur. Cell Mater*. 24:e65. doi: 10.22203/eCM.v024a18

Burgoyne, J. R., Oka, S.-I., Ale-Agha, N., and Eaton, P. (2013). Hydrogen peroxide sensing and signaling by protein kinases in the cardiovascular system. *Antioxid. Redox Sign*. 18, 1042–1052. doi: 10.1089/ars.2012.4817

Butterfield, D. A., and Lauderback, C. M. (2002). Lipid peroxidation and protein oxidation in Alzheimer's disease brain: potential causes and consequences involving amyloid β-peptide-associated free radical oxidative stress. *Free Radic. Biol. Med*. 32, 1050–1060. doi: 10.1016/S0891-5849(02)00794-3

Cadet, J. L., and Brannock, C. (1998). Invited review free radicals and the pathobiology of brain dopamine systems. *Neurochem. Int*. 32, 117–131. doi: 10.1016/S0197-0186(97)00031-4

Cairns, R. A., Harris, I. S., and Mak, T. W. (2011). Regulation of cancer cell metabolism. *Nat. Rev. Cancer* 11, 85–95. doi: 10.1038/nrc2981

Cao, W., Gu, Y., Li, T., and Xu, H. (2015). Ultra-sensitive ROS-responsive tellurium-containing polymers. *Chem. Commun*. 51, 7069–7071. doi: 10.1039/C5CC01779C

Chan, H.-K., and Kwok, P. C. L. (2011). Production methods for nanodrug particles using the bottom-up approach. *Adv. Drug Deliver. Rev*. 63, 406–416. doi: 10.1016/j.addr.2011.03.011

Chaudhary, S., Umar, A., and Mehta, S. (2016). Selenium nanomaterials: an overview of recent developments in synthesis, properties and potential applications. *Prog. Mater. Sci*. 83, 270–329. doi: 10.1016/j.pmatsci.2016.07.001

Cheignon, C., Tomas, M., Bonnefont-Rousselot, D., Faller, P., Hureau, C., and Collin, F. (2018). Oxidative stress and the amyloid beta peptide in Alzheimer's disease. *Redox Bio*. 14, 450–464. doi: 10.1016/j.redox.2017.10.014

Chen, D., Zhang, G., Li, R., Guan, M., Wang, X., Zou, T., et al. (2018). Biodegradable, hydrogen peroxide, and glutathione dual responsive nanoparticles for potential programmable paclitaxel release. *J. Am. Chem. Soc*. 140, 7373–7376. doi: 10.1021/jacs.7b12025

Chen, M., Daddy, J., Amerigos, K., Su, Z., Guissi, N. E. I., Xiao, Y., et al. (2019). Folate receptor-targeting and reactive oxygen species-responsive liposomal formulation of methotrexate for treatment of rheumatoid arthritis. *Pharmaceutics* 11:582. doi: 10.3390/pharmaceutics11110582

Cheng, Y., Jiao, X., Xu, T., Wang, W., Cao, Y., Wen, Y., et al. (2017). Free-blockage mesoporous anticancer nanoparticles based on ROS-responsive wetting behavior of nanopores. *Small* 13:1701942. doi: 10.1002/smll.201701942

Chung, M.-F., Chia, W.-T., Wan, W.-L., Lin, Y.-J., and Sung, H.-W. (2015). Controlled release of an anti-inflammatory drug using an ultrasensitive ROS-responsive gas-generating carrier for localized inflammation inhibition. *J. Am. Chem. Soc*. 137, 12462–12465. doi: 10.1021/jacs.5b08057

Clark, R. A. (1999). Activation of the neutrophil respiratory burst oxidase. *J. Inf. Dis*. 179(Supplement_2), S309–S317. doi: 10.1086/513849

Clerkin, J., Naughton, R., Quiney, C., and Cotter, T. (2008). Mechanisms of ROS modulated cell survival during carcinogenesis. *Cancer Lett*. 266, 30–36. doi: 10.1016/j.canlet.2008.02.029

Commoner, B., Townsend, J., and Pake, G. E. (1954). Free radicals in biological materials. *Nature* 174, 689–691. doi: 10.1038/174689a0

Deng, Z., Qian, Y., Yu, Y., Liu, G., Hu, J., Zhang, G., et al. (2016). Engineering intracellular delivery nanocarriers and nanoreactors from oxidation-responsive polymersomes via synchronized bilayer cross-linking and permeabilizing inside live cells. *J. Am. Chem. Soc*. 138, 10452–10466. doi: 10.1021/jacs.6b04115

Denko, N. C. (2008). Hypoxia, HIF1 and glucose metabolism in the solid tumour. *Nat. Rev. Cancer* 8, 705–713. doi: 10.1038/nrc2468

Di Rosanna, P., and Salvatore, C. (2012). Reactive oxygen species, inflammation, and lung diseases. *Curr. Pharm. Des*. 18, 3889–3900. doi: 10.2174/138161212802083716

Dickinson, B. C., and Chang, C. J. (2011). Chemistry and biology of reactive oxygen species in signaling or stress responses. *Nat. Chem. Biol*. 7:504. doi: 10.1038/nchembio.607

Dou, Y., Chen, Y., Zhang, X., Xu, X., Chen, Y., Guo, J., et al. (2017). Non-proinflammatory and responsive nanoplatforms for targeted treatment of atherosclerosis. *Biomaterials* 143, 93–108. doi: 10.1016/j.biomaterials.2017.07.035

Droge, W. (2002). Free radicals in the physiological control of cell function. *Physiol. Rev*. 82, 47–95. doi: 10.1152/physrev.00018.2001

Erdamar, H., Demirci, H., Yaman, H., Erbil, M. K., Yakar, T., Sancak, B., et al. (2008). The effect of hypothyroidism, hyperthyroidism, and their treatment on parameters of oxidative stress and antioxidant status. *Clin. Chem. Lab. Med*. 46, 1004–1010. doi: 10.1515/CCLM.2008.183

Fan, Z., and Xu, H. (2020). Recent progress in the biological applications of reactive oxygen species-responsive polymers. *Polym. Rev*. 60, 114–143. doi: 10.1080/15583724.2019.1641515

Fang, J., Seki, T., and Maeda, H. (2009). Therapeutic strategies by modulating oxygen stress in cancer and inflammation. *Adv. Drug Deliver. Rev*. 61, 290–302. doi: 10.1016/j.addr.2009.02.005

Fang, R., Xu, H., Cao, W., Yang, L., and Zhang, X. (2015). Reactive oxygen species (ROS)-responsive tellurium-containing hyperbranched polymer. *Polym. Chem*. 6, 2817–2821. doi: 10.1039/C5PY00050E

Feng, C., Ouyang, J., Tang, Z., Kong, N., Liu, Y., Fu, L., et al. (2020). Germanene-based theranostic materials for surgical adjuvant treatment: inhibiting tumor recurrence and wound infection. *Matter*. 3, 127–144. doi: 10.1016/j.matt.2020.04.022

Feng, S., Hu, Y., Peng, S., Han, S., Tao, H., Zhang, Q., et al. (2016). Nanoparticles responsive to the inflammatory microenvironment for targeted treatment of arterial restenosis. *Biomaterials* 105, 167–184. doi: 10.1016/j.biomaterials.2016.08.003

Finkel, T. (2011). Signal transduction by reactive oxygen species. *J. Cell Biol*. 194, 7–15. doi: 10.1083/jcb.201102095

Folgueras, A. R., Pendas, A. M., Sanchez, L. M., and Lopez-Otin, C. (2004). Matrix metalloproteinases in cancer: from new functions to improved inhibition strategies. *Int. J. Dev. Biol*. 48, 411–424. doi: 10.1387/ijdb.041811af

Forman, H. J., and Torres, M. (2001). Redox signaling in macrophages. *Mol. Aspects Med*. 22, 189–216. doi: 10.1016/S0098-2997(01)00010-3

Fraisl, P., Aragonés, J., and Carmeliet, P. (2009). Inhibition of oxygen sensors as a therapeutic strategy for ischaemic and inflammatory disease. *Nat. Revi. Drug Discov*. 8, 139–152. doi: 10.1038/nrd2761

Franceschi, C., Garagnani, P., Parini, P., Giuliani, C., and Santoro, A. (2018). Inflammaging: a new immune–metabolic viewpoint for age-related diseases. *Nat. Rev. Endocrinol*. 14, 576–590. doi: 10.1038/s41574-018-0059-4

Freitas, M., Lima, J. L., and Fernandes, E. (2009). Optical probes for detection and quantification of neutrophils' oxidative burst. A review. *Anal. Chim. Acta* 649, 8–23. doi: 10.1016/j.aca.2009.06.063

Gadoth, N., and Göbel, H. H. (2011). *Oxidative Stress and Free Radical Damage in Neurology*. New York, NY: Humana

Geng, J., Li, M., Wu, L., Chen, C., and Qu, X. (2012). Mesoporous silica nanoparticle-based H2O2 responsive controlled-release system used for Alzheimer's disease treatment. *Adv. Healthc. Mater*. 1, 332–336. doi: 10.1002/adhm.201200067

Gerschman, R. (1954). "Oxygen poisoning and x-irradiation: a mechanism in common," in *Glutathione*, eds S. Colowick, A. Lazarow, E. Racker, D.R. Schwarz, E. Stadtman, and H. Waelsch (Elsevier Inc.), 288–291.

Giorgio, M., Trinei, M., Migliaccio, E., and Pelicci, P. G. (2007). Hydrogen peroxide: a metabolic by-product or a common mediator of ageing signals? *Nat. Rev. Mol. Cell Biol.* 8:722. doi: 10.1038/nrm2240

Gligorovski, S., Strekowski, R., Barbati, S., and Vione, D. (2015). Environmental implications of hydroxyl radicals (· OH). *Chem. Rev*. 115, 13051–13092. doi: 10.1021/cr500310b

Gomberg, S. (2020). The microenvironment of chronic disease," in *Integrative and Functional Medical Nutrition Therapy,* eds D. Noland, J. A. Drisko, and L. Wagner (New York, NY: Humana, Cham), 437–446.

Grzelczak, M., Liz-Marzán, L. M., and Klajn, R. (2019). Stimuli-responsive self-assembly of nanoparticles. *Chem. Soc. Rev*. 48, 1342–1361. doi: 10.1039/C8CS00787J

Guo, C., Sun, L., Chen, X., and Zhang, D. (2013). Oxidative stress, mitochondrial damage and neurodegenerative diseases. *Neural Regen. Res.* 8:2003. doi: 10.3969/j.issn.1673-5374.2013.21.009

Han, X., Yang, N., Xu, Y., Zhu, J., Chen, Z., Liu, Z., et al. (2011). Simvastatin treatment improves functional recovery after experimental spinal cord injury by upregulating the expression of BDNF and GDNF. *Neurosci. Lett*. 487, 255–259. doi: 10.1016/j.neulet.2010.09.007

Harman, D. (1956). Aging: a theory based on free radical and radiation chemistry. *J. Gerontol.* 11, 298–300. doi: 10.1093/geronj/11.3.298

Hatfield, D. L., Yoo, M.-H., Carlson, B. A., and Gladyshev, V. N. (2009). Selenoproteins that function in cancer prevention and promotion. *Biochim. Biophys. Acta* 1790, 1541–1545. doi: 10.1016/j.bbagen.2009.03.001

Hayyan, M., Hashim, M. A., and AlNashef, I. M. (2016). Superoxide ion: generation and chemical implications. *Chem. Rev*. 116, 3029–3085. doi: 10.1021/acs.chemrev.5b00407

He, L., Huang, G., Liu, H., Sang, C., Liu, X., and Chen, T. (2020). Highly bioactive zeolitic imidazolate framework-8–capped nanotherapeutics for efficient reversal of reperfusion-induced injury in ischemic stroke. *Sci. Adv*. 6:eaay9751. doi: 10.1126/sciadv.aay9751

Hitchon, C. A., and El-Gabalawy, H. S. (2004). Oxidation in rheumatoid arthritis. *Arthritis Res. Ther*. 6:265. doi: 10.1186/ar1447

Hoetzenecker, W., Echtenacher, B., Guenova, E., Hoetzenecker, K., Woelbing, F., Brück, J., et al. (2012). ROS-induced ATF3 causes susceptibility to secondary infections during sepsis-associated immunosuppression. *Nat. Med*. 18:128. doi: 10.1038/nm.2557

Hoffman, A. S. (2013). Stimuli-responsive polymers: biomedical applications and challenges for clinical translation. *Adv. Drug Deliver. Rev*. 65, 10–16. doi: 10.1016/j.addr.2012.11.004

Hotamisligil, G. S. (2017). Inflammation, metaflammation and immunometabolic disorders. *Nature* 542:177. doi: 10.1038/nature21363

Houstis, N., Rosen, E. D., and Lander, E. S. (2006). Reactive oxygen species have a causal role in multiple forms of insulin resistance. *Nature* 440, 944–948. doi: 10.1038/nature04634

Hsu, H.-Y., and Wen, M.-H. (2002). Lipopolysaccharide-mediated reactive oxygen species and signal transduction in the regulation of interleukin-1 gene expression. *J. Biol. Chem*. 277, 22131–22139. doi: 10.1074/jbc.M111883200

Hu, B., Dai, F., Fan, Z., Ma, G., Tang, Q., and Zhang, X. (2015). Nanotheranostics: congo Red/Rutin-MNPs with enhanced magnetic resonance imaging and h2o2-responsive therapy of alzheimer's disease in APPswe/PS1dE9 transgenic Mice. *Adv. Mater*. 27, 5499–5505. doi: 10.1002/adma.201502227

Hu, K., Xie, L., Zhang, Y., Hanyu, M., Yang, Z., Nagatsu, K., et al. (2020). Marriage of black phosphorus and Cu2+ as effective photothermal agents for PET-guided combination cancer therapy. *Nat. Commun*. 11:2778. doi: 10.1038/s41467-020-16513-0

Hu, X., Yu, J., Qian, C., Lu, Y., Kahkoska, A. R., Xie, Z., et al. (2017). H2O2-responsive vesicles integrated with transcutaneous patches for glucose-mediated insulin delivery. *ACS Nano* 11, 613–620. doi: 10.1021/acsnano.6b06892

Huang, L. E., Arany, Z., Livingston, D. M., and Bunn, H. F. (1996). Activation of hypoxia-inducible transcription factor depends primarily upon redox-sensitive stabilization of its α subunit. *J. Biol. Chem*. 271, 32253–32259. doi: 10.1074/jbc.271.50.32253

Huang, W., Huang, Y., You, Y., Nie, T., and Chen, T. (2017). High-yield synthesis of multifunctional tellurium nanorods to achieve simultaneous chemo-photothermal combination cancer therapy. *Adv. Funct. Mater*. 27:1701388. doi: 10.1002/adfm.201701388

Huang, Y., Chen, Q., Ma, P., Song, H., Ma, X., Ma, Y., et al. (2018). Facile fabrication of oxidation-responsive polymeric nanoparticles for effective anticancer drug delivery. *Mol. Pharmaceut*. 16, 49–59. doi: 10.1021/acs.molpharmaceut.8b00634

Huang, Y., Fu, Y., Li, M., Jiang, D., Kutyreff, C. J., Engle, J. W., et al. (2020). Chirality-driven transportation and oxidation prevention by chiral selenium nanoparticles. *Angew. Chem. Int. Edit*. 132, 4436–4444. doi: 10.1002/ange.201910615

Hughes, M. M., and O'Neill, L. A. (2018). Metabolic regulation of NLRP 3. *Immunol. Rev*. 281, 88–98. doi: 10.1111/imr.12608

Imlay, J. A. (2003). Pathways of oxidative damage. *Annu. Rev. Microbiol*. 57, 395–418. doi: 10.1146/annurev.micro.57.030502.090938

Ishikawa, K., Takenaga, K., Akimoto, M., Koshikawa, N., Yamaguchi, A., Imanishi, H., et al. (2008). ROS-generating mitochondrial DNA mutations can regulate tumor cell metastasis. *Science* 320, 661–664. doi: 10.1126/science.1156906

Jiang, X. C., Xiang, J. J., Wu, H. H., Zhang, T. Y., Zhang, D. P., Xu, Q. H., et al. (2019). Neural stem cells transfected with reactive oxygen species–responsive polyplexes for effective treatment of ischemic stroke. *Adv. Mater*. 31:1807591. doi: 10.1002/adma.201807591

Jiang, Y., Wei, N., Zhu, J., Lu, T., Chen, Z., Xu, G., et al. (2010). Effects of brain-derived neurotrophic factor on local inflammation in experimental stroke of rat. *Mediat. Inflamm*. 2010:372423. doi: 10.1155/2010/372423

Kaelin, W. G., and Thompson, C. B. (2010). Clues from cell metabolism. *Nature* 465, 562–564. doi: 10.1038/465562a

Kang, C., Cho, W., Park, M., Kim, J., Park, S., Shin, D., et al. (2016). H2O2-triggered bubble generating antioxidant polymeric nanoparticles as ischemia/reperfusion targeted nanotheranostics. *Biomaterials* 85, 195–203. doi: 10.1016/j.biomaterials.2016.01.070

Kinscherf, R., Wagner, M., Kamencic, H., Bonaterra, G. A., Hou, D., Schiele, R. A., et al. (1999). Characterization of apoptotic macrophages in atheromatous tissue of humans and heritable hyperlipidemic rabbits. *Atherosclerosis* 144, 33–39. doi: 10.1016/S0021-9150(99)00037-4

Kong, H., and Chandel, N. S. (2020). Reactive oxygen species and cancer. *Free Radic Res.* 2020, 619–637. doi: 10.1016/B978-0-12-818606-0.00030-4

Kong, N., Ji, X., Wang, J., Sun, X., Chen, G., Fan, T., et al. (2020). ROS-mediated selective killing effect of black phosphorus: mechanistic understanding and its guidance for safe biomedical applications. *Nano Lett*. 20, 3943–3955. doi: 10.1021/acs.nanolett.0c01098

Kumar, B., Koul, S., Khandrika, L., Meacham, R. B., and Koul, H. K. (2008). Oxidative stress is inherent in prostate cancer cells and is required for aggressive phenotype. *Cancer Res*. 68, 1777–1785. doi: 10.1158/0008-5472.CAN-07-5259

Kunkemoeller, B., and Kyriakides, T. R. (2017). Redox signaling in diabetic wound healing regulates extracellular matrix deposition. *Antioxid. Redox Sign*. 27, 823–838. doi: 10.1089/ars.2017.7263

Kwon, J., Kim, J., Park, S., Khang, G., Kang, P. M., and Lee, D. (2013). Inflammation-responsive antioxidant nanoparticles based on a polymeric prodrug of vanillin. *Biomacromolecules* 14, 1618–1626. doi: 10.1021/bm400256h

Lacy, F., Kailasam, M. T., O'connor, D. T., Schmid-Schönbein, G. W., and Parmer, R. J. (2000). Plasma hydrogen peroxide production in human essential

hypertension: role of heredity, gender, and ethnicity. *Hypertension* 36, 878–884. doi: 10.1161/01.HYP.36.5.878

Lai, H., Zhang, X., Song, Z., Yuan, Z., He, L., and Chen, T. (2019). Facile synthesis of antioxidative nanotherapeutics using a microwave for efficient reversal of cisplatin-induced nephrotoxicity. *Chem. Eng. J.* 391:123563. doi: 10.1016/j.cej.2019.123563

Lambeth, J. D. (2004). NOX enzymes and the biology of reactive oxygen. *Nat. Rev. Immun*. 4, 181–189. doi: 10.1038/nri1312

Lamkanfi, M., and Dixit, V. M. (2012). Inflammasomes and their roles in health and disease. *Annu. Rev. Cell Dev. Biol*. 28, 137–161. doi: 10.1146/annurev-cellbio-101011-155745

Le Belle, J. E., Orozco, N. M., Paucar, A. A., Saxe, J. P., Mottahedeh, J., Pyle, A. D., et al. (2011). Proliferative neural stem cells have high endogenous ROS levels that regulate self-renewal and neurogenesis in a PI3K/Akt-dependant manner. *Cell Stem Cell* 8, 59–71. doi: 10.1016/j.stem.2010.11.028

Lee, D., Bae, S., Ke, Q., Lee, J., Song, B., Karumanchi, S. A., et al. (2013). Hydrogen peroxide-responsive copolyoxalate nanoparticles for detection and therapy of ischemia–reperfusion injury. *J. Control. Release* 172, 1102–1110. doi: 10.1016/j.jconrel.2013.09.020

Lee, D., Khaja, S., Velasquez-Castano, J. C., Dasari, M., Sun, C., Petros, J., et al. (2007). *In vivo* imaging of hydrogen peroxide with chemiluminescent nanoparticles. *Nat. Mater*. 6, 765–769. doi: 10.1038/nmat1983

Lee, Y., Lee, S., and Jon, S. (2018). Biotinylated bilirubin nanoparticles as a tumor microenvironment-responsive drug delivery system for targeted cancer therapy. *Adv. Sci*. 5:1800017. doi: 10.1002/advs.201800017

Li, C., Zhao, Y., Cheng, J., Guo, J., Zhang, Q., Zhang, X., et al. (2019). A proresolving peptide nanotherapy for site-specific treatment of inflammatory bowel disease by regulating proinflammatory microenvironment and gut microbiota. *Adv. Sci*. 6:1900610. doi: 10.1002/advs.201900610

Li, F., Li, T., Cao, W., Wang, L., and Xu, H. (2017a). Near-infrared light stimuli-responsive synergistic therapy nanoplatforms based on the coordination of tellurium-containing block polymer and cisplatin for cancer treatment. *Biomaterials* 133, 208–218. doi: 10.1016/j.biomaterials.2017.04.032

Li, L., Wang, Y., Guo, R., Li, S., Ni, J., Gao, S., et al. (2020). Ginsenoside Rg3-loaded, reactive oxygen species-responsive polymeric nanoparticles for alleviating myocardial ischemia-reperfusion injury. *J. Control. Release* 317, 259–272. doi: 10.1016/j.jconrel.2019.11.032

Li, M., Shi, P., Xu, C., Ren, J., and Qu, X. (2013). Cerium oxide caged metal chelator: anti-aggregation and anti-oxidation integrated H2O2-responsive controlled drug release for potential Alzheimer's disease treatment. *Chem. Sci*. 4, 2536–2542. doi: 10.1039/c3sc50697e

Li, X., Gao, M., Xin, K., Zhang, L., Ding, D., Kong, D., et al. (2017b). Singlet oxygen-responsive micelles for enhanced photodynamic therapy. *J. Control. Release* 260, 12–21. doi: 10.1016/j.jconrel.2017.05.025

Li, Y., Li, Y., Ji, W., Lu, Z., Liu, L., Shi, Y., et al. (2018). Positively charged polyprodrug amphiphiles with enhanced drug loading and reactive oxygen species-responsive release ability for traceable synergistic therapy. *J. Am. Chem. Soc.* 140, 4164–4171. doi: 10.1021/jacs.8b01641

Liang, J., and Liu, B. (2016). ROS-responsive drug delivery systems. *Bio. Transl. Med*. 1, 239–251. doi: 10.1002/btm2.10014

Liang, X., Zhang, Q., Wang, X., Yuan, M., Zhang, Y., Xu, Z., et al. (2018). Reactive oxygen species mediated oxidative stress links diabetes and atrial fibrillation. *Mol. Med. Report*. 17, 4933–4940. doi: 10.3892/mmr.2018.8472

Lin, L., Gong, H., Li, R., Huang, J., Cai, M., Lan, T., et al. (2020). Nanodrug with ROS and pH dual-sensitivity ameliorates liver fibrosis via multicellular regulation. *Adv. Sci*. 7:1903138. doi: 10.1002/advs.201903138

Liou, G.-Y., and Storz, P. (2010). Reactive oxygen species in cancer. *Free Radic. Res*. 44, 479–496. doi: 10.3109/10715761003667554

Liu, J., Pang, Y., Zhu, Z., Wang, D., Li, C., Huang, W., et al. (2013). Therapeutic nanocarriers with hydrogen peroxide-triggered drug release for cancer treatment. *Biomacromolecules* 14, 1627–1636. doi: 10.1021/bm4002574

Liu, J., Yang, G., Zhu, W., Dong, Z., Yang, Y., Chao, Y., et al. (2017a). Light-controlled drug release from singlet-oxygen sensitive nanoscale coordination polymers enabling cancer combination therapy. *Biomaterials* 146, 40–48. doi: 10.1016/j.biomaterials.2017.09.007

Liu, T., Lai, L., Song, Z., and Chen, T. (2016). A sequentially triggered nanosystem for precise drug delivery and simultaneous inhibition of cancer growth, migration, and invasion. *Adv. Funct. Mater*. 26, 7775–7790. doi: 10.1002/adfm.201604206

Liu, T., Zeng, L., Jiang, W., Fu, Y., Zheng, W., and Chen, T. (2015). Rational design of cancer-targeted selenium nanoparticles to antagonize multidrug resistance in cancer cells. *Nanomedicine* 11, 947–958. doi: 10.1016/j.nano.2015.01.009

Liu, Y., Ai, K., Ji, X., Askhatova, D., Du, R., Lu, L., et al. (2017b). Comprehensive insights into the multi-antioxidative mechanisms of melanin nanoparticles and their application to protect brain from injury in ischemic stroke. *J. Am. Chem. Soc*. 139, 856–862. doi: 10.1021/jacs.6b11013

Liu, Z., Zhou, T., Ziegler, A. C., Dimitrion, P., and Zuo, L. (2017c). Oxidative stress in neurodegenerative diseases: from molecular mechanisms to clinical applications. *Oxid. Med. Cell. Longev*. 2017:2525967. doi: 10.1155/2017/2525967

Lobanov, A. V., Hatfield, D. L., and Gladyshev, V. N. (2009). Eukaryotic selenoproteins and selenoproteomes. *Biochim. Biophys. Acta* 1790, 1424–1428. doi: 10.1016/j.bbagen.2009.05.014

Lu, Y., Aimetti, A. A., Langer, R., and Gu, Z. (2016). Bioresponsive materials. *Nat. Rev. Mater*. 2, 1–17. doi: 10.1038/natrevmats.2016.75

Lu, Y., Li, C., Chen, Q., Liu, P., Guo, Q., Zhang, Y., et al. (2019). Microthrombus-targeting micelles for neurovascular remodeling and enhanced microcirculatory perfusion in acute ischemic stroke. *Adv. Mater*. 31:1808361. doi: 10.1002/adma.201808361

Luo, C., Sun, J., Liu, D., Sun, B., Miao, L., Musetti, S., et al. (2016). Self-assembled redox dual-responsive prodrug-nanosystem formed by single thioether-bridged paclitaxel-fatty acid conjugate for cancer chemotherapy. *Nano Lett*. 16, 5401–5408. doi: 10.1021/acs.nanolett.6b01632

Luo, M., Fan, T., Zhou, Y., Zhang, H., and Mei, L. (2019). 2D black phosphorus–based biomedical applications. *Adv. Funct. Mater*. 29:1808306. doi: 10.1002/adfm.201808306

Lv, W., Xu, J., Wang, X., Li, X., Xu, Q., and Xin, H. (2018). Bioengineered boronic ester modified dextran polymer nanoparticles as reactive oxygen species responsive nanocarrier for ischemic stroke treatment. *ACS Nano* 12, 5417–5426. doi: 10.1021/acsnano.8b00477

Ma, N., Li, Y., Ren, H., Xu, H., Li, Z., and Zhang, X. (2010a). Selenium-containing block copolymers and their oxidation-responsive aggregates. *Polym. Chem*. 1, 1609–1614. doi: 10.1039/c0py00144a

Ma, N., Li, Y., Xu, H., Wang, Z., and Zhang, X. (2010b). Dual redox responsive assemblies formed from diselenide block copolymers. *J. Am. Chem. Soc.* 132, 442–443. doi: 10.1021/ja908124g

Manoharan, S., Guillemin, G. J., Abiramasundari, R. S., Essa, M. M., Akbar, M., and Akbar, M. D. (2016). The role of reactive oxygen species in the pathogenesis of Alzheimer's disease, Parkinson's disease, and Huntington's disease: a mini review. *Oxid. Med. Cell. Longev*. 2016:8590578. doi: 10.1155/2016/8590578

Maruf, A., Wang, Y., Luo, L., Zhong, Y., Nurhidayah, D., Liu, B., et al. (2020). Nanoerythrocyte membrane–enveloped ros-responsive 5-aminolevulinic acid prodrug nanostructures with robust atheroprotection. *Part. Part. Syst. Char*. 37:2000021. doi: 10.1002/ppsc.202000021

Marusyk, A., and Polyak, K. (2010). Tumor heterogeneity: causes and consequences. *Biochim. Biophys. Acta* 1805, 105–117. doi: 10.1016/j.bbcan.2009.11.002

Mei, C., Wang, N., Zhu, X., Wong, K. H., and Chen, T. (2018). Photothermal-controlled nanotubes with surface charge flipping ability for precise synergistic therapy of triple-negative breast cancer. *Adv. Funct. Mater*. 28:1805225. doi: 10.1002/adfm.201805225

Melo, A., Monteiro, L., Lima, R. M., de Oliveira, D. M., de Cerqueira, M. D., and El-Bachá, R. S. (2011). Oxidative stress in neurodegenerative diseases: mechanisms and therapeutic perspectives. *Oxid. Med. Cell. Longev*. 2011:467180. doi: 10.1155/2011/467180

Mercanzini, A., Reddy, S. T., Velluto, D., Colin, P., Maillard, A., Bensadoun, J.-C., et al. (2010). Controlled release nanoparticle-embedded coatings reduce the tissue reaction to neuroprostheses. *J. Control. Release* 145, 196–202. doi: 10.1016/j.jconrel.2010.04.025

Missiroli, S., Genovese, I., Perrone, M., Vezzani, B., Vitto, V. A., and Giorgi, C. (2020). The Role of mitochondria in inflammation: from cancer to neurodegenerative disorders. *J. Clin. Med*. 9:740. doi: 10.3390/jcm9030740

Mittal, M., Siddiqui, M. R., Tran, K., Reddy, S. P., and Malik, A. B. (2014). Reactive oxygen species in inflammation and tissue injury. *Antioxid. Redox Sign.* 20, 1126–1167. doi: 10.1089/ars.2012.5149

Moreno, J. C., Bikker, H., Kempers, M. J., Van Trotsenburg, A. P., Baas, F., de Vijlder, J. J., et al. (2002). Inactivating mutations in the gene for thyroid oxidase 2 (THOX2) and congenital hypothyroidism. *N. Engl. J. Med.* 347, 95–102. doi: 10.1056/NEJMoa012752

Morgan, M. J., and Liu, Z.-G. (2011). Crosstalk of reactive oxygen species and NF-κB signaling. *Cell Res.* 21, 103–115. doi: 10.1038/cr.2010.178

Morry, J., Ngamcherdtrakul, W., and Yantasee, W. (2017). Oxidative stress in cancer and fibrosis: Opportunity for therapeutic intervention with antioxidant compounds, enzymes, and nanoparticles. *Redox Bio.* 11, 240–253. doi: 10.1016/j.redox.2016.12.011

Mouthuy, P.-A., Snelling, S. J., Dakin, S. G., Milković, L., Gašparović, A. C., Carr, A. J., et al. (2016). Biocompatibility of implantable materials: An oxidative stress viewpoint. *Biomaterials* 109, 55–68. doi: 10.1016/j.biomaterials.2016.09.010

Nakajima, K., and Kohsaka, S. (2001). Microglia: activation and their significance in the central nervous system. *J. Biochem.* 130, 169–175. doi: 10.1093/oxfordjournals.jbchem.a002969

Nathan, C., and Cunningham-Bussel, A. (2013). Beyond oxidative stress: an immunologist's guide to reactive oxygen species. *Nat. Rev. Immunol.* 13, 349–361. doi: 10.1038/nri3423

Newsholme, P., Cruzat, V. F., Keane, K. N., Carlessi, R., and de Bittencourt, P. I. H. Jr. (2016). Molecular mechanisms of ROS production and oxidative stress in diabetes. *Biochem. J.* 473, 4527–4550. doi: 10.1042/BCJ20160503C

Ni, R., Song, G., Fu, X., Song, R., Li, L., Pu, W., et al. (2020). Reactive oxygen species-responsive dexamethasone-loaded nanoparticles for targeted treatment of rheumatoid arthritis via suppressing the iRhom2/TNF-α/BAFF signaling pathway. *Biomaterials* 232:119730. doi: 10.1016/j.biomaterials.2019.119730

Nosaka, Y., and Nosaka, A. Y. (2017). Generation and detection of reactive oxygen species in photocatalysis. *Chem. Rev.* 117, 11302–11336. doi: 10.1021/acs.chemrev.7b00161

Ovais, M., Mukherjee, S., Pramanik, A., Das, D., Mukherjee, A., Raza, A., et al. (2020). Designing stimuli-responsive upconversion nanoparticles that exploit the tumor microenvironment. *Adv. Mater.* 32:2000055. doi: 10.1002/adma.202000055

Panagiotou, S., and Saha, S. (2015). Therapeutic benefits of nanoparticles in stroke. *Front. Neurosci.* 9:182. doi: 10.3389/fnins.2015.00182

Park, J. S., Park, W., Park, S., j., Larson, A. C., Kim, D. H., et al. (2017). Multimodal magnetic nanoclusters for gene delivery, directed migration, and tracking of stem cells. *Adv. Funct. Mater.* 27:1700396. doi: 10.1002/adfm.201700396

Pu, H.-L., Chiang, W.-L., Maiti, B., Liao, Z.-X., Ho, Y.-C., Shim, M. S., et al. (2014). Nanoparticles with dual responses to oxidative stress and reduced pH for drug release and anti-inflammatory applications. *ACS Nano* 8, 1213–1221. doi: 10.1021/nn4058787

Qiao, C., Yang, J., Shen, Q., Liu, R., Li, Y., Shi, Y., et al. (2018). Traceable nanoparticles with Dual tareting and ROS response for RNAi-based immunochemotherapy of intracranial glioblastoma treatment. *Adv. Mater.* 30:1705054. doi: 10.1002/adma.201705054

Qiu, M., Singh, A., Wang, D., Qu, J., Swihart, M., Zhang, H., et al. (2019). Biocompatible and biodegradable inorganic nanostructures for nanomedicine: silicon and black phosphorus. *Nano Today* 25, 135–155. doi: 10.1016/j.nantod.2019.02.012

Qiu, M., Wang, D., Liang, W., Liu, L., Zhang, Y., Chen, X., et al. (2018). Novel concept of the smart NIR-light–controlled drug release of black phosphorus nanostructure for cancer therapy. *Proc. Natl. Acad. Sci. U.S.A.* 115, 501–506. doi: 10.1073/pnas.1714421115

Radi, E., Formichi, P., Battisti, C., and Federico, A. (2014). Apoptosis and oxidative stress in neurodegenerative diseases. *J. Alzheimers Dis.* 42, S125–S152. doi: 10.3233/JAD-132738

Ray, P. D., Huang, B.-W., and Tsuji, Y. (2012). Reactive oxygen species (ROS) homeostasis and redox regulation in cellular signaling. *Cell. Signal.* 24, 981–990. doi: 10.1016/j.cellsig.2012.01.008

Reczek, C. R., and Chandel, N. S. (2017). The two faces of reactive oxygen species in cancer. *Annu. Rev. Cancer Biol.* 1, 77–98. doi: 10.1146/annurev-cancerbio-041916-065808

Ren, H., Wu, Y., Li, Y., Cao, W., Sun, Z., Xu, H., et al. (2013). Visible-light-induced disruption of diselenide-containing layer-by-layer films: toward combination of chemotherapy and photodynamic therapy. *Small* 9, 3981–3986. doi: 10.1002/smll.201300628

Riley, R. S., June, C. H., Langer, R., and Mitchell, M. J. (2019). Delivery technologies for cancer immunotherapy. *Nat. Rev. Drug Discov.* 18, 175–196. doi: 10.1038/s41573-018-0006-z

Saravanakumar, G., Kim, J., and Kim, W. J. (2017). Reactive-oxygen-species-responsive drug delivery systems: promises and challenges. *Adv. Sci.* 4:1600124. doi: 10.1002/advs.201600124

Sarmah, D., Kaur, H., Saraf, J., Vats, K., Pravalika, K., Wanve, M., et al. (2019). Mitochondrial dysfunction in stroke: implications of stem cell therapy. *Transl. Stroke Res.* 10, 121–136. doi: 10.1007/s12975-018-0642-y

Schapira, A. (1998). Human complex I defects in neurodegenerative diseases. *Biochim. Biophys. Acta* 1364, 261–270. doi: 10.1016/S0005-2728(98)00032-2

Schumacker, P. T. (2015). Reactive oxygen species in cancer: a dance with the devil. *Cancer Cell* 27, 156–157. doi: 10.1016/j.ccell.2015.01.007

Sun, B., Chen, Y., Yu, H., Wang, C., Zhang, X., Zhao, H., et al. (2019). Photodynamic PEG-coated ROS-sensitive prodrug nanoassemblies for core-shell synergistic chemo-photodynamic therapy. *Acta Biomater.* 92, 219–228. doi: 10.1016/j.actbio.2019.05.008

Suzukawa, K., Miura, K., Mitsushita, J., Resau, J., Hirose, K., Crystal, R., et al. (2000). Nerve growth factor-induced neuronal differentiation requires generation of Rac1-regulated reactive oxygen species. *J. Biol. Chem.* 275, 13175–13178. doi: 10.1074/jbc.275.18.13175

Sznajder, J. I., Fraiman, A., Hall, J. B., Sanders, W., Schmidt, G., Crawford, G., et al. (1989). Increased hydrogen peroxide in the expired breath of patients with acute hypoxemic respiratory failure. *Chest* 96, 606–612. doi: 10.1378/chest.96.3.606

Tafani, M., Sansone, L., Limana, F., Arcangeli, T., De Santis, E., Polese, M., et al. (2016). The interplay of reactive oxygen species, hypoxia, inflammation, and sirtuins in cancer initiation and progression. *Oxid. Med. Cell. Longev.* 2016:3907147. doi: 10.1155/2016/3907147

Tang, Z., Kong, N., Ouyang, J., Feng, C., Kim, N. Y., Ji, X., et al. (2020). Phosphorus science-oriented design and synthesis of multifunctional nanomaterials for biomedical applications. *Matter* 2, 297–322. doi: 10.1016/j.matt.2019.12.007

Tao, W., Ji, X., Xu, X., Islam, M. A., Li, Z., Chen, S., et al. (2017). Antimonene quantum dots: synthesis and application as near-infrared photothermal agents for effective cancer therapy. *Angew. Chem. Int. Edit.* 129, 12058–12062. doi: 10.1002/ange.201703657

Tao, W., Kong, N., Ji, X., Zhang, Y., Sharma, A., Ouyang, J., et al. (2019). Emerging two-dimensional monoelemental materials (Xenes) for biomedical applications. *Chem. Soc. Rev.* 48, 2891–2912. doi: 10.1039/C8CS00823J

Tapeinos, C., Larrañaga, A., Tomatis, F., Bizeau, J., Marino, A., Battaglini, M., et al. (2020). Advanced functional materials and cell-based therapies for the treatment of ischemic stroke and postischemic stroke effects. *Adv. Funct. Mater.* 30, 1906283. doi: 10.1002/adfm.201906283

Tapeinos, C., and Pandit, A. (2016). Physical, chemical, and biological structures based on ros-sensitive moieties that are able to respond to oxidative microenvironments. *Adv. Mater.* 28, 5553–5585. doi: 10.1002/adma.201505376

Tian, T., Wang, Z., and Zhang, J. (2017). Pathomechanisms of oxidative stress in inflammatory bowel disease and potential antioxidant therapies. *Oxid. Med. Cell. Longev.* 2017:4535194. doi: 10.1155/2017/4535194

Touyz, R. M. (2003). Reactive oxygen species in vascular biology: role in arterial hypertension. *Expert Rev. Cardiovasc. Ther.* 1, 91–106. doi: 10.1586/14779072.1.1.91

Trachootham, D., Alexandre, J., and Huang, P. (2009). Targeting cancer cells by ROS-mediated mechanisms: a radical therapeutic approach? *Nat. Rev Drug Discov.* 8, 579–591. doi: 10.1038/nrd2803

Uthaman, S., Pillarisetti, S., Mathew, A. P., Kim, Y., Bae, W. K., Huh, K. M., et al. (2020). Long circulating photoactivable nanomicelles with tumor localized activation and ROS triggered self-accelerating drug release for enhanced locoregional chemo-photodynamic therapy. *Biomaterials* 232:119702. doi: 10.1016/j.biomaterials.2019.119702

Uttara, B., Singh, A. V., Zamboni, P., and Mahajan, R. (2009). Oxidative stress and neurodegenerative diseases: a review of upstream and downstream antioxidant therapeutic options. *Curr. Neuropharmacol.* 7, 65–74. doi: 10.2174/157015909787602823

Valko, M., Rhodes, C., Moncol, J., Izakovic, M., and Mazur, M. (2006). Free radicals, metals and antioxidants in oxidative stress-induced

cancer. *Chem. Biol. Interact.* 160, 1–40. doi: 10.1016/j.cbi.2005.12.009

Wang, L., Fan, F., Cao, W., and Xu, H. (2015). Ultrasensitive ROS-responsive coassemblies of tellurium-containing molecules and phospholipids. *ACS Appli. Mater. Inter.* 7, 16054–16060. doi: 10.1021/acsami.5b04419

Wang, M., Sun, S., Neufeld, C. I., Perez-Ramirez, B., and Xu, Q. (2014). Reactive oxygen species-responsive protein modification and its intracellular delivery for targeted cancer therapy. *Angew. Chem. Int. Edit.* 53, 13444–13448. doi: 10.1002/anie.201407234

Wang, X., Meng, G., Zhang, S., and Liu, X. (2016). A reactive 1O2-responsive combined treatment system of photodynamic and chemotherapy for cancer. *Sci. Rep.* 6:29911. doi: 10.1038/srep29911

Wang, Y., Deng, Y., Luo, H., Zhu, A., Ke, H., Yang, H., et al. (2017). Light-responsive nanoparticles for highly efficient cytoplasmic delivery of anticancer agents. *ACS Nano* 11, 12134–12144. doi: 10.1021/acsnano.7b05214

Weekley, C. M., and Harris, H. H. (2013). Which form is that? *the importance of selenium speciation and metabolism in the prevention and treatment of disease. Chem. Soc. Rev.* 42, 8870–8894. doi: 10.1039/c3cs60272a

Weinberg, F., Hamanaka, R., Wheaton, W. W., Weinberg, S., Joseph, J., Lopez, M., et al. (2010). Mitochondrial metabolism and ROS generation are essential for Kras-mediated tumorigenicity. *Proc. Natl. Acad. Sci. U.S.A.* 107, 8788–8793. doi: 10.1073/pnas.1003428107

West, A. P., Shadel, G. S., and Ghosh, S. (2011). Mitochondria in innate immune responses. *Nat. Rev. Immunol.* 11, 389–402. doi: 10.1038/nri2975

Wilson, D. S., Dalmasso, G., Wang, L., Sitaraman, S. V., Merlin, D., and Murthy, N. (2010). Orally delivered thioketal nanoparticles loaded with TNF-α-siRNA target inflammation and inhibit gene expression in the intestines. *Nat. Mater.* 9, 923–928. doi: 10.1038/nmat2859

Winterbourn, C. C. (2008). Reconciling the chemistry and biology of reactive oxygen species. *Nat. Chem. Biol.* 4:278. doi: 10.1038/nchembio.85

Xiang, J., Liu, X., Zhou, Z., Zhu, D., Zhou, Q., Piao, Y., et al. (2018). Reactive Oxygen Species (ROS)-responsive charge-switchable nanocarriers for gene therapy of metastatic cancer. *ACS Appli. Mater. Inter.* 10, 43352–43362. doi: 10.1021/acsami.8b13291

Xiao, C., Ding, J., Ma, L., Yang, C., Zhuang, X., and Chen, X. (2015). Synthesis of thermal and oxidation dual responsive polymers for reactive oxygen species (ROS)-triggered drug release. *Polym. Chem.* 6, 738–747. doi: 10.1039/C4PY01156B

Xie, A., Hanif, S., Ouyang, J., Tang, Z., Kong, N., Kim, N. Y., et al. (2020). Stimuli-responsive prodrug-based cancer nanomedicine. *EBioMedicine* 56:102821. doi: 10.1016/j.ebiom.2020.102821

Xu, Q., He, C., Xiao, C., and Chen, X. (2016). Reactive oxygen species (ROS) responsive polymers for biomedical applications. *Macromol. Biosci.* 16, 635–646. doi: 10.1002/mabi.201500440

Yang, G., Sun, X., Liu, J., Feng, L., and Liu, Z. (2016). Light-responsive, singlet-oxygen-triggered on-demand drug release from photosensitizer-doped mesoporous silica nanorods for cancer combination therapy. *Adv. Funct. Mater.* 26, 4722–4732. doi: 10.1002/adfm.201600722

Yang, N., Xiao, W., Song, X., Wang, W., and Dong, X. (2020a). Recent advances in tumor microenvironment hydrogen peroxide-responsive materials for cancer photodynamic therapy. *Nano Micro. Lett.* 12:15. doi: 10.1007/s40820-019-0347-0

Yang, X., Li, Y., Li, Y., Ren, X., Zhang, X., Hu, D., et al. (2017). Oxidative stress-mediated atherosclerosis: mechanisms and therapies. *Front. Physiol.* 8:600. doi: 10.3389/fphys.2017.00600

Yang, X., Shi, X., Zhang, Y., Xu, J., Ji, J., Ye, L., et al. (2020b). Photo-triggered self-destructive ROS-responsive nanoparticles of high paclitaxel/chlorin e6 co-loading capacity for synergetic chemo-photodynamic therapy. *J. Control. Release* 323, 333–349. doi: 10.1016/j.jconrel.2020.04.027

Yang, Y., Wang, Y., Xu, L., and Chen, T. (2020c). Dual-functional Se/Fe complex facilitates TRAIL treatment against resistant tumor cells via modulating cellular endoplasmic reticulum stress. *Chinese Chem. Lett.* 31, 1801–1806. doi: 10.1016/j.cclet.2020.03.004

Yao, Y., Zhang, H., Wang, Z., Ding, J., Wang, S., Huang, B., et al. (2019). Reactive oxygen species (ROS)-responsive biomaterials mediate tissue microenvironments and tissue regeneration. *J. Mater. Chem. B* 7, 5019–5037. doi: 10.1039/C9TB00847K

Ye, J., Fan, J., Venneti, S., Wan, Y.-W., Pawel, B. R., Zhang, J., et al. (2014). Serine catabolism regulates mitochondrial redox control during hypoxia. *Cancer Discov.* 4, 1406–1417. doi: 10.1158/2159-8290.CD-14-0250

Youdim, K. A., Martin, A., and Joseph, J. A. (2000). Essential fatty acids and the brain: possible health implications. *Int. J. Dev. Neurosci.* 18, 383–399. doi: 10.1016/S0736-5748(00)00013-7

Yu, L.-Y., Su, G.-M., Chen, C.-K., Chiang, Y.-T., and Lo, C.-L. (2016). Specific cancer cytosolic drug delivery triggered by reactive oxygen species-responsive micelles. *Biomacromolecules* 17, 3040–3047. doi: 10.1021/acs.biomac.6b00916

Zhang, D., Wei, Y., Chen, K., Zhang, X., Xu, X., Shi, Q., et al. (2015). Biocompatible reactive oxygen species (ROS)-responsive nanoparticles as superior drug delivery vehicles. *Adv. Healthc. Mater.* 4, 69–76. doi: 10.1002/adhm.201400299

Zhang, Q., Zhang, F., Chen, Y., Dou, Y., Tao, H., Zhang, D., et al. (2017). Structure–property correlations of reactive oxygen species-responsive and hydrogen peroxide-eliminating materials with anti-oxidant and anti-inflammatory activities. *Chem. Mater.* 29, 8221–8238. doi: 10.1021/acs.chemmater.7b02412

Zhang, R., Liu, R., Liu, C., Pan, L., Qi, Y., Cheng, J., et al. (2020). A pH/ROS dual-responsive and targeting nanotherapy for vascular inflammatory diseases. *Biomaterials* 230:119605. doi: 10.1016/j.biomaterials.2019.119605

Zhang, Y., Li, Y., Tian, H., Zhu, Q., Wang, F., Fan, Z., et al. (2019). Redox-responsive and dual-targeting hyaluronic acid–methotrexate prodrug self-assembling nanoparticles for enhancing intracellular drug self-delivery. *Mol. Pharm.* 16, 3133–3144. doi: 10.1021/acs.molpharmaceut.9b00359

Zhang, Y., Ma, C., Zhang, S., Wei, C., Xu, Y., and Lu, W. (2018). ROS-responsive selenium-containing polyphosphoester nanogels for activated anticancer drug release. *Mater. Today Chem.* 9, 34–42. doi: 10.1016/j.mtchem.2018.04.002

Zhao, C., Sun, G., Li, S., Lang, M.-F., Yang, S., Li, W., et al. (2010). MicroRNA let-7b regulates neural stem cell proliferation and differentiation by targeting nuclear receptor TLX signaling. *Proc. Natl. Acad. Sci. U.S.A.* 107, 1876–1881. doi: 10.1073/pnas.0908750107

Zhao, Z., Gao, P., Ma, L., and Chen, T. (2020). A highly X-ray sensitive iridium prodrug for visualized tumor radiochemotherapy. *Chem. Sci.* 11, 3780–3789. doi: 10.1039/D0SC00862A

Zhou, Z., Song, J., Nie, L., and Chen, X. (2016). Reactive oxygen species generating systems meeting challenges of photodynamic cancer therapy. *Chem. Soc. Rev.* 45, 6597–6626. doi: 10.1039/C6CS00271D

Zuccato, C., and Cattaneo, E. (2009). Brain-derived neurotrophic factor in neurodegenerative diseases. *Nat. Rev. Neurol.* 5:311. doi: 10.1038/nrneurol.2009.54

Conflict of Interest: The authors declare that the research was conducted in the absence of any commercial or financial relationships that could be construed as a potential conflict of interest.

frontiers in Chemistry

ORIGINAL RESEARCH
published: 06 October 2020
doi: 10.3389/fchem.2020.00741

Surface Modification of Monolayer MoS_2 by Baking for Biomedical Applications

Yan Wang[1], Yuanjun Ma[2], Jinping Shi[1], Xiangyu Yan[3], Jun Luo[3], Huilong Zhu[3], Kunpeng Jia[3], Juan Li[1]* and Can Yang Zhang[4]**

[1] School of Physics, Beijing Institute of Technology, Beijing, China, [2] School of Optics and Photonics, Beijing Institute of Technology, Beijing, China, [3] Institute of Microelectronics, Chinese Academy of Sciences, Beijing, China, [4] Antimicrobial Resistance Interdisciplinary Research Group, Singapore-MIT Alliance for Research and Technology, Singapore, Singapore

OPEN ACCESS

Edited by:
Dalong Ni,
Shanghai Jiao Tong University, China

Reviewed by:
Zhimin Wu,
Xiangtan University, China
Xin Dong Guo,
Beijing University of Chemical Technology, China
Wenjing Lin,
Guangdong University of Technology, China

***Correspondence:**
Kunpeng Jia
jiakunpeng@ime.ac.cn
Juan Li
jli@bit.edu.cn
Can Yang Zhang
canyang.zhang@smart.mit.edu

Specialty section:
This article was submitted to Nanoscience, a section of the journal Frontiers in Chemistry

Received: 29 May 2020
Accepted: 17 July 2020
Published: 06 October 2020

Citation:
Wang Y, Ma Y, Shi J, Yan X, Luo J, Zhu H, Jia K, Li J and Zhang CY (2020) Surface Modification of Monolayer MoS_2 by Baking for Biomedical Applications. Front. Chem. 8:741. doi: 10.3389/fchem.2020.00741

Molybdenum disulfide (MoS_2), a transition metal dichalcogenide material, possesses great potential in biomedical applications such as chemical/biological sensing, drug/gene delivery, bioimaging, phototherapy, and so on. In particular, monolayer MoS_2 has more extensive applications because of its superior physical and chemical properties; for example, it has an ultra-high surface area, is easily modified, and has high biodegradability. It is important to prepare advanced monolayer MoS_2 with enhanced energy exchange efficiency (EEE) for the development of MoS_2-based nanodevices and therapeutic strategies. In this work, a monolayer MoS_2 film was first synthesized through a chemical vapor deposition method, and the surface of MoS_2 was further modified via a baking process to develop p-type doping of monolayer MoS_2 with high EEE, followed by confirmation by X-ray photoelectron spectroscopy and Raman spectroscopy analysis. The morphology, surface roughness, and layer thickness of monolayer MoS_2 before and after baking were thoroughly investigated using atomic force microscopy. The results showed that the surface roughness and layer thickness of monolayer MoS_2 modified by baking were obviously increased in comparison with MoS_2 without baking, indicating that the surface topography of the monolayer MoS_2 film was obviously influenced. Moreover, a photoluminescence spectrum study revealed that p-type doping of monolayer MoS_2 displayed much greater photoluminescence ability, which was taken as evidence of higher photothermal conversion efficiency. This study not only developed a novel MoS_2 with high EEE for future biomedical applications but also demonstrated that a baking process is a promising way to modify the surface of monolayer MoS_2.

Keywords: MoS_2, surface modification, p-type doping, baking, biomedical application

INTRODUCTION

Two-dimensional materials (2DMs) have attracted extremely wide attention in the biomedical science field because of their various unique properties (Yin et al., 2016; Liu and Liu, 2018). 2DMs are a large family of materials that include semimetals (graphene), semiconductors (molybdenum disulfide (MoS_2), black phosphorus, etc.), insulators (h-BN), superconductors (carbon nanotubes), thermoelectric materials (PbTe), and topological insulators (HgTe quantum wells) (Frindt, 1966; Wilson and Yoffe, 1969; Clement et al., 1978; Abruna and Bard, 1982; Mishra et al., 1997; Prasad and Zabinski, 1997; Poizot et al., 2000; Frey et al., 2003; Kane and Mele, 2005). In recent years, another class of 2DMs, transition metal dichalcogenides (TMDCs), have emerged and also received much attention as next-generation applications in electronics and optoelectronics because of their various unique optical, electrochemical, catalytic, and lubrication properties (Radisavljevic et al., 2011a,b; Choi et al., 2012; Wang et al., 2012; Sundaram et al., 2013). The chemical formula of two-dimensional (2D) TMDCs is MX_2, where M stands for a transition metal element, such as Mo, W, etc., and X stands for a chalcogen element, such as S, Se, etc. (Wu et al., 2016). TMDCs are a series of compounds with layered structures, and the bulk MX_2 is composed of multiple X–M–X layers that are held in stacks by weak van der Waals forces. The single-layer MX_2 has a unique sandwich-like structure, with a plane of M atoms wedged into two planes of X atoms. The M and X atoms are held together by strong covalent bonds (Lee et al., 2012). MoS_2 is a typical 2D TMDC compound, with the height of each layer being 0.65 nm (Eda et al., 2011). In its bulk structure, MoS_2 is a semiconductor with an indirect bandgap of about 1 eV, while monolayer MoS_2 has direct bandgap of 1.8 eV (Li and Zhu, 2015). Because of its outstanding properties, MoS_2 has been widely studied and used in various applications, including transistors, sensors, and memory and optoelectronic devices in the biomedical sciences (Kim et al., 2012; Singh et al., 2016). Recently, MoS_2-based nanoplatforms have been reported as photothermal agents used for cancer therapy and treatment of bacteria-induced infections because of their good biocompatibility and high photothermal conversion efficiency in the near-infrared region (Chou et al., 2013; Yin et al., 2014, 2016; Gao et al., 2018). Chou et al. (2013) synthesized and prepared MoS_2 nanosheets that were used in photothermal therapy (PTT) for cancer. The study showed that MoS_2 nanosheets had much higher photothermal conversion efficiency than graphene and gold nanorods, thereby improving the therapeutic efficacy in cancer therapy (Chou et al., 2013). Inspired by the effective photothermal conversion of MoS_2, Yin et al. (2016) developed polyethylene glycol-functionalized MoS_2-based nanoflowers that showed high antimicrobial activity for Gram-negative ampicillin-resistant *Escherichia coli* and Gram-positive endospore-forming *Bacillus subtilis*.

Broadly speaking, the methods to obtain MoS_2 films include top-down and bottom-up methods, such as micro-mechanical stripping, lithium-ion intercalation, liquid-phase ultrasonic stripping, and chemical vapor deposition (CVD) (Ramakrishna Matte et al., 2010; Coleman et al., 2011; Lee et al., 2012; Baugher et al., 2013; Zhang et al., 2014). The technology of the micro-mechanical stripping method is completely mature; nevertheless, achieving large-scale production using this method remains a challenge (Baugher et al., 2013). The lithium-ion intercalation method is quite time-consuming and has extremely strict requirements for the preparation conditions (Ramakrishna Matte et al., 2010), while the degree and efficiency of the liquid-state ultrasonic stripping method are relatively low and the resulting single-layer product content is low (Coleman et al., 2011). Therefore, it is necessary to optimize large-area deposition methods for MoS_2 films to scale up these technologies. In recent years, a method of growing MoS_2 by CVD on insulating substrates has been developed. The CVD method is easy to operate and can achieve high-quality, large-area continuous synthesis batches with high efficiency (Zhang et al., 2014); this method is better suited to industrialization and can quickly adapt to the large-scale application of MoS_2. In 2012, Lee and co-workers reported the synthesis of large-area monolayers of MoS_2 thin films on silicon dioxide substrates by CVD for the first time (Lee et al., 2012). Indeed, a native n-doping behavior of not intentionally doped MoS_2 was confirmed by previous investigations (Mak et al., 2013; Fang et al., 2014) because of hypothetical sulfur vacancies (Qiu et al., 2013; Tongay et al., 2013). The n-type doping limits carrier conduction in MoS_2 to its conduction bands, and p-type doping is more desirable for MoS_2-based field-effect transistor devices (Zhang et al., 2013). Inspired by this demand, research on the doping of MoS_2 has been extensively encouraged (Chuang et al., 2016). The p-type doping of MoS_2 has lower resistance and better performance than the original MoS_2 (Laskar et al., 2014; Neal et al., 2017), the basic mechanism of which is to suppress n-type conductivity. Moreover, 2DMs also enable new methods such as surface charge transfer (Zhang et al., 2016) and intercalation (Jung et al., 2016) to be used. But these methods are neither easy nor convenient. Another commonly used doping method is chemical doping. Rhenium and chlorine are used as substitution donors, while niobium and phosphorus are used as substitution acceptors (Tiong et al., 1999; Laskar et al., 2014; Suh et al., 2014; Yang et al., 2014; Das et al., 2015; Park et al., 2015). The p-type doping of MoS_2 films is carried out by fluorine plasma treatment or the spin-on $AuCl_3$ method (Chen et al., 2013; Liu et al., 2016; Xue et al., 2016). In addition, oxygen is frequently used for doping as pure physical adsorption of oxygen will have only a small effect, which can cause an increase in the threshold voltage and a decrease in the on-current; however, the interaction between oxygen and MoS_2 films is too weak to overcome the intrinsic n-type doping. In this case, some of the intrinsic properties of MoS_2 can be altered by the oxygen plasma method (Nan et al., 2014), which is widely used to prepare p-type doping of MoS_2. However, the aforementioned methods of preparing p-type doping of MoS_2 have some limitations. (i) There is residual organic solvent after chemical doping. (ii) Plasma treatment is carried out under harsh reaction conditions and requires careful control of the power to decrease damage to the sample surface. (iii) In addition, spin-on $AuCl_3$ is mainly used for achieving high performance in p-type field-effect transistors (Park et al., 2015; Xue et al., 2016).

Therefore, it is of great importance to efficiently and effectively synthesize and prepare p-type doping of MoS_2 films to enhance the energy exchange efficiency (EEE) for PTT in biomedical applications. In this work, we report a simple and convenient method for the preparation of p-type doping of monolayer MoS_2 through baking under ambient conditions. The monolayer MoS_2 film was synthesized using the CVD method first. Optical microscopy (OM) and atomic force microscopy (AFM) were used to directly image and evaluate the morphology associated with monolayer MoS_2 grown by CVD onto a SiO_2/Si substrate. Then, the monolayer MoS_2 film was modified via baking at different temperatures under ambient conditions. Finally, the physicochemical properties of the modified monolayer MoS_2 film were thoroughly investigated using AFM, Raman spectroscopy, photoluminescence (PL), and X-ray photoelectron spectroscopy (XPS). This study not only prepared a p-type doping MoS_2 film with high EEE, but also demonstrated that the baking process is a promising way to modify the surface of an MoS_2 film, which encourages further investigations for biomedical applications.

MATERIALS AND METHODS

Materials

N-type silicon covered with 30 nm silicon dioxide was purchased from Suzhou Ruicai Semiconductor Co. Ltd. MoO_3 (AR) was obtained from Nanjing Muke Nanotechnology Co. Ltd. S powder (99.95 %) was ordered from Aladdin Reagent Co. Ltd. Ar (99.99%) was purchased from Harbin Dawn Gas. Acetone, anhydrous ethanol, and deionized water were obtained from Wuxi Ledong Microelectronics Co. Ltd. The CVD oven was purchased from Hefei Kejing Material Technology Co. Ltd.

Synthesis of MoS_2 Films

MoS_2 films were synthesized using the CVD method. N-type silicon covered with 30 nm silicon dioxide was used as the substrate to grow the MoS_2 films. A silicon wafer was cleaned through sonication for 10 min with acetone, anhydrous ethanol, and deionized water, respectively. Subsequently, after drying under argon, the silicon wafer was further cleaned by plasma oxygen cleaner. MoO_3 and elemental S powder were used as the precursor and reactant materials, respectively, to grow a single layer of MoS_2 at a temperature of 700°C under atmospheric pressure. The whole experiment was carried out under Ar. MoS_2 films were obtained after 25 min.

Baking of the MoS_2 Film

Four monolayer MoS_2 samples was prepared under the same conditions using the CVD method. One was used as a control sample without any further treatment. The other three were baked under atmosphere in an oven for 2 h, at 150, 200, and 250°C, respectively.

X-Ray Photoelectron Spectroscopy Analysis

The control sample and the MoS_2 sample baked at 250°C were prepared for XPS. Using X-rays to radiate the samples, spectra can be obtained after software processing. XPS was performed to verify whether MoS_2 can form an Mo–O bond via baking.

Optical Microscopy Imaging

The number of layers of MoS_2 films was confirmed by OM. A silicon wafer with MoS_2 films was placed on a glass slide, which was put on the objective stage with two clamps to hold it. An appropriate objective was used to observe the MoS_2 films with a clear view. The OM image can be displayed by a CCD camera mounted on the OM.

Atomic Force Microscopy Imaging

AFM was carried out on MoS_2 films on a silicon wafer to characterize the morphology, roughness, and thickness of the samples. An AFM tapping mode (Dimension FastScan, Bruker) was used to scan the samples.

Raman Spectroscopy Analysis

Raman spectroscopy was carried out on the MoS_2/Si samples at room temperature with a 532 nm laser as the excitation light source and the laser power was limited to 50 μW to prevent self-heating-induced damage during the measurement. Raman spectra were observed using a micro-confocal Raman spectrometer (Horiba).

Photoluminescence Analysis

In order to determine the luminescence of MoS_2 before and after baking, PL was carried on the monolayer MoS_2 at different baking temperatures. PL spectra were observed using the same machine as used for the Raman spectra. The only difference was that during Raman measurement the sample was placed directly in the machine at room temperature under air, while during PL measurement the sample was placed in a cryostat.

RESULTS AND DISCUSSIONS

Preparation and Characterization of MoS_2 Films

The monolayer MoS_2 film was prepared by the CVD method, as shown in **Figure 1A**. The n-type silicon substrate covered with 30 nm silicon dioxide was cleaned by plasma oxygen cleaner, followed by the growth of the monolayer MoS_2 film using MoO_3 and elemental S powder as the precursor and reactant materials, respectively. The reaction was carried out at 700°C at atmospheric pressure under Ar for 25 min. Representative OM images of the as-deposited samples are shown in **Figures 1B,C**, demonstrating the presence of large MoS_2 domains with uniform and smooth morphology, as indicated by the homogeneous purple color on the silicon substrate (Castellanos-Gomez et al., 2010; Li et al., 2012). Some irregular parts of the silicon wafer (orange) were exposed that were not covered with MoS_2 film because of the rupture of the monolayer MoS_2 film during the CVD process. Collectively, the monolayer MoS_2 film was successfully prepared by the CVD method on the silicon substrate.

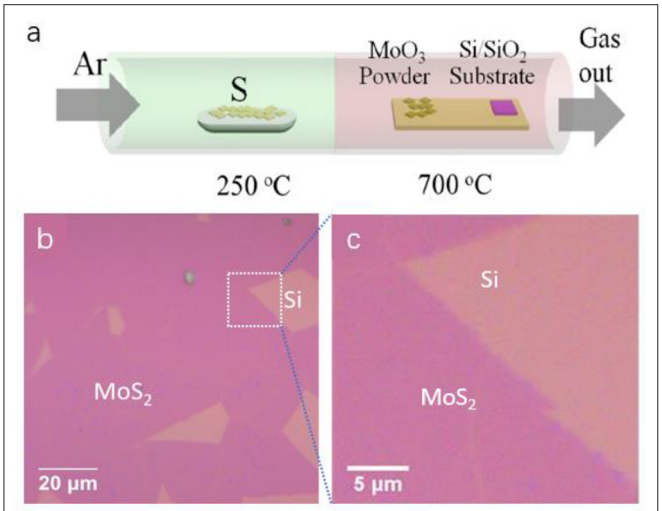

FIGURE 1 | (A) A schematic of the synthesis of a monolayer MoS_2 film using the chemical vapor deposition (CVD) method. **(B,C)** Optical micrographs of monolayer MoS_2 prepared by the CVD method on a silicon substrate. **(B)** Scale bar, 20 μm. **(C)** Scale bar, 5 μm.

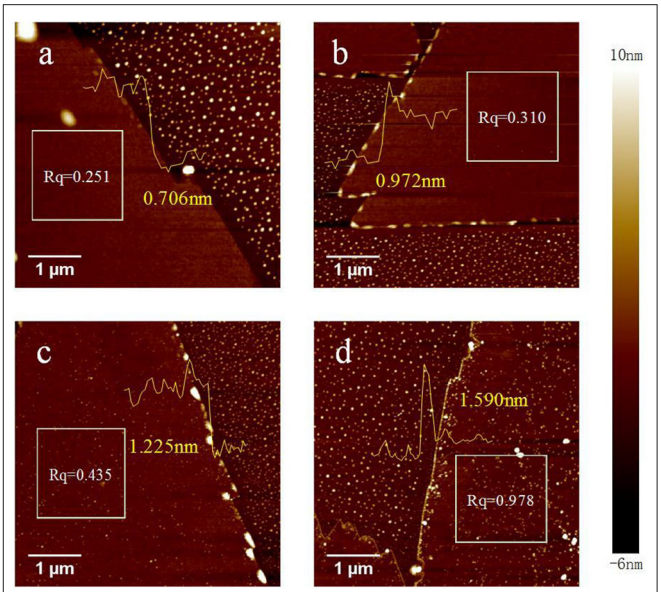

FIGURE 2 | Atomic force microscopy images of the monolayer MoS_2 film before and after baking at different temperatures for 2 h under air. **(A)** The original monolayer MoS_2 film prepared by the chemical vapor deposition method. The monolayer MoS_2 film baked at **(B)** 150°C, **(C)** 200°C, and **(D)** 250°C. The yellow line indicates the surface height of the monolayer MoS_2 film. The area indicated with the white square was measured to confirm the roughness. Scale bar, 1 μm.

Study of the Baking Effect on the MoS_2 Film

Atomic Force Microscopy Imaging

Next, we treated the monolayer MoS_2 film via baking at 150, 200, or 250°C for 2 h under air, followed by imaging through AFM. To further confirm the morphology and size (especially the thickness) of the monolayer MoS_2 film, the border of the MoS_2 film and wafer was imaged, as shown in **Figure 2**. The areas with white dots are the silicon wafer, and the integrated and smooth areas are the monolayer MoS_2 film. To further characterize the morphology and size of the samples, the perpendicular height (thickness) of the monolayer MoS_2 film and roughness of the area indicated by the white square were measured. **Figure 2A** shows a higher resolution tapping mode AFM morphological image of an MoS_2 domain partially covering the SiO_2 surface without the baking process. A uniform and smooth MoS_2 film was observed, and the result was consistent with that of OM imaging. The thickness and roughness (R_q) were, respectively, confirmed as 0.706 nm and 0.251, which further proved the successful synthesis of the monolayer MoS_2 film (Giannazzo et al., 2020). After baking at 150°C (**Figure 2B**), the thickness and the R_q of the treated MoS_2 film were increased to 0.972 nm and 0.310, respectively. Moreover, after baking at 200°C (**Figure 2C**) and 250°C (**Figure 2D**), the thickness was obviously increased to 1.225 nm and 1.590 nm, respectively. In addition, the R_q was significantly increased (0.435 at 200°C and 0.978 at 250°C). These results show that the thickness and roughness of the monolayer MoS_2 film were increased with an increase in baking temperature. In addition, the surface topography of the sample was also changed with an increase in the baking temperature. Compared with the original sample, the monolayer MoS_2 film baked at 150°C still showed a smooth and clear surface, indicating no obvious changes in the surface topography. However, some white dots were observed in the sample after baking at 200°C, and denser and larger white dots appeared on the surface of the sample after baking at 250°C. These changes possibly resulted in the increase in the roughness of the monolayer MoS_2 film. As reported previously, the white dots could be the etched parts of the monolayer MoS_2 flake, which would break down at 300°C (Zhou et al., 2013). This can be explained by the composition of the surface of the MoS_2 film being disturbed or changed, possibly as a result of a chemical reaction that led to the adsorption or formation of elements. In this etching process, some sulfur vacancies might arise, followed by adsorption and reaction with the oxygen in the air and water vapor, finally resulting in p-type doping of the monolayer MoS_2 film. In summary, the thickness and surface topography of the monolayer MoS_2 film were obviously influenced by the baking process and were dependent on the baking temperature.

Raman Spectroscopy Analysis

To further investigate the effect of baking on the monolayer MoS_2 film, the Raman spectra of samples before and after baking at different temperatures were measured, as shown in **Figure 3**. Two characteristic vibrational peaks were observed for the MoS_2 film, namely the in-plane vibration mode E^1_{2g} (385 cm^{-1}) and the out-of-plane vibration mode A_{1g} (403 cm^{-1}) (**Figure 3A**). The wavenumber difference ($\Delta = 17.9\ cm^{-1}$) between the peaks' positions is consistent with the presence of the monolayer MoS_2 domains (Kim et al., 2018). **Figures 3B,C** shows the changes in the frequency shift and full width at half-maximum (FWHM) of two modes with the increase in the baking temperature,

respectively. With the increase in the baking temperature, no obvious shift was observed for the E^1_{2g} mode, whereas the A_{1g} mode showed a right shift with an increase of ∼2 cm^{-1}, from about 403 cm^{-1} to 405 cm^{-1} (**Figures 3A,B**). The different changes in the E^1_{2g} and A_{1g} modes demonstrated the presence of p-type doping of MoS_2 (Chakraborty et al., 2012; Mao et al., 2013). Moreover, the FWHM of the A_{1g} mode was obviously decreased with the increase in the baking temperature. However, the E^1_{2g} mode showed negligible changes compared with those of the A_{1g} mode with the increase in the baking temperature. As reported previously, both the doping and strain showed an effect on the vibrational modes of the Raman spectra of the monolayer MoS_2 film (Scalise et al., 2014). If the changes were induced by strain, Raman modes E^1_{2g} and A_{1g} would shift together, compressive strain could cause blue shift of E^1_{2g} and A_{1g}, tensile strain could cause red shift of E^1_{2g} and A_{1g}, therefore there was no strain effect in above results. In contrast, if the changes were caused by doping, the wavenumber and the FWHM of the A_{1g} mode were obviously changed, and the E^1_{2g} mode was maintained stable. Furthermore, blue shift of the A_{1g} mode and a decrease in the FWHM corresponded to p-type doping, and red shift and an increase in the FWHM corresponded to n-type doping (Chakraborty et al., 2012). In this case, the results revealed that the p-type doping of the MoS_2 film was caused by the baking process.

X-Ray Photoelectron Spectroscopy Analysis

To further confirm the p-type doping of MoS_2 after baking, XPS spectra of samples in the Mo(3d) and O(1s) regions before and after baking at 250°C for 2 h under air were monitored, as shown in **Figures 4A,B**, respectively. First, the peaks at S 2s, Mo^{4+} $3d_{5/2}$, and Mo^{4+} $3d_{3/2}$ were observed (**Figure 4A**), showing the successful synthesis of the monolayer MoS_2 film. After the baking process, the signals of the Mo^{4+} $3d_{3/2}$ and Mo^{6+} peaks were significantly enhanced (**Figure 4A**), indicating the generation of MoO_3, which proved the p-type doping of MoS_2. Furthermore, the signal of the O(1s) peak of the sample after baking was also significantly enhanced in comparison with that of the original sample (**Figure 4B**), implying p-type doping of MoS_2 after the baking process. This can be explained by elemental oxygen being adsorbed on the surface of the sample, followed by reaction with the S vacancy during the baking process. In summary, the results of the XPS spectra further confirmed the presence of p-type doping of MoS_2 after the baking process.

Photoluminescence Analysis

Since we successfully synthesized the monolayer MoS_2 film and prepared the p-type doping of the MoS_2 film, we next evaluated whether the luminescence of MoS_2 was enhanced after the baking process using PL measurement (**Figure 5**). **Figure 5A** shows the PL spectrum of the monolayer MoS_2 film before and after baking at different temperatures. There are two major peaks in the PL spectrum, which correspond to A1 and B1 excitons, respectively. The two peaks are associated with the direct excitonic transitions at the Brillouin zone K point. The energy difference between the two peaks is due to the spin-orbital splitting of the valence band. These PL characteristics are consistent with previous work (Coehoorn et al., 1987a,b; Mak et al., 2010; Splendiani et al., 2010). Therefore, the PL spectra of the samples were divided into two peaks, where (X, Y) represents the nature of the curve after each subpeak. X represents the center of the peak, and Y represents the overall height of the peak as well as the luminous intensity of the sample, as shown in **Figures 5B–E**. For the first peak in the PL spectra, the PL intensity was enhanced step by step with the increase in the baking temperature. In particular, the PL intensity was obviously enhanced after baking at 250°C, demonstrating a 2.7-fold higher intensity than that of the original sample. The shape of the PL spectrum also changed after baking, becoming sharper with the baking treatment. The first peak energy was right (blue) shifted with an increase in the baking temperature. The right (blue) shift and the enhancement of the PL intensity could be explained by the contributions of the exciton and the charged exciton (trion) in the first peak. As previous works have shown, the charged exciton transformed to an exciton after the baking process, and the exciton was dominant in the first peak, which induced the changes in the PL spectrum. The combination of the two peaks corresponding to the A1 and B1 excitons improved the PL capacity compared with the original sample (Mak et al., 2013; Mouri et al., 2013). In addition, the unique sandwich-like structure (S–Mo–S triatomic layer) also increased the PL ability of MoS_2 after baking (Splendiani et al., 2010; Coleman et al., 2014). As mentioned above, during the baking process, the surface of the MoS_2 was active for air adsorption, which was manifested in the active physical adsorption of oxygen and water vapor. In addition, Mo–O bonds and MoO_3 might be generated by the chemical reactions, facilitating the transformation of the charged exciton to the exciton, thereby leading to the enhanced PL intensity and higher EEE (Wei et al., 2014). In conclusion, these results proved that the p-type doping of MoS_2 prepared by the baking process exhibited much higher EEE than the control sample, in which p-type doping of MoS_2 might be a promising nanoplatform for PTT in biomedical science.

CONCLUSIONS

In this work, we successfully prepared a monolayer MoS_2 film using the CVD method. Following this, OM and AFM were used to characterize the morphology of the sample. Furthermore, a baking process was utilized to treat the monolayer MoS_2 film at different temperatures under air. The surface topography of the monolayer MoS_2 film before and after the baking process was investigated by AFM, especially the thickness and roughness. Subsequently, the Raman and XPS spectra of the samples were used to confirm p-type doping of the monolayer MoS_2 film and the mechanism of generation through baking. To further evaluate the energy exchange capacity, the PL of the samples before and after the baking process was measured, and the results showed that p-type doping of the monolayer MoS_2 film exhibited much higher EEE than the original control. This study not only developed a monolayer MoS_2 film with high EEE that might be a promising platform for PTT or imaging in biomedical

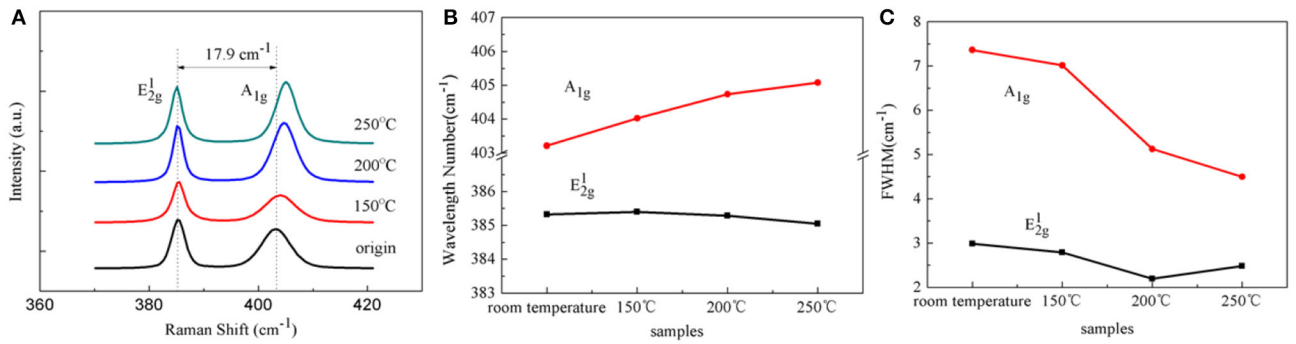

FIGURE 3 | (A) Raman spectra of the samples before and after baking at different temperatures for 2 h under air. The wavelength number **(B)** and full width at half-maximum **(C)** of the A_{1g} and E^1_{2g} modes before and after baking at 150, 200, and 250°C for 2 h under air.

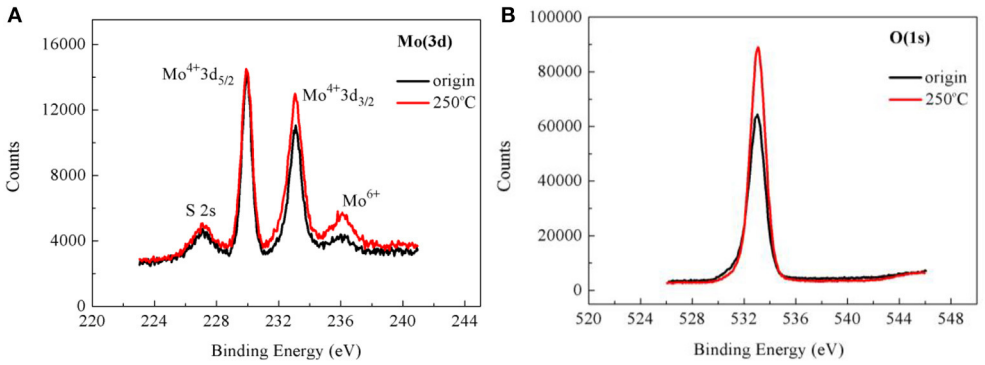

FIGURE 4 | X-ray photoelectron spectroscopy (XPS) spectra of the monolayer MoS_2 film before and after baking at 250°C for 2 h under air. **(A)** The XPS spectra of Mo(3d) atoms in the samples before and after baking. **(B)** The XPS spectra of O(1s) atoms in the samples before and after baking.

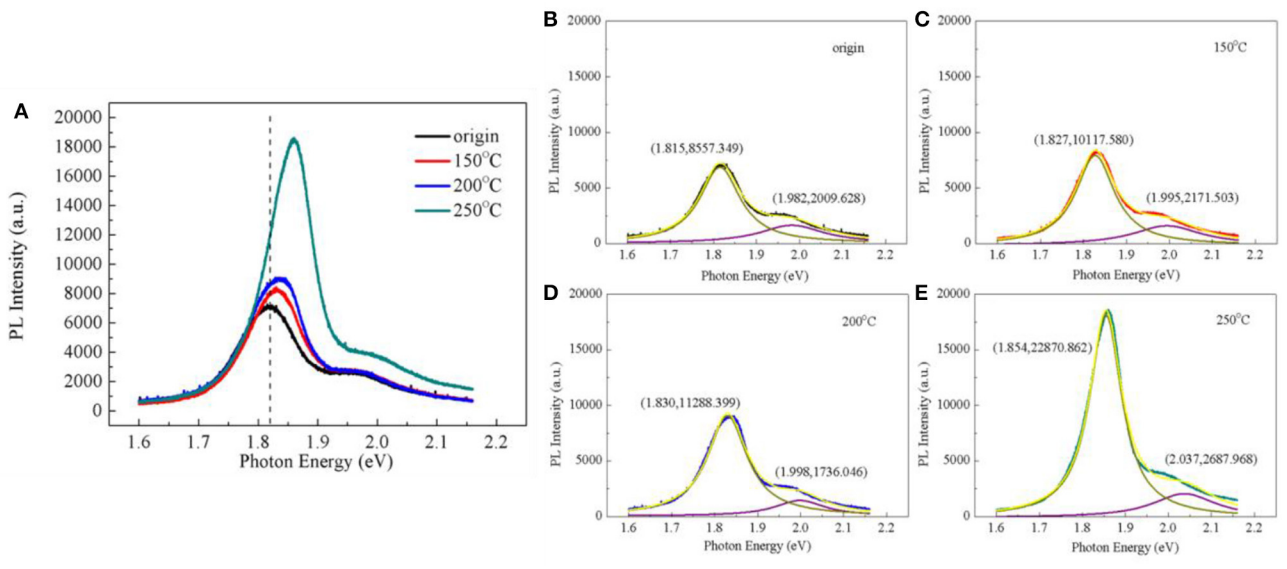

FIGURE 5 | (A) Photoluminescence (PL) spectra of the monolayer MoS_2 film before and after baking at different temperatures. PL peak fitting spectra of the original sample **(B)** and after baking at 150°C **(C)**, 200°C **(D)**, and 250°C **(E)**.

applications, but also showed that the baking process could be a convenient method to prepare p-type doping of MoS_2 with improved properties by surface modification.

DATA AVAILABILITY STATEMENT

The raw data supporting the conclusions of this article will be made available by the authors. Additional data related to this paper may be requested from the authors.

AUTHOR CONTRIBUTIONS

YW and YM: methodology and investigation. XY: software. JL and HZ: validation. YW and JL: formal analysis. YW: resources. JS: data curation. YW and JS: writing-original draft preparation. CZ: writing-review and editing. YW and XY: visualization. JL, KJ, and CZ: supervision. JL: project administration and funding acquisition. All authors contributed to the article and approved the submitted version.

FUNDING

This work was financially supported by the Beijing Institute of Technology Research Fund Program for Young Scholars and the National Natural Science Foundation of China (no. 21902012).

REFERENCES

Abruna, H. D., and Bard, A. J. (1982). Semiconductor electrodes. 44. photoelectrochemistry at polycrystalline p-Type WSe2 films. *J. Electrochem. Soc.* 129, 673–675. doi: 10.1149/1.2123949

Baugher, B. W., Churchill, H. O., Yang, Y., and Jarillo-Herrero, P. (2013). Intrinsic electronic transport properties of high-quality monolayer and bilayer MoS_2. *Nano Lett.* 13, 4212–4216. doi: 10.1021/nl401916s

Castellanos-Gomez, A., Agraït, N., and Rubio-Bollinger, G. (2010). Optical identification of atomically thin dichalcogenide crystals. *Appl. Phys. Lett.* 96:213116. doi: 10.1063/1.3442495

Chakraborty, B., Bera, A., Muthu, D., Bhowmick, S., Waghmare, U. V., and Sood, A. (2012). Symmetry-dependent phonon renormalization in monolayer MoS_2 transistor. *Phys. Rev. B* 85:161403. doi: 10.1103/PhysRevB.85.161403

Chen, M., Nam, H., Wi, S., Ji, L., Ren, X., Bian, L., et al. (2013). Stable few-layer MoS_2 rectifying diodes formed by plasma-assisted doping. *Appl. Phys. Lett.* 103:142110. doi: 10.1063/1.4824205

Choi, W., Cho, M. Y., Konar, A., Lee, J. H., Cha, G. B., Hong, S. C., et al. (2012). High-detectivity multilayer MoS_2 phototransistors with spectral response from ultraviolet to infrared. *Adv. Mater.* 24, 5832–5836. doi: 10.1002/adma.201201909

Chou, S. S., Kaehr, B., Kim, J., Foley, B. M., De, M., Hopkins, P. E., et al. (2013). Chemically exfoliated MoS_2 as near-infrared photothermal agents. *Angew. Chem. Int. Edn.* 52, 4160–4164. doi: 10.1002/anie.201209229

Chuang, H.-J., Chamlagain, B., Koehler, M., Perera, M. M., Yan, J., Mandrus, D., et al. (2016). Low-resistance 2D/2D ohmic contacts: a universal approach to high-performance WSe2, MoS_2, and $MoSe_2$ transistors. *Nano Lett.* 16, 1896–1902. doi: 10.1021/acs.nanolett.5b05066

Clement, R. P., Davies, W. B., Ford, K. A., Green, M. L., and Jacobson, A. J. (1978). Organometallic intercalates of the layered transition-metal dichalcogenides tantalum sulfide (TaS2) and zirconium sulfide. *Inorg. Chem.* 17, 2754–2758. doi: 10.1021/ic50188a013

Coehoorn, R., Haas, C., and De Groot, R. (1987a). Electronic structure of $MoSe_2$, MoS_2, and WSe_2. II. The nature of the optical band gaps. *Phys. Rev. B* 35:6203. doi: 10.1103/PhysRevB.35.6203

Coehoorn, R., Haas, C., Dijkstra, J., Flipse, C., d., De Groot, R., et al. (1987b). Electronic structure of $MoSe_2$, MoS_2, and WSe_2. I. Band-structure calculations and photoelectron spectroscopy. *Phys. Rev. B* 35:6195. doi: 10.1103/PhysRevB.35.6195

Coleman, A. F., Flores, R. L., and Xu, Y.-Q. (2014). Effects of ozone plasma treatment and X-ray irradiation on optical properties of atomically thin molybdenum disulfide. *Young Sci.* 4:1016. doi: 10.1186/s11671-019-3119-3

Coleman, J. N., Lotya, M., O'Neill, A., Bergin, S. D., King, P. J., Khan, U., et al. (2011). Two-dimensional nanosheets produced by liquid exfoliation of layered materials. *Science* 331, 568–571. doi: 10.1126/science.1194975

Das, S., Demarteau, M., and Roelofs, A. (2015). Nb-doped single crystalline MoS_2 field effect transistor. *Appl. Phys. Lett.* 106:173506. doi: 10.1063/1.4919565

Eda, G., Yamaguchi, H., Voiry, D., Fujita, T., Chen, M., and Chhowalla, M. (2011). Photoluminescence from chemically exfoliated MoS_2. *Nano Lett.* 11, 5111–5116. doi: 10.1021/nl201874w

Fang, H., Battaglia, C., Carraro, C., Nemsak, S., Ozdol, B., Kang, J. S., et al. (2014). Strong interlayer coupling in van der Waals heterostructures built from single-layer chalcogenides. *Proc. Natl. Acad. Sci. U.S.A.* 111, 6198–6202. doi: 10.1073/pnas.1405435111

Frey, G. L., Reynolds, K. J., Friend, R. H., Cohen, H., and Feldman, Y. (2003). Solution-processed anodes from layer-structure materials for high-efficiency polymer light-emitting diodes. *J. Am. Chem. Soc.* 125, 5998–6007. doi: 10.1021/ja020913o

Frindt, R. (1966). Single crystals of MoS_2 several molecular layers thick. *J. Appl. Phys.* 37, 1928–1929. doi: 10.1063/1.1708627

Gao, Q., Zhang, X., Yin, W., Ma, D., Xie, C., Zheng, L., et al. (2018). Functionalized MoS_2 nanovehicle with near-infrared laser-mediated nitric oxide release and photothermal activities for advanced bacteria-infected wound therapy. *Small* 14:1802290. doi: 10.1002/smll.201802290

Giannazzo, F., Bosi, M., Fabbri, F., Schilirò, E., Greco, G., and Roccaforte, F. (2020). Direct probing of grain boundary resistance in chemical vapor deposition-grown monolayer MoS_2 by conductive atomic force microscopy. *Rapid Res. Lett.* 14:1900393. doi: 10.1002/pssr.201900393

Jung, Y., Zhou, Y., and Cha, J. J. (2016). Intercalation in two-dimensional transition metal chalcogenides. *Inorgan. Chem. Front.* 3, 452–463. doi: 10.1039/C5QI00242G

Kane, C. L., and Mele, E. J. (2005). Quantum spin hall effect in graphene. *Phys. Rev. Lett.* 95:226801. doi: 10.1103/PhysRevLett.95.226801

Kim, H. J., Kim, D., Jung, S., Bae, M. H., Yun, Y. J., Yi, S. N., et al. (2018). Changes in the Raman spectra of monolayer MoS_2 upon thermal annealing. *J. Raman Spectrosc.* 49, 1938–1944. doi: 10.1002/jrs.5476

Kim, S., Konar, A., Hwang, W.-S., Lee, J. H., Lee, J., Yang, J., et al. (2012). High-mobility and low-power thin-film transistors based on multilayer MoS_2 crystals. *Nat. Commun.* 3:1011. doi: 10.1038/ncomms2018

Laskar, M. R., Nath, D. N., Ma, L., Lee, E. W., Lee, C. H., Kent, T., et al. (2014). p-type doping of MoS_2 thin films using Nb. *Appl. Phys. Lett.* 104:092104. doi: 10.1063/1.4867197

Lee, Y. H., Zhang, X. Q., Zhang, W., Chang, M. T., Lin, C. T., Chang, K. D., et al. (2012). Synthesis of large-area MoS_2 atomic layers with chemical vapor deposition. *Adv. Mater.* 24, 2320–2325. doi: 10.1002/adma.201104798

Li, H., Zhang, Q., Yap, C. C. R., Tay, B. K., Edwin, T. H. T., Olivier, A., et al. (2012). From bulk to monolayer MoS_2: evolution of Raman scattering. *Adv. Funct. Mater.* 22, 1385–1390. doi: 10.1002/adfm.201102111

Li, X., and Zhu, H. (2015). Two-dimensional MoS_2: properties, preparation, and applications. *J. Materiomics* 1, 33–44. doi: 10.1016/j.jmat.2015.03.003

Liu, T., and Liu, Z. (2018). 2D MoS_2 nanostructures for biomedical applications. *Adv. Healthc. Mater.* 7:1701158. doi: 10.1002/adhm.201701158

Liu, X., Qu, D., Ryu, J., Ahmed, F., Yang, Z., Lee, D., et al. (2016). P-type polar transition of chemically doped multilayer MoS_2 transistor. *Adv.Mater.* 28, 2345–2351. doi: 10.1002/adma.201505154

Mak, K. F., He, K., Lee, C., Lee, G. H., Hone, J., Heinz, T. F., et al. (2013). Tightly bound trions in monolayer MoS_2. *Nat. Mater.* 12, 207–211. doi: 10.1038/nmat3505

Mak, K. F., Lee, C., Hone, J., Shan, J., and Heinz, T. F. (2010). Atomically thin MoS_2: a new direct-gap semiconductor. *Phys. Rev. Lett.* 105:136805. doi: 10.1103/PhysRevLett.105.136805

Mao, N., Chen, Y., Liu, D., Zhang, J., and Xie, L. (2013). Solvatochromic effect on the photoluminescence of MoS_2 monolayers. *Small* 9, 1312–1315. doi: 10.1002/smll.201202982

Mishra, S., Satpathy, S., and Jepsen, O. (1997). Electronic structure and thermoelectric properties of bismuth telluride and bismuth selenide. *J. Condens. Matter Phys.* 9:461. doi: 10.1088/0953-8984/9/2/014

Mouri, S., Miyauchi, Y., and Matsuda, K. (2013). Tunable photoluminescence of monolayer MoS_2 via chemical doping. *Nano Lett.* 13, 5944–5948. doi: 10.1021/nl403036h

Nan, H., Wang, Z., Wang, W., Liang, Z., Lu, Y., Chen, Q., et al. (2014). Strong photoluminescence enhancement of MoS_2 through defect engineering and oxygen bonding. *ACS Nano* 8, 5738–5745. doi: 10.1021/nn500532f

Neal, A. T., Pachter, R., and Mou, S. (2017). P-type conduction in two-dimensional MoS_2 via oxygen incorporation. *Appl. Phys. Lett.* 110:193103. doi: 10.1063/1.4983092

Park, T.-E., Suh, J., Seo, D., Park, J., Lin, D.-Y., Huang, Y.-S., et al. (2015). Hopping conduction in p-type MoS_2 near the critical regime of the metal-insulator transition. *Appl. Phys. Lett.* 107:223107. doi: 10.1063/1.4936571

Poizot, P., Laruelle, S., Grugeon, S., Dupont, L., and Tarascon, J. (2000). Nano-sized transition-metal oxides as negative-electrode materials for lithium-ion batteries. *Nature* 407:496. doi: 10.1038/35035045

Prasad, S., and Zabinski, J. (1997). Super slippery solids. *Nature* 387, 761–763. doi: 10.1038/42820

Qiu, H., Xu, T., Wang, Z., Ren, W., Nan, H., Ni, Z., et al. (2013). Hopping transport through defect-induced localized states in molybdenum disulphide. *Nat. Commun.* 4:2642. doi: 10.1038/ncomms3642

Radisavljevic, B., Radenovic, A., Brivio, J., Giacometti, V., and Kis, A. (2011a). Single-layer MoS_2 transistors. *Nat. Nanotechnol.* 6:147. doi: 10.1038/nnano.2010.279

Radisavljevic, B., Whitwick, M. B., and Kis, A. (2011b). Integrated circuits and logic operations based on single-layer MoS_2. *ACS Nano* 5, 9934–9938. doi: 10.1021/nn203715c

Ramakrishna Matte, H., Gomathi, A., Manna, A. K., Late, D. J., Datta, R., Pati, S. K., et al. (2010). MoS_2 and WS2 analogues of graphene. *Angew. Chem. Int. Edn.* 49, 4059–4062. doi: 10.1002/anie.201000009

Scalise, E., Houssa, M., Pourtois, G., Afanas, V., and Stesmans, A. (2014). First-principles study of strained 2D MoS_2. *Phys. E Low Dimens. Syst. Nanostruct.* 56, 416–421. doi: 10.1016/j.physe.2012.07.029

Singh, V. V., Kaufmann, K., de Ávila, B. E. F., Karshalev, E., and Wang, J. (2016). Molybdenum disulfide-based tubular microengines: toward biomedical applications. *Adv. Funct. Mater.* 26, 6270–6278. doi: 10.1002/adfm.201602005

Splendiani, A., Sun, L., Zhang, Y., Li, T., Kim, J., Chim, C.-Y., et al. (2010). Emerging photoluminescence in monolayer MoS_2. *Nano Lett.* 10, 1271–1275. doi: 10.1021/nl903868w

Suh, J., Park, T.-E., Lin, D.-Y., Fu, D., Park, J., Jung, H. J., et al. (2014). Doping against the native propensity of MoS_2: degenerate hole doping by cation substitution. *Nano Lett.* 14, 6976–6982. doi: 10.1021/nl503251h

Sundaram, R., Engel, M., Lombardo, A., Krupke, R., Ferrari, A., Avouris, P., et al. (2013). Electroluminescence in single layer MoS_2. *Nano Lett.* 13, 1416–1421. doi: 10.1021/nl400516a

Tiong, K., Liao, P., Ho, C., and Huang, Y. (1999). Growth and characterization of rhenium-doped MoS_2 single crystals. *J. Cryst. Growth* 205, 543–547. doi: 10.1016/S0022-0248(99)00296-1

Tongay, S., Suh, J., Ataca, C., Fan, W., Luce, A., Kang, J. S., et al. (2013). Defects activated photoluminescence in two-dimensional semiconductors: interplay between bound, charged, and free excitons. *Sci. Rep.* 3:2657. doi: 10.1038/srep02657

Wang, Q. H., Kalantar-Zadeh, K., Kis, A., Coleman, J. N., and Strano, M. S. (2012). Electronics and optoelectronics of two-dimensional transition metal dichalcogenides. *Nat. Nanotechnol.* 7:699. doi: 10.1038/nnano.2012.193

Wei, X., Yu, Z., Hu, F., Cheng, Y., Yu, L., Wang, X., et al. (2014). Mo-O bond doping and related-defect assisted enhancement of photoluminescence in monolayer MoS_2. *AIP Adv.* 4:123004. doi: 10.1063/1.4897522

Wilson, J. A., and Yoffe, A. (1969). The transition metal dichalcogenides discussion and interpretation of the observed optical, electrical and structural properties. *Adv. Phys.* 18, 193–335. doi: 10.1080/00018736900101307

Wu, D., Huang, H., Zhu, X., He, Y., Xie, Q., Chen, X., et al. (2016). ERaman mode in thermal strain-fractured CVD-MoS_2. *Crystals* 6:151. doi: 10.3390/cryst6110151

Xue, F., Chen, L., Chen, J., Liu, J., Wang, L., Chen, M., et al. (2016). p-Type MoS_2 and n-Type ZnO diode and its performance enhancement by the piezophototronic effect. *Adv. Mater.* 28, 3391–3398. doi: 10.1002/adma.201506472

Yang, L., Majumdar, K., Liu, H., Du, Y., Wu, H., Hatzistergos, M., et al. (2014). Chloride molecular doping technique on 2D materials: WS2 and MoS_2. *Nano Lett.* 14, 6275–6280. doi: 10.1021/nl502603d

Yin, W., Yan, L., Yu, J., Tian, G., Zhou, L., Zheng, X., et al. (2014). High-throughput synthesis of single-layer MoS_2 nanosheets as a near-infrared photothermal-triggered drug delivery for effective cancer therapy. *ACS Nano* 8, 6922–6933. doi: 10.1021/nn501647j

Yin, W., Yu, J., Lv, F., Yan, L., Zheng, L. R., Gu, Z., et al. (2016). Functionalized nano-MoS_2 with peroxidase catalytic and near-infrared photothermal activities for safe and synergetic wound antibacterial applications. *ACS Nano* 10, 11000–11011. doi: 10.1021/acsnano.6b05810

Zhang, S.-L., Choi, H.-H., Yue, H.-Y., and Yang, W.-C. (2014). Controlled exfoliation of molybdenum disulfide for developing thin film humidity sensor. *Curr. Appl. Phys.* 14, 264–268. doi: 10.1016/j.cap.2013.11.031

Zhang, X., Shao, Z., Zhang, X., He, Y., and Jie, J. (2016). Surface charge transfer doping of low-dimensional nanostructures toward high-performance nanodevices. *Adv. Mater. Weinheim* 28, 10409–10442. doi: 10.1002/adma.201601966

Zhang, Y. J., Ye, J. T., Yomogida, Y., Takenobu, T., and Iwasa, Y. (2013). Formation of a stable p-n junction in a liquid-gated MoS_2 ambipolar transistor. *Nano Lett.* 13, 3023–3028. doi: 10.1021/nl400902v

Zhou, H., Yu, F., Liu, Y., Zou, X., Cong, C., Qiu, C., et al. (2013). Thickness-dependent patterning of MoS_2 sheets with well-oriented triangular pits by heating in air. *Nano Res.* 6, 703–711. doi: 10.1007/s12274-013-0346-2

Conflict of Interest: The authors declare that the research was conducted in the absence of any commercial or financial relationships that could be construed as a potential conflict of interest.

frontiers in Chemistry

ORIGINAL RESEARCH
published: 07 October 2020
doi: 10.3389/fchem.2020.00755

pH-Triggered Assembly of Natural Melanin Nanoparticles for Enhanced PET Imaging

Qingyao Liu[1,2], *Hanyi Fang*[1,2], *Yongkang Gai*[1,2] *and Xiaoli Lan*[1,2]*

[1] *Department of Nuclear Medicine, Union Hospital, Tongji Medical College, Huazhong University of Science and Technology, Wuhan, China,* [2] *Hubei Province Key Laboratory of Molecular Imaging, Wuhan, China*

Natural melanin nanoplatforms have attracted attention in molecular imaging. Natural melanin can be made into small-sized nanoparticles, which penetrate tumor sites deeply, but unfortunately, the particles continue to backflow into the blood or are cleared into the surrounding tissues, leading to loss of retention within tumors. Here, we report a pH-triggered approach to aggregate natural melanin nanoparticles by introducing a hydrolysis-susceptible citraconic amide on the surface. Triggered by pH values lower than 7.0, such as the tumor acid environment, the citraconic amide moiety tended to hydrolyze abruptly, resulting in both positive and negative surface charges. The electrostatic attractions between nanoparticles drove nanoparticle aggregation, which increased accumulation in the tumor site because backflow was blocked by the increased size. Melanin nanoparticles have the natural ability to bind metal ions, which can be labeled with isotopes for nuclear medicine imaging. When the melanin nanoparticles were labeled by ^{68}Ga, we observed that the pH-induced physical aggregation in tumor sites resulted in enhanced PET imaging. The pH-triggered assembly of natural melanin nanoparticles could be a practical strategy for efficient tumor targeted imaging.

Keywords: natural melanin nanoparticles, pH-triggered aggregation, ^{68}Ga labeling, PET imaging, enhanced tumor retention

OPEN ACCESS

Edited by:
Hyung-Jun Im,
Seoul National University, South Korea

Reviewed by:
Weiyu Chen,
Stanford University, United States
Yifan Zhang,
Shenzhen University, China

***Correspondence:**
Xiaoli Lan
xiaoli_lan@hust.edu.cn;
LXL730724@hotmail.com

Specialty section:
This article was submitted to Nanoscience, a section of the journal Frontiers in Chemistry

Received: *29 May 2020*
Accepted: *21 July 2020*
Published: *07 October 2020*

Citation:
Liu Q, Fang H, Gai Y and Lan X (2020) pH-Triggered Assembly of Natural Melanin Nanoparticles for Enhanced PET Imaging. Front. Chem. 8:755. doi: 10.3389/fchem.2020.00755

INTRODUCTION

With the continuing development of nanotechnology, there is still strong demand for the design of new nanoparticles that have the properties of biocompatibility, long circulation time, low immune response, low toxicity, and biodegradability for biomedical applications (Jiao et al., 2018; Yang et al., 2019; Ou et al., 2020). Nature has inspired scientists to mimic precise dimensional biopolymer systems that play crucial roles in the physiology of many organisms and disease processes. Great efforts have been devoted to the modification of natural nanoparticles with high applicability potential (Cormode et al., 2010; Carrera et al., 2017; Aqil et al., 2019).

Among potential nanoparticles, melanin has attracted increasing attention because of its physicochemical properties. Melanin is an endogenous pigment that is distributed widely throughout human tissues and organs such as skin, mucous membranes, retinas, gallbladder, and ovaries, making it safe for *in vivo* application (Watts et al., 1981). Recent investigations demonstrated that melanin could serve as a photothermal agent (Liu Y. et al., 2013; Chu et al., 2016) and a photoacoustic probe (Ju et al., 2016; Liu et al., 2018) because of its strong near-infrared light absorption and high photothermal conversion efficiency. Moreover, melanin is an effective drug delivery system that can load chemotherapeutic drugs with aromatic structures *via* π-π stacking

and/or hydrogen binding (Zhang et al., 2015), and the drug release can be stimulated by multiple methods, including near infrared light, pH, and reactive oxygen species (Araújo et al., 2014; Wang et al., 2016; Kim et al., 2017). As the structure of melanin includes abundant carboxyl groups, amino groups, and phenolic hydroxyl groups, it can serve as a natural multi-site metal chelating agent, making it capable of complexing many metal ions under mild conditions (Kim et al., 2012; Thaira et al., 2019). Many radionuclides are metallic elements, such as ^{64}Cu, ^{89}Zr, ^{68}Ga, ^{177}Lu, and ^{99m}Tc. Much effort is required to synthesize bifunctional chelators by labeling these radionuclides and optimizing the labeling conditions (Kang et al., 2015; Gai et al., 2016, 2018). Melanin may provide a facile strategy for labeling with radiometals. Cheng's group actively chelated melanin to $^{64}Cu^{2+}$ and Fe^{3+} for PET and MRI imaging with high loading capacity and stability, indicating that melanin is a promising multimodality imaging nanoplatform (Fan et al., 2014; Hong et al., 2017).

Melanin can be made into nanoparticles with controllable sizes from a few nanometers to hundreds of nanometers (Ren et al., 2016; Amin et al., 2017; Lemaster et al., 2019). Studies have shown that small nanoparticles (<20 nm) can avoid macrophage recognition and penetrate tissues more deeply (Perrault et al., 2009; Liu C. et al., 2013). However, unfortunately, when small nanoparticles reach the tumor site, they continue to backflow into the bloodstream or are cleared into the surrounding tissues, decreasing retention within the tumor (Larsen et al., 2009; Zeng et al., 2016). Nanoparticles about 100 nm in size have been reported to have good retention but still high accumulation in the liver and pancreas before reaching the tumor, resulting in relatively low drug concentrations at the tumor site (Jain and Stylianopoulos, 2010; Albanese et al., 2012).

To overcome these limitations, we introduce a pH-triggered approach to aggregate small-sized melanin nanoparticles (pH-MNPs). The MNPs are redecorated with hydrolysis-susceptible citraconic amide, which can maintain a small size in the blood. When they reach the tumor site, spontaneous aggregation occurs in response to the tumor's acidic microenvironment. The aggregation of melanin nanoparticles cannot exceed the size of the blood vessels, and they become trapped in the extracellular matrix between cells because of their increased size, resulting in enhanced retention in the tumor site (Liu X. et al., 2013). In addition, the pH-melanin was labeled by ^{68}Ga, and the *in vivo* PET imaging and biodistribution profiles of ^{68}Ga-pH-MNPs were evaluated. We ascertained that the pH-triggered assembly of natural melanin nanoparticles could result in enhanced PET imaging, which could be a practical strategy for efficient tumor imaging.

MATERIALS AND METHODS

Materials and Reagents

Melanin was purchased from Sigma-Aldrich. Methoxy polyethylene glycol amine (mPEG2000-NH_2) was purchased from the Shanghai Aladdin Biochemical Technology Co., Ltd.

Cell Line and Animal

H22 mouse hepatocarcinoma cells were purchased from the American Type Culture Collection (ATCC) and cultured in standard cell medium recommended by ATCC. Male BALB/c mice (6–8 weeks, 20–22 g) were provided by the animal center of Tongji Medical College (Wuhan, China). The mice were raised at an animal facility under special pathogen-free (SPF) conditions with a 12 h light/dark cycle and free access to food and water. The animal study was reviewed and approved by the Laboratory Animal Management Committee of Tongji Medical College of Huazhong University of Science and Technology.

Preparation of PEG-Functionalized Melanin Nanoparticles (PEG-MNPs)

Thirty mg of the melanin granule was dissolved in 10 ml of NaOH (0.1 N) and sonicated for 30 min with a bath type sonicator. Then, 90 mg of mPEG2000-NH_2 (Mw = 2,000) aqueous solution was dropped into the above aqueous solution and stirred with a magnetic stirrer. After vigorous stirring for 12 h, the mixed solution was retrieved by centrifugation (MWCO-10,000, Millipore) at 4,000 rpm for 30 min and washed several times with deionized water.

Preparation of pH-Sensitive Melanin Nanoparticles (pH-MNPs)

Thirty mg of the melanin granule was dissolved in 10 ml of NaOH (0.1 N) and sonicated for 30 min with a bath type sonicator. Then, 90 mg of mPEG2000-NH_2 (Mw = 2,000) and 270 μmol of ethylenediamine were added into the above aqueous solution and stirred with a magnetic stirrer. After vigorous stirring for 12 h, the mixed solution was retrieved by centrifugation (MWCO-10,000, Millipore) at 4,000 rpm for 30 min and washed several times with deionized water. Then, 200 μmol of citraconic anhydride was added into the obtained 10 ml of melanin aqueous solution (1 mg/ml of water) and the pH was adjusted to 9.0 with NaOH (0.1 N). After vigorous stirring for 12 h, mPEG and the citraconic amide modified MNPs were retrieved by centrifugation (MWCO-10,000, Millipore) at 4,000 rpm for 30 min and washed several times with deionized water.

Characterization of Melanin Nanoparticles

The size and zeta potential of MNPs under pH 9, 7.4, and 6 were measured by a dynamic light scattering (DLS) instrument (Malvern instruments Ltd). The morphologies of MNPs were obtained under a transmission electronic microscope (TEM) at 100 kV.

$^{68}Ga^{2+}$ Radiolabeling

$^{68}GaCl_2$ was washed from a ^{68}Ge/^{68}Ga radionuclide generator by 4 × 1 ml high purity hydrochloric acid (HCl, 0.05 M), and we took the one with the highest radioactivity. One ml of $^{68}GaCl_2$ nearly 5 mCi in 0.05 M HCl was added into 200 μl PEG-MNPs or pH-MNPs (0.5 mg/ml of MNPs), then 0.25 M NaOAc was added dropwise to adjust the pH to 4, 5, 6, 7.4, respectively and incubated at room temperature for 30 min. The radiolabeled MNPs were purified by a PD-10 column (GE Healthcare) to remove the free ^{68}Ga. The final product was

washed out by PBS and passed through a 0.22 μm Millipore filter into a sterile vial for *in vivo* PET imaging. The radiolabeling yield was evaluated by dividing the radioactivity of the purified radiolabeled MNPs by the total radioactivity added. The stability of ^{68}Ga-labeled MNPs was determined *in vitro* by incubating in saline or human plasma at a physiologic temperature for 3 h. An aliquot of ^{68}Ga-labeled MNPs was removed at 1, 2, and 3 h intervals and the radiochemical purity was determined by ITLC (TLC scanner, BIOSCAN, USA). GF254 silica gel plates were used as the stationary phase and citrate buffer (0.1 M) was used as the mobile phase.

Cell Viability

The *in vitro* cytotoxicity of MNPs was determined in H22 mouse hepatocarcinoma cells by the CCK-8 assay. H22 cells were cultured in DMEM (GIBCO, Carlsbad, CA, USA), supplemented with 10% fetal calf serum (FCS), 2 mmol/l glutamine, 100 U/ml penicillin, and 100 μg/ml streptomycin. Cells (5,000/well) were seeded in 96-well plates with 100 μL/well medium and incubated overnight with 10% fetal bovine serum DMEM medium at 37°C and in an atmosphere of 5% CO_2. Cells were then cultured in the medium supplemented with different doses of PEG-MNPs and pH-MNPs. The final concentrations of MNPs in the culture medium were fixed at 100, 50, 25, 10, and 5 μg/ml, untreated cells were used as the control (with 100% cell viability), and the medium without cells was used as the blank. After treatment for 24 and 48 h, respectively, the medium was removed and DMEM medium containing 10% CCK-8 was added. After incubation for 30 min at 37°C, the absorbance at 450 nm was measured by using an automatic enzyme standard instrument (Bio-Rad iMark).

Subcutaneous Tumor Models

The H22 cells were maintained in the ascitic form by sequential passages into the peritoneal cavities of BALB/c mice, by weekly intraperitoneally (i.p.) transplanting 1×10^7 tumor cells in 0.2 ml. The ascites were collected, diluted with sterile saline, and the cell concentration was adjusted to 1×10^7/ml. The diluted solution (0.2 ml) was administered subcutaneously in the right shoulder of each mouse. When the tumors reached 0.5–0.8 cm in diameter, the tumor-bearing mice were subjected to *in vivo* PET imaging and biodistribution studies.

Small Animal PET Imaging

Small animal PET imaging of tumor-bearing mice was performed on a microPET-CT (TransPET Discoverist 180 system, Raycan Technology Co., Ltd, Suzhou, China). ^{68}Ga-labeled PEG-MNPs and ^{68}Ga-labeled pH-MNPs (180.0 ± 5.0 μCi) were injected *via* the tail vein, respectively ($n = 4$). At different times after injection (1, 2, and 3 h), mice bearing H22 tumors were anesthetized with 2% isoflurane in 100% oxygen for maintenance during imaging, and placed prone near the center of the FOV of the scanner. PET/CT images were obtained with the static mode for 10 min followed by a CT scan in the normal mode. The PET images were reconstructed using the three-dimensional (3D) ordered-subsets expectation maximization (OSEM) algorithm with a voxel size of $0.5 \times 0.5 \times 0.5$ mm^3. CT images were reconstructed using the FDK algorithm with $256 \times 256 \times 256$ matrix. Images were displayed with software Carimas (Turku PET Center, Turku, Finland). No background correction was performed. The radioactivity uptake in the tumor and normal tissues were calculated using a region of interest (ROI) drawn over the whole organ region and expressed as a percentage of the injected radioactive dose per gram of tissue (% ID/g).

Biodistribution Studies

The biodistribution studies were performed in H22 tumor-bearing BALB/c mice (6–8 weeks), weighing 20–22 g, which were randomly divided into six groups (five mice per group). ^{68}Ga-labeled PEG-MNPs and ^{68}Ga-labeled pH-MNPs were intravenously injected through a tail vein and the mice were sacrificed at 1, 2, and 3 h intervals. The blood and organs of interest (e.g., brain, heart, lungs, liver, spleen, kidneys, stomach, small intestine, large intestine, muscle, bones, and tumor) were harvested, then weighed and measured using an automated gamma counter (2470 WIZARD, PerkinElmer, Norwalk CT, USA). The amount of radioactivity in each tissue sample was reported as the percentage of the injected dose per gram of tissue (%ID/g).

Statistical Analysis

Quantitative data are expressed as means ± standard deviation (SD). Means were compared using Student's *t*-test (two-tailed) with a *P*-value <0.05 indicating significance.

RESULT AND DISCUSSION

Preparation and Characterization of pH-MNPs

The design and synthetic procedures of pH-MNPs are schematically illustrated in **Figure 1**. Firstly, the natural melanin was modified with mPEG-NH_2 and ethylenediamine to provide many terminal amine groups on the surface. Then, the primary amine groups were reacted with citraconic anhydride to form amide bonds (**Figure 1**). The citraconic amide moiety on the surface is selectively hydrolysis-susceptible in mildly acidic environments. Under neutral and alkaline conditions, the citraconic amide bonds are stable and maintain negative charges. Triggered by pH values lower than 7.0, such as those present in tumor tissues that are often rendered acidic by hypoxia, the citraconic amide moiety tended to hydrolyze abruptly, resulting in both positive and negative surface charges as its terminal group changed from a carboxylate anion to a protonated amine group (Nam et al., 2009). The electrostatic attraction between nanoparticles drove nanoparticle aggregation (**Supplementary Figure 1**). The steric effect of mPEG may have hindered the electrostatic attraction, but the reduction of the surface modification of mPEG affected the water solubility of the MNPs. A ratio of ethylenediamine to mPEG of about 6 was reported to achieve a balance between steric hindrance and water solubility.

The product of each step of the synthesis was measured by the zeta potential and FT-IR spectra. In the FTIR spectrum of pristine melanin, the broad and strong bands in the 3,300 ∼ 3,400 cm^{-1} region were due to the -OH and -NH stretching.

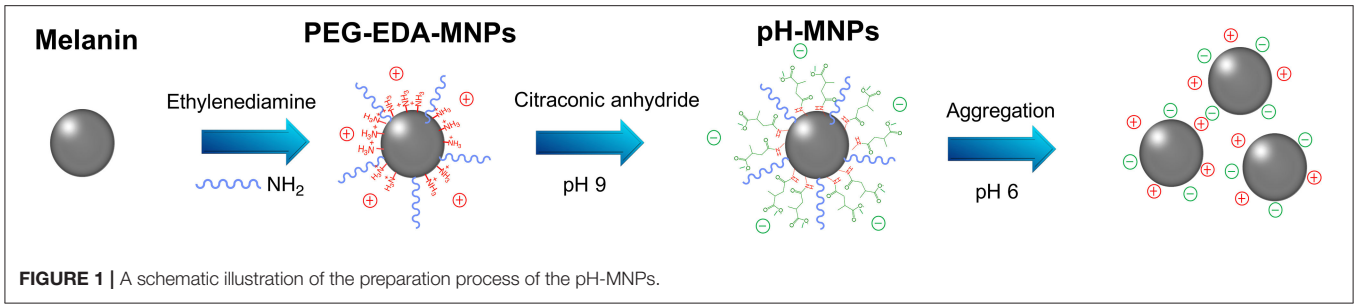

FIGURE 1 | A schematic illustration of the preparation process of the pH-MNPs.

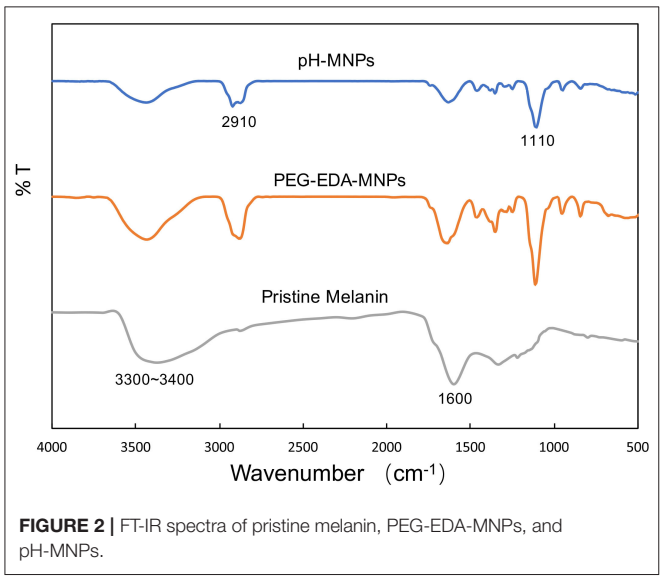

FIGURE 2 | FT-IR spectra of pristine melanin, PEG-EDA-MNPs, and pH-MNPs.

The characteristic peaks at 1,600 cm^{-1} were attributed to the aromatic ring C=C, C=N bending, and C=O stretching in indole and indoline structures. The FT-IR spectra detected characteristic alkyl C-H bands around 2,910 cm^{-1} and C-O-C stretching bands from PEG at 1,100 cm^{-1} after the introduction of ethylenediamine and PEG on the surface (**Figure 2**). Although the FT-IR spectra did not provide any additional information about the pH-MNPs, the zeta potential described a considerable change in the surface charge at each step of the surface modification (**Figure 3A**). Melanin itself is a negatively charged polymer, and the surface potential after the introduction of PEG remained negative (-12.8 ± 1.3 mV). After a reaction with a large amount of ethylenediamine, the surface charge changed from negative to positive (6.7 ± 0.9 mV) because of the presence of the protonated amine. The surface charge then became negative again after a reaction with citraconic anhydride, indicating successful conjugation and conversion of the amine group to a carboxylate anion. Dynamic light scattering was employed to examine the size of the MNPs after surface modification. The hydrodynamic diameters of the PEG-MNPs, PEG-EDA-MNPs, and pH-MNPs were all ~12 nm, demonstrating no significant size differences between nanoparticle type (**Figure 3B**).

To characterize pH-induced aggregation behavior in solution, we compared the stability of pristine melanin, PEG-MNPs, PEG-EDA-MNPs, and pH-MNPs under different pH conditions. As shown in **Figure 4**, pristine melanin only dissolved in the alkaline solution, while the PEG-MNPs and PEG-EDA-MNPs maintained good solubility in acidic, neutral, and alkaline conditions. However, pH-MNPs exhibited specific aggregation in response to acidic conditions. At pH 9 and 7.4, the solution of pH-MNPs was clear and translucent, and at a mildly acidic pH 6, flocculation and precipitation occurred. All of the photos were taken after the samples had been standing at room temperature for ~12 h, and the pH-MNPs maintained a stable precipitation state, indicating that the aggregation was irreversible after complete hydrolysis. The hydrodynamic size and zeta potential of pH-MNPs at different pH values were measured by dynamic light scattering (DLS), with PEG-MNPs as the control group. As shown in **Supplementary Figure 2**, the size of pH-MNPs was found to be $3{,}316 \pm 271$ nm with a wide size distribution at pH 6, while the particles showed a small size and narrow size distribution at pH 7.4 and 9. In the control group, the size of PEG-MNPs did not change and maintained at 12.2 ± 1.3 nm under different pH values. **Supplementary Figure 3** showed the zeta potentials of pH-MNPs and PEG-MNPs at different pH values. At pH value of 9, the zeta potentials of pH-MNPs was -12.6 ± 1.0 mV, and the value positively shifted to -9.3 ± 1.8 mV under neutral conditions. After exposure to an acidic environment (pH 6), the surface charge of pH-MNPs shifted to a positive value (4.9 ± 0.3 mV), indicating the citraconic amide moieties had been hydrolyzed into protonated amine groups. PEG-MNPs also showed a trend in that the zeta potential shifted positively as the pH value decreased. At pH 9, the zeta potential was -16.4 ± 0.7 mV, and it became -12.8 ± 1.3 mV at pH 7.4. After exposure to pH 6 buffer, the zeta potential positively shifted to -9.3 ± 0.3 mV, but remained negative. This result was due to the protonation of phenolic and amino groups of PEG-MNPs.

Dynamic light scattering (DLS) and transmission electron microscopy (TEM) were conducted to monitor the variation of particle size and morphology between different time points during the pH-triggering process of pH-MNPs. The TEM images in **Figure 5A** illustrate that the average size of the prepared pH-MNPs was nearly 10 nm with a narrow size distribution, which is consistent with the results obtained by DLS. Upon pH triggering, the agglomeration degree of pH-MNPs gradually grew, and the size to which the pH-MNPs aggregated became larger. After 10 min of exposure to an acidic environment (pH 6), the size increased to 100–160 nm with messy shapes observed by TEM, and DLS

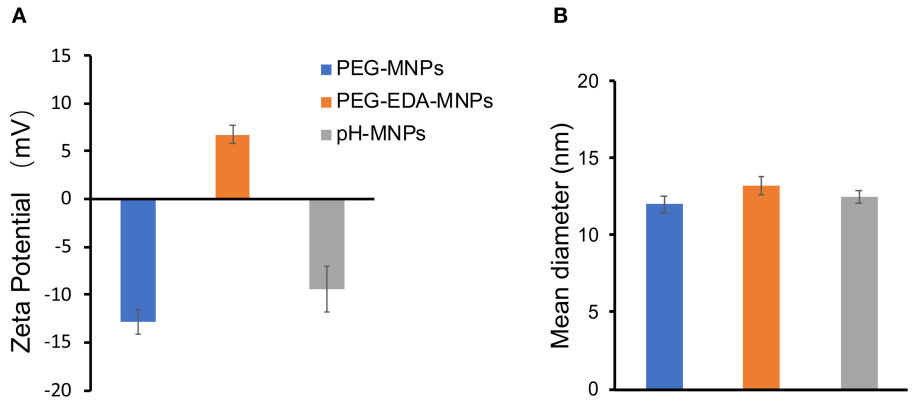

FIGURE 3 | Characteristics of MNPs. **(A)** Zeta potential of PEG-MNPs, PEG-EDA-MNPs, and pH-MNPs. **(B)** Hydrodynamic size of PEG-MNPs, PEG-EDA-MNPs, and pH-MNPs. Bars represent means ± SD ($n = 3$). All of the samples are adjusted to neutral pH value by buffer solution.

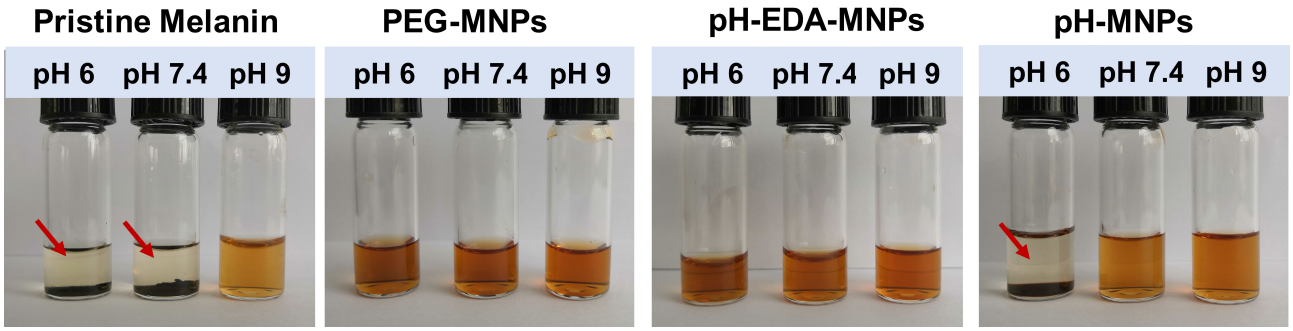

FIGURE 4 | Stability of pristine melanin, PEG-MNPs, PEG-EDA-MNPs, and pH-MNPs under different pH conditions. Standing ~12 h, photos taken of all samples. The red arrow indicates precipitation at the bottom of the bottle.

measurement showed two peaks with PDI 0.542, indicating a wide size distribution (**Figure 5B**). TEM measurement after 2 h of exposure confirmed the growth of some aggregates over time: the hydrodynamic size of pH-MNPs continually increased to the micron level in **Figure 5C**, whereas such pH-induced aggregation was not observed in PEG-MNPs (**Supplementary Figure 4**). These results strongly support that pH-MNPs had the ability to undergo pH-triggered aggregation. The aggregation of pH-MNPs began early (within 10 min), and flocculation occurred within 2 h. This rapid pH-response ability provides the possibility of subsequently ^{68}Ga-labeling for PET imaging, which is desirable because the half-life of the ^{68}Ga nuclide is only 67.7 min.

Radiolabeling With ^{68}Ga and Stability *in vitro*

Melanin has the ability to coordinate with metal ions without an additional chelator because of its inherent structure. That enables us to prepare radiometal-labeled melanin nanoparticles for molecular imaging. Furthermore, melanin can bind metal ions at a wide pH range because of different chelating sites on the molecule function at different pH ranges. Under acidic conditions, the carboxyl groups are mainly involved in binding metal ions to form complexes, whereas under alkaline conditions, the phenolic hydroxyl groups play a major role (Sarna et al., 1980). In this research, we used ^{68}Ga to radiolabel pH-MNPs without any linker at different pH values. The ^{68}Ga-pH-MNPs exhibited high loading capacities at pH 4 and 5 with non-decay-corrected yields of 89.6 ± 6.2 and 87.5 ± 8.3%, respectively (**Figure 6A**). As the pH increased, the labeling yield gradually decreased, with only 52.3 ± 12.4% yield at pH 7. Considering the acid-triggered assembly of pH-MNPs, we still tried to use ^{68}Ga for labeling under neutral conditions for subsequent *in vivo* studies, but the labeling yield was not very high. The ^{68}Ga-pH-MNPs were prepared under the labeling conditions of pH 7, 37°C, and 30 min incubation. After purification using a PD-10 column, the radiochemical purity of the ^{68}Ga-pH-MNPs was determined by ITLC. On the ITLC plate, ^{68}Ga-pH-MNPs remained close to the origin ($Rf = 0.12$), and no free ^{68}Ga was observed at the solvent front (radiochemical purity: >96%; **Supplementary Figure 5**). The stability assay of ^{68}Ga-pH-MNPs in saline solution and human plasma showed that the radiochemical purity of ^{68}Ga-pH-MNPs remained above

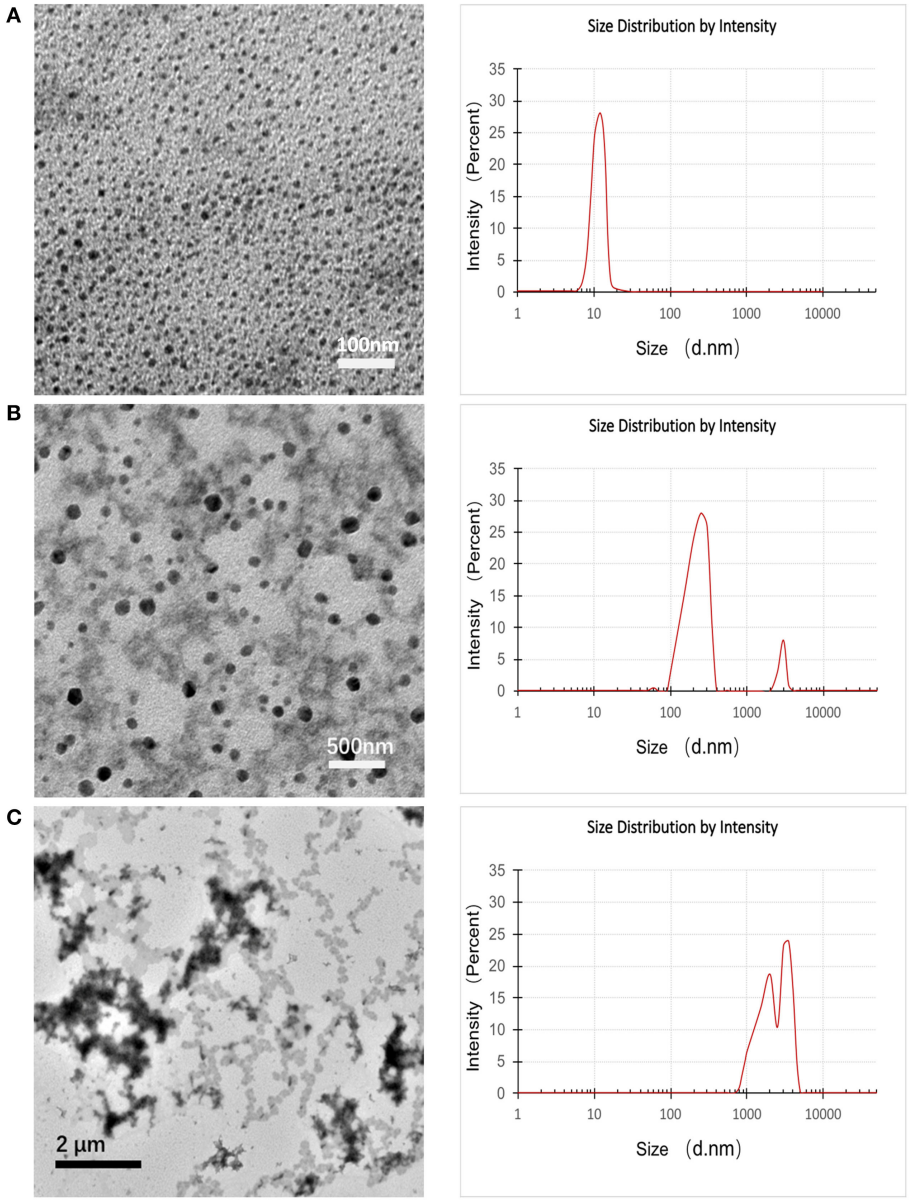

FIGURE 5 | TEM images (left) and DLS images (right) of pH-MNPs in pH 6 buffer at different elapsed times of **(A)** 0, **(B)** 10, and **(C)** 120 min.

95% throughout the 3 h incubation period, indicating excellent stability *in vitro* (**Figure 6B**).

Biocompatibility of MNPs

To evaluate the *in vitro* cytotoxicity of the synthesized MNPs, CCK-8 assays were performed on H22 mouse hepatocarcinoma cells. For these assays, cultured cells were exposed to PEG-MNPs and pH-MNPs (5–100 μg/mL) for 24 and 48 h. The results showed that PEG-MNPs and pH-MNPs did not inhibit H22 cell viability at any concentration at either time point (**Supplementary Figure 6**), indicating that the synthesized MNPs have high biocompatibility *in vitro*.

Small Animal PET Imaging

For PET imaging, ∼6.66 MBq (180 μCi) of ^{68}Ga-pH-MNPs and ^{68}Ga-PEG-MNPs were injected intravenously into H22 tumor-bearing mice. At different time points after injection (1, 2, and 3 h), tomographic images were acquired. **Figure 7** shows representative decay-corrected whole-body images. A stronger PET signal in the tumor was observed for ^{68}Ga-pH-MNPs than ^{68}Ga-PEG-MNPs at all time points. The difference in tumor accumulation when ^{68}Ga-PEG-MNPs are employed may be due to backflow into the bloodstream over time. In contrast, the pH-triggered aggregation of ^{68}Ga-pH-MNPs, which can be trapped in tumor tissue, led to enhanced PET imaging. In addition

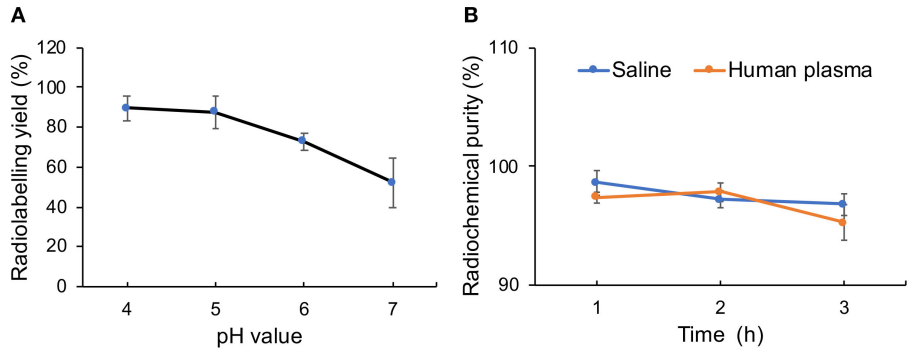

FIGURE 6 | Characterization of radiolabeling with ^{68}Ga. **(A)** Radiolabeling yield of ^{68}Ga-pH-MNPs at different pH and **(B)** stability of ^{68}Ga-labeled MNPs incubated in saline or human plasma for 1, 2, and 3 h.

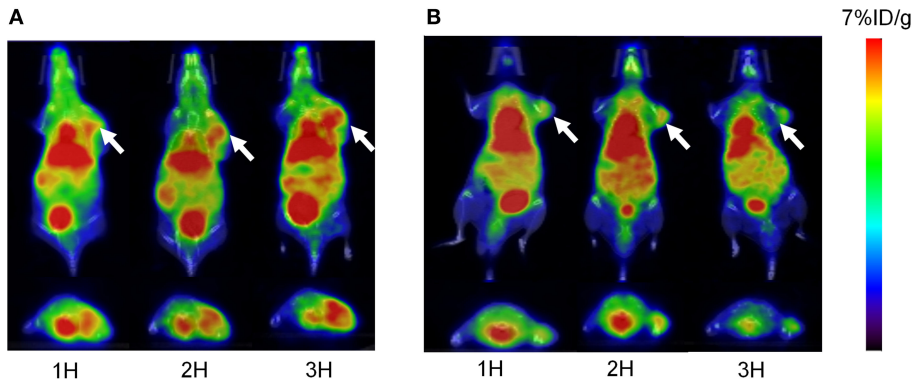

FIGURE 7 | The overlaying of the PET and CT images of H22 tumors acquired at 1, 2, and 3 h after the intravenous injection of **(A)** ^{68}Ga-pH-MNPs and **(B)** ^{68}Ga-PEG-MNPs. Representative decay-corrected coronal and transaxial are displayed on the top and bottom respectively. The white arrow indicates tumor site.

to that within the tumor, moderate activity accumulation was found in the liver because nanoparticles are easily captured by the reticuloendothelial system. The heart was visible, perhaps because of the circulation of small-sized melanin nanoparticles in the blood. Quantitative analysis of three-dimensional regions of interest over multiple image slices revealed that the tumor uptake of ^{68}Ga-pH-MNPs was up to 2.4 times higher than that of ^{68}Ga-PEG-MNPs at 3 h post-injection (4.47 ± 0.73 vs. 1.87 ± 0.56% ID/g, respectively, $p < 0.01$; **Supplementary Figure 7**).

Biodistribution Study

The biodistribution results are shown in **Figure 8**. The radioactivity in blood gradually decreased over time, indicating that ^{68}Ga-pH-MNPs were gradually cleared from circulation (**Figure 8A**). The liver showed the highest uptake among the tissues studied (7.47 ± 0.76% ID/g at 1 h), and then the level reduced gradually but was still prominent at 3 h post-injection (4.51 ± 0.72% ID/g). Relatively lower activity accumulation was observed in the spleen and kidney. The ^{68}Ga-pH-MNPs was mainly cleared through the hepatobiliary system. The tumor uptake of ^{68}Ga-pH-MNPs consistently increased, and the enhanced retention was maintained throughout all time points (2.54 ± 0.38, 3.35 ± 0.13, and 3.86 ± 0.25% ID/g at 1, 2, and 3 h p.i., respectively). In contrast, the tumor uptake of ^{68}Ga-PEG-MNPs decreased from 2.14 ± 0.38% ID/g (1 h p.i.) to 1.34 ± 0.25% ID/g (3 h p.i.) (**Figure 8B**). The results were consistent with the PET images above. The tumor-to-muscle ratio of ^{68}Ga-pH-melanin increased significantly from 4.74 ± 0.76 at 1 h p.i. to 29.30 ± 5.64 at 3 h p.i., a much greater increase than that of ^{68}Ga-PEG-melanin (2.88 ± 0.74 at 3 h p.i.). However, the tumor-to-blood ratio was relatively low, probably because nanoparticles were still circulating in the blood (**Supplementary Table 1**). Therefore, the pH-MNPs can achieve enhanced tumor retention for PET imaging.

CONCLUSIONS

In this work, we have successfully designed and prepared natural melanin nanoparticles that can form aggregates in response to pH changes. Under mildly acidic conditions, the pH-MNPs began to aggregate and became trapped by their increasing size, resulting in enhanced tumor retention. We also demonstrated that the pH-MNPs could be successfully radiolabeled with the ^{68}Ga nuclide in a pH-neutral environment by simple mixing. The resultant ^{68}Ga-pH-MNPs exhibited enhanced PET imaging, which could

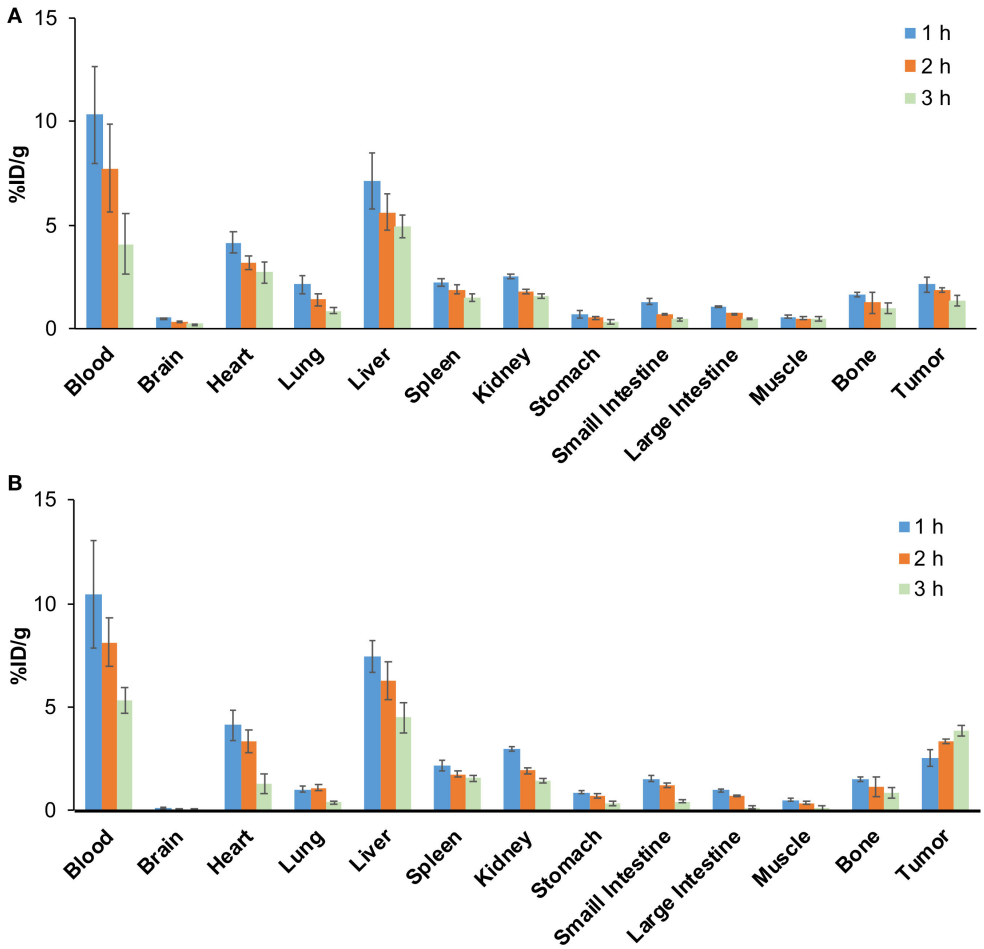

FIGURE 8 | Biodistribution study of H22 tumor-bearing mice ($n = 5$) at different time points in **(A)** the ^{68}Ga-PEG-MNPs group and **(B)** the ^{68}Ga-pH-MNPs group.

provide a promising strategy for molecular imaging and future clinical trials.

DATA AVAILABILITY STATEMENT

The raw data supporting the conclusions of this article will be made available by the authors, without undue reservation.

ETHICS STATEMENT

The animal study was reviewed and approved by Laboratory Animal Management Committee of Tongji Medical College of Huazhong University of Science and Technology.

AUTHOR CONTRIBUTIONS

QL conceived the idea and supervised the research work overall. HF and YG contributed to the experiment methods and data analysis. QL wrote the manuscript and drew all the figures. YG came up with ideas for the manuscript. XL contributed to the revision of the paper. All authors contributed to the article and approved the submitted version.

FUNDING

This work was supported by the National Natural Science Foundation of China (No. 81501532).

ACKNOWLEDGMENTS

We thank Richard Lipkin, PhD, from Liwen Bianji, Edanz Group China (www.liwenbianji.cn/ac), for edited the English text of a draft of this manuscript.

SUPPLEMENTARY MATERIAL

The Supplementary Material for this article can be found online at: https://www.frontiersin.org/articles/10.3389/fchem.2020.00755/full#supplementary-material

REFERENCES

Albanese, A., Tang, P. S., and Chan, W. C. (2012). The effect of nanoparticle size, shape, and surface chemistry on biological systems. *Annu. Rev. Biomed. Eng.* 14, 1–16. doi: 10.1146/annurev-bioeng-071811-150124

Amin, D. R., Sugnaux, C., Lau, K. H. A., and Messersmith, P. B. (2017). Size control and fluorescence labeling of polydopamine melanin-mimetic nanoparticles for intracellular imaging. *Biomimetics* 2:17. doi: 10.3390/biomimetics2030017

Aqil, F., Munagala, R., Jeyabalan, J., Agrawal, A. K., Kyakulaga, A.-H., Wilcher, S. A., et al. (2019). Milk exosomes-natural nanoparticles for siRNA delivery. *Cancer Lett.* 449, 186–195. doi: 10.1016/j.canlet.2019.02.011

Araújo, M., Viveiros, R., Correia, T. R., Correia, I. J., Bonifácio, V. D., Casimiro, T., et al. (2014). Natural melanin: a potential pH-responsive drug release device. *Int. J. Pharm.* 469, 140–145. doi: 10.1016/j.ijpharm.2014.04.051

Carrera, P., Espinoza-Montero, P. J., Fernández, L., Romero, H., and Alvarado, J. (2017). Electrochemical determination of arsenic in natural waters using carbon fiber ultra-microelectrodes modified with gold nanoparticles. *Talanta* 166, 198–206. doi: 10.1016/j.talanta.2017.01.056

Chu, M., Hai, W., Zhang, Z., Wo, F., Wu, Q., Zhang, Z., et al. (2016). Melanin nanoparticles derived from a homology of medicine and food for sentinel lymph node mapping and photothermal *in vivo* cancer therapy. *Biomaterials* 91, 182–199. doi: 10.1016/j.biomaterials.2016.03.018

Cormode, D. P., Jarzyna, P. A., Mulder, W. J., and Fayad, Z. A. (2010). Modified natural nanoparticles as contrast agents for medical imaging. *Adv. Drug Deliv. Rev.* 62, 329–338. doi: 10.1016/j.addr.2009.11.005

Fan, Q., Cheng, K., Hu, X., Ma, X., Zhang, R., Yang, M., et al. (2014). Transferring biomarker into molecular probe: melanin nanoparticle as a naturally active platform for multimodality imaging. *J. Am. Chem. Soc.* 136, 15185–15194. doi: 10.1021/ja505412p

Gai, Y., Sun, L., Hui, W., Ouyang, Q., Anderson, C. J., Xiang, G., et al. (2016). New bifunctional chelator p-SCN-PhPr-NE3TA for copper-64: synthesis, peptidomimetic conjugation, radiolabeling, and evaluation for PET imaging. *Inorg. Chem.* 55, 6892–6901. doi: 10.1021/acs.inorgchem.6b00395

Gai, Y., Sun, L., Lan, X., Zeng, D., Xiang, G., and Ma, X. (2018). Synthesis and evaluation of new bifunctional chelators with Phosphonic acid arms for Gallium-68 based PET imaging in melanoma. *Bioconjug. Chem.* 29, 3483–3494. doi: 10.1021/acs.bioconjchem.8b00642

Hong, S. H., Sun, Y., Tang, C., Cheng, K., Zhang, R., Fan, Q., et al. (2017). Chelator-free and biocompatible melanin nanoplatform with facile-loading gadolinium and copper-64 for bioimaging. *Bioconjug. Chem.* 28, 1925–1930. doi: 10.1021/acs.bioconjchem.7b00245

Jain, R. K., and Stylianopoulos, T. (2010). Delivering nanomedicine to solid tumors. *Nature Rev. Clin. Oncol.* 7:653. doi: 10.1038/nrclinonc.2010.139

Jiao, M., Zhang, P., Meng, J., Li, Y., Liu, C., Luo, X., et al. (2018). Recent advancements in biocompatible inorganic nanoparticles towards biomedical applications. *Biomater. Sci.* 6, 726–745. doi: 10.1039/C7BM01020F

Ju, K.-Y., Kang, J., Pyo, J., Lim, J., Chang, J. H., and Lee, J.-K. (2016). pH-Induced aggregated melanin nanoparticles for photoacoustic signal amplification. *Nanoscale* 8, 14448–14456. doi: 10.1039/C6NR02294D

Kang, C. S., Chen, Y., Lee, H., Liu, D., Sun, X., Kweon, J., et al. (2015). Synthesis and evaluation of a new bifunctional NETA chelate for molecular targeted radiotherapy using 90Y or 177Lu. *Nucl. Med. Biol.* 42, 242–249. doi: 10.1016/j.nucmedbio.2014.10.004

Kim, D. J., Ju, K.-Y., and Lee, J.-K. (2012). The synthetic melanin nanoparticles having an excellent binding capacity of heavy metal ions. *Bull. Korean Chem. Soc.* 33, 3788–3792. doi: 10.5012/bkcs.2012.33.11.3788

Kim, M. A., Do Yoon, S., and Lee, C.-M. (2017). A drug release system induced by near infrared laser using alginate microparticles containing melanin. *Int. J. Biol. Macromol.* 103, 839–844. doi: 10.1016/j.ijbiomac.2017.05.139

Larsen, E. K., Nielsen, T., Wittenborn, T., Birkedal, H., Vorup-Jensen, T., Jakobsen, M. H., et al. (2009). Size-dependent accumulation of PEGylated silane-coated magnetic iron oxide nanoparticles in murine tumors. *ACS Nano* 3, 1947–1951. doi: 10.1021/nn900330m

Lemaster, J. E., Jeevarathinam, A. S., Kumar, A., Chandrasekar, B., Chen, F., and Jokerst, J. V. (2019). Synthesis of ultrasmall synthetic melanin nanoparticles by UV irradiation in acidic and neutral conditions. *ACS Appl. Bio Mater.* 2, 4667–4674. doi: 10.1021/acsabm.9b00747

Liu, C., Gao, Z., Zeng, J., Hou, Y., Fang, F., Li, Y., et al. (2013). Magnetic/upconversion fluorescent NaGdF4: Yb, Er nanoparticle-based dual-modal molecular probes for imaging tiny tumors *in vivo*. *ACS Nano* 7, 7227–7240. doi: 10.1021/nn4030898

Liu, M., Wang, Y., Li, M., Feng, H., Liu, Q., Qin, C., et al. (2018). Using tyrosinase as a tri-modality reporter gene to monitor transplanted stem cells in acute myocardial infarction. *Exp. Mol. Med.* 50, 1–10. doi: 10.1038/s12276-018-0088-z

Liu, X., Chen, Y., Li, H., Huang, N., Jin, Q., Ren, K., et al. (2013). Enhanced retention and cellular uptake of nanoparticles in tumors by controlling their aggregation behavior. *ACS Nano* 7, 6244–6257. doi: 10.1021/nn402201w

Liu, Y., Ai, K., Liu, J., Deng, M., He, Y., and Lu, L. (2013). Dopamine-melanin colloidal nanospheres: an efficient near-infrared photothermal therapeutic agent for *in vivo* cancer therapy. *Adv. Mater.* 25, 1353–1359. doi: 10.1002/adma.201204683

Nam, J., Won, N., Jin, H., Chung, H., and Kim, S. (2009). pH-induced aggregation of gold nanoparticles for photothermal cancer therapy. *J. Am. Chem. Soc.* 131, 13639–13645. doi: 10.1021/ja902062j

Ou, J., Liu, K., Jiang, J., Wilson, D. A., Liu, L., Wang, F., et al. (2020). Micro-/nanomotors toward biomedical applications: the recent progress in biocompatibility. *Small* 16:1906184. doi: 10.1002/smll.201906184

Perrault, S. D., Walkey, C., Jennings, T., Fischer, H. C., and Chan, W. C. (2009). Mediating tumor targeting efficiency of nanoparticles through design. *Nano Lett.* 9, 1909–1915. doi: 10.1021/nl900031y

Ren, X., Zheng, R., Fang, X., Wang, X., Zhang, X., Yang, W., et al. (2016). Red blood cell membrane camouflaged magnetic nanoclusters for imaging-guided photothermal therapy. *Biomaterials* 92, 13–24. doi: 10.1016/j.biomaterials.2016.03.026

Sarna, T., Froncisz, W., and Hyde, J. S. (1980). Cu2+ probe of metal-ion binding sites in melanin using electron paramagnetic resonance spectroscopy: II. Natural melanin. *Arch. Biochem. Biophys.* 202, 304–313. doi: 10.1016/0003-9861(80)90431-2

Thaira, H., Raval, K., Manirethan, V., and Balakrishnan, R. M. (2019). Melanin nano-pigments for heavy metal remediation from water. *Sep. Sci. Technol.* 54, 265–274. doi: 10.1080/01496395.2018.1443132

Wang, X., Zhang, J., Wang, Y., Wang, C., Xiao, J., Zhang, Q., et al. (2016). Multi-responsive photothermal-chemotherapy with drug-loaded melanin-like nanoparticles for synergetic tumor ablation. *Biomaterials* 81, 114–124. doi: 10.1016/j.biomaterials.2015.11.037

Watts, K. P., Fairchild, R. G., Slatkin, D. N., Greenberg, D., Packer, S., Atkins, H. L., et al. (1981). Melanin content of hamster tissues, human tissues, and various melanomas. *Cancer Res.* 41, 467–472.

Yang, G., Phua, S. Z. F., Bindra, A. K., and Zhao, Y. (2019). Degradability and clearance of inorganic nanoparticles for biomedical applications. *Adv. Mater.* 31:1805730. doi: 10.1002/adma.201805730

Zeng, J., Cheng, M., Wang, Y., Wen, L., Chen, L., Li, Z., et al. (2016). pH-responsive Fe (III)–gallic acid nanoparticles for *in vivo* photoacoustic-imaging-guided photothermal therapy. *Adv. Healthc. Mater.* 5, 772–780. doi: 10.1002/adhm.201500898

Zhang, R., Fan, Q., Yang, M., Cheng, K., Lu, X., Zhang, L., et al. (2015). Engineering melanin nanoparticles as an efficient drug–delivery system for imaging-guided chemotherapy. *Adv. Mater.* 27, 5063–5069. doi: 10.1002/adma.201502201

Conflict of Interest: The authors declare that the research was conducted in the absence of any commercial or financial relationships that could be construed as a potential conflict of interest.

frontiers in Chemistry

REVIEW
published: 10 November 2020
doi: 10.3389/fchem.2020.598100

Moving Beyond the Pillars of Cancer Treatment: Perspectives From Nanotechnology

Cerise M. Siamof[1†], *Shreya Goel*[2*†‡] *and Weibo Cai*[3,4,5*]

[1] Department of Biochemistry, University of Wisconsin-Madison, Madison, WI, United States, [2] Department of Materials Science and Engineering, University of Wisconsin-Madison, Madison, WI, United States, [3] Department of Radiology, University of Wisconsin-Madison, Madison, WI, United States, [4] Department of Medical Physics, University of Wisconsin-Madison, Madison, WI, United States, [5] Department of Pharmaceutical Sciences, University of Wisconsin-Madison, Madison, WI, United States

OPEN ACCESS

Edited by:
Dalong Ni,
Shanghai Jiao Tong University, China

Reviewed by:
Wei Tao,
Harvard Medical School, United States
Wenpei Fan,
China Pharmaceutical University, China

***Correspondence:**
Shreya Goel
shreya.goel.shreya@gmail.com
Weibo Cai
wcai@uwhealth.org

[†] These authors have contributed equally to this work

[‡]Present address:
Shreya Goel,
Department of Cancer Systems Imaging, MD Anderson Cancer Center, Houston, TX, United States

Specialty section:
This article was submitted to Nanoscience, a section of the journal Frontiers in Chemistry

Received: 23 August 2020
Accepted: 20 October 2020
Published: 10 November 2020

Citation:
Siamof CM, Goel S and Cai W (2020) Moving Beyond the Pillars of Cancer Treatment: Perspectives From Nanotechnology. Front. Chem. 8:598100. doi: 10.3389/fchem.2020.598100

Nanotechnology has made a significant impact on basic and clinical cancer research over the past two decades. Owing to multidisciplinary advances, cancer nanotechnology aims to address the problems in current cancer treatment paradigms, with the ultimate goal to improve treatment efficacy, increase patient survival, and decrease toxic side-effects. The potential for use of nanomedicine in cancer targeting and therapy has grown, and is now used to advance the four traditional pillars of cancer treatment: surgery, chemotherapy, radiation therapy and the newest pillar, immunotherapy. In this review we provide an overview of notable advances of nanomedicine in improving drug delivery, radiation therapy and immunotherapy. Potential barriers in the translation of nanomedicine from bench to bedside as well as strategies to overcome these barriers are also discussed. Promising preclinical findings highlight the translational and clinical potential of integrating nanotechnology approaches into cancer care.

Keywords: drug delivery, radiation therapy, immunotherapy, theranosctics, nanomedcine

INTRODUCTION

Cancer is a leading cause of death globally, with 18 million cases and 9 million deaths worldwide each year (Bray et al., 2018). Despite a promising decline in mortality rates over the past 10 years, more than half a million people die annually of cancer in the United States alone (Miller et al., 2019; Siegel et al., 2019). Traditional cancer treatment options can be classified into distinct pillars: surgery, chemotherapy, radiation therapy (hereon referred to as external radionuclide therapy, or ERT) and a more recently added fourth pillar; immunotherapy. Decades of concerted efforts have radically transformed the face of clinical cancer care and has identified specific weaknesses in each of these pillars that are now being targeted by designer personalized therapies aimed at improving survival rates and reducing treatment side-effects.

Since the first FDA approval of the liposomal doxorubicin (Doxil) in the 1990s (Grodzinski et al., 2019), nanomedicine approaches have emerged as a formidable means to improve the outcomes of traditional pillars of cancer therapy, each of which has its own set of advantages and disadvantages. Surgery is by nature more invasive than other treatment options, but can be used as a frontline treatment for primary tumor masses, for example in cases of prostate cancer (Petrelli et al., 2014).

Of course, the location of tumor site must be known for surgery to be effective, which is not always possible, especially in cases where cancers have become invasive or metastasized to different organs. Smart nanomedicine can enhance efficacy of traditional surgical procedures through advances in lymph node mapping (Ravizzini et al., 2009; Erogbogbo et al., 2011; Rubio et al., 2015) and intraoperative image-guided surgery to achieve complete oncological resection (Bradbury et al., 2013; Zheng et al., 2015; Sun et al., 2017). Further, novel approaches such as NP-mediated phototherapy of non-resectable or residual tumor margins can potentially improve curative rates in several cancer types, for example, thoracic malignancies (Keereweer et al., 2011; Bradbury et al., 2013; Lee et al., 2015; Locatelli et al., 2015; Hofferberth et al., 2016; Owens et al., 2016). Theranostic nanomedicine (combination of diagnostic and therapeutic entities into a single platform) can potentially improve outcomes in the post-operative settings as well (Feng et al., 2020). Synergism of precision surgery and nanomedicine has been explored in depth in other excellent reviews, and thus the intersection of nanomedicine with surgical oncology is not a main focus of this review (Singhal et al., 2010; Wang et al., 2019).

By contrast, chemotherapy, ERT and immunotherapy are minimally invasive options, and chemotherapy in particular is now a hallmark of modern cancer treatments (Schirrmacher et al., 2003). However, basic ERT and chemotherapy often pose the risk of damage to benign body cells, causing toxicity and undesirable side effects to the patient, accompanied by very modest treatment outcomes. In regards to the problem of non-specificity with chemotherapy, advances in the multidisciplinary fields of chemistry, biomedical engineering, materials sciences, biophysical, and biochemical sciences have enabled development of novel targeted therapies to improve drug formulations and delivery, as well as overcoming drug resistance (Peer et al., 2007). ERT has benefitted from multidisciplinary advances in irradiation techniques and effective nanoscale radiosensitizers that ensure accurate dose distributions that spare normal tissues. Immunotherapy, on the other hand, has shown mixed results, with efficacy varying drastically from patient to patient and among different cancer types. Nanotechnology has benefitted immunotherapy through improved delivery of immunomodulatory compounds that induce local/systemic anti-tumor immunity or have a tumor priming effect (Martin et al., 2020). Furthermore, high-performance combinations of these fundamental pillars themselves or with other emerging treatment modalities afforded by nano-engineering promises significant implications across preclinical and clinical settings (Kobayashi et al., 2010).

In this work, we provide an overview of the recent research advances in the field of nanotechnology that have dramatically impacted the pillars of cancer treatment, and discuss the opportunities and challenges in these emerging areas. We begin by reviewing advances in targeted drug delivery system, focusing on the use of NPS in stimuli-responsive chemotherapy, such as pH, enzyme, ROS, and hypoxia-sensitive systems. We then move to another traditional pillar of cancer treatment: ERT, and review the uses of nanotechnology within ERT, paying special attention to the ability of nanotechnology to combine ERT with other types of therapy, including both chemotherapy and immunotherapy. Lastly, we review exciting advances in the newest pillar: immunotherapy, describing how nanotechnology may improve therapies targeted to both the innate and adaptive immune system, including nanovaccines, innate immune cell-activation, and immune checkpoint inhibition.

TARGETED CHEMOTHERAPY AND DRUG DELIVERY SYSTEMS

The inability of traditional chemotherapy drugs to distinguish cancer from self and suboptimal pharmacokinetics, pose several complications to cancer treatment. Chemotherapy can result in cardiomyopathy (Shakir and Rasul, 2009; Kumar et al., 2012; Higgins et al., 2015), neuropathy (Kannarkat et al., 2007; Windebank and Grisold, 2008), and nephrotoxicity (Weiss and Poster, 1982; Hanigan and Devarajan, 2003), causing significant concerns for patient morbidity and mortality. NPs have a high surface area to volume ratio which makes them efficient in use for drug loading and delivery (Singh and Lillard, 2009) and have been recognized as a promising approach to selectively target the tumor site by passive [enhanced permeability and retention (EPR) effect (Torchilin, 2011)] or active targeting (Byrne et al., 2008) approaches, to reduce normal tissue uptake and undesirable side-effects of chemotherapeutics. Passive targeting exploits characteristic features of tumors, particularly leaky vasculature, to enhance the accumulation of drug-loaded NPs in the tumor. Active targeting approaches achieve enhanced drug delivery by conjugating drug-loaded NPs with moieties that specifically bind to receptors overexpressed on target cells, such as proteins, polysaccharides, and other small molecules (Yoo et al., 2019). Several recent reviews describe these paradigms in detail (Byrne et al., 2008; Bazak et al., 2015). Furthermore, external stimuli such as temperature, light and magnetically-guided delivery and release of chemotherapeutics are emerging strategies that promise significant advances in targeted drug delivery (Dai et al., 2017). For more in depth review stimuli-responsive drug delivery systems, readers are referred to other more detailed reviews (Ruoslahti et al., 2010; Mura et al., 2013; Zhou L. et al., 2018).

Despite being promising, the final outcomes of such strategies are severely influenced by the intrinsic physiological factors within the tumor. Hence, smart nanomedicine approaches have focused on developing NPs carefully engineered to specifically harness the unique tumor microenvironment (TME) to increase the specificity and efficacy of the treatment. There are several distinct physiological features of the TME that can be exploited by NPs for improved chemotherapy outcomes, including acidic pH, reactive oxygen species (ROS), overexpression of certain enzymes, and lack of intratumoral oxygen or hypoxia. In the following sections, we highlight promising TME-responsive NPs that offer a universal approach for anti-cancer therapy by targeting the genral physiological abnormalities found in all tumors.

pH-Responsive Nanosystems

The body varies considerably in pH: physiological pH is ∼7.4, while that at the tumor site ranges from pH 5.7–7.8 (Gao et al., 2010), due to altered metabolism (glycolysis) and hypoxia resulting in lactic acid formation (Feron, 2009; Danhier et al., 2010). This known physiological difference allows for the development of pH-sensitive nanocarriers that can release their cargo in a more targeted fashion. These systems generally rely on change in structure or size upon exposure to acidicity, or the breaking of a bond sensitive to the acidic pH, which allows for controlled release of the cargo drug at the tumor site (Gao et al., 2010; Tao et al., 2018). pH sensitivity can be conferred to NPs through the use of acid-labile moieties (Li et al., 2016). For example, platinum pro-drug conjugated polymeric NPs form large (∼100 nm) nanoclusters (NC) in physiological pH that enhances their accumulation at the tumor site through prolonged blood circulation and EPR effect (Li et al., 2016). On exposure to acidic pH, an amide bond in cleaved, and NCs release small polyamidoamine prodrug dendrimers (∼ 5 nm) that facilitates greater tumor penetration and cellular internalization. Another redox-responsive moiety that has been used to respond to high concentrations of glutathione is poly(disulfide amide) (PDSA) (Kong et al., 2019). Other examples of pH sensitive moieties used to develop acidosis-responsive NPs include acetals, hydrazones, anhydrides, and Schiff bases (He et al., 2013; Zhang et al., 2016).

Multifunctional inorganic NPs have also been designed for pH-responsive imaging and drug delivery applications. For example, Yang et al. reported a novel biodegradable hollow MnO_2 nanocarrier (H- MnO_2) co-loaded with chemotherapeutic doxorubicin (DOX) and a photosensitizer chlorin e6 (Ce6), utilizing pH sensitivity for both specific imaging and on-demand drug release (Yang et al., 2017). The NPs were stable at neutral pH but exhibited time-dependent degradation behavior in increasingly acidic pH, from 6.5 to 5.5 (**Figure 1A**), resulting in enhanced release of both DOX and Ce6 (**Figure 1B**). pH-responsiveness of the NPs derived from reaction with either H^+ ions or glutathione present in the TME. H- MnO_2 NPs enabled tumor-specific magnetic resonance (MR) imaging (**Figure 1C**) as well as efficient drug release, which translated to greatly reduced tumor burdens when coupled with Ce6-enabled photodynamic therapy (PDT) (**Figure 1D**). Of note, H-MnO_2 triggered hypoxia alleviation in the tumor resulted in enhanced combination chemo-PDT efficacy as well as reversal of immunosuppressive TME. When further combined with immune checkpoint inhibitors, the pH-responsive chemo-PDT by H-MnO_2 demonstrated effective abscopal effect by not only inhibiting the growth of primary tumors, but also of distant tumor sites that were not irradiated with the laser. The work highlights a multi-pronged approach to tumor eradication by pH responsive NPs and makes a compelling case for exploring experimental therapeutic approaches in conjunction with the established paradigms for more effective outcomes, that is desirable for both researchers and patients.

Enzyme-Sensitive Nanosystems

The overexpression of different enzymes in tumors has been exploited to develop smart microenvironment-responsive nanomedicine. Tumors are characterized by elevated levels of enzymes such as galactosidases, phospholipases, cathepsins, and matrix metalloproteinases (MMPs) (Kessenbrock et al., 2010; Cal and López-Otín, 2015; Zhang et al., 2019). MMPs in particular, have been widely harnessed to develop enzyme-responsive drug delivery systems owing to their involvement in signaling pathways important for tumor cell growth and migration and apoptosis (Kessenbrock et al., 2010). Conveniently, one substrate of MMPs is gelatin, which is biocompatible and non-immunogenic (Xu et al., 2013). Exploiting this, the authors prepared mesoporous silica nanoparticles (MSNs) which were coated with a gelatin matrix, then loaded with DOX (MSN-Gel-DOX) (Xu et al., 2013). The gelatin matrix prevented premature release of DOX, and on exposure to MMP-9 in the TME, was degraded, allowing for enhanced DOX release. This was confirmed *in vitro* where MMP-9 triggered increased DOX release from the MSN-Gel-DOX platform in colon carcinoma cells, as well as *in vivo* where the as-developed nanoplatform showed significantly decreased tumor volumes in HT-29 xenografts when compared to DOX alone. Importantly, MSN-Gel-DOX depicted lower systemic toxicity in mice compared to free DOX administration, highlighting the advantage of rationally-designed nanomedicine approach over conventional chemotherapy.

Highlighting the possibility for multimodal agents, Wang et al. developed a cisplatin polyprodrug nanoplatform for cascade photo-chemotherapy, through co-assembly of near infrared dye, indocyanine green (ICG) and polyethylene glycol (PEG) moieties, with repeating cathepsin-B degradable peptides and cisplatin prodrug units [ICG/Poly(Pt); **Figure 2A**] (Wang W. et al., 2018). Cathepsin B is a cysteine protease usually present in lysosomes that has been shown to be present in increased levels in tumors, particularly those that are metastatic and invasive (Gondi and Rao, 2013). In the paper noted, upon exposure to cathepsin B, the nanoplatform was degraded, resulting in the cascade chemotherapy beginning with release of ICG and cisplatin prodrug (**Figure 2B**). Further, irradiation with 808 nm light resulted in formation of ROS and hyperthermia for phototherapy (mediated by ICG) which promoted subsequent uptake of the cisplatin prodrugs to the cytosol and resulted in enhanced apoptosis in cathepsin B positive A549 cells (**Figure 2C**) *in vitro*. Enzyme-responsive treatment efficacy was also observed *in vivo*, where ICG/Poly(Pt) + laser treatment demonstrated higher survival rates in in resistant A549/DDP mice compared to untreated controls, or mice treated with only Pt, only cisplatin, or free ICG+laser (**Figure 2D**).

A major concern for enzyme-responsive treatment is the heterogenous expression of target enzymes in different cancer types. As the exploration of the TME continues, a better understanding of the expression patterns of enzymes at tumor sites will enable effective and precise enzyme-responsive drug delivery systems. It is also expected that newer and more universally expressed enzymes may discovered that may be exploited by nanotechnology for drug delivery. For a deeper overview of the current knowledge and future perspectives in the field, readers are directed to these excellent reviews on

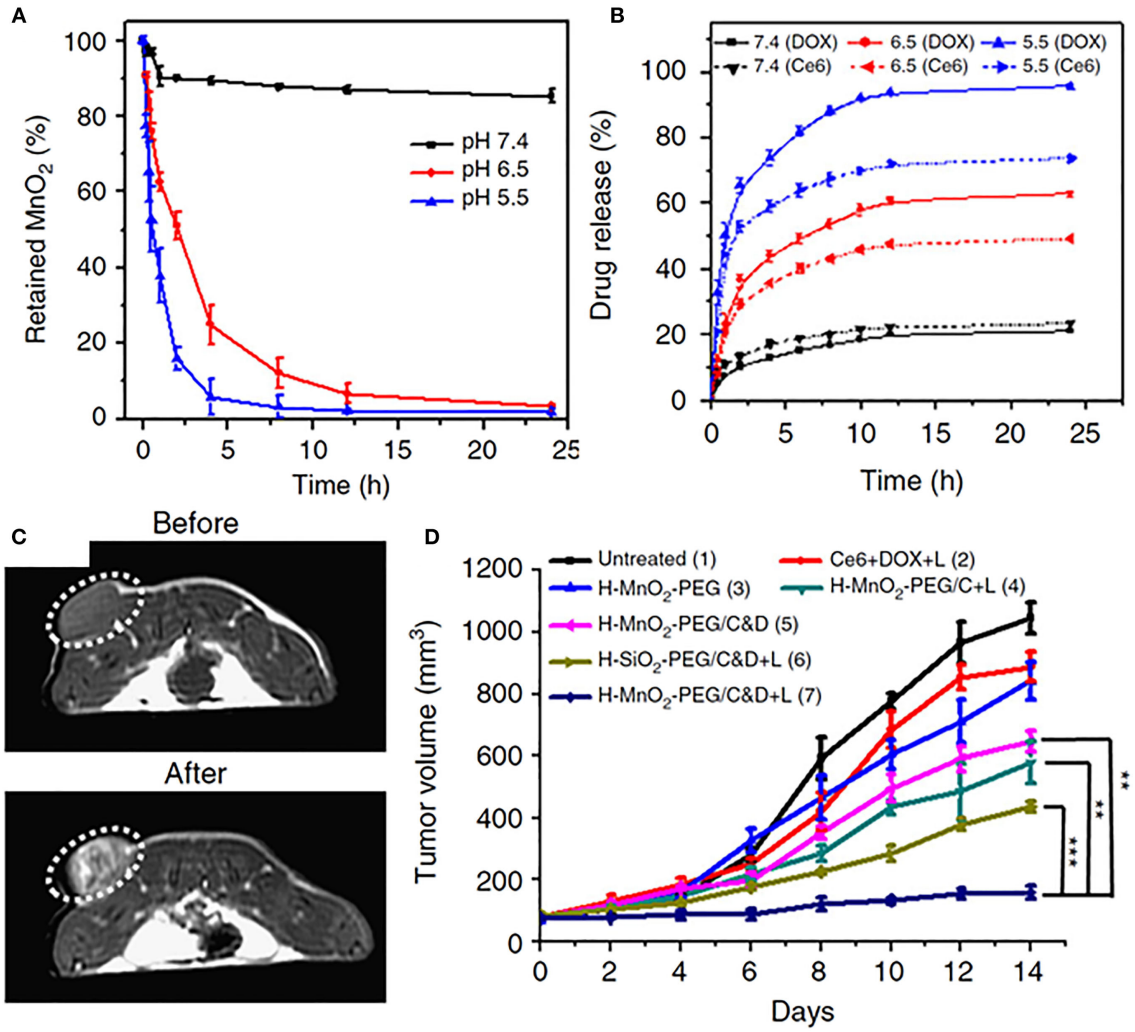

FIGURE 1 | (A) pH-dependent nanoparticle decomposition of hollow MnO_2-PEG nanoparticles dispersed in solutions of different pH (7.4, 6.5, and 5.5) determined by the absorbance of MnO_2. **(B)** Percentages of released Ce6 and DOX from H-MnO_2-PEG/C&D over time in the presence of 10% fetal bovine serum (FBS) at different pH values. **(C)** *In vivo* axial T1-MR images of a 4T1- tumor bearing mouse taken before and 24 h post i.v. injection of H-MnO_2-PEG/C&D. **(D)** Tumor growth curves in different groups after various treatments as indicated. Chemo-PDT treatment after injection of pH-responsive H-MnO_2-PEF/C&D nanoparticles depicted most significant reduction in tumor volumes. With permission from Yang et al. (2017). p values were calculated by Tukey's post-test (***$p < 0.001$, **$p < 0.01$, and *$p < 0.05$).

enzyme-stimulated drug delivery systems (de la Rica et al., 2012; Mu et al., 2018).

ROS-Responsive Nanosystems

The physiology of the tumor site is notable also for the elevated presence of ROS, a byproduct of several physiological processes such as oncogene activation, metabolism, and mitochondrial dysfunction, that has been associated with abnormal cancer cell growth (Trachootham et al., 2009). Interestingly, NPs may also be used to selectively increase the ROS concentration within the tumor site to a level toxic to the cells, though this is not a focus of our discussion of ROS-mediated therapy (Ji et al., 2019; Kong et al., 2020). Rather, we focus here on endogenous ROS sensitivity. Several types of NPs have been recognized as promising for treatment of ROS-related diseases, most notably cerium oxide, carbon, and manganese NPs (Ferreira et al., 2018). Of these, ceria (cerium dioxide) NPs have been the most widely explored for cancer owing to their biocompatibility and antioxidant behavior (Wason and Zhao, 2013).

Endogenous ROS exploitation for drug delivery has been achieved through modifying MSNs with hydrophobic phenyl sulfide (PHS) moieties which protect the nanopores from being wetted by water and thereby inhibits premature release of drugs, such as DOX. Conversely, under the stimulation of endogenous ROS, the PHS groups are oxidized and the nanopores are wetted, resulting in enhanced DOX release (Cheng et al., 2017). Although confined to *in vitro* studies only, the system represents an excellent example of nanoengineering approaches to design simple but effective stimuli-responsive drug delivery nanomedicines. ROS-responsive NPs have also

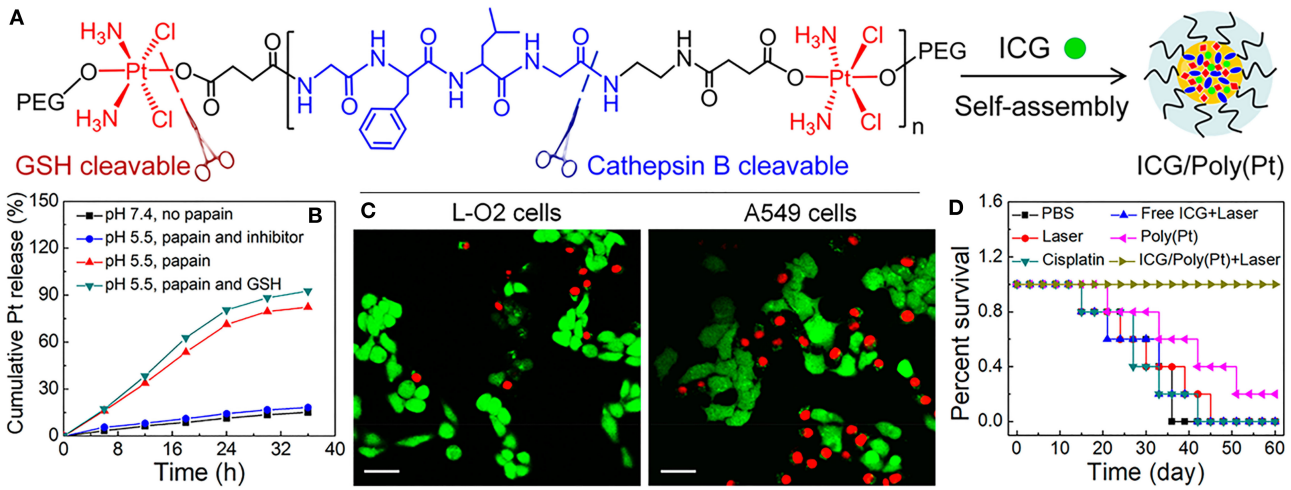

FIGURE 2 | (A) Schematic illustration of Enzyme-Responsive Polyprodrug Nanoplatforms, composed of ICG and cisplatin polyprodrug amphiphiles tethered with repeating cathepsin-B degradable GFLG peptides, PEG-*b*-P(Pt-*co*-GFLG)-*b*-PEG. **(B)** *In vitro* Pt release under different treatment conditions: (i) pH 7.4 without papain (physiological condition), (ii) pH 5.5 with papain, simulating the acidic and enzymatic condition of lysosomes, (iii) pH 5.5 with papain in the presence of a papain inhibitor, and (iv) pH 5.5 with papain followed by GSH treatment at pH 7.4, mimicking the lysosomal escape into the reductive cytosolic environment. **(C)** Fluorescence images of cathepsin B positive A549 cells and cathepsin B negative L-O2 cells upon incubation with ICG/Poly(Pt) after irradiation with 808 nm, 1 W/cm^2, 5 min. Viable cells were stained with green Calcein-AM, while dead and late apoptotic cells were stained with red PI. Scale bar: 40 um. **(D)** Survival curves of resistant A549/DDP cancerous mice after cascade photo-chemotherapy. Figure adapted with permission from Wang W. et al. (2018).

been designed by exploiting thioketal (TK) containing linkers in an elegant study by Xu et al. (2017b). The authors designed a polyprodrug platform from a model drug mitoxantrone (MTO) polymerized with TK linkers and polyethylene glycol. Further tumor specificity was endowed via integrin-targeting RGD ligand. Self-assembled NPs demonstrated enhanced MTO delivery and tumor inhibition *in vivo* in LNCaP prostate tumors, known to have high ROS concentration, compared to free MTO drug, as well as NPs without ROS-sensitive TK linkers (Xu et al., 2017b).

Since the levels of ROS change with tumor status, an innovative strategy was used to combine chemotherapeutic DOX and photodynamic agent Ce6 in polymeric NPs, capable of *in situ* ROS generation and enhanced anti-cancer therapy (Cao et al., 2018). When irradiated with 660 nm laser, ROS generated by the activation of Ce6 resulted in cleavage of the TK linker, causing shrinkage of the NP backbone and enhanced release of DOX. Compared to control, the treatment groups demonstrated remarkable therapeutic outcomes *in vivo*, highlighting the promising potential of remotely-controlled light-activated targeted drug delivery systems. Notably, TK-PPEs administered without internalized Ce6 did not demonstrate ROS-responsiveness, possibly owing to the lower intrinsic ROS levels in the tumor. The approach was mirrored by another group, who reported TK linked, PEGylated NPs with a Ce6 photosensitizer loaded with paclitaxel (PTX; TK-Ce6-PTX NPs) (Li et al., 2018). *In vivo* studies revealed prolonged circulation time of PEGylated NPs. TK-Ce6-PTX NPs with laser irradiation showed increased tumor tissue concentration of PTX compared to TK-NP-Ce6-PTX-NPs without irradiation, and had little PTX uptake in off-target organs. Overall, this strategy overcomes tumor heterogeneity and can be effective for highly targeted ROS-mediated multimodal therapy in tumors that typically demonstrate low ROS concentrations.

Hypoxia-Responsive NPs

Hypoxia is an important biomarker of aggressive tumors, which is widely associated with poor clinical outcomes for the three pillars of cancer treatment (Harris, 2002). Hypoxia is a regulator of numerous pathways that are critical to tumor development and maintenance, such as angiogenesis and metastasis, though it may also induce cell death by apoptosis (Harris, 2002). Resulting from accelerated metabolism or deficient oxygen delivery, hypoxic TME provides a reducing environment with increased presence of nitroreductases and azoreductases (Cui et al., 2011; Liu et al., 2017). Thus, targets of these species such as nitroaromatic, quinone, and azobenzene derivatives have been exploited as hypoxia-sensitive moieties in the development of TME-responsive nanomedicine (Cui et al., 2011; Liu et al., 2017). For example, hypoxia-activated prodrugs (HAPs), which are non-toxic compounds designed to undergo reduction to cytotoxic compounds in the hypoxic environment, have been widely reported for cancer therapy (Hunter et al., 2016). A number of HAPs have been interrogated in clinical trials with limited efficacy that has been attributed to various factors, including poor extravascular transport and suboptimal micropharmacokinetic properties (Jackson et al., 2019). Thus nanocarriers have been designed to improve the accumulation of HAPs at the tumor sites (Liu et al., 2015a).

More innovative strategies have utilized endogenous hypoxia sensitivity as a trigger to enhance drug delivery. Son et al. reported a carboxymethyl dextran (CMD) NP containing a

hypoxia-sensitive azo moiety as well as black hole quencher 3 (BHQ3) dye (Son et al., 2018). Under hypoxic conditions, CMD-BHQ3-NPs were reduced to aniline derivative by tumor intrinsic reductases. These NPs were also loaded with DOX and demonstrated increased drug release in hypoxic conditions compared to normoxic conditions. *In vivo*, the NPs showed high tumor accumulation, demonstrating potential for the system to be used for hypoxia-induced drug delivery. Later, a nanosystem was synthesized with a nitro-imidazole derivative conjugated to CMD, forming hypoxia-responsive NPs (HR-NPs) that were loaded with DOX (Thambi et al., 2014). On exposure to hypoxic conditions, the nitro-imidazole group of the HR-NPs was reduced to aminoimidazole, successfully demonstrating hypoxia-responsiveness, and the NPs showed increased DOX release compared to NPs in the normoxic condition. *In vivo* studies showed high accumulation of the HR-NPs in the tumor site, and slowed tumor growth compared to mice treated with saline or free DOX. The use of a nitroimidazole derivative to create hypoxia-responsiveness has also been seen elsewhere (Ahmad et al., 2016).

Recently, increased attention has been paid to the potential of combination of PDT and hypoxia-responsive nanoplatforms (Qian et al., 2016), again highlighting the importance of multifaceted nanomedicine that can target one tumor in many ways to improve therapeutic outcomes. Along these lines, there is room for hypoxia-responsive or hypoxia-alleviating NPs that can also result in enhanced ERT, which is known to be adversely affected by hypoxia(also discussed further in the next section) (Rockwell et al., 2009). Using hypoxia-sensitive NPs followed by hypoxia alleviating or radiosensitizing NPs may present an effective strategy for multipronged attack on the tumor site in future explorations.

A consideration for all stimuli-responsive systems discussed thus far, is the ability of the NP to maintain the full dose of drug with which it is loaded during its transport to the tumor site, and release the full dose upon exposure to the TME. In other words, NPs need to maintain their specificity for only TME triggers, and respond only when necessary, to avoid undesirable side effects which have become a hallmark of traditional chemotherapy. As our knowledge of tumor physiology as well as tumor vasculature and how it relates to the TME triggers improves, so does the potential for improvement in stimuli-responsive nanomedicine.

NANOTECHNOLOGY FOR ENHANCING EXTERNAL RADIATION THERAPY (ERT)

ERT is one of the long-standing pillars of cancer therapy, performed either alone in cases where surgery is not possible, or in conjunction with surgery or chemotherapy. Adjuvant radiotherapy is a standard in clinical care, whereby residual tumor margins after debulking surgery are irradiated to prevent recurrence and relapse (Coffey et al., 2003). ERT utilizes high energy ionizing beams to directly target the tumor site (Haume et al., 2016). This poses short term risks such as skin irritation as well as long term risks such as fibrosis and atrophy to nearby healthy tissue (Bentzen, 2006). In addition to this complication, there is evidence to show that hypoxic areas within the tumor site are more resistant to standard ERT than non-hypoxic areas (Rockwell et al., 2009). Nanotechnology can play an integral role in improving radiotherapy through improved treatment delivery, combination with other treatment modalities and companion diagnostics (Erdi et al., 2002).

Nanomaterials with high photoelectric cross-sections have been shown to amplify effective radiation dose locally at the tumor site, thereby significantly reducing unwanted side effects and overexposure to radiation (Goel et al., 2017). In an noteworthy study, Shen et. al. reported a biocompatible, renal-clearable nanosystem composed of PEGylated tungsten-gallic acid coordination polymers (W-GA-PEG CPNS) ∼5 nm in diameter (**Figure 3A**) (Shen et al., 2017). ^{64}Cu-labeled W-GA-PEG CPNS demonstrated significant uptake in 4T1 tumor bearing mice within 4 h post-injection, as revealed by positron emission tomography (PET, **Figure 3B**) along with rapid renal clearance and little long-term retention (**Figure 3C**). Mice treated with W-GA-PEG CPN combined with RT demonstrated significantly reduced tumor volumes and prolonged survival compared to mice treated with RT alone (**Figures 3D,E**). Given that many of the nanoplatforms researched for combination with RT involve heavy metals, this study addresses a major concern in improving biocompatibility and natural clearance to avoid long term toxicity in cancer treatment. Nanoformulations have also been designed to improve the delivery of radiosensitizers such as Wortmannin, a potent inhibitor of DNA-dependent kinases, limited by its insolubility and poor pharmacokinetic profule (Karve et al., 2012). Uses of nanomaterials in radiosensitization have been widely explored, becoming the subject of several reviews (Kwatra et al., 2013; Mi et al., 2016; Goel et al., 2017; Song et al., 2017).

Another relevant target for NP intervention to improve ERT is modulating the hypoxic center that exists within solid tumor sites, as was alluded to previously (Goel et al., 2017; Graham and Unger, 2018). Anti-cancer effect of ionizing radiations is dependent on the generation of ROS, which is turn depends of the oxygen availability in the TME. Thus, hypoxic centers cause tumor cells to become radiation-resistant and decrease the efficacy of ERT (Moulder and Rockwell, 1987). Nanotechnology has enabled a two-pronged attack on this issue: nanocarriers loaded with hypoxia-activated drugs have been designed for combinatorial chemo-radiation therapies. A recent noteworthy study reported a rattle-type nanostructure comprised of an upconversion nanoparticle core with a mesoporous silica shell (UCHM) (Liu et al., 2015b). UCHMs loaded with the hypoxia-sensitive agent tirapazamine (TPZ) demonstrated complete tumor remission when combined with RT. On the other hand control mice treated with RT or TPZ alone saw slowed tumor growth initially, which accelerated significantly over time. This effect was also seen in the mice treated with UCHMs and RT, while groups treated with TPZ and RT saw significantly decreased tumor growth.

Nanomaterials have also been engineered to alleviate hypoxia and reoxygenate the tumor microenvironment through enhanced oxygen delivery (Zhou Z. et al., 2018) or *in situ* oxygen production (Prasad et al., 2014). An example of the latter strategy

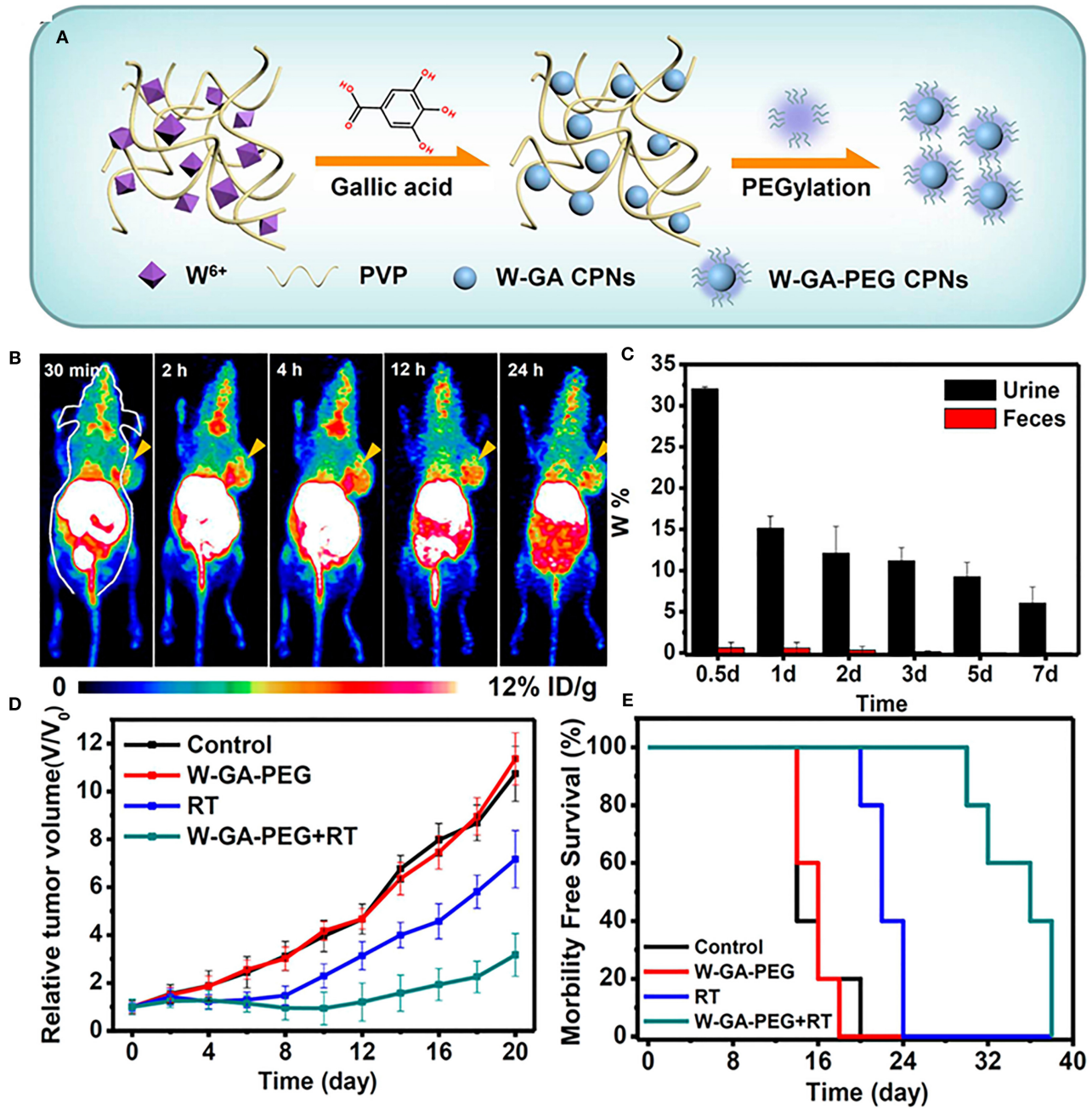

FIGURE 3 | (A) Schematic illustration for the synthesis and structure of W-GA-PEG CPNs. **(B)** *In vivo* PET images of 4T1-tumor-bearing mice after i.v. injection of 64Cu-W-GA-PEG CPNs at different time points. The tumors are indicated with yellow arrows. **(C)** The W levels in urine and feces of healthy mice after i.v. administration of W-GA-PEG CPNs (dose = 40 mg/kg) collected at different intervals. **(D)** Tumor growth curves and **(E)** survival curves of animals treated with W-GA-PEG CPN or radiotherapy or both (five mice per group; irradiation dose of X-ray (RT): 6 Gy; injection dose of W-GA-PEG CPNs: 20 mg/kg). Figures adapted from Shen et al. (2017).

comes from Prasad et al. who developed manganese dioxide (MnO_2) nanoparticles conjugated with albumin that react with endogenous H_2O_2 to produce O_2, with the beneficial side effect of increasing the local pH to combat tumor acidosis, previously mentioned as a hallmark of the TME (Prasad et al., 2014). When injected intratumorally into EMT6 tumor bearing mice, the MnO_2-Albumin NPs caused 45% increase in saturated O_2 levels at tumor periphery compared to mice without NP treatment. In the future, the ability of NPs to alleviate the hypoxic center may be employed to sensitize the tumor to lower doses of radiation, so as to achieve an enhanced treatment with even further reduced side effects.

The ability to extend beyond the three pillars and combine different therapies into one system is one of the biggest advantages that nanomedicine brings to traditional treatment regimes. In an exciting study, nanoscale metal-organic frameworks (nMOFS) were harnessed to combine radiotherapy-radiodynamic therapy and immune checkpoint blockade for local and systemic tumor elimination (Lu et al., 2018). The authors synthesized hafnium nMOFS, which absorbed X-Ray photons that directly excited a coordinated porphyrin photosensitizer. This resulted in both radiotherapy and the production of singlet oxygen species for enhanced radiodynamic therapy even at low doses. To achieve dual radiotherapy and immunotherapy, the nMOFs were loaded with an inhibitor of indoleamine 2,3, dioxygenase, an immunoregulatory enzyme establishes immune tolerance in the TME. The study ultimately demonstrated *in vivo* regression of primary tumors as well as untreated distant tumors via abscopal effect. Importantly, the authors demonstrated systemic tumor rejection when re-challenged, indicating the potential of X-radiation induced *in situ* vaccination. Overall, this study serves as a key example of innovative and effective nanomedicines that synergistically combine multiple pillars of cancer therapy with promising outcomes.

NANOMEDICINE APPROACHES IN IMMUNOTHERAPY

The immune system has limited natural ability to fight cancer, and the TME is often marked by immunosuppressive and immune-evasive mechanisms (Couzin-Frankel, 2013). Immunotherapy seeks to re-train the body's immune system to recognize cancer as non-self and appropriately respond, without triggering undesirable autoimmune processes (Pardoll, 2012). There are several described ways of initiating immunotherapy, including T cell priming and therapy (Schirrmacher et al., 2003), antigen release, and checkpoint inhibition (Pardoll, 2012), and nanotechnology has interacted with all of these domains (Liu et al., 2018; Goldberg, 2019; Irvine and Dane, 2020).

NPs have been used to deliver immunostimulatory agents, antigens, cytokines, chemokines, nucleotides, and toll-like receptor (TLR) agonists that target various immune cells (Fan and Moon, 2015; Da Silva et al., 2016). In other cases, NP design has been carefully modulated to help mount anti-tumor immune responses through their material compositions, geometries, or surface modifications (Moon et al., 2012; Wang J. et al., 2018).

In cases where adaptive immune responses cannot be mounted, nanomedicine approaches have been employed to trigger the innate immune system. In this regard, cancer nanovaccines and more recently nanotherapies activating anti-tumor phagocytes (macrophages) and NK cells are particularly noteworthy (Yuan et al., 2017). For example, a multivalent nanobioconjugate engager (mBiNE) was developed to simultaneously target human epidermal growth factor 2 (HER2), which is overexpressed in certain breast cancers, and calreticulin, a prophagocytic protein (Yuan et al., 2017). The mBiNe led to enhanced phagocytosis of cancer cells and enhanced antigen presentation by macrophages in HER2 positive cells. *In vivo* studies showed that mBiNE had enhanced antitumor efficacy in HER2 positive tumors compared to HER2 negative tumors. Treatment with mBiNE led to increased presence of macrophages and T cells in the tumor site. Interestingly, mice treated with mBiNE also demonstrated resistance to re-challenge and enhanced antitumor immunity in both HER2 negative and HER2 positive tumors. Further, cancer nanovaccines based on dendritic cells (DC vaccines) and NK cells have also shown significant promise in preclinical studies. The development of nanovaccines is a highly active area of research, covered extensively in excellent prior reviews (Irvine et al., 2015; Luo et al., 2017).

An immunotherapy strategy focusing on the adaptive immune system, immune checkpoint inhibition (ICI), has demonstrated excellent therapeutic outcomes and has now become a subject of intense research both in the clinical and preclinical settings (Alsaab et al., 2017). Among many targets, ICI may exploit the unusually high density of the protein, programmed death ligand (PD-L1) on the tumors, that orchestrates immune evasion by inhibiting cytotoxic lymphocyte (CTL) function. Anti-PD-L1 antibodies have shown significant clinical benefit in response rate, survival, and side effects, making it popular as of late (Alsaab et al., 2017). However, ICI has been shown to be effective in only a small subset of patients, and only against certain cancer types, calling for innovation (Alsaab et al., 2017). An interesting study utilized the PD-L1 checkpoint inhibition strategy along with an aldehyde-functionalized dextran superparamagnetic iron oxide NPs, which were conjugated with a checkpoint inhibitor and T cell activators. The NPs could be targeted to the tumor site using an external magnetic field, and once there, modulated the immunosuppressive environment by increasing T cell proliferation as well as ICI (Chiang et al., 2018). This created a twofold immune response that inhibited the tumor growth in different tumor models *in vivo*; 4T1 breast cancer and CT-26 colon cancer, providing a promising avenue for future research in nanotechnology and immunotherapy (Chiang et al., 2018). Nanotechnology may also combine delivery of PD-L1 antibodies with PDT for enhanced response, as was done with non-toxic core-shell NPs (Duan et al., 2016). Apoptosis/necrosis of tumor cells as well as disrupted vasculature after PDT increased the tumor immunogenicity by activating both the innate and adaptive immune systems in the TME. When combined with the PD-L1 blockade, not only localized but systemic antitumor response was successfully mounted in syngeneic breast cancer models (Duan et al., 2016).

ICI targeting cytotoxic T-lymphocyte-associated antigen 4 (CTLA4) has also been thoroughly studied and enhanced by nanotechnology. Mechanism of action of CTLA4 is under intense research. CTLA4 has been shown to outcompete T cell co-stimulatory receptor, CD28 to bind CD80 and CD86 ligands, and creating an immunosuppressive environment which is conducive to tumor growth (Pardoll, 2012). It also sequesters CD80 and CD86 ligands from binding CD28 moeities on the surface of T cells, thus blocking the co-stimulatory signal required for T cell activation, as well as actively removing these ligands from APC surface. CTLA4 blockade serves to enhance $CD4^+$ T cell activity as well as reverse the immunosuppressive environment normally

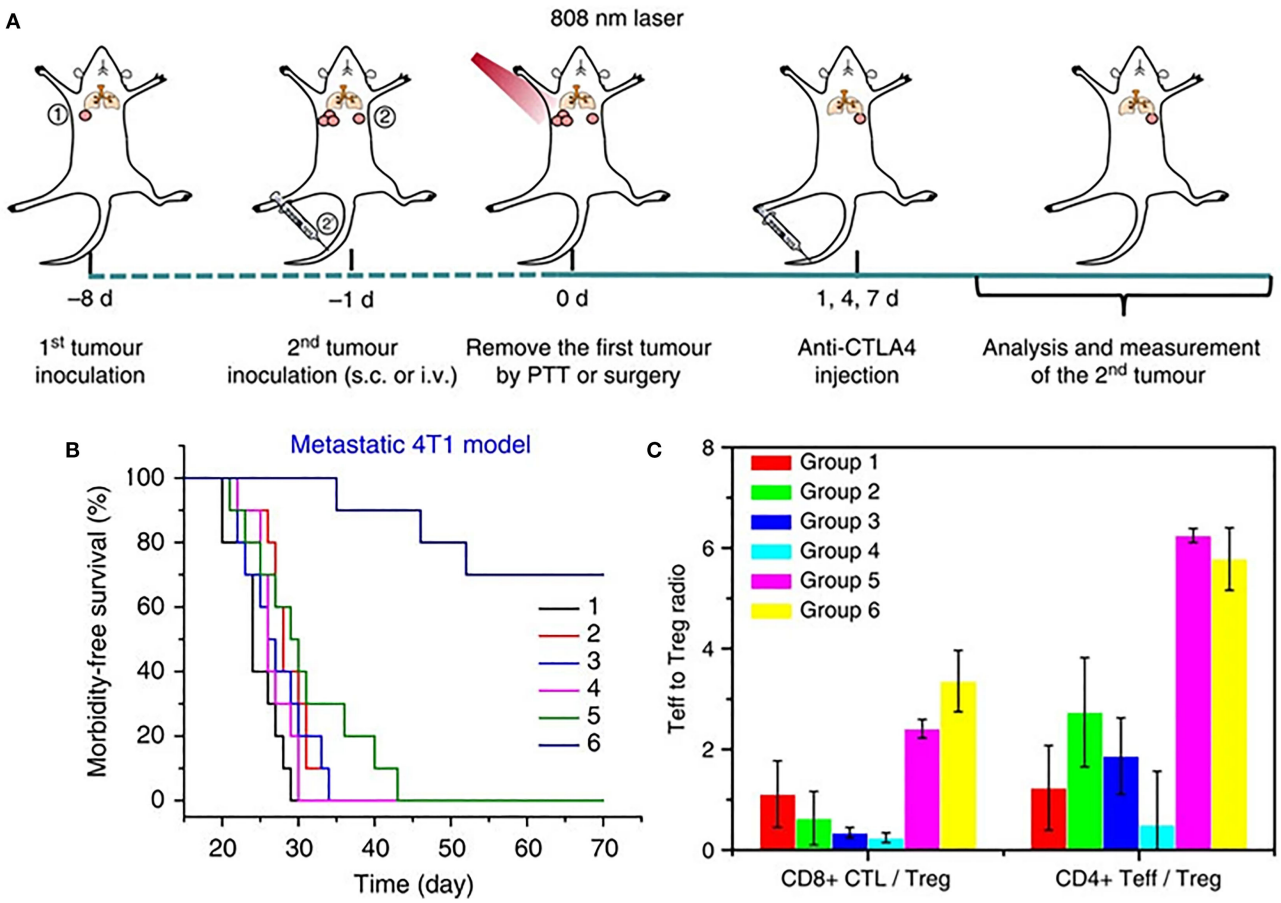

FIGURE 4 | (A) Schematic illustration of PLGA-ICG-R837-based PTT and anti-CTLA-4 combination therapy to inhibit tumor growth at distant sites. **(B)** Morbidity-free survival of different groups of mice with metastatic 4T1 tumors after various treatments to eradicate their primary tumors: (1) Surgery, (2) Surgery+antiCTLA4, (3) Surgery+ PLGA-ICG-R837, (4) PLGA-ICG-R837+laser, (5) Surgery+ PLGA-ICG-R837+antiCTLA4, and (6) PLGA-ICG-R837+ laser + antiCTLA4. **(C)** CD8+ CTL: Treg ratios and CD4+ effector T cells: Treg ratios in the secondary tumors upon various treatments. Both ratios were significantly enhanced after combination treatment with PLGA-ICG-R837-based PTT and anti-CTLA4 therapy. Figure adapted with permission from Chen et al. (2016).

maintained by an increased presence of T_{reg} cells. CTLA4-blocking antibodies have been an area of ongoing research and were the first class of immunotherapeutics to be FDA approved (Pardoll, 2012). However, as with other ICI strategies, CTLA4-based treatment shows heterogeneous responses. Recently, PLGA NPs combining ICG and the toll like receptor ligand R387 (PLGA-ICG-R387) were used in combination photothermal-immunotherapy, such that the photothermal ablation triggered the release of tumor-associated antigens, which in combination with anti-CTLA4 checkpoint blockade, resulted in strong immunological response both locally and at distant tumor sites (**Figure 4A**) (Chen et al., 2016). This response led to increased DC maturation *in vitro* and *in vivo,* as well as demonstrated slowed growth of off-target tumors (**Figure 4B**). In a long-term immune-memory study, secondary tumors that were re-inoculated 40 days after treatment with the PLGA-ICG-R387 and ablation, showed increased levels of T-cells, IFN-δ, and TNF-α and delayed tumor growth compared to tumors that had been re-inoculated 40 days post-surgery alone (**Figure 4C**). This, along with other notable work using upconversion NPs triggered by NIR light to combine CTLA4 checkpoint blockade with PDT (Xu et al., 2017a), shows the potential for multifunctional NPs to effectively consolidate treatment options while delivering improved therapeutic outcomes.

The use of immunotherapy in cancer treatment is a recent and exciting development. Much is left to be discovered about the role of the natural immune system in preventing, managing, and fighting cancer. As more is learned about immunotherapeutics, the uses of nanotechnology in the domain will almost certainly evolve beyond those discussed here, especially with regards to innate immunity and nanovaccines. Further, nanotechnology may allow for more streamlined combination of immunotherapy with other modalities such as chemo or radiation therapies as well as image-guided stratification of immunologically "hot" and "cold" tumors, all of which can work together to improve patient outcomes in the future.

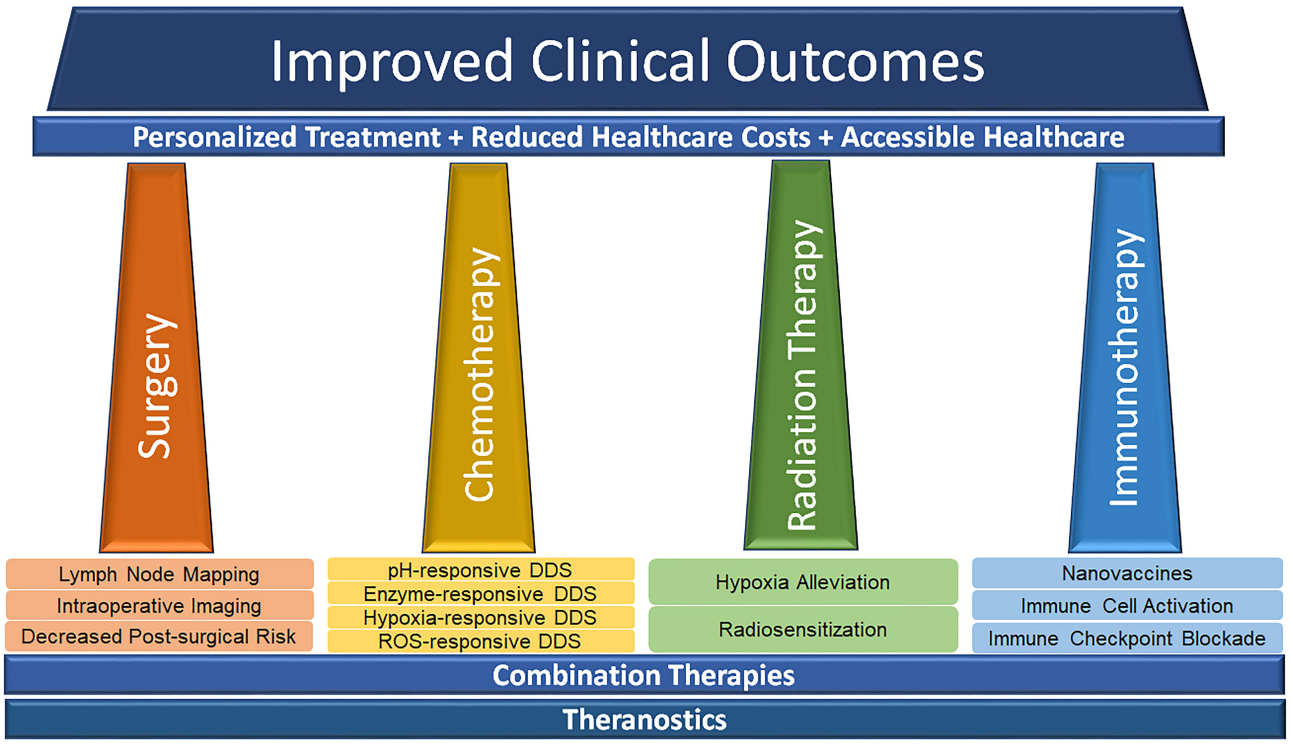

FIGURE 5 | Schematic illustrating the potential of nanotechnology in advancing the pillars of modern cancer treatment toward effective, affordable and accessible personalized medicine to improve healthcare outcomes.

CONCLUSIONS AND FUTURE PERSPECTIVES

The level of innovation demonstrated by nanotechnology, as applied to the pillars of cancer treatment has been phenomenal in the preclinical arena. As we have covered here, nanotechnology both has the ability to improve the pillars individually, as well as facilitate combination therapies with the ultimate goal of improving clinical outcomes (**Figure 5**). Translation of these novel strategies to the clinic, however, has not progressed in accordance with the literature. In the clinical domain, this innovation has been conspicuous by its absence, as doxil and abraxane continue to dominate the clinical utility of nanotechnology, accounting for > $1 B dollars in sale annually (Grodzinski et al., 2019). While these figures are impressive, there is much work to improve, particularly when the balance of efficacy and safety are concerned. In terms of chemotherapy and targeted drug delivery, while NPs have already been used for drugs that are generally hydrophobic or otherwise display poor pharmacokinetics *in vivo*, there is room for repurposing drugs that have been previously rejected (or orphan drugs). If appropriately formulated, NPs show significant promise in making them viable options for treatment in the clinic.

As nanotechnology progresses from the research setting to the clinical one, attention must be paid to the toxicity of not only drugs themselves, but the delivery systems which are being developed. Clinical translation of nanosystems depends on their stability in circulation, ability to negotiate physiological barriers to access the tumor site and their safety profile. This latter point has significantly impeded the clinical successes of nanomedicine so far. As such, NPs which can be cleared naturally by the body or which degrade after treatment are desirable. It is important to thoroughly characterize and deconstruct nanoparticle transport and toxicity not only in the short term, but also long term. Continued progress of nanofabrication methodologies provides the potential for incorporating imaging labels onto therapeutic nanomaterials to develop modular designs that enable non-invasive delineation of nanoparticles kinetics *in vivo* in real time (Goel et al., 2020). Better understanding of NP transport in different animal models over longer timescales would function not only to improve treatment outcomes, but also to help anticipate long term off-target side effects during translational studies. Avoiding cumulative buildup of NPs in the body is a crucial long term consideration that remains an important hurdle to overcome prior to nanomedicines becoming clinically and commercially viable. Similar considerations are paramount in the use of nanotechnology for radiation therapy.

Cancer immunotherapy is a rapidly evolving and highly promising area of research, with great potential for improvement with nanotechnology. NPs may be used in numerous contexts encompassing both innate and adaptive immunity, as well as potential cancer vaccines. The combination of immunotherapy

and other therapies such as chemo or radiation therapies facillitated ny nanotechnology may not only increase the efficacy of treatment and overcome innate immunological "coldness" of certain tumors, but also lead to more convenient administration in the clinic. As immunotherapy grows, more emphasis may be placed on individualized therapies, and the ability to potentially combine a more general chemotherapeutic treatment with an individualized immunotherapy could be exciting, both weakening the tumor and specifically strengthening the host's immune response. Furthermore, given the systemic nature of immunomodulatory therapies, particularly cancer nanovaccines that are trafficked through the lymphoid structures, it is essential that thorough biodistribution studies are performed at both organ and cellular levels. As such, the role of integrated multiscale imaging methods is indispensable.

Finally, the versatility of nanotechnology in cancer requires concerted efforts and interdisciplinary cooperation between scientists, academics, clinicians and regulatory authorities. Continued support from funding agencies and improved cross-talk between academia and industry will be essential to move cancer nanomedicine forward. While significant attention is paid to improving nanomedicine design, it is equally important to design rigorous clinical trials based on appropriate patient selection and stratification, as well as identification of unique avenues in cancer treatment that will benefit from integration of nanotechnology.

AUTHOR CONTRIBUTIONS

CS and SG co-wrote the article. SG and WC contributed to planning and guidance. All authors approve the submitted version.

FUNDING

This work was supported by the University of Wisconsin—Madison, the National Institutes of Health P30CA014520, and the University of Wisconsin—Madison Hilldale Undergraduate/Faculty Research Fellowship.

REFERENCES

Ahmad, Z., Lv, S., Tang, Z., Shah, A., and Chen, X. (2016). Methoxy poly (ethylene glycol)-block-poly (glutamic acid)-graft-6-(2-nitroimidazole) hexyl amine nanoparticles for potential hypoxia-responsive delivery of doxorubicin. *J. Biomater. Sci. Polym. Ed* 27, 40–54. doi: 10.1080/09205063.2015.1107707

Alsaab, H. O., Sau, S., Alzhrani, R., Tatiparti, K., Bhise, K., Kashaw, S., et al. (2017). PD-1 and PD-L1 checkpoint signaling inhibition for cancer immunotherapy: mechanism, combinations, and clinical outcome. *Front. Pharmacol.* 8:561. doi: 10.3389/fphar.2017.00561

Bazak, R., Houri, M., El Achy, S., Kamel, S., and Refaat, T. (2015). Cancer active targeting by nanoparticles: a comprehensive review of literature. *J Cancer Res. Clin. Oncol.* 141, 769–784. doi: 10.1007/s00432-014-1767-3

Bentzen, S. M. (2006). Preventing or reducing late side effects of radiation therapy: radiobiology meets molecular pathology. *Nat. Rev. Cancer* 6, 702–713. doi: 10.1038/nrc1950

Bradbury, M. S., Phillips, E., Montero, P. H., Cheal, S. M., Stambuk, H., Durack, J. C., et al. (2013). Clinically-translated silica nanoparticles as dual-modality cancer-targeted probes for image-guided surgery and interventions. *Integr. Biol.* 5, 74–86. doi: 10.1039/c2ib20174g

Bray, F., Ferlay, J., Soerjomataram, I., Siegel, R. L., Torre, L. A., and Jemal, A. (2018). Global cancer statistics 2018: GLOBOCAN estimates of incidence and mortality worldwide for 36 cancers in 185 countries. *CA Cancer J. Clin.* 68, 394–424. doi: 10.3322/caac.21492

Byrne, J. D., Betancourt, T., and Brannon-Peppas, L. (2008). Active targeting schemes for nanoparticle systems in cancer therapeutics. *Adv. Drug Deliv. Rev.* 60, 1615–1626. doi: 10.1016/j.addr.2008.08.005

Cal, S., and López-Otín, C. (2015). ADAMTS proteases and cancer. *Matrix Biol.* 44–46:77–85. doi: 10.1016/j.matbio.2015.01.013

Cao, Z., Yinchu, M., Chunyang, S., Zidong, L., Zeyu, Y., Junxia, W., et al. (2018). ROS-sensitive polymeric nanocarriers with red light-activated size shrinkage for remotely controlled drug release. *Chem. Materials* 30, 517–525. doi: 10.1021/acs.chemmater.7b04751

Chen, Q., Xu, L., Liang, C., Wang, C., Peng, R., and Liu, Z. (2016). Photothermal therapy with immune-adjuvant nanoparticles together with checkpoint blockade for effective cancer immunotherapy. *Nat. Commun.* 7:13193. doi: 10.1038/ncomms13193

Cheng, Y., Jiao, X., Xu, T., Wang, W., Cao, Y., Wen, Y., et al. (2017). Free-blockage mesoporous anticancer nanoparticles based on ROS-responsive wetting behavior of nanopores. *Small* 13:1701942. doi: 10.1002/smll.201701942

Chiang, C. S., Lin, Y. J., Lee, R., Lai, Y. H., Cheng, H. W., Hsieh, C. H., et al. (2018). Combination of fucoidan-based magnetic nanoparticles and immunomodulators enhances tumour-localized immunotherapy. *Nat. Nanotechnol.* 13, 746–754. doi: 10.1038/s41565-018-0146-7

Coffey, J. C., Wang, J. H., Smith, M. J., Bouchier-Hayes, D., Cotter, T. G., and Redmond, H. P. (2003). Excisional surgery for cancer cure: therapy at a cost. *Lancet Oncol.* 4, 760–768. doi: 10.1016/S1470-2045(03)01282-8

Couzin-Frankel, J. (2013). Breakthrough of the year 2013. *Cancer Immunother. Sci.* 342, 1432–1433. doi: 10.1126/science.342.6165.1432

Cui, L., Zhong, Y., Zhu, W., Xu, Y., Du, Q., Wang, X., et al. (2011). A new prodrug-derived ratiometric fluorescent probe for hypoxia: high selectivity of nitroreductase and imaging in tumor cell. *Org. Lett.* 13, 928–931. doi: 10.1021/ol102975t

Da Silva, C. G., Rueda, F., Löwik, C. W., Ossendorp, F., and Cruz, L. J. (2016). Combinatorial prospects of nano-targeted chemoimmunotherapy. *Biomaterials* 83, 308–320. doi: 10.1016/j.biomaterials.2016.01.006

Dai, Y., Xu, C., Sun, X., and Chen, X. (2017). Nanoparticle design strategies for enhanced anticancer therapy by exploiting the tumour microenvironment. *Chem. Soc. Rev.* 46, 3830–3852. doi: 10.1039/C6CS00592F

Danhier, F., Feron, O., and Préat, V. (2010). To exploit the tumor microenvironment: passive and active tumor targeting of nanocarriers for anti-cancer drug delivery. *J. Control Release* 148, 135–146. doi: 10.1016/j.jconrel.2010.08.027

de la Rica, R., Aili, D., and Stevens, M. M. (2012). Enzyme-responsive nanoparticles for drug release and diagnostics. *Adv. Drug Deliv. Rev.* 64, 967–978. doi: 10.1016/j.addr.2012.01.002

Duan, X., Chan, C., Guo, N., Han, W., Weichselbaum, R. R., and Lin, W. (2016). Photodynamic therapy mediated by nontoxic core-shell nanoparticles synergizes with immune checkpoint blockade to elicit antitumor immunity and antimetastatic effect on breast cancer. *J. Am. Chem. Soc.* 138, 16686–16695. doi: 10.1021/jacs.6b09538

Erdi, Y. E., Rosenzweig, K., Erdi, A. K., Macapinlac, H. A., Hu, Y. C., Braban, L. E., et al. (2002). Radiotherapy treatment planning for patients with non-small cell lung cancer using positron emission tomography (PET). *Radiother. Oncol.* 62, 51–60. doi: 10.1016/S0167-8140(01)00470-4

Erogbogbo, F., Yong, K. T., Roy, I., Hu, R., Law, W. C., Zhao, W., et al. (2011). *In vivo* targeted cancer imaging, sentinel lymph node mapping and multi-channel imaging with biocompatible silicon nanocrystals. *ACS Nano* 5, 413–423. doi: 10.1021/nn1018945

Fan, Y., and Moon, J. J. (2015). Nanoparticle drug delivery systems designed to improve cancer vaccines and immunotherapy. *Vaccines* 3, 662–685. doi: 10.3390/vaccines3030662

Feng, C., Jiang, O., Zhongmin, T., Na, K., Yuan, L., Liyi, F., et al. (2020). Germanene-based theranostic materials for surgical adjuvant treatment: inhibiting tumor recurrence and wound infection. *Matter* 3, 127–144. doi: 10.1016/j.matt.2020.04.022

Feron, O. (2009). Pyruvate into lactate and back: from the Warburg effect to symbiotic energy fuel exchange in cancer cells. *Radiother. Oncol.* 92, 329–333. doi: 10.1016/j.radonc.2009.06.025

Ferreira, C. A., Ni, D., Rosenkrans, Z. T., and Cai, W. (2018). Scavenging of reactive oxygen and nitrogen species with nanomaterials. *Nano Res.* 11, 4955–4984. doi: 10.1007/s12274-018-2092-y

Gao, W., Chan, J. M., and Farokhzad, O. C. (2010). pH-Responsive nanoparticles for drug delivery. *Mol. Pharm.* 7, 1913–1920. doi: 10.1021/mp100253e

Goel, S., Ni, D., and Cai, W. (2017). Harnessing the power of nanotechnology for enhanced radiation therapy. *ACS Nano* 11, 5233–5237. doi: 10.1021/acsnano.7b03675

Goel, S., Zhang, G., Dogra, P., Nizzero, S., Cristini, V., Wang, Z., et al. (2020). Sequential deconstruction of composite drug transport in metastatic breast cancer. *Sci. Adv.* 6:eaba4498. doi: 10.1126/sciadv.aba4498

Goldberg, M. S. (2019). Improving cancer immunotherapy through nanotechnology. *Nat. Rev. Cancer* 19, 587–602. doi: 10.1038/s41568-019-0186-9

Gondi, C. S., and Rao, J. S. (2013). Cathepsin B as a cancer target. *Expert Opin Ther. Targets* 17, 281–291. doi: 10.1517/14728222.2013.740461

Graham, K., and Unger, E. (2018). Overcoming tumor hypoxia as a barrier to radiotherapy, chemotherapy and immunotherapy in cancer treatment. *Int. J. Nanomed.* 13, 6049–6058. doi: 10.2147/IJN.S140462

Grodzinski, P., Kircher, M., Goldberg, M., and Gabizon, A. (2019). Integrating nanotechnology into cancer care. *ACS Nano* 13, 7370–7376. doi: 10.1021/acsnano.9b04266

Hanigan, M. H., and Devarajan, P. (2003). Cisplatin nephrotoxicity: molecular mechanisms. *Cancer Ther.* 1, 47–61.

Harris, A. L. (2002). Hypoxia–a key regulatory factor in tumour growth. *Nat Rev Cancer* 2, 38–47. doi: 10.1038/nrc704

Haume, K., Rosa, S., Grellet, S., Smiałek, M. A., Butterworth, K. T., Solov'yov, A. V., et al. (2016). Gold nanoparticles for cancer radiotherapy: a review. *Cancer Nanotechnol.* 7:8. doi: 10.1186/s12645-016-0021-x

He, H., Chen, S., Zhou, J., Dou, Y., Song, L., Che, L., et al. (2013). Cyclodextrin-derived pH-responsive nanoparticles for delivery of paclitaxel. *Biomaterials* 34, 5344–5358. doi: 10.1016/j.biomaterials.2013.03.068

Higgins, A. Y., O'Halloran, T. D., and Chang, J., D. (2015). Chemotherapy-induced cardiomyopathy. *Heart Fail Rev.* 20, 721–730. doi: 10.1007/s10741-015-9502-y

Hofferberth, S. C., Grinstaff, M. W., and Colson, Y., L. (2016). Nanotechnology applications in thoracic surgery. *Eur. J. Cardiothorac. Surg.* 50, 6–16. doi: 10.1093/ejcts/ezw002

Hunter, F. W., Wouters, B. G., and Wilson, W. R. (2016). Hypoxia-activated prodrugs: paths forward in the era of personalised medicine. *Br. J. Cancer* 114, 1071–1077. doi: 10.1038/bjc.2016.79

Irvine, D. J., and Dane, E. L. (2020). Enhancing cancer immunotherapy with nanomedicine. *Nat. Rev. Immunol.* 20, 321–334. doi: 10.1038/s41577-019-0269-6

Irvine, D. J., Hanson, M. C., Rakhra, K., and Tokatlian, T. (2015). Synthetic nanoparticles for vaccines and immunotherapy. *Chem. Rev.* 115, 11109–11146. doi: 10.1021/acs.chemrev.5b00109

Jackson, R. K., Liew, L. P., and Hay, M. P. (2019). Overcoming radioresistance: small molecule radiosensitisers and hypoxia-activated prodrugs. *Clin. Oncol.* 31, 290–302. doi: 10.1016/j.clon.2019.02.004

Ji, X., Kang, Y., Ouyang, J., Chen, Y., Artzi, D., Zeng, X., et al. (2019). Synthesis of ultrathin biotite nanosheets as an intelligent theranostic platform for combination cancer therapy. *Adv. Sci.* 6:1901211. doi: 10.1002/advs.201901211

Kannarkat, G., Lasher, E. E., and Schiff, D. (2007). Neurologic complications of chemotherapy agents. *Curr. Opin Neurol.* 20, 719–725. doi: 10.1097/WCO.0b013e3282f1a06e

Karve, S., Werner, M. E., Sukumar, R., Cummings, N. D., Copp, J. A., Wang, E. C., et al. (2012). Revival of the abandoned therapeutic wortmannin by nanoparticle drug delivery. *Proc. Natl. Acad. Sci. U.S.A* 109, 8230–8235. doi: 10.1073/pnas.1120508109

Keereweer, S., Kerrebijn, J. D., van Driel, P. B., Xie, B., Kaijzel, E. L., Snoeks, T. J., et al. (2011). Optical image-guided surgery–where do we stand? *Mol. Imaging Biol.* 13, 199–207. doi: 10.1007/s11307-010-0373-2

Kessenbrock, K., Plaks, V., and Werb, Z. (2010). Matrix metalloproteinases: regulators of the tumor microenvironment. *Cell* 141, 52–67. doi: 10.1016/j.cell.2010.03.015

Kobayashi, K., Usami, N., Porcel, E., Lacombe, S., and Le Sech, C. (2010). Enhancement of radiation effect by heavy elements. *Mutat Res.* 704, 123–131. doi: 10.1016/j.mrrev.2010.01.002

Kong, N., Ji, X., Wang, J., Sun, X., Chen, G., Fan, T., et al. (2020). ROS-mediated selective killing effect of black phosphorus: mechanistic understanding and its guidance for safe biomedical applications. *Nano Lett.* 20, 3943–3955. doi: 10.1021/acs.nanolett.0c01098

Kong, N., Tao, W., Ling, X., Wang, J., Xiao, Y., Shi, S., et al. (2019). Synthetic mRNA nanoparticle-mediated restoration of p53 tumor suppressor sensitizes p53-deficient cancers to mTOR inhibition. *Sci. Transl. Med.* 11:eaaw1565. doi: 10.1126/scitranslmed.aaw1565

Kumar, S., Marfatia, R., Tannenbaum, S., Yang, C., and Avelar, E. (2012). Doxorubicin-induced cardiomyopathy 17 years after chemotherapy. *Tex Heart Inst. J.* 39, 424–427.

Kwatra, D., Anand, V., and Shrikant, A. (2013). Nanoparticles in radiation therapy: a summary of various approaches to enhance radiosensitization in cancer. *Transl. Cancer Res.* 2, 330–342.

Lee, H., Lee, Y., Song, C., Cho, H. R., Ghaffari, R., Choi, T. K., et al. (2015). An endoscope with integrated transparent bioelectronics and theranostic nanoparticles for colon cancer treatment. *Nat. Commun.* 6:10059. doi: 10.1038/ncomms10059

Li, H. J., Du, J. Z., Du, X. J., Xu, C. F., Sun, C. Y., Wang, H. X., et al. (2016). Stimuli-responsive clustered nanoparticles for improved tumor penetration and therapeutic efficacy. *Proc. Natl. Acad. Sci. U.S.A.* 113, 4164–4169. doi: 10.1073/pnas.1522080113

Li, J., Sun, C., Tao, W., Cao, Z., Qian, H., Yang, X., and Wang, J. (2018). Photoinduced PEG deshielding from ROS-sensitive linkage-bridged block copolymer-based nanocarriers for on-demand drug delivery. *Biomaterials* 170, 147–155. doi: 10.1016/j.biomaterials.2018.04.015

Liu, J. N., Bu, W., and Shi, J. (2017). Chemical design and synthesis of functionalized probes for imaging and treating tumor hypoxia. *Chem. Rev.* 117, 6160–6224. doi: 10.1021/acs.chemrev.6b00525

Liu, Y., Liu, Y., Bu, W., Cheng, C., Zuo, C., Xiao, Q., et al. (2015a). Hypoxia induced by upconversion-based photodynamic therapy: towards highly effective synergistic bioreductive therapy in tumors. *Angew. Chem. Int. Ed. Engl.* 54, 8105–8109. doi: 10.1002/anie.201500478

Liu, Y., Liu, Y., Bu, W., Xiao, Q., Sun, Y., Zhao, K., et al. (2015b). Radiation-/hypoxia-induced solid tumor metastasis andregrowth inhibited by hypoxia-specific upconversion nanoradiosensitizer. *Biomaterials* 49, 1–8. doi: 10.1016/j.biomaterials.2015.01.028

Liu, Z., Jiang, W., Nam, J., Moon, J. J., and Kim, B. Y. S. (2018). Immunomodulating nanomedicine for cancer therapy. *Nano Lett.* 18, 6655–6659. doi: 10.1021/acs.nanolett.8b02340

Locatelli, E., Ilaria, M., and Mauro Comes, F. (2015). Hard and soft nanoparticles for image-guided surgery in nanomedicine. *J. Nanoparticle Res.* 17:328. doi: 10.1007/s11051-015-3135-x

Lu, K., He, C., Guo, N., Chan, C., Ni, K., Lan, G., et al. (2018). Low-dose X-ray radiotherapy-radiodynamic therapy via nanoscale metal-organic frameworks enhances checkpoint blockade immunotherapy. *Nat. Biomed. Eng.* 2, 600–610. doi: 10.1038/s41551-018-0203-4

Luo, M., Samandi, L. Z., Wang, Z., Chen, Z. J., and Gao, J. (2017). Synthetic nanovaccines for immunotherapy. *J. Control Release* 263, 200–210. doi: 10.1016/j.jconrel.2017.03.033

Martin, J. D., Cabral, H., Stylianopoulos, T., and Jain, R. K. (2020). Improving cancer immunotherapy using nanomedicines: progress, opportunities and challenges. *Nat. Rev. Clin. Oncol.* 17, 251–266. doi: 10.1038/s41571-019-0308-z

Mi, Y., Shao, Z., Vang, J., Kaidar-Person, O., and Wang, A. Z. (2016). Application of nanotechnology to cancer radiotherapy. *Cancer Nanotechnol.* 7:11. doi: 10.1186/s12645-016-0024-7

Miller, K. D., Nogueira, L., Mariotto, A. B., Rowland, J. H., Yabroff, K. R., Alfano, C. M., et al. (2019). Cancer treatment and survivorship statistics. *CA Cancer J. Clin.* (2019) 69, 363–385. doi: 10.3322/caac.21565

Moon, J. J., Huang, B., and Irvine, D. J. (2012). Engineering nano- and microparticles to tune immunity. *Adv. Mater.* 24, 3724–3746. doi: 10.1002/adma.201200446

Moulder, J. E., and Rockwell, S. (1987). Tumor hypoxia: its impact on cancer therapy. *Cancer Metastasis Rev.* 5, 313–341. doi: 10.1007/BF00055376

Mu, J., Lin, J., Huang, P., and Chen, X. (2018). Development of endogenous enzyme-responsive nanomaterials for theranostics. *Chem. Soc. Rev.* 47, 5554–5573. doi: 10.1039/C7CS00663B

Mura, S., Nicolas, J., and Couvreur, P. (2013). Stimuli-responsive nanocarriers for drug delivery. *Nat. Mater.* 12, 991–1003. doi: 10.1038/nmat3776

Owens, E. A., Hyun, H., Dost, T. L., Lee, J. H., Park, G., Pham, D. H., et al. (2016). Near-infrared illumination of native tissues for image-guided surgery. *J. Med. Chem.* 59, 5311–5323. doi: 10.1021/acs.jmedchem.6b00038

Pardoll, D. M. (2012). The blockade of immune checkpoints in cancer immunotherapy. *Nat. Rev. Cancer* 12, 252–264. doi: 10.1038/nrc3239

Peer, D., Karp, J. M., Hong, S., Farokhzad, O. C., Margalit, R., and Langer, R. (2007). Nanocarriers as an emerging platform for cancer therapy. *Nat. Nanotechnol.* 2, 751–760. doi: 10.1038/nnano.2007.387

Petrelli, F., Vavassori, I., Coinu, A., Borgonovo, K., Sarti, E., and Barni, S. (2014). Radical prostatectomy or radiotherapy in high-risk prostate cancer: a systematic review and metaanalysis. *Clin. Genitourin Cancer* 12, 215–224. doi: 10.1016/j.clgc.2014.01.010

Prasad, P., Gordijo, C. R., Abbasi, A. Z., Maeda, A., Ip, A., Rauth, A. M., et al. (2014). Multifunctional albumin-MnO_2 nanoparticles modulate solid tumor microenvironment by attenuating hypoxia, acidosis, vascular endothelial growth factor and enhance radiation response. *ACS Nano* 8, 3202–3212. doi: 10.1021/nn405773r

Qian, C., Yu, J., Chen, Y., Hu, Q., Xiao, X., Sun, W., et al. (2016). Light-activated hypoxia-responsive nanocarriers for enhanced anticancer therapy. *Adv. Mater.* 28, 3313–3320. doi: 10.1002/adma.201505869

Ravizzini, G., Turkbey, B., Barrett, T., Kobayashi, H., and Choyke, P. L. (2009). Nanoparticles in sentinel lymph node mapping. *Wiley Interdiscip Rev. Nanomed. Nanobiotechnol.* 1, 610–623. doi: 10.1002/wnan.48

Rockwell, S., Dobrucki, I. T., Kim, E. Y., Marrison, S. T., and Vu, V. T. (2009). Hypoxia and radiation therapy: past history, ongoing research, and future promise. *Curr. Mol. Med.* 9, 442–458. doi: 10.2174/156652409788167087

Rubio, I. T., Diaz-Botero, S., Esgueva, A., Rodriguez, R., Cortadellas, T., Cordoba, O., et al. (2015). The superparamagnetic iron oxide is equivalent to the Tc99 radiotracer method for identifying the sentinel lymph node in breast cancer. *Eur. J. Surg Oncol.* 41, 46–51. doi: 10.1016/j.ejso.2014.11.006

Ruoslahti, E., Bhatia, S. N., and Sailor, M. J. (2010). Targeting of drugs and nanoparticles to tumors. *J. Cell Biol.* 188, 759–768. doi: 10.1083/jcb.200910104

Schirrmacher, V., Feuerer, M., Fournier, P., Ahlert, T., Umansky, V., and Beckhove, P. (2003). T-cell priming in bone marrow: The potential for long-lasting protective anti-tumor immunity. *Trends Mol. Med.* doi: 10.1016/j.molmed.2003.10.001

Shakir, D. K., and Rasul, K. I. (2009). Chemotherapy induced cardiomyopathy: pathogenesis, monitoring and management. *J. Clin. Med. Res.* 1, 8–12. doi: 10.4021/jocmr2009.02.1225

Shen, S., Jiang, D., Cheng, L., Chao, Y., Nie, K., Dong, Z., et al. (2017). Renal-clearable ultrasmall coordination polymer nanodots for chelator-Free (64)Cu-labeling and imaging-guided enhanced radiotherapy of cancer. *ACS Nano* 11, 9103–9111. doi: 10.1021/acsnano.7b03857

Siegel, R. L., Miller, K. D., and Jemal, A. (2019). Cancer statistics. *CA Cancer J. Clin.* (2019) 69, 7–34. doi: 10.3322/caac.21551

Singh, R., and Lillard, J. W., Jr. (2009). Nanoparticle-based targeted drug delivery. *Exp. Mol. Pathol.* 86, 215–223. doi: 10.1016/j.yexmp.2008.12.004

Singhal, S., Nie, S., and Wang, M. D. (2010). Nanotechnology applications in surgical oncology. *Annu. Rev. Med.* 61, 359–373. doi: 10.1146/annurev.med.60.052907.094936

Son, S., Rao, N. V., Ko, H., Shin, S., Jeon, J., Han, H. S., et al. (2018). Carboxymethyl dextran-based hypoxia-responsive nanoparticles for doxorubicin delivery. *Int. J. Biol. Macromol.* 110, 399–405. doi: 10.1016/j.ijbiomac.2017.11.048

Song, G., Cheng, L., Chao, Y., Yang, K., and Liu, Z. (2017). Emerging nanotechnology and advanced materials for cancer radiation therapy. *Adv. Mater.* 29:170099632. doi: 10.1002/adma.201700996

Sun, Y., Ding, M., Zeng, X., Xiao, Y., Wu, H., Zhou, H., et al. (2017). Novel bright-emission small-molecule NIR-II fluorophores for *in vivo* tumor imaging and image-guided surgery. *Chem. Sci.* 8, 3489–3493. doi: 10.1039/C7SC00251C

Tao, W., Ji, X., Zhu, X., Li, L., Wang, J., Zhang, Y., et al. (2018). Two-dimensional antimonene-based photonic nanomedicine for cancer theranostics. *Adv Mater.* 30:e1802061. doi: 10.1002/adma.201802061

Thambi, T., Deepagan, V. G., Yoon, H. Y., Han, H. S., Kim, S. H., Son, S., et al. (2014). Hypoxia-responsive polymeric nanoparticles for tumor-targeted drug delivery. *Biomaterials* 35, 1735–1743. doi: 10.1016/j.biomaterials.2013.11.022

Torchilin, V. (2011). Tumor delivery of macromolecular drugs based on the EPR effect. *Adv. Drug Deliv. Rev.* 63, 131–135. doi: 10.1016/j.addr.2010.03.011

Trachootham, D., Alexandre, J., and Huang, P. (2009). Targeting cancer cells by ROS-mediated mechanisms: a radical therapeutic approach? *Nat. Rev. Drug Discov.* 8, 579–591. doi: 10.1038/nrd2803

Wang, C., Fan, W., Zhang, Z., Wen, Y., Xiong, L., and Chen, X. (2019). Advanced nanotechnology leading the way to multimodal imaging-guided precision surgical therapy. *Adv. Mater.* 31:e1904329. doi: 10.1002/adma.201904329

Wang, J., Chen, H. J., Hang, T., Yu, Y., Liu, G., He, G., et al. (2018). Physical activation of innate immunity by spiky particles. *Nat. Nanotechnol.* 13, 1078–1086. doi: 10.1038/s41565-018-0274-0

Wang, W., Guohai, L., Wenjia, Z., Da, X., and Xianglong, H. (2018). Cascade-promoted photo-chemotherapy against resistant cancers by enzyme-responsive polyprodrug nanoplatforms. *Chem. Mater.* 30, 3486–3498. doi: 10.1021/acs.chemmater.8b01149

Wason, M. S., and Zhao, J. (2013). Cerium oxide nanoparticles: potential applications for cancer and other diseases. *Am. J. Transl. Res* 5, 126–131.

Weiss, R. B., and Poster, D. S. (1982). The renal toxicity of cancer chemotherapeutic agents. *Cancer Treat Rev.* 9, 37–56. doi: 10.1016/S0305-7372(82)80004-2

Windebank, A. J., and Grisold, W. (2008). Chemotherapy-induced neuropathy. *J. Peripher. Nerv. Syst.* 13, 27–46. doi: 10.1111/j.1529-8027.2008.00156.x

Xu, J., Xu, L., Wang, C., Yang, R., Zhuang, Q., Han, X., et al. (2017a). Near-infrared-triggered photodynamic therapy with multitasking upconversion nanoparticles in combination with checkpoint blockade for immunotherapy of colorectal cancer. *ACS Nano* 11, 4463–4474. doi: 10.1021/acsnano.7b00715

Xu, J. H., Fu-Ping, G., Li-Li, L., Horse Ma, L., Yun-Shan, F., Wei, L., et al. (2013). Gelatin-mesoporous silica nanoparticles as matrix metalloproteinases-degradable drug delivery systems *in vivo*. *Microporous Mesoporous Mater.* 182, 165–172. doi: 10.1016/j.micromeso.2013.08.050

Xu, X., Saw, P. E., Tao, W., Li, Y., Ji, X., Bhasin, S., et al. (2017b). ROS-responsive polyprodrug nanoparticles for triggered drug delivery and effective cancer therapy. *Adv. Mater* 29:1700141. doi: 10.1002/adma.201700141

Yang, G., Xu, L., Chao, Y., Xu, J., Sun, X., Wu, Y., et al. (2017). Hollow MnO(2) as a tumor-microenvironment-responsive biodegradable nano-platform for combination therapy favoring antitumor immune responses. *Nat. Commun.* 8:902. doi: 10.1038/s41467-017-01050-0

Yoo, J., Park, C., Yi, G., Lee, D., and Koo, H. (2019). Active targeting strategies using biological ligands for nanoparticle drug delivery systems. *Cancers* 11:640. doi: 10.3390/cancers11050640

Yuan, H., Jiang, W., von Roemeling, C. A., Qie, Y., Liu, X., Chen, Y., et al. (2017). Multivalent bi-specific nanobioconjugate engager for targeted cancer immunotherapy. *Nat. Nanotechnol.* 12, 763–769. doi: 10.1038/nnano.2017.69

Zhang, Y., Yang, C., Wang, W., Liu, J., Liu, Q., Huang, F., et al. (2016). Co-delivery of doxorubicin and curcumin by pH-sensitive prodrug nanoparticle for combination therapy of cancer. *Sci. Rep.* 6:21225. doi: 10.1038/srep21225

Zhang, Z. T., Huang-Fu, M. Y., Xu, W. H., and Han, M. (2019). Stimulus-responsive nanoscale delivery systems triggered by the enzymes in the tumor microenvironment. *Eur. J. Pharm. Biopharm.* 137, 122–130. doi: 10.1016/j.ejpb.2019.02.009

Zheng, J., Muhanna, N., De Souza, R., Wada, H., Chan, H., Akens, M. K., et al. (2015). A multimodal nano agent for image-guided cancer surgery. *Biomaterials* 67, 160–168. doi: 10.1016/j.biomaterials.2015.07.010

Zhou, L., Wang, H., and Li, Y. (2018). Stimuli-responsive nanomedicines for overcoming cancer multidrug resistance. *Theranostics* 8, 1059–1074. doi: 10.7150/thno.22679

Zhou, Z., Zhang, B., Wang, H., Yuan, A., Hu, Y., and Wu, J. (2018). Two-stage oxygen delivery for enhanced radiotherapy by perfluorocarbon nanoparticles. *Theranostics* 8, 4898–4911. doi: 10.7150/thno.27598

Conflict of Interest: The authors declare that the research was conducted in the absence of any commercial or financial relationships that could be construed as a potential conflict of interest.

frontiers in Chemistry

ORIGINAL RESEARCH
published: 29 March 2021
doi: 10.3389/fchem.2021.637754

Cinobufagin-Loaded and Folic Acid-Modified Polydopamine Nanomedicine Combined With Photothermal Therapy for the Treatment of Lung Cancer

Jianwen Li[1†], *Zhanxia Zhang*[2†*], *Haibin Deng*[1] *and Zhan Zheng*[1*]

[1]*Department of Oncology, Longhua Hospital, Shanghai University of Traditional Chinese Medicine, Shanghai, China,* [2]*Cancer Institute, Longhua Hospital, Shanghai University of Traditional Chinese Medicine, Shanghai, China*

Cinobufagin is used as a traditional Chinese medicine for cancer therapy. However, it has some disadvantages, such as poor water solubility, short circulating half-life, and low bioavailability. In the present study, a targeted delivery and smart responsive polydopamine (PDA)-based nanomedicine for delivering cinobufagin was rationally designed to improve the anticancer efficacy of the compound for the treatment of lung cancer. The modification of the nanomedicine using folic acid first mediated tumor targeting via the interaction between folic acid and its receptors on tumor cells. After lysosomes escape, the PDA nanomedicine was triggered by the low pH and released its cargo into the tumor microenvironment. The nanomedicine had a better therapeutic effect against lung cancer when used in combination with photothermal therapy. Compared with other nanomedicines used with photothermal therapy, this nanocarrier was not only sensitive to biologically low pH levels for on-demand drug release, but was also biodegradable, breaking down into biocompatible terminal products. Therefore, the proposed drug delivery system with targeted delivery and smart release demonstrated potential as a multifunctional nanoplatform that can enhance the bioavailability and reduce the side effects of chemotherapeutic agents.

Keywords: anticancer nanomedicine, photothermal therapy, targeted delivery, stimuli response, biodegradation

OPEN ACCESS

Edited by:
Dawei Jiang,
Huazhong University of Science and Technology, China

Reviewed by:
Lei Wang,
Harbin Institute of Technology, China
Renren Deng,
Zhejiang University, China

***Correspondence:**
Zhan Zheng
zhengzhan@shutcm.edu.cn
Zhanxia Zhang
zhanxiazhang@shutcm.edu.cn

[†]*These authors contributed equally to this work*

Specialty section:
This article was submitted to Nanoscience, a section of the journal Frontiers in Chemistry

Received: *04 December 2020*
Accepted: *11 February 2021*
Published: *29 March 2021*

Citation:
Li J, Zhang Z, Deng H and Zheng Z (2021) Cinobufagin-Loaded and Folic Acid-Modified Polydopamine Nanomedicine Combined With Photothermal Therapy for the Treatment of Lung Cancer. Front. Chem. 9:637754. doi: 10.3389/fchem.2021.637754

INTRODUCTION

Malignant tumors pose a major threat to human health and are characterized by rapid growth, strong metastasis, and high recurrence rate (Quail and Joyce, 2013). In addition, their morbidity and mortality rates are on the rise (Siegel et al., 2020). Although many chemotherapeutic agents used clinically can inhibit tumor growth significantly, they have various toxic and side effects, and have a low drug utilization rate (Kroschinsky et al., 2017). Therefore, new therapies need to be developed to circumvent these issues.

Photothermal therapy (PTT) is a novel noninvasive tumor treatment strategy that can transform near-infrared (NIR) light into heat using organic photosensitive molecules or inorganic nanomaterials (Hussein et al., 2018). The main advantages of PTT for treating cancer include thermal ablation, reversal of drug resistance, and inhibition of tumor metastasis (Jiang et al., 2015). Dong et al. developed a new method to efficiently produce Mo-based POM using β-Mo_2C as the raw

material, and revealed its REDOX cycle behavior in the tumor microenvironment, and successfully applied it to second near-infrared window (NIR-II) photoacoustic imaging-mediated photothermal and chemodynamic synergistic therapy (Liu et al., 2019). At present, organic photosensitive molecules mainly include indocyanine green (ICG) and methylene blue (Fan et al., 2020). However, the blood circulation half-life of these compounds is short, and they cannot be enriched selectively in the tumor area (Gonçalves et al., 2020). Although a large variety of nanomaterials, including noble metal nanoparticles (NPs), chalcogenide nanomaterials, carbon nanomaterials, and quantum dots, have been reported to exhibit photothermal activities, their poor biocompatibility limits their application in PTT (Zhang et al., 2016; Wang et al., 2020). Recently, polydopamine (PDA), derived from the self-polymerization of dopamine, has received attention as a biocompatible (natural melanin) photothermal material as well as a nanocarrier containing amino groups to facilitate surface modification (Farokhi et al., 2019).

Nanomedicine has the advantages of enhanced permeability and retention (EPR), extending the biological half-life of drugs, targeted delivery, and controlled release, even across the blood brain barrier (Zhao et al., 2020). To date, the FDA has approved various nanomedicines, such as doxil (liposome doxil), abraxane (albumin paclitaxel), and onivyde (liposome irityde) for treating cancer (Gaitanis and Staal, 2010). Although nanomedicines have achieved some success in anti-tumor therapy, the safety and toxicity of nanocarriers need to be evaluated and their clinical efficacy needs to be improved. Recent studies have found that the modification of nanomedicines by targeting molecules on their surface (positive targeting) can improve the specific delivery of these nanomedicines at tumor sites (Hill and Mohs, 2016). Targeting molecules usually include small molecules such as folic acid (FA), lectin, peptides, polysaccharides, antibodies, and nucleic acid aptamers (Rashidi et al., 2016). Previous studies demonstrate the use of RGD polypeptide, cetuximab, and EGFR (epidermal growth factor receptor) aptamer, all of which have targeted effects on tumor tissues (Wang et al., 2016; Narmani et al., 2019; Zhang et al., 2019). Overexpression of the FA receptor (FR) in various tumor cells makes it a good candidate for targeted delivery of nanomedicine (Zhang et al., 2020). The new generation of nanomedicine not only has the advantage of targeted delivery but can also release the cargo, according to the stimulation of the tumor microenvironment. Many smart nanomedicines that respond to external stimuli, such as light, magnetic field, and ultrasound, as well as internal stimuli, such as pH, temperature, enzyme, and redox potential responses have been explored (Zhou et al., 2018). Previous studies have demonstrated the release of nanomedicines in response to redox potential, DNAzyme, nuclease, crown ether, visible–ultraviolet light, and autophagy-lysosome processes (Zhang et al., 2013a; Zhang et al., 2013b; Zhang et al., 2013c; Zhang et al., 2014; Wang et al., 2016; Narmani et al., 2019). A large number of studies have shown that the pH level of tumor tissues (6.5–6.9) is generally lower than that of para-carcinoma tissue (7.2–7.4), which is mainly due to the anaerobic metabolism (Warburg effect) of tumor tissues and the production of a large number of acidic metabolites, such as lactic acid (Liu et al., 2014). Although there have been some reports on pH-responsive nanomedicines (Tang et al., 2018), there are only a few studies

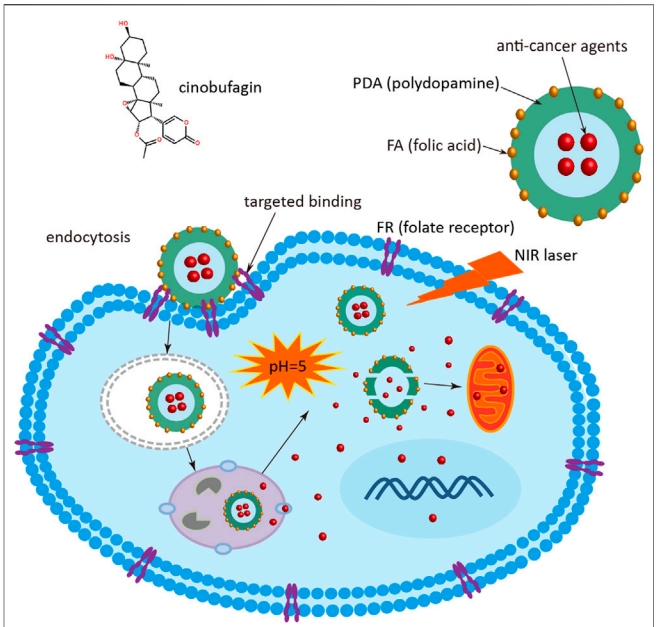

FIGURE 1 | Schematic diagram of Cino nanomedicine with targeted delivery and smart response. Cino, cinobufagin; PDA, polydopamine; FA, folic acid; FR, folate receptor; NIR, near infrared.

on biodegradable nanomedicines, such as PLGA (poly(lactic-co-glycolic acid), cyclodextrin, and chitosan, as well as treatment in combination with PTT (Zhang et al., 2018), which markedly restricts the prospects of nanomedicines.

The main components of cinobufagin (Cino) are indole alkaloids, which are extracted from the dry epidermis of *Bufo gargarizans* Cantor or *B. melanostictus* Schneider (Xie et al., 2012; Dai et al., 2018). Cino aids in clearing away heat and detoxification, relieving pain, relieving swelling, and removing stasis. According to the "Compendium of Materia Medica" the smell of Cino is symplectic cool, and it has the effect of clearing fever and damp elimination. Currently, Cino is used as a traditional anti-tumor medicine in China. It has shown significant efficacy in the treatment of various malignant tumors, especially lung, liver, and pancreatic cancers, when used alone or in combination with other chemotherapy drugs (Qi et al., 2011). However, due to the poor water solubility, short circulating half-life, and low bioavailability of Cino, improving its anticancer efficacy is an urgent clinical problem that needs to be solved (Ren et al., 2019).

In order to improve the therapeutic efficacy and enhanced solubility of the anticancer agent, a stimuli-responsive and targeting molecule-modified organic nanomedicine was developed. The biodegradable PDA nanomedicine was firstly synthesized via a classical Stöber method (by the reduction of dopamine hydrochloride to PDA in an aqueous alkaline solution) (Ren et al., 2019). Subsequently, the surface of the PDA nanomedicine was modified by the targeting molecule FA through the covalent coupling reaction of amino and carboxyl groups in the presence of EDC and NHS. The process of

delivering the nanomedicine is described in **Figure 1**. At the beginning, the FA-modified nanomedicine is recognized by FR, which is highly expressed in tumor cells. The nanomedicine is then delivered into the cytoplasm via the endosome through FA and FR-mediated endocytosis. After lysosome escape, the nanomedicine is delivered into the cell cytoplasm. Then the PDA nanomedicine is stimulated by the low intracellular pH due to the accumulation of acidic metabolites (e.g., lactic acid) produced by the high-rate of anaerobic glycolysis in tumor cells, and the anticancer agent Cino is released for inhibiting the proliferation of cancer cells. Finally, the PDA nanomedicine possesses a better therapeutic effect when combined with PTT.

MATERIALS AND METHODS

Materials

Cino was purchased from Absin. Dopamine hydrochloride, doxorubicin (DOX), and FA were purchased from Aladdin. N-(3-Dimethylaminopropyl)-N′-ethylcarbodiimide hydrochloride (EDC) and N-hydroxysuccinimide (NHS) were purchased from Sigma. All other organic solvents used in this study were of an analytical grade. Cleaved caspase-3 antibody was purchased from Abcam. Cell counting kit-8 (CCK-8) was purchased from MedChemExpress. Alanine transaminase (ALT), aspartate aminotransferase (AST), and creatinine (CRE) activity assay kits were purchased from the Nanjing Jiancheng Bioengineering Institute.

Synthesis of Anticancer Agent-Loaded Polydopamine Nanomedicine

A classical Stöber method with some modifications was used to synthesize the PDA nanomedicine (Bao et al., 2018). Briefly, a mixture of 290 ml of ultrapure water, 110 ml of ethanol, and 1.5 ml of NH_4OH was stirred at room temperature for 30 min. Then, 50 mg of Cino or 50 mg of DOX in 10 ml of ethanol was added to the above mixture. Subsequently, 0.5 g of dopamine hydrochloride in 10 ml of ultrapure water was added, and the reaction was stirred overnight. Finally, the nanomedicine was collected by centrifugation to remove the unloaded drug at 10,000 rpm for 10 min, washed twice with ultrapure water using a centrifuge at room temperature, and dried overnight on a lyophilizer.

As for the modification using FA, the obtained nanomedicine (100 mg) was first dispersed in 10 ml of phosphate buffered saline (PBS) (10 mM, pH 6.0). Subsequently, 50 mg of FA in 1 ml of ultrapure water was added to the above mixture. Next, 50 mg of EDC and 50 mg of NHS were added, and the mixture was stirred for 2 h. Finally, the FA-modified nanomedicine was collected by centrifugation at 5,000 rpm for 10 min, washed twice with ultrapure water using a centrifuge at room temperature, and dried overnight. Similarly, the blank PDA NPs were synthesized using the above-mentioned method, except for the addition of the anticancer agent.

Characterization of Polydopamine Nanoparticles

Transmission electron microscopy (TEM) and dynamic light scattering (DLS) were used to characterize the PDA NPs. Aliquots of PDA NP suspension were first dispensed onto parafilm sheets in a humidified Petri dish, and the vesicles were deposited on a carbon-coated grid (300-mesh) for 3 min. Subsequently, the grids were analyzed using a TEM (JEM-1230, JEOL). For DLS studies, the size distribution and zeta potential of the NPs were analyzed using a Malvern ZetaSizer Nano ZS90 particle size analyzer.

Assessment of Encapsulation Efficiency and Loading Content of Cino in the Polydopamine Nanomedicine

To measure the Cino content in the Cino-loaded PDA nanomedicine, the nanomedicine was diluted in acetonitrile. Subsequently, the concentration of Cino in the samples was determined using a Waters Acquity UPLC apparatus equipped with a Waters Acquity UPLC HSS T3 (2.1 × 100 mm, 1.8 μm) chromatographic column. The mobile phase consisted of acetonitrile (A) and 0.1% formic acid (B). The gradient elution program was as follows: 0–19 min, 10–95% (A); 19–20 min, 95–100% (A); 20–21 min, 100–10% (A); and 21–25 min, 10% (A). The other parameters were flow velocity: 0.4 ml/min; column temperature: 40°C; and sample volume: 2 μL. The monitoring wavelength range was 190–800 nm. The amount of Cino in the PDA nanomedicine was measured at 254 nm using a standard curve (absorbance vs. concentration). Cino encapsulation efficiency was 21.3% and was calculated as the ratio of the amount of Cino encapsulated in the NPs to the total amount of Cino fed for encapsulation. Cino loading content in the PDA nanomedicine was 9.1% and was calculated as the ratio of the amount of Cino encapsulated in the NPs to the total amount of NPs including Cino. Loading content of DOX in the PDA nanomedicine (dissolved in Tris buffer (pH = 9.0) for 20 min) for targeted delivery and pH release was measured using a nano-drop UV-Vis spectrophotometer at 539 nm using a standard curve (absorbance vs. concentration). The excitation and emission spectra of DOX is shown in **Suplementary Figure S5** (**Supplementary Material**).

Cell Culture and Cell Viability

Human lung/brunch normal epithelial (Beas2B), human lung adenocarcinoma (A549), and Lewis lung carcinoma (LLC) cell lines were purchased from the Cell Center of the Chinese Academy of Medical Sciences. Beas2B and LLC cells were cultured in DMEM (Hyclone, Logan, UT), and A549 cells were cultured in RPMI 1640 medium (Hyclone, Logan, UT), containing 10% fetal bovine serum (Biochrom AG, Berlin, Germany) and 1% penicillin-streptomycin solution at 37°C with 5% carbon dioxide.

For the cell viability assay, the cells were plated in 96-well plates at a density of 2×10^3 cells per well in quadruplicate and cultured overnight. After incubation with different reagents for 48 h, the cells were subjected to the CCK-8 assay according to the manufacturer's specifications.

Targeted Effect of Folic Acid -Modified Nanomedicine

For analysis of the targeted effect of FA, the Beas2B, A549, and LLC cells were first seeded in confocal dishes at 2×10^5 cells per well and cultured for 24 h. The cells were then incubated with 0.5 mg/ml of DOX-loaded FA-modified PDA nanomedicine for 4 h. Subsequently, the samples were washed with PBS and fixed with 4% paraformaldehyde for 30 min. Next, 0.5 μg/ml of Hoechst 33,258 was used to stain the cell nuclei for 5 min after washing with PBS. Finally, the targeted effect of FA was observed using a fluorescence microscope (Leica) at the red channel, after washing with ultrapure water and drying.

For analysis of the targeted effect of FA using a flow cytometry, the Beas2B, A549, and LLC cells were first seeded in 6-well plates at 2×10^5 cells per well, and cultured for 24 h. The cells were then incubated with 0.5 mg/ml of DOX-loaded FA-modified PDA nanomedicine for 4 h. Finally, the cells were harvested and analyzed on a flow cytometer (BD) at the PE (red) channel.

Stimuli Response of Doxorubicin-Loaded Polydopamine Nanomedicine

For the pH-responsive release of the PDA nanomedicine, Cino-loaded nanomedicine was used to stimulate the release of the PDA nanomedicine. First, 2.5 mg of Cino-loaded PDA nanomedicine was dissolved in 5 ml of 1 × PBS buffer (pH = 7.4) and divided into five portions of 1 ml each for use as control (pH = 7.4). Simultaneously, 5 mg of Cino-loaded PDA nanomedicine was dissolved in 10 ml of 1 × PBS buffer (pH = 5.0) and divided into ten portions of 1 ml each. Five of them were used as the pH (pH = 5.0) release group, and the other five were used as the pH (pH = 5.0) release with laser irradiation (808 nm, 2 W cm^{-2}, 5 min) group. Then, three samples from the different groups were precipitated at predetermined time intervals, and the content of Cino in the supernatant was determined using the UPLC apparatus.

In Vitro Anti-Tumor Efficacy of Cino-Loaded Polydopamine Nanomedicine in Lung Cancer Cells

For the cell viability assay, Beas2B, A549, and LLC cells were seeded in 96-well plates at 2×10^3 cells per well in quadruplicate and cultured overnight. After incubation with different concentrations of free Cino, Cino-loaded PDA nanomedicine, and Cino-loaded PDA nanomedicine with laser irradiation (808 nm, 2 W cm^{-2}, 5 min) for 48 h, the cells were subjected to CCK-8 assay according to the manufacturer's specifications.

In Vivo Anti-Tumor Efficacy of Cino-Loaded Polydopamine Nanomedicine

To establish xenograft tumors, six-week-old male nude mice (weighing approximately 20 g) were purchased from the Sippr-BK Laboratory Animal Co. Ltd (Shanghai, China). They were randomly divided into five groups (n = 6 for each group) and subcutaneously injected with 2×10^5 of LLC cells on the left side of the armpit. The length and width of tumors were measured using calipers every two days, and the tumor volume was calculated as (length × $width^2$)/2.

To evaluate the anticancer activity of the Cino-loaded PDA nanomedicine *in vivo*, the mice were intraperitoneally injected with saline, blank PDA NPs (~5 mg/kg), free Cino (1 mg/kg), Cino-loaded nanomedicine (at a Cino dose of 1 mg/kg), and Cino-loaded nanomedicine (at a Cino dose of 2 mg/kg) with laser irradiation (808 nm, 2 W cm^{-2}, 5 min), and treated every two days after the tumor volume reached approximately 50 mm^3. All mice were sacrificed, and their tumor weights and gross volumes were measured when the largest tumor volume was less than 800 mm^3. In addition, orbital blood obtained before mice sacrifice was mainly used for the detection of hepatorenal function. The tumor tissues were fixed in formalin for immunohistochemical analyses.

Immunohistochemical Staining

Tumors in each group were fixed with 5 ml of formalin overnight, dehydrated in ethanol, embedded in paraffin, and sectioned (at a thickness of 5 μm). Next, slides were deparaffinized in xylene and ethanol, and rehydrated in water. Subsequently, antigen retrieval was performed by heating in a microwave for 30 min in sodium citrate buffer (pH = 6.0). Slides were then quenched in hydrogen peroxide (3%) to block endogenous peroxidase activity and washed with TBST buffer. Finally, the primary antibodies were incubated at 4°C overnight, followed by the use of a SuperPicture™ Polymer Detection kit (Life Technologies) according to the manufacturer's instructions, along with antibodies against cleaved caspase-3 (Abcam).

Statistical Analysis

Data are presented as mean ± standard deviation (SD). Statistically significant differences between two groups were analyzed by hypothesis testing with the two-sample t-test, and indicated by $^*p < 0.05$, $^{**}p < 0.01$, and $^{***}p < 0.001$; $p < 0.05$ was considered statistically significant in all analyses (95% confidence level).

RESULTS AND DISCUSSION

Synthesis and Characterization of Polydopamine Nanoparticles

A classical Stöber approach was used to prepare the PDA NPs. During the reaction, the mixture quickly turned from colorless to black, indicating the formation of PDA NPs, because dopamine is a natural melanin. TEM and DLS were employed to characterize the morphology and size of the PDA NPs. As shown in **Figure 2A**, the TEM image indicates that the PDA NPs possessed a spherical and uniform morphology. As shown in **Figure 2B**, the DLS image correlates well with the TEM results, and the size of most of the NPs was approximately 330 nm.

The zeta potentials of the blank PDA NPs and Cino-loaded nanomedicine were measured using DLS. As shown in **Supplementary Figure S1** (**Supplementary Material**), the zeta potentials of the PDA NPs and Cino-loaded nanomedicine were

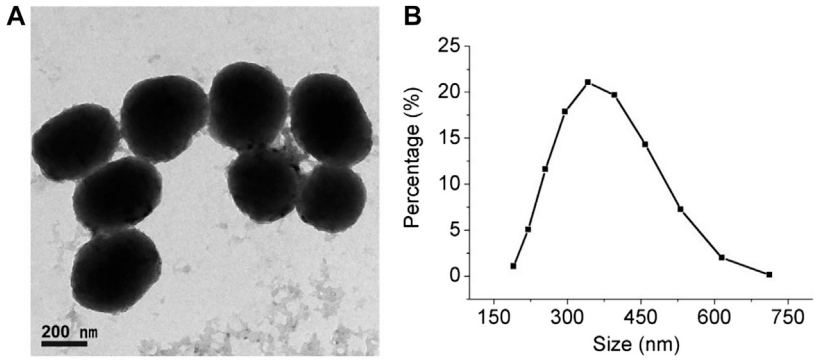

FIGURE 2 | Characterization of synthesized PDA NPs. **(A)** TEM image of PDA NPs (scale bar = 200 nm). **(B)** Particle size distribution using dynamic light scattering (DLS).

−42 mV and −31 mV, respectively, indicating that Cino was successfully embedded in the PDA nanomedicine. The negative charge may be caused by the modification of FA on the surface of the nanomedicine.

Furthermore, Fourier transform infrared spectroscopy (FITR) of PDA NPs, FA, and FA-modified PDA NPs were recorded. As shown in **Supplementary Figure S2** (**Supplementary Material**), the characteristic peak of FA (at 1700 cm^{-1}) can be observed in FA-modified PDA NPs, revealing that FA was successfully modified on the surface of the PDA NPs.

The absorption spectrum and the photostability of the PDA NPs were also measured. As shown in **Supplementary Figure S3** (**Supplementary Material**), the PDA NPs possess broad absorption in the NIR region at 750–900 nm, exhibiting the capability to convert NIR into heat similar to other photothermal materials (Ding et al., 2019). Importantly, the PDA NPs have excellent photothermal stability and repeatability in which the conversion efficiency was virtually unchanged after five rounds of ON/OFF irradiation cycles. These results indicated that the PDA NPs had good photothermal conversion efficiency and photothermal stability. Thus, the NPs were suitable for use as PTT agents.

Biocompatibility of the Blank Polydopamine Nanoparticles

PDA, a natural melanin, was chosen as the basic component to guarantee the favorable biocompatibility of the nanocarrier. In theory, the blank PDA NPs should have excellent biocompatibility because of the biodegradable metabolites homovanillic acid and trihydroxyphenylacetic acid (Marín-Valencia et al., 2008). As shown in **Supplementary Figure S4** (**Supplementary Material**), blank PDA NPs showed no obvious cytotoxicity to Beas2B, A549, or LLC cells, indicating that the PDA NPs are biocompatible.

In this study, PDA is not only used as the nanomedicine carrier but also has the property of PTT. Hence, we also explored the influence of the 808 laser on cell growth. As shown in the last panel of **Supplementary Figure S4** (**Supplementary Material**), the 808 laser used at 2 W cm^{-2} for 5 min had little effect on the proliferation of Beas2B, A549, and LLC cells. Furthermore, the *in vitro* anti-tumor efficacy of the blank PDA NPs with NIR treatment in lung cancer was also recorded. As shown in **Supplementary Figure S6** (**Supplementary Material**), the cell viability of A549 cells and LLC cells had some influence after incubation with the blank PDA NPs with NIR treatment, indicating that the NPs had the property of photothermal therapy.

Targeted Delivery of Folic Acid

In order to improve the efficacy and reduce the side effects of the nanomedicine, FA was used as the targeting molecule for modifying the surface of the PDA nanomedicine. For verifying the targeted effect of FA, DOX-loaded FA-modified PDA nanomedicine was incubated with Beas2B, A549, and LLC cells due to the optical signal of DOX (Chen et al., 2018). As depicted in **Figure 3A**, fluorescence microscopy indicated the presence of a small amount of PDA nanomedicine around the Beas2B cells. The red color around the Beas2B cells might be due to nonspecific adsorption of the PDA nanomedicine, like the right (red) shift of Beas2B cells observed in the flow cytometry analysis (**Figure 3B**). In contrast, there was a large amount of targeted adsorption of the nanomedicine around the A549 and LLC cells, suggesting the excellent targeted effect of FA in tumor cells. As depicted in **Figure 3B**, flow cytometry analysis is consistent with the results of fluorescence microscopy. These data demonstrated that the modification by FA as a targeting molecule can help deliver anticancer drugs specifically to tumor cells.

Controlled Release and Optothermal Response of the Polydopamine Nanomedicine

A large number of studies have shown that the pH of tumor tissues (6.5–6.9) is generally lower than that of normal tissues, which is mainly due to the aerobic glycolysis (Warburg effect) of tumor tissues, and the production of a large number of acidic metabolites, such as lactic acid (Marín-Valencia et al., 2008). The pH-responsive release and optothermal response of the Cino-loaded PDA nanomedicine were studied under low pH conditions (pH = 5.0) with NIR laser irradiation. As shown in

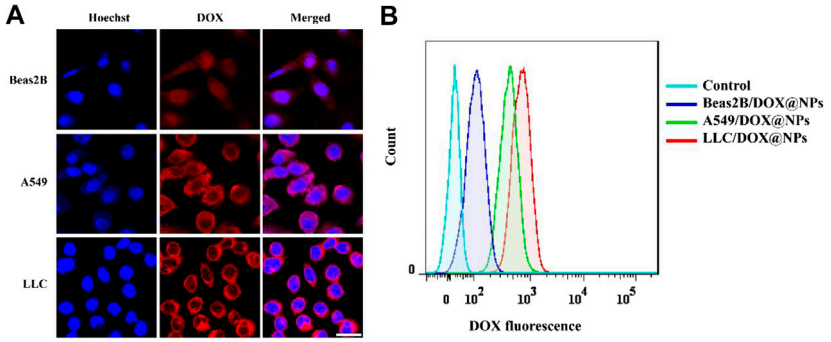

FIGURE 3 | Targeted effect of DOX-loaded FA-modified nanomedicine. **(A)** Fluorescence microscopy images of normal Beas2B, lung cancer A549, and LLC cells after treatment with DOX-loaded FA-modified nanomedicine (0.5 mg/ml) for 4 h. The red color indicates DOX, and the blue color indicates Hoechst; scale bar = 25 μm. **(B)** Flow cytometry analysis of the above samples at PE (red) channel.

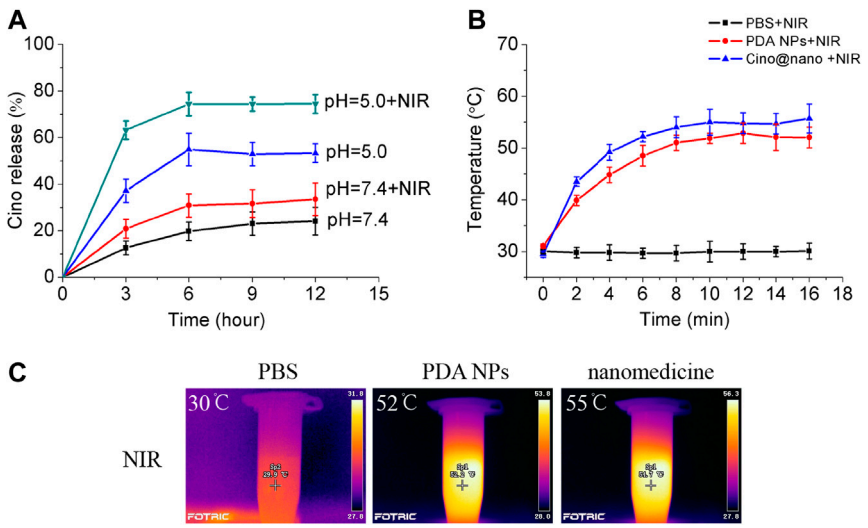

FIGURE 4 | Controlled release and optothermal response of the PDA nanomedicine. **(A)** Cino release from Cino-loaded PDA nanomedicine (0.5 mg/ml) after treatment with pH = 5.0 PBS buffer, without or with an 808 laser (2 W cm^{-2}, 5 min). Data are presented as the mean ± SD (standard deviation, $n = 3$). The temperature curves **(B)** and pictures **(C)** of PBS buffer, blank PDA NPs, and Cino-loaded PDA nanomedicine after treatment with the 808 laser.

Figure 4A, the release curve showed that only 24% of Cino was released in the control group (pH = 7.4 of PBS buffer). The minor leakage of Cino was caused by the relative stability of the PDA nanocarrier under normal conditions. The Cino release reached up to 33% with NIR laser treatment. Importantly, the Cino release reached up to 53 and 74% without and with NIR laser treatment, respectively, at pH = 5.0 within 12 h. The pH-dependent release may be due to the pH sensitivity of the PDA nanocarrier (Crayton and Tsourkas, 2011). After treatment with the 808 laser (2 W cm^{-2}, 5 min) at pH = 5.0, the temperature of the PDA nanomedicine was gradually increased, which led to a significant increase in cumulative Cino release. In addition, most of the anticancer agents were released from PDA nanomedicine during the first 6 h. These results confirmed that the PDA nanomedicine could respond to low pH levels and be triggered for on-demand drug release. Further, the laser treatment (808 nm) can accelerate the release of the anticancer agents from PDA nanomedicine.

Next, we explored the photothermal response of the PDA nanomedicine. thermographic images and curves of the PBS buffer, blank PDA NPs, and Cino-loaded PDA nanomedicine after treatment with the 808 laser are shown in **Figure 4B**. The temperature of the PBS buffer did not change when treated with the 808 laser. However, the temperature of the blank PDA NPs and Cino-loaded PDA nanomedicine increased over time and reached a saturation state; the rate of increase in temperature was proportional to the power of the laser. Furthermore, the temperature curves of the blank PDA NPs and Cino-loaded PDA nanomedicine showed similar trends. Collectively, the efficacy of Cino-loaded PDA nanomedicine was found to be enhanced by PTT in lung cancer therapy.

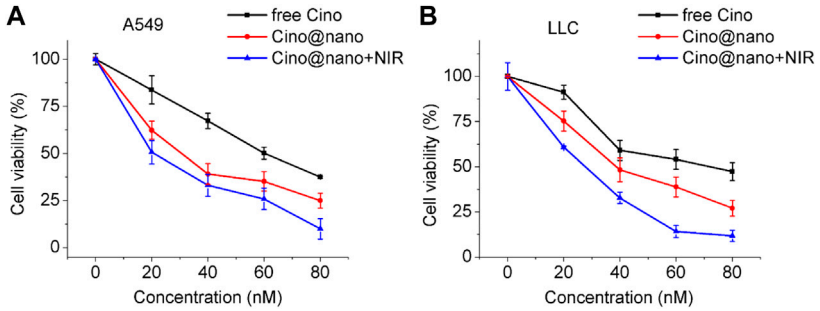

FIGURE 5 | *In vitro* anti-tumor efficacy of Cino-loaded PDA nanomedicine in lung cancer cells. **(A)** Viability of A549 cells after incubation with various concentrations of free Cino, Cino-loaded PDA nanomedicine, and Cino-loaded PDA nanomedicine with NIR treatment. Data are presented as mean ± SD (standard deviation, $n = 4$). **(B)** Viability of LLC cells after incubation with various concentrations of free Cino, Cino-loaded PDA nanomedicine, and PDA nanomedicine with NIR treatment (2 W cm^{-2}, 5 min). Data are presented as the mean ± SD (standard deviation, $n = 4$).

In Vitro Inhibitory Effect of Polydopamine Nanomedicine on Lung Cancer Cells

To explore the anticancer effect of the PDA nanomedicine, lung cancer cells were incubated with free Cino (control group), Cino-loaded PDA nanomedicine, and Cino-loaded PDA nanomedicine with laser irradiation at 808 nm. As shown in **Figure 5A**, the half maximal inhibitory concentration (IC_{50}) of free Cino was 61 nM in A549 cells. Conversely, the IC_{50} of Cino-loaded nanomedicine was only 32 nM, which is almost half. The IC_{50} of Cino-loaded nanomedicine combined with laser irradiation at 808 nm was even lower, at 21 nM. These results revealed that PDA nanomedicine has a better inhibition potential than its free drug form. In addition, PDA nanomedicine combined with laser irradiation at 808 nm possesses the potential for PTT. Concurrently, the inhibitory effects of the PDA nanomedicine on lung cancer LLC cells were also assessed. As shown in **Figure 5B**, the IC_{50} of free Cino was 74 nM, whereas that of the PDA nanomedicine was 39 nM. The IC_{50} of the nanomedicine combined with laser irradiation at 808 nm was 31 nM, indicating that the PDA nanomedicine, used along with laser irradiation at 808 nm, has the ability to greatly suppress the proliferation of LLC cells, not only with its chemotherapeutic agents, but also with PTT. The PDA nanomedicine has a better inhibitory effect, which might be due to the different methods of cellular uptake for these agents. For example, free Cino enters cells via diffusion, whereas the PDA nanomedicine enters through endocytosis. In this aspect, endocytosis seems more efficient for carrying a high amount of Cino in contrast to simple diffusion through the cell membrane (Rashidi et al., 2016). Importantly, the PDA nanomedicine posed a much higher selective cytotoxicity to the lung cancer cells, having high FR expression and lower pH than normal cells. In addition, treatment with laser irradiation at 808 nm showed an inhibitory effect on lung cancer cells mainly due to thermal ablation (Li et al., 2018). All the observations demonstrated that the PDA nanomedicine with targeted delivery and controlled release had the best therapeutic effect in the presence of laser irradiation at 808 nm.

In Vivo Anti-Tumor Activities of the Polydopamine Nanomedicine

We firstly investigated the *in vivo* targeted delivery capacity of the PDA nanomedicine. *In vivo* biodistribution of free ICG, ICG-loaded PDA nanomedicine, and ICG-loaded PDA nanomedicine with FA modification was monitored using an *in vivo* imaging system due to the NIR fluorescence signal of ICG (Li et al., 2018). As shown in **Supplementary Figure S7** (**Supplementary Material**), only weak ICG fluorescence in the tumor could be visualized for the free ICG group at 24 h post-injection. In contrast, the fluorescence intensity of PDA nanomedicine without FA modification in the tumor tissues was still very strong. However, strong ICG fluorescence in the liver was observed, indicating that PDA nanomedicine without FA modification could prolong systemic circulation in blood due to the EPR effect. Importantly, the ICG fluorescence of PDA nanomedicine with FA modification was much stronger at the tumor site than that of PDA nanomedicine without FA modification, and weaker in the liver, demonstrating a good tumor-targeting ability. These results reveal that PDA nanomedicine with targeted modification could improve the therapeutic effect and reduce toxic and side effects.

The anti-tumor efficacy of the blank PDA nanoplatform, free Cino, PDA nanomedicine, and PDA nanomedicine with PTT was studied in LLC tumor-bearing mice. During the monitoring period, neither mouse death nor a significant drop in body weight was observed in any group (**Supplementary Figure S8**, **Supplementary Material**), indicating that the treatments did not produce serious toxicity and side effects in the tumor-bearing mice. When the LLC subcutaneous xenograft reached 50 mm^3 in size, mice were randomly divided into five groups of six mice per group. The mice were then administered saline only, blank PDA NPs (~5 mg/kg), free Cino (1 mg/kg), PDA nanomedicine (1 mg/kg), and PDA nanomedicine (1 mg/kg) with NIR laser (2 W cm^{-2}, 5 min, after treatment) by intraperitoneal injection every alternate day. Before each treatment, body weight and tumor volume were measured. As shown in **Figure 6A**, the blank PDA NP group showed a similar tendency to that of the control group, indicating the biocompatibility of the PDA

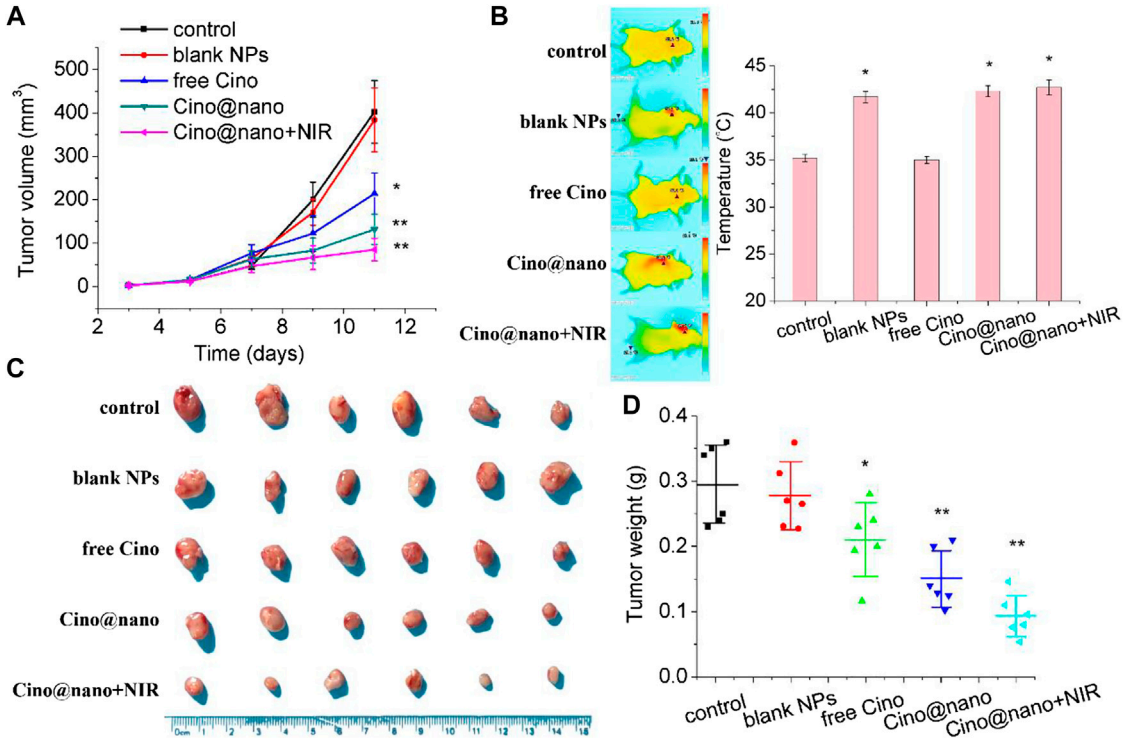

FIGURE 6 | *In vivo* anti-tumor efficacy of Cino-loaded PDA nanomedicine. **(A)** Tumor volume growth curves **(B)** optothermal response **(C)** tumor photo, and **(D)** tumor weight of LLC tumor-bearing mice after systemic administration of saline, blank NPs, free Cino (1 mg/kg), Cino-loaded PDA nanomedicine (1 mg/kg of Cino), and Cino-loaded PDA nanomedicine (1 mg/kg of Cino) treated with 808 NIR laser (2 W cm^{-2}, 5 min). Data are presented as the mean ± SD (standard deviation, $n = 6$), $^{*}p < 0.05$, $^{**}p < 0.01$.

nanocarrier. Free Cino effectively inhibited tumor growth. In contrast, PDA nanomedicine had a better therapeutic efficacy than free Cino. Importantly, the PDA nanomedicine combined with laser irradiation at 808 nm almost suppressed the growth of subcutaneous tumors. As shown in **Figures 6C,D**, photos and the weight of tumors support the results of tumor volume (**Figure 6A**), clearly showing that free Cino, PDA nanomedicine, and PDA nanomedicine with NIR laser could effectively inhibit tumor growth, with inhibition rates of 29, 48, and 67% on the 11th day, respectively. The temperature increase in the tumor region during NIR laser irradiation is shown in **Figure 6B**. For the groups treated with saline and free Cino, the temperature increased to 35.2 and 34.9°C, respectively, after irradiation for 5 min (2 W cm^{-2}). Conversely, the temperature increased to 41.7, 42.3, and 42.7°C for the groups treated with blank PDA NPs, PDA nanomedicine, and PDA nanomedicine with NIR laser, respectively. These results revealed that the PDA nanomedicine with NIR laser inhibits tumor development most effectively, which is due to the targeted delivery and low pH level stimuli of the PDA nanomedicine in the tumor microenvironment. In addition, the thermal ablation of laser irradiation also increases the therapeutic effect of the PDA nanomedicine.

To further determine the anticancer efficacy of the PDA nanomedicine with NIR laser, immunohistochemical analysis was also performed. As shown in **Figures 7A,B**, compared with the control group, the blank PDA NPs showed similar results for the apoptosis factors (cleaved caspase-3). However, free Cino treatment showed significantly increased positive staining for cleaved caspase-3. In addition, Cino-loaded nanomedicine showed more positive staining of cleaved caspase-3 than free Cino. Notably, compared with the tumors treated with Cino@nano, the groups treated with Cino@nano plus NIR irradiation showed typical features of thermal damage in tumor tissues, and possessed the largest number of apoptotic cells, demonstrating the most significant anti-tumor activity of Cino@nano under NIR laser irradiation.

Furthermore, hepatorenal toxicity of the PDA nanomedicine was assessed in terms of ALT, AST, and CRE in mouse serum. As shown in **Supplementary Figure S9** (**Supplementary Material**), the free Cino had the highest ALT, AST, and CRE levels, while the PDA nanomedicine and the PDA nanomedicine with NIR laser had a lesser influence on the liver function of the mice compared with free Cino; the blank NPs had no significant influence. These results indicated that PDA is biodegradable, and that the PDA nanomedicine has properties conducive for targeted delivery and smart response in the tumor microenvironment. The low hepatorenal toxicity of the PDA nanomedicine with PTT is also demonstrated. Altogether, the PDA nanomedicine with NIR laser possesses a significant therapeutic effect and low hepatorenal toxicity.

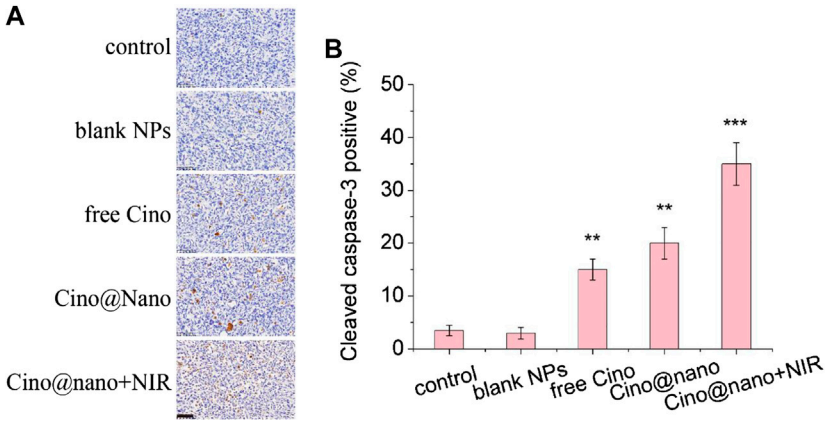

FIGURE 7 | Immunohistochemical staining. **(A)** Cleaved caspase-3 immunohistochemical staining of LLC tumor-bearing mice after systemic administration of saline, blank NPs, free Cino, Cino loaded nanomedicine, and Cino loaded nanomedicine with NIR laser (scale bar = 50 μm). **(B)** Statistical analysis of immunohistochemical staining. Data are presented as the mean ± SD (standard deviation, $n = 15$), $^{**}p < 0.01$, $^{***}p < 0.001$.

CONCLUSION

A targeting molecule-modified multifunctional drug delivery platform was designed to improve the therapeutic effect of an anticancer agent. PDA nanomedicine can be delivered to tumor cells through FA and FR-mediated cellular endocytosis. In addition, pH-responsive and NIR irradiation-triggered drug release was observed. Both *in vitro* and *in vivo* studies showed that the PDA nanomedicine exerted excellent multimodal (anticancer agent and photothermal) therapeutic effects in inhibiting tumor cell proliferation. This nanomedicine delivery platform is biocompatible and biodegradable due to natural melanin. Importantly, other chemotherapeutic agents and a combination of multiple anticancer drugs as well as genetic agents can be selectively delivered by this smart, responsive, multifunctional nanocarrier. Furthermore, because of the easy introduction of other functional modules onto the surface of the PDA nanomedicine, this work opens up a new avenue to tailor precise PTT nanosystems with high drug accumulation in tumor tissue for a specific patient or disease. Altogether, the present study illustrates the great potential of NIR-responsive and targeted delivery PDA nanomedicine for fast *in situ* drug release to achieve augmented cancer therapy.

DATA AVAILABILITY STATEMENT

The original contributions presented in the study are included in the article/**Supplementary Material**, further inquiries can be directed to the corresponding author.

ETHICS STATEMENT

The animal study was reviewed and approved. All animal experiments were approved by the Institutional Animal Ethics Committees of Shanghai University of Traditional Chinese Medicine (PZSHUTCM200522005).

AUTHOR CONTRIBUTIONS

ZZ (4th author) and ZZ (1st author) designed the experiments; JL and HD performed the experiments; ZZ (4th author) and ZZ (1st author) analyzed the data; ZZ (1st author) and JL wrote the manuscript.

FUNDING

This work was supported by the Natural Science Foundation of Shanghai (No. 20ZR1459200, 17ZR1430600) and the Innovation Program of Shanghai Municipal Education Commission (2017-01-07-00-10-E00064).

SUPPLEMENTARY MATERIAL

The Supplementary Material for this article can be found online at: https://www.frontiersin.org/articles/10.3389/fchem.2021.637754/full#supplementary-material.

REFERENCES

Bao, X., Zhao, J., Sun, J., Hu, M., and Yang, X. (2018). Polydopamine nanoparticles as efficient scavengers for reactive oxygen species in periodontal disease. *ACS Nano* 12, 8882–8892. doi:10.1021/acsnano.8b04022

Chen, D., Zhang, G., Li, R., Guan, M., Wang, X., Zou, T., et al. (2018). Biodegradable, hydrogen peroxide, and glutathione dual responsive nanoparticles for potential programmable paclitaxel release. *J. Am. Chem. Soc.* 140, 7373–7376. doi:10.1021/jacs.7b12025

Crayton, S. H., and Tsourkas, A. (2011). pH-titratable superparamagnetic iron oxide for improved nanoparticle accumulation in acidic tumor microenvironments. *ACS Nano* 5, 9592–9601. doi:10.1021/nn202863x

Dai, G., Zheng, D., Guo, W., Yang, J., and Cheng, A. Y. (2018). Cinobufagin induces apoptosis in osteosarcoma cells via the mitochondria-mediated apoptotic pathway. *Cell. Physiol. Biochem.* 46, 1134–1147. doi:10.1159/000488842

Ding, Y., Du, C., Qian, J., and Dong, C. (2019). NIR-responsive polypeptide nanocomposite generates no gas, mild photothermia and chemotherapy to reverse multidrug Resistant Cancer. *Nano Lett.* 19, 4362–4370. doi:10.1021/acs.nanolett.9b00975

Fan, Z., Zong, J., Lau, W. Y., and Zhang, Y. (2020). Indocyanine green and its nanosynthetic particles for the diagnosis and treatment of hepatocellular carcinoma. *Am. J. Transl. Res.* 12, 2344–2352.

Farokhi, M., Mottaghitalab, F., Saeb, M. R., and Thomas, S. (2019). Functionalized theranostic nanocarriers with bio-inspired polydopamine for tumor imaging and chemo-photothermal therapy. *J. Control Release* 309, 203–219. doi:10.1016/j.jconrel.2019.07.036

Gaitanis, A., and Staal, S. (2010). Liposomal doxorubicin and nab-paclitaxel: nanoparticle cancer chemotherapy in current clinical use. *Methods Mol. Biol.* 624, 385–392. doi:10.1007/978-1-60761-609-2_26

Gonçalves, A. S. C., Rodrigues, C. F., Moreira, A. F., and Correia, I. J. (2020). Strategies to improve the photothermal capacity of gold-based nanomedicines. *Acta Biomater.* 116, 105–137. doi:10.1016/j.actbio.2020.09.008

Hill, T. K., and Mohs, A. M. (2016). Image-guided tumor surgery: will there be a role for fluorescent nanoparticles?. *Wiley Interdiscip. Rev. Nanomed. Nanobiotechnol.* 8, 498–511. doi:10.1002/wnan.1381

Hussein, E. A., Zagho, M. M., Nasrallah, G. K., and Elzatahry, A. A. (2018). Recent advances in functional nanostructures as cancer photothermal therapy. *Int. J. Nanomed.* 13, 2897–2906. doi:10.2147/ijn.s161031

Jiang, Y., Fei, W., Cen, X., Tang, Y., and Liang, X. (2015). Near-infrared light activatable multimodal gold nanostructures platform: an emerging paradigm for cancer therapy. *Curr. Cancer Drug Targets* 15, 406–422. doi:10.2174/1568009615666150407125333

Kroschinsky, F., Stölzel, F., von Bonin, S., Beutel, G., Kochanek, M., Kiehl, M., et al. (2017). Intensive Care in Hematological and Oncological Patients (iCHOP) Collaborative GroupNew drugs, new toxicities: severe side effects of modern targeted and immunotherapy of cancer and their management. *Crit. Care* 21, 89. doi:10.1186/s13054-017-1678-1

Li, M., Sun, X., Zhang, N., Wang, W., Yang, Y., Jia, H., et al. (2018). NIR-activated polydopamine-coated carrier-free "nanobomb" for *in situ* on-demand drug release. *Adv. Sci. (Weinh)* 5, 1800155. doi:10.1002/advs.201800155

Liu, G., Zhu, J., Guo, H., Sun, A., Chen, P., Xi, L., et al. (2019). Mo_2C-Derived polyoxometalate for NIR-II photoacoustic imaging-guided chemodynamic/photothermal synergistic therapy. *Angew. Chem. Int. Ed. Engl.* 58, 18641–18646. doi:10.1002/anie.201910815

Liu, J., Huang, Y., Kumar, A., Tan, A., Jin, S., Mozhi, A., et al. (2014). pH-sensitive nano-systems for drug delivery in cancer therapy. *Biotechnol. Adv.* 32, 693–710. doi:10.1016/j.biotechadv.2013.11.009

Marín-Valencia, I., Serrano, M., Ormazabal, A., Pérez-Dueñas, B., García-Cazorla, A., Campistol, J., et al. (2008). Biochemical diagnosis of dopaminergic disturbances in paediatric patients: analysis of cerebrospinal fluid homovanillic acid and other biogenic amines. *Clin. Biochem.* 41, 1306–1315. doi:10.1016/j.clinbiochem.2008.08.077

Narmani, A., Rezvani, M., Farhood, B., Darkhor, P., Mohammadnejad, J., Amini, B., et al. (2019). Folic acid functionalized nanoparticles as pharmaceutical carriers in drug delivery systems. *Drug Dev. Res.* 80, 404–424. doi:10.1002/ddr.21545

Qi, F., Li, A., Inagaki, Y., Kokudo, N., Tamura, S., Nakata, M., et al. (2011). Antitumor activity of extracts and compounds from the skin of the toad *Bufo gargarizans* Cantor. *Int. Immunopharmacol.* 11, 342–349. doi:10.1016/j.intimp.2010.12.007

Quail, D. F., and Joyce, J. A. (2013). Microenvironmental regulation of tumor progression and metastasis. *Nat. Med.* 19, 1423–1437. doi:10.1038/nm.3394

Rashidi, L. H., Homayoni, H., Zou, X., Liu, L., and Chen, W. (2016). Investigation of the strategies for targeting of the afterglow nanoparticles to tumor cells. *Photodiagnosis Photodyn. Ther.* 13, 244–254. doi:10.1016/j.pdpdt.2015.08.001

Ren, W., Chen, S., Liao, Y., Li, S., Ge, J., Tao, F., et al. (2019). Near-infrared fluorescent carbon dots encapsulated liposomes as multifunctional nano-carrier and tracer of the anticancer agent cinobufagin *in vivo* and *in vitro*. *Colloids Surf. B Biointerfaces* 174, 384–392. doi:10.1016/j.colsurfb.2018.11.041

Siegel, R. L., Miller, K. D., and Jemal, A. (2020). Cancer statistics, 2020. *CA Cancer J. Clin.* 70, 7–30. doi:10.3322/caac.21332

Tang, H., Zhao, W., Yu, J., Li, Y., and Zhao, C. (2018). Recent development of pH-responsive polymers for cancer nanomedicine. *Molecules* 24, 4. doi:10.3390/molecules24010004

Wang, J., Wu, X., Shen, P., Wang, J., Shen, Y., Shen, Y., et al. (2020). Applications of inorganic nanomaterials in photothermal therapy based on combinational cancer treatment. *Int. J. Nanomed.* 15, 1903–1914. doi:10.2147/ijn.s239751

Wang, Y., Huang, H. Y., Yang, L., Zhang, Z., and Ji, H. (2016). Cetuximab-modified mesoporous silica nano-medicine specifically targets EGFR-mutant lung cancer and overcomes drug resistance. *Sci. Rep.* 6, 25468. doi:10.1038/srep25468

Xie, R. F., Li, Z. C., Gao, B., Shi, Z. N., and Zhou, X. (2012). Bufothionine, a possible effective component in cinobufocini injection for hepatocellular carcinoma. *J. Ethnopharmacol.* 141, 692–700. doi:10.1016/j.jep.2011.12.018

Zhang, P., Hu, C., Ran, W., Meng, J., Yin, Q., and Li, Y. (2016). Recent progress in light-triggered nanotheranostics for cancer treatment. *Theranostics* 6, 948–968. doi:10.7150/thno.15217

Zhang, L., Qin, Y., Zhang, Z., Fan, F., Huang, C., Lu, L., et al. (2018). Dual pH/reduction-responsive hybrid polymeric micelles for targeted chemo-photothermal combination therapy. *Acta Biomater.* 75, 371–385. doi:10.1016/j.actbio.2018.05.026

Zhang, Z., Balogh, D., Wang, F., Sung, S. Y., Nechushtai, R., and Willner, I. (2013a). Biocatalytic release of an anticancer drug from nucleic-acids-capped mesoporous SiO_2 Using DNA or molecular biomarkers as triggering stimuli. *ACS Nano* 7, 8455–8468. doi:10.1021/nn403772j

Zhang, Z., Balogh, D., Wang, F., Tel-Vered, R., Levy, N., Sung, S. Y., et al. (2013b). Light-induced and redox-triggered uptake and release of substrates to and from mesoporous SiO_2 nanoparticles. *J. Mater. Chem. B* 1, 3159–3166. doi:10.1039/c3tb20292e

Zhang, Z., Balogh, D., Wang, F., and Willner, I. (2013c). Smart mesoporous SiO_2 nanoparticles for the DNAzyme-induced multiplexed release of substrates. *J. Am. Chem. Soc.* 135, 1934–1940. doi:10.1021/ja311385y

Zhang, Z., Wang, F., Sohn, Y. S., Nechushtai, R., and Willner, I. (2014). Gated mesoporous SiO_2 nanoparticles using K^+-stabilized G-quadruplexes. *Adv. Funct. Mater.* 24, 5662–5670. doi:10.1002/adfm.201400939

Zhang, Z., Dong, C., Yu, G., Cheng, W., Liang, Y., Pan, Y., et al. (2019). Smart and dual-targeted BSA nanomedicine with controllable release by high autolysosome levels. *Colloids Surf. B Biointerfaces* 182, 110325. doi:10.1016/j.colsurfb.2019.06.055

Zhang, Z., Cheng, W., Pan, Y., and Jia, L. (2020). An anticancer agent-loaded PLGA nanomedicine with glutathione-response and targeted delivery for the treatment of lung cancer. *J. Mater. Chem. B* 8, 655–665. doi:10.1039/c9tb02284h

Zhao, M., van Straten, D., Broekman, M. L. D., Préat, V., and Schiffelers, R. M. (2020). Nanocarrier-based drug combination therapy for glioblastoma. *Theranostics* 10, 1355–1372. doi:10.7150/thno.38147

Zhou, Q., Zhang, L., Yang, T., and Wu, H. (2018). Stimuli-responsive polymeric micelles for drug delivery and cancer therapy. *Int. J. Nanomed.* 13, 2921–2942. doi:10.2147/ijn.s158696

Conflict of Interest: The authors declare that the research was conducted in the absence of any commercial or financial relationships that could be construed as a potential conflict of interest.

Advantages of publishing in Frontiers

OPEN ACCESS
Articles are free to read for greatest visibility and readership

FAST PUBLICATION
Around 90 days from submission to decision

HIGH QUALITY PEER-REVIEW
Rigorous, collaborative, and constructive peer-review

TRANSPARENT PEER-REVIEW
Editors and reviewers acknowledged by name on published articles

Frontiers
Avenue du Tribunal-Fédéral 34
1005 Lausanne | Switzerland

Visit us: www.frontiersin.org
Contact us: frontiersin.org/about/contact

REPRODUCIBILITY OF RESEARCH
Support open data and methods to enhance research reproducibility

DIGITAL PUBLISHING
Articles designed for optimal readership across devices

FOLLOW US
@frontiersin

IMPACT METRICS
Advanced article metrics track visibility across digital media

EXTENSIVE PROMOTION
Marketing and promotion of impactful research

LOOP RESEARCH NETWORK
Our network increases your article's readership